

ELECTROCHEMICAL STUDIES OF CONDUCTING POLYMERS

CENTRE FOR NEWFOUNDLAND STUDIES

**TOTAL OF 10 PAGES ONLY  
MAY BE XEROXED**

(Without Author's Permission)

KAVITHAA LOGANATHAN





# **ELECTROCHEMICAL STUDIES OF CONDUCTING POLYMERS**

by

**Kavithaa Loganathan**

A thesis submitted to the School of Graduate Studies in partial fulfillment of the  
requirements for the degree of Doctor of Philosophy



Department of Chemistry

Memorial University of Newfoundland

St. John's, Newfoundland, Canada

December, 2005



## Abstract

This project addresses the development of low band gap organic materials with high intrinsic conductivity which remains a big challenge for many conducting polymer based applications. New bridged bithiophene and fluorene systems were investigated. Results proved that the linkage of two bridged bithiophene moieties by a double bond, and bridging fluorene moieties by sulphur atoms can produce low band gap materials with low-lying LUMO energy levels. This new approach to the design of low band gap materials compliments the strategy of introducing electron withdrawing groups at an  $sp^2$  carbon bridging a bithienyl precursor for producing n-type conjugated low band gap systems.

Advanced polymerization techniques such as copolymerization (polymerization from solution of two monomers), homopolymerization of a comonomer (a molecule containing both monomer units) and working electrode rotation during polymer growth were developed to tune band gaps and enhance intrinsic conductivities. Investigations of copolymers with conjugated bridged bithiophene and fluorene systems support the donor acceptor strategy for band gap reduction. Hence, by advanced synthetic strategies, the band gap of a polythiophene derivative was tuned from 1.0 eV to 0.1 eV and its intrinsic conductivity was improved by an order of magnitude. Further, a variety of polyfluorene derivatives with band gaps ranging from 1.2 eV to 0.8 eV were synthesized and structure-conductivity relationships were studied. These materials may have potential uses in electrochromic displays and related applications.

## Acknowledgements

I would like to thank my supervisor, Dr. Peter G. Pickup, University Research Professor, and Deputy Head of Graduate Studies and Research, Memorial University of Newfoundland, for his guidance and support throughout this program.

I take this opportunity to thank Dr. Robert Helleur, Dr. Laurence K. Thompson, Dr. Michael Mackey, Dr. Graham Bodwell, Dr. David W. Thompson, Dr. Ray Poirier, Dr. Paris Georghiou, Dr. Erika F. Merschrod, and Dr. Yuming Zhao, for their kind help during the course of this program. Many thanks to Dr. Graham Bodwell and Ms. Marie Manning for their care and timely help delivered to my family.

Thanks to Ms. Linda Winsor, Ms. Rose, Ms. Kai Zhang (C-CART), Ms. Linda Thompson (Phys. Chem. Lab), Ms. Lisa Lee (SEM, Biology) for their assistance. My hearty thanks to Ms. Linda Corbett, Ms. Mary Flinn, Ms. Teresa Toope, Ms. Bonita Smith, Ms. Viola Martin, and Ms. Joan Squires for their help and lovingness.

Thanks to my present and past group members, Brandi Langsdorf (PDF; from the US), Brad Easton (PhD; from Canada), Fang Huang (MSc; from China), Mohammad Khanfer (MSc; from Jordan), Jun Zhu (MSc; from China), Wanda Aylward (PhD; from Canada), Gaungchun Li (PhD; from China), Hongchao Li (PDF; from China), Chaojie Song (PDF; from China), Omar Yopez (PDF; from Venezuela), Rita Satler (PDF; from Germany), Amit Kundale and Vikrant Adsool (GB & SP group) for their help and friendship.

Thanks to my family members for their sacrifice and patience. Special thanks to my father Mr. T. Krishnan for his encouragement and invaluable help delivered to my family and me. This thesis is dedicated to him.

## **Table of Contents**

Title

Abstract

Acknowledgements

Table of Contents

List of Figures

List of Schemes

List of Tables

Glossary of Abbreviations

Glossary of Symbols

### **Chapter 1- Introduction**

1.1	Conjugated Polymers- A Brief Introduction	1
1.2	Conjugated Polymers as Organic Semiconductors	2
1.3	Strategies for Band Gap Engineering	5
1.4	Electrochemistry of Conducting Polymers	9
1.4.1	Electrochemical Synthesis of Conducting Polymers	10
1.4.2	Cyclic Voltammetry of Conducting Polymers	12

1.4.4	UV-VIS-NIR Spectroelectrochemical Measurements	17
1.5	Evaluation of Band Gaps	17
1.5.1	Cyclic Voltammetry	18
1.5.2	Electronic Spectroscopy	20
1.5.3	Conductivity	23
1.6	Techniques for Electronic Conductivity Measurement	23
1.6.1	Dual Electrode Sandwich Voltammetry	24
1.7	Goals of this Work	24

## **Chapter 2- Experimental Section**

2.1	Chemicals and Reagents	33
2.2	Electrochemical Synthesis and Studies	33
2.3	Rotating Disc Voltammetry	34
2.4	Dual Electrode Sandwich Voltammetry	35
2.5	Electrochemical Impedance Spectroscopy	36
2.6	UV-VIS-NIR Spectroscopy	37
2.7	FT-IR Spectroscopy	37
2.8	Scanning Electron Microscope	37
2.9	Elemental Analysis	38
2.10	NMR Spectroscopy	38



## **Chapter 3- $\Delta^{4,4'}$ -Dicyclopenta[2,1-*b*:3,4-*b'*]dithiophene. A Conjugated Bridging Unit for Low Band Gap Conducting Polymers**

3.1	Introduction	40
3.2	Experimental Section	42
3.2.1	Chemicals and Electrodes	42
3.2.2	Synthesis of 3-3	42
3.2.3	Polymerization of 3-3	43
3.2.4	Polymer Film Thickness	43
3.2.5	Conductivity Measurements	43
3.3	Results and Discussion	44
3.3.1	Monomer Synthesis	44
3.3.2	Electrochemistry of the Monomer and Electrochemical Polymerization	45
3.3.3	Electronic Absorption Spectroscopy	49
3.3.4	IR Spectroscopy	53
3.3.5	Electrochemistry of Poly (3-3) Films	55
3.3.6	In Situ Conductivity Measurements	57
3.4	Conclusions	61

## **Chapter 4 - Poly ( $\Delta^{4,4'}$ -Dicyclopenta[2,1-*b*:3,4-*b'*]dithiophene-co-3, 4-ethylenedioxythiophene): Electrochemically Generated Low Band Gap Conducting copolymers**

4.1	Introduction	66
4.2	Experimental	67
4.2.1	Chemicals and Electrodes	67
4.2.2	IR Spectroscopy	68
4.2.3	Spectroelectrochemistry	68
4.2.4	Conductivity Measurements	68
4.3	Results and Discussion	69
4.3.1	Synthesis of Poly-(4-2-co-EDOT) Copolymers	69
4.3.2	IR Spectra	71
4.3.3	Electrochemistry of Copolymers	73
4.3.4	Spectroelectrochemical Studies of Copolymers	79
4.3.5	In Situ Conductivity Measurements	83
4.4	Conclusions	86

## **Chapter 5 - The Influence of Electrode Rotation on Morphologies and Conductivities of Poly-( $\Delta^{4,4'}$ -Dicyclopenta[2,1-*b*:3,4-*b'*]dithiophene) and Copolymers with 3,4-Ethylenedioxythiophene**

5.0	Introduction	89
5.1	Effect of Electrode Rotation on Polymer Growth	91
5.1.1	Electrochemical Polymerization of Dicyclopenta[2,1- <i>b</i> :3,4- <i>b'</i> ]dithiophene	91
5.1.2	Morphology of Polymer Films	91

5.2	Characterization of the Films	94
5.2.1	Cyclic Voltammetry	94
5.2.2	Electrochemical Impedance Spectroscopy	96
5.3	Discussion	103
5.4	Characterization of Copolymers of (5-1) and EDOT (CP1, CP2 and CP3)	109
5.4.1	Cyclic Voltammetry	109
5.4.2	Electrochemical Impedance Spectroscopy	112
5.5	Discussion	118
5.6	Conclusions	121

## **Chapter 6 - Studies on Fluorenone Based Copolymers**

6.1	Experimental	127
6.1.1	PFKB, PFKT, and PFKF Coated Electrodes	127
6.1.2	Conversion of Ketals to Fluorenone Copolymers	127
6.2	Characterization of PFB, PFT and PFF Films	128
6.2.1	IR Spectroscopy	128
6.2.2	UV-Vis Spectroscopy	130
6.2.3	Cyclic Voltammetry	134
6.3	Discussion	137
6.4	Conclusions	139

## **Chapter 7 - Synthesis of Fluorene Based Donor-Acceptor Conjugated Molecules**

7.1	Introduction	141
7.2	Syntheses	144
7.2.1	Synthesis of 2,7-Di-2-thienyl-9H-fluoren-9-one, 7-3	144
7.2.2	Synthesis of 2-(2-Thienyl)-9H-fluoren-9-one, 7-4	146
7.2.3	Synthesis of (2,7-Di-2-thienyl-9H-fluoren-9-ylidene) malononitrile, 7-5	147
7.2.4	Attempted Synthesis of 2,7-Di-2-thienyl-9H-fluorene-9-thione, 7-6 and/or 2,7,2',7'-Tetra-2-thienyl-[9,9']bifluorenylidene, 7-7	150
7.3	Conclusions	155
7.4	Experimental	155

## **Chapter 8 - The Influence of Donor Acceptor Units on the Band Gaps of Fluorene Based Copolymers**

8.1	Introduction	163
8.2	Redox Potentials and Band Gaps of ThFl, Th <sub>2</sub> Fl and CNTh <sub>2</sub> Fl	166
8.2.1	Redox Potentials of ThFl, Th <sub>2</sub> Fl and CNTh <sub>2</sub> Fl	167
8.2.2	UV-Visible Spectroscopic Results of ThFl, Th <sub>2</sub> Fl and CNTh <sub>2</sub> Fl	170
8.3	Electropolymerizations of ThFl, Th <sub>2</sub> Fl and CNTh <sub>2</sub> Fl	170
8.4	Electrochemical Studies of Poly-ThFl, Poly-Th <sub>2</sub> Fl and Poly-CNTh <sub>2</sub> Fl	173

8.5	<i>In Situ</i> Conductivity Measurements	175
8.5.1	Dual Electrode Sandwich Method	175
8.6	Band Gap of Poly-(S <sub>2</sub> Th <sub>4</sub> Fl <sub>2</sub> ) (8-4)	179
8.6.1	Electrochemical and Optical Band Gap	179
8.6.2	Theoretical Estimation of Band Gap	180
8.7	Discussion	182
8.8	Conclusion	188
 <b>Chapter 9 – Summary and Future Work</b>		 190
Appendix		194

### **List of Figures**

1.1	Development of the band structure of polythiophene from energy levels of monomer through tetramer of thiophene	3
1.2	Low band gap polymers	6
1.3	Examples of bithienyl precursors for low band gap polymers	7
1.4	3, 4-(ethylenedioxythiophene) and donor acceptor comonomers	9
1.5	Cyclic voltammogram at 100 mV/s in CH <sub>3</sub> CN/0.1 M Bu <sub>4</sub> NPF <sub>6</sub> of poly(ThFl) (Structure 8-5, Chapter 8) on a platinum electrode	14
1.6	Circuit for a finite transmission line in series with an uncompensated solution resistance	16

1.7	Representation of an ideal complex plane impedance plot	16
1.8	Relationship between electrochemically measured band gaps ( $E_g$ ) (Experimental results, Chapter 8) and density of states	19
1.9a	Potential energy diagram for a diatomic molecule illustrating Franck-Condon excitation	21
1.9b	Intensity distribution among vibronic bands as determined by the Franck-Condon principle	21
2.1	Rotating disk electrode with hydrodynamic flow pattern	34
2.2	Schematic dual-electrode used in the measurement of conductivity against potential	35
3.1	Cyclic voltammograms ( $100 \text{ mV s}^{-1}$ ) of 3-3 ( $<1 \text{ mM}$ ) in acetonitrile containing $0.01 \text{ M Bu}_4\text{NPF}_6$	46
3.2	Cyclic voltammograms ( $100 \text{ mV s}^{-1}$ ) recorded during the formation of a poly(3-3) film on a Pt electrode under potential cycling conditions from $5 \text{ mM}$ 3-3 in nitrobenzene containing $0.01 \text{ M Bu}_4\text{NPF}_6$ . Currents increased during cycling	48
3.3	Electronic absorption spectra of 3-3 in acetonitrile and a poly(3-3) film on an indium/tin oxide electrode	51
3.4	Expected structure of poly(3-3)	52
3.5	IR Spectra (KBr disks) of 3-3 and poly(3-3)	54
3.6	Cyclic voltammograms ( $10\text{-}100 \text{ mV s}^{-1}$ ) of a poly(3-3) coated Pt electrode in acetonitrile containing $0.01 \text{ M Bu}_4\text{NPF}_6$	56

- 3.7 Cyclic voltammograms ( $100 \text{ mV s}^{-1}$ ) and in situ conductivity as a function of potential (in acetonitrile containing  $0.01 \text{ mol dm}^{-3} \text{ Bu}_4\text{NPF}_6$ ) for a poly(3-3) film sandwiched between Pt disk electrode and a porous gold film. Conductivity data were obtained with a fixed  $10 \text{ mV}$  potential difference between the Pt and Au contacts to the film. 58
- 3.8 Log plot of in situ conductivity as a function of potential (in acetonitrile containing  $0.01 \text{ mol dm}^{-3} \text{ Bu}_4\text{NPF}_6$ ) for a poly-(3-3) film sandwiched between a Pt disk electrode and a porous gold film. The gold film was maintained at  $0 \text{ V}$  vs SSCE in this experiment. 60
- 4.1 Multisweep cyclic voltammograms ( $100 \text{ mV/s}$ ) at a Pt electrode ( $0.0052 \text{ cm}^2$ ) of mixtures of 4-2 ( $2 \text{ mM}$ ) and EDOT(A  $1 \text{ mM}$ ; B  $2 \text{ mM}$ ; C  $5 \text{ mM}$ ) in nitrobenzene containing  $0.1 \text{ M Bu}_4\text{NPF}_6$ . The current has been multiplied by a factor of five in A to facilitate comparison. Peak anodic currents on the last cycle shown were  $3.0 \text{ (A)}$ ,  $20 \text{ (B)}$ , and  $27 \mu\text{A (C)}$ . 70
- 4.2 IR spectra (KBr discs) of a) poly(4-2), b) CP1, c) CP2, d), CP3, and e) poly-EDOT 72
- 4.3 Comparison of an IR spectrum of CP3 (solid line) with a composite spectrum obtained by adding the spectra (absorbances) of poly(4-2) and PEDOT in a ratio of  $0.75:1$  (i.e.  $A_{\text{comp}} = 0.9 A_{\text{poly(4-2)}} + 1.2 A_{\text{PEDOT}}$ ). 74

4.4	Cyclic voltammograms at 100 mV/s for films of CP1 and poly(4-2) on Pt in acetonitrile containing 0.1 M Bu <sub>4</sub> NPF <sub>6</sub>	76
4.5	Comparison of cyclic voltammograms of (a) CP1, (b) CP2 and (c) CP3 in acetonitrile containing 0.1 M Bu <sub>4</sub> NPF <sub>6</sub> Scan rate: 100 mV/s	77
4.6	Electronic absorption spectra of CP1, CP2, and CP3 films on ITO electrodes at controlled potential (-0.3 V, -0.3 V, and -0.5 V, respectively) in acetonitrile containing 0.1 M Bu <sub>4</sub> NPF <sub>6</sub>	80
4.7	Electronic absorption spectra of a CP1 film on an ITO electrode at potentials of -0.3 V, 0 V, +0.3 V and +0.6 V in acetonitrile containing 0.1 M Bu <sub>4</sub> NPF <sub>6</sub>	82
4.7	Normalized conductivities of copolymer films as a function of potential in acetonitrile containing 0.1 M Bu <sub>4</sub> NPF <sub>6</sub> . Both p-type (potentials > -0.3 V), and n-type (potentials < -0.5 V) conductivities were observed for CP1 (open and solid triangles, respectively), while only p-type conductivity was observed for CP2 (open squares) and CP3 (open circles).	84
5.1	Repetitive sweep polymerizations of 2 mM 5-1 at rotation rates of (a) 0 rpm, (b) 400 rpm, (c) 800 rpm, and (d) 1200 rpm	92
5.2	Scanning electron micrographs of poly-(5-1) films deposited on stationary (a) or rotating [(b) 400 rpm (c) 800 rpm (d) 1200 rpm] Pt electrodes	93



5.3	Cyclic voltammograms in acetonitrile containing 0.1 M Bu <sub>4</sub> NPF <sub>6</sub> of the poly-(5-1) films prepared in the polymerizations depicted in Fig. 5.1. Insets show variations of cathodic and anodic peak currents with electrode rotation rates.	95
5.4	Impedance plots for Pt electrodes coated with poly(5-1) in 0.1 M Bu <sub>4</sub> NPF <sub>6</sub> -CH <sub>3</sub> CN. Film thicknesses: (a) poly-(0), 0.3 μm; (b) poly-(400), 0.8 μm; (c) poly-(800), 1.3 μm; (d) poly-(1200), 1.4 μm.	97
5.5	Impedances of p-doped poly-(1200) in 0.1 M Bu <sub>4</sub> NPF <sub>6</sub> acetonitrile solution	98
5.6	Capacitance vs real impedance plots for p-doped (+0.8 V) poly-(5-1) films.	100
5.7	Capacitance vs real impedance plots for n-doped (-0.8 V) poly(5-1) films	101
5.8	In situ conductivity (calculated from AC impedance data) as a function of potential for poly-(1200). Inset shows capacitance vs frequency profiles	102
5.9	Cyclic voltammograms (100 mV/s) of A CP1; B CP2; C CP3 coated Pt electrodes in Bu <sub>4</sub> NPF <sub>6</sub> -CH <sub>3</sub> CN. (a to d; doping processes of CP films polymerized under stationary to hydrodynamic conditions 400- 1200 rpm)	111
5.10	Impedance plots for Pt electrodes coated with p-doped CP1	113

in 0.1M Bu<sub>4</sub>NPF<sub>6</sub>-CH<sub>3</sub>CN at various electrode rotation rates.

Film thicknesses: CP1-(0), 0.35 μm; CP1-(400), 0.99 μm;

CP1-(800), 1.1 μm; CP1-(1200), 1.2 μm

- |      |   |     |
|------|---|-----|
| 5.11 | Impedance plots for Pt electrodes coated with p-doped copolymer films in 0.1M Bu <sub>4</sub> NPF <sub>6</sub> -CH <sub>3</sub> CN at various electrode rotation rates. Film thicknesses: CP2-(0), 0.37 μm; CP2-(400), 1.1 μm; CP2-(800), 1.4 μm; CP2-(1200), 1.4 μm; CP3-(0), 0.60 μm; CP3-(400), 0.97 μm; CP3-(800), 1.2 μm; CP3-(1200), 1.4 μm | 114 |
| 5.12 | Capacitance vs. real impedance plots for p-doped (CP1 and CP2 at +0.8 V; CP3 at +0.6 V) and n-doped (-0.9 V) CP films.  | 115 |
| 5.13 | Capacitance vs. potential plots for copolymer films shown in Fig 5.9  | 116 |
| 5.14 | Conductivity vs potential plots of copolymer films polymerized at 1200 rpm  | 116 |
| 6.1  | IR spectra of PFB, PFT and PFF films on Si discs compared with their respective ketyl copolymers.   | 129 |
| 6.2  | Electronic absorption spectra of a PFKB film on a quartz disc before and following exposure to trifluoroacetic acid vapour (PFB). The graphical method for estimating the absorption onset (*) is illustrated.  | 131 |
| 6.3  | Electronic absorption spectra of a PFKT film on a   | 132 |

	quartz disc before and following exposure to trifluoroacetic acid vapour (PFT)	
6.4	Electronic absorption spectra of a PFKF film on a quartz disc before and following exposure to trifluoroacetic acid vapour (PFF)	133
6.5	Cyclic voltammograms (100 mV/s) of films of (a) PFKB, (b) PFB, (c) PFT, and (d) PFF films on glassy carbon electrodes in acetonitrile containing 0.01 M Bu <sub>4</sub> NPF <sub>6</sub>	135
7.1	IR spectra (KBr) of (a) 7-3 and (b) 7-5	149
7.2	IR spectra (KBr discs) of (a) 7-3, (b) 7-8	153
7.3	NMR spectra (CDCl <sub>3</sub> ) of (a) 7-3 (b) 7-8 (c) decomposition of 7-8 to 7-7	154
8.1	Structures of fluorene based comonomers	164
8.2	Structures of fluorene based copolymers	165
8.3	Cyclic voltammograms (100 mV s <sup>-1</sup> ) of ThFl (2 mM) in dichloromethane containing 0.1 M Bu <sub>4</sub> NPF <sub>6</sub>	167
8.4	Cyclic voltammograms (100 mV s <sup>-1</sup> ) of Th <sub>2</sub> Fl (2 mM) in dichloromethane containing 0.1 M Bu <sub>4</sub> NPF <sub>6</sub>	168
8.5	Cyclic voltammograms (100 mV s <sup>-1</sup> ) of CNTh <sub>2</sub> Fl (2 mM) in dichloromethane containing 0.1 M Bu <sub>4</sub> NPF <sub>6</sub>	169
8.6	Comparison of UV-Vis spectra of (a) ThFl, (b) Th <sub>2</sub> Fl and (c) CNTh <sub>2</sub> Fl recorded in CHCl <sub>3</sub> solution	171

8.7	Multisweep cyclic voltammograms (100 mV/s) at a Pt electrode of 2 mM precursors (A- ThFl; B- Th <sub>2</sub> Fl; C- CNTh <sub>2</sub> Fl) in dichloromethane containing 0.1 M Bu <sub>4</sub> NPF <sub>6</sub>	172
8.8	Comparision of cyclic voltammogarms of (A) poly-ThFl, (B) poly-Th <sub>2</sub> Fl and (C) poly-CNTh <sub>2</sub> Fl in acetonitrile containing 0.1 M Bu <sub>4</sub> NFP <sub>6</sub> . Scan rate: 100 mV/s	174
8.9	In situ conductivity as a function of potential (in acetonitrile containing 0.01 MBu <sub>4</sub> NPF <sub>6</sub> ) for a 0.02 μm poly-ThFl film sandwiched between a Pt disk electrode and a porous gold film	176
8.10	In situ conductivity as a function of potential (in acetonitrile containing 0.01 M Bu <sub>4</sub> NPF <sub>6</sub> ) for a 0.1 mm poly-Th <sub>2</sub> Fl film sandwiched between a Pt disk electrode and a porous gold film	177
8.11	In situ conductivity as a function of potential (in acetonitrile containing 0.01 MBu <sub>4</sub> NPF <sub>6</sub> ) for a 0.1 mm poly-CNTh <sub>2</sub> Fl film sandwiched between a Pt disk electrode and a porous gold film	178
8.12.	Electrochemistry of S <sub>2</sub> Th <sub>4</sub> Fl in acetonitrile containing 0.01 M Bu <sub>4</sub> NPF <sub>6</sub> . Inset: UV-Visible absorption spectrum of S <sub>2</sub> Th <sub>4</sub> Fl in chloroform	181
8.13	Structure of S <sub>2</sub> Th <sub>4</sub> Fl <sub>2</sub> representing LUMO population	180

## List of Schemes

1.1	Structural changes in polythiophene upon doping with a suitable oxidant	4
1.2	Mechanism of the electrochemical polymerization	11
3.1	Monomer synthesis	45
5.1	Circuit for a finite transmission line in series with an uncompensated solution resistance	96
5.2	A schematic representation of the electrogeneration of a polymer at a rotating disc electrode	105
6.1.	Polyketal precursors and their respective polyfluorenone structures	126
6.2	Conversion of ketals to fluorenone copolymers	128
7.1	Possible structures of copolymers synthesized by electrochemical oxidation of two monomers	142
7.2	Synthesis of 2,7-di-2-thienyl-9H-fluoren-9-one	144
7.3	Synthesis of 2-(2-thienyl)-9H-fluoren-9-one	147
7.4	Synthesis of (2,7-di-2-thienyl-9H-fluoren-9-ylidene)malononitrile	148
7.5	Attempted Synthesis of 2,7-di-2-thienyl-9H-fluorene-9-thione and/or 2,7,2',7'-tetra-2-thienyl-[9,9']bifluorenylidene	151

## List of Tables

5.1	Polymerization peak currents and thicknesses of the polymer films prepared at various rotation rates shown in Fig 5.1	104
5.2	Electrochemical data for poly-(5-1) films shown in Fig. 5.3	104
5.3	Capacitances and conductivities from the impedance data for poly-(5-1) coated Pt electrodes shown in Fig. 5.3	107
5.4	Capacitances and conductivities from the impedance data for poly-(1200) coated Pt electrodes illustrated in Fig. 5.3d	107
5.5	Electrochemical data for copolymer films shown in Fig. 5.9 capacitances and resistances from the impedance data for copolymer film coated Pt electrodes shown in Fig.5.9	119
6.1	Electrochemical data for the copolymers	136
6.2	Optical properties of copolymers as films on quartz	136
8.1	Summary of electrochemical properties of fluorene based molecules	183
8.2	Summary of spectroscopic properties of fluorene based molecules	183
8.3	Summary of electrochemical properties of fluorene based polymers	184
8.4	Conductivities of fluorene based copolymers	184

## Glossary of Abbreviations

Abs	absorbance
CNTh <sub>2</sub> Fl	(2,7-di-2-thienyl-9H-fluoren-9-ylidene)malononitrile
Ca.	circa
CP	conducting polymer
CP1	copolymer1
CP2	copolymer2
CP3	copolymer3
CV	cyclic voltammetry
DA	donor-acceptor
DiCNDT	4-dicyanomethylene-cyclopenta[2,1- <i>b</i> :3,4, <i>b'</i> ]bithiophene
DiCNFl	dicyanomethylene fluorene
EC	electrochromism
EDOT	3,4-ethylenedioxythiophene
EDT	3,4-ethylenedioxythiophene
FTIR	fourier transform infrared spectrophotometry
HOMO	highest occupied molecular orbital
IR	infrared
ITO	indium-tin oxide
LR	Lawesson's reagent
LUMO	lowest unoccupied molecular orbital

MS	mass spectrometry
NMR	nuclear magnetic resonance
OLEDs	organic light emitting diodes
PEDOT	poly(3,4-ethylenedioxythiophene)
PFB	poly(2,7-9-fluorene-one-co-1,4-benzene)
PFF	poly(2,7-9-fluorene-one-co-1,4-furan)
PFKB	poly{2,7-spiro[4,4'-dioctyl-2',6'-dioxycyclohexane]-1',9-fluorene-co-1,4-benzene}
PFKF	poly{2,7-spiro[4,4'-dioctyl-2',6'-dioxycyclohexane]-1',9-fluorene-co-1,4-furan}
PFKT	poly{2,7-spiro[4,4'-dioctyl-2',6'-dioxycyclohexane]-1',9-fluorene-co-1,4-thiophene)}
PFT	poly(2,7-9-fluorene-one-co-1,4-thiophene)
RDE	rotating disk electrode
RDV	rotating disk voltammetry
S <sub>2</sub> ThFl <sub>2</sub>	2,7,2',7'-tetra-2-thienyl-[9,9']bifluorenyl-dithietane
SCE	standard calomel electrode
SSCE	saturated sodium chloride calomel electrode
Th <sub>2</sub> Fl	2,7-di-2-thienyl-9H-fluoren-9-one
ThFl	2-(2-thienyl)-9H-fluoren-9-one
UV-Vis-NIR	ultraviolet-visible-near infrared



## Glossary of Symbols

A	electrode area
AC	alternating current
c	speed of light
C	capacitance
$C_F$	faradaic capacitance
$\delta$	chemical shift
d	film thickness
d	distance
$\Delta E$	potential difference
E	potential
E	energy
$E^{0'}$	formal potential
$E_{1/2}$	half wave potential
$E_g$	band gap
$E_{\text{onset}}^{\text{ox}}$	oxidation onset potential
$E_{\text{onset}}^{\text{red}}$	reduction onset potential
$E_{p,a}$	anodic peak potential
$E_{p,c}$	cathodic peak potential
eV	electron volt
F	Faraday's constant

$h$	Planck's constant
Hz	hertz
I	current
K	kelvin
$k$	Boltzmann constant
$\lambda$	wavelength
$\lambda_{\max}$	wavelength of maximum absorption
$\mu$	micron
$m/z$	mass-to-charge ratio
$\nu$	scan rate
$n$	conjugation length
Q	charge
$\rho$	resistivity
$R_E$	electronic resistance
$R_I$	ionic resistance
rpm	rotation per minute
$R_S$	solution resistance
$s$	slope
$\sigma$	conductivity
S	Siemens
V	volt
$\omega$	rotation rate

$\Omega$	Ohm
$Z'$	real impedance
$Z''$	imaginary impedance
$Z$	impedance

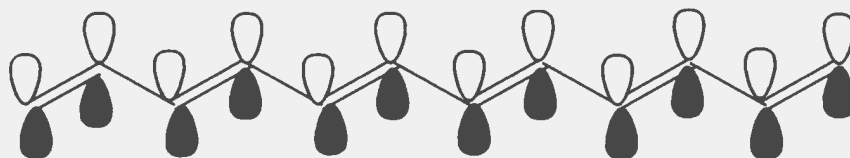
## Chapter 1

### Introduction

Like inorganic semiconductors, organic materials with extended  $\pi$ -electron conjugation possess interesting electrical, optical, and magnetic properties. Such features of organic materials have been translated into a variety of useful devices [1-20].

However, organic  $\pi$ -electron materials, unlike elemental semiconductors, are not atomic solids but rather are typically amorphous polymeric materials. Properties such as charge transport in organic materials are quite different from those encountered in inorganic semiconductors. There are numerous polymer structures and processing protocols reported to date [21-30] and the possibilities for molecular engineering of conducting polymers are very large indeed.

The intrinsic conductivity of conducting polymers (CP; also termed conjugated polymers or organic polymeric conductors), which generally consist of C, H and heteroatoms such as N and S, arise uniquely from  $\pi$ -conjugation, an extended and delocalized framework originating from overlap of  $\pi$ -orbitals. Such conjugation is illustrated below for poly(acetylene).



Schematic representation of  $\pi$ -conjugation in poly(acetylene)

## 1.2 Conjugated Polymers as Organic Semiconductors

The band structure of a conducting polymer originates from interaction of the  $\pi$ -orbitals of the repeating units throughout the chain as illustrated in **Fig. 1.1**. The calculated energy levels of oligothiophenes with  $n = 1-4$  and of polythiophene are shown as a function of oligomer length [31]. Addition of every new thiophene ring causes mixing of the energy levels yielding more and more levels until a point is reached at which there are bands rather than discrete levels. Interactions between the  $\pi$ -electrons of neighboring molecules lead to a three-dimensional band structure. The highest occupied band (which originates from the HOMO of a single thiophene unit) is called the valence band, whereas the lowest unoccupied band (originating from the LUMO of a single thiophene unit) is called the conduction band. The difference in energy ( $E_g$ ) between these levels is called the band gap.

Highly conducting polymers are obtained through simple chemical or electrochemical oxidation (p-doping), and in some cases reduction (n-doping). The resulting materials are salts doped with anionic or cationic species and belong to the class of extrinsically conducting polymers.

Removal of one electron from the CP chain produces a polaron, as shown in **Scheme 1.1b**. Further oxidation can either convert the polaron into a bipolaron (Scheme 1.1c) or introduce another polaron as shown in Scheme 1.1d. When a great many bipolarons are formed (highly p-doped), their energy states overlap at the edges, which creates narrow bipolaron bands in the gap.

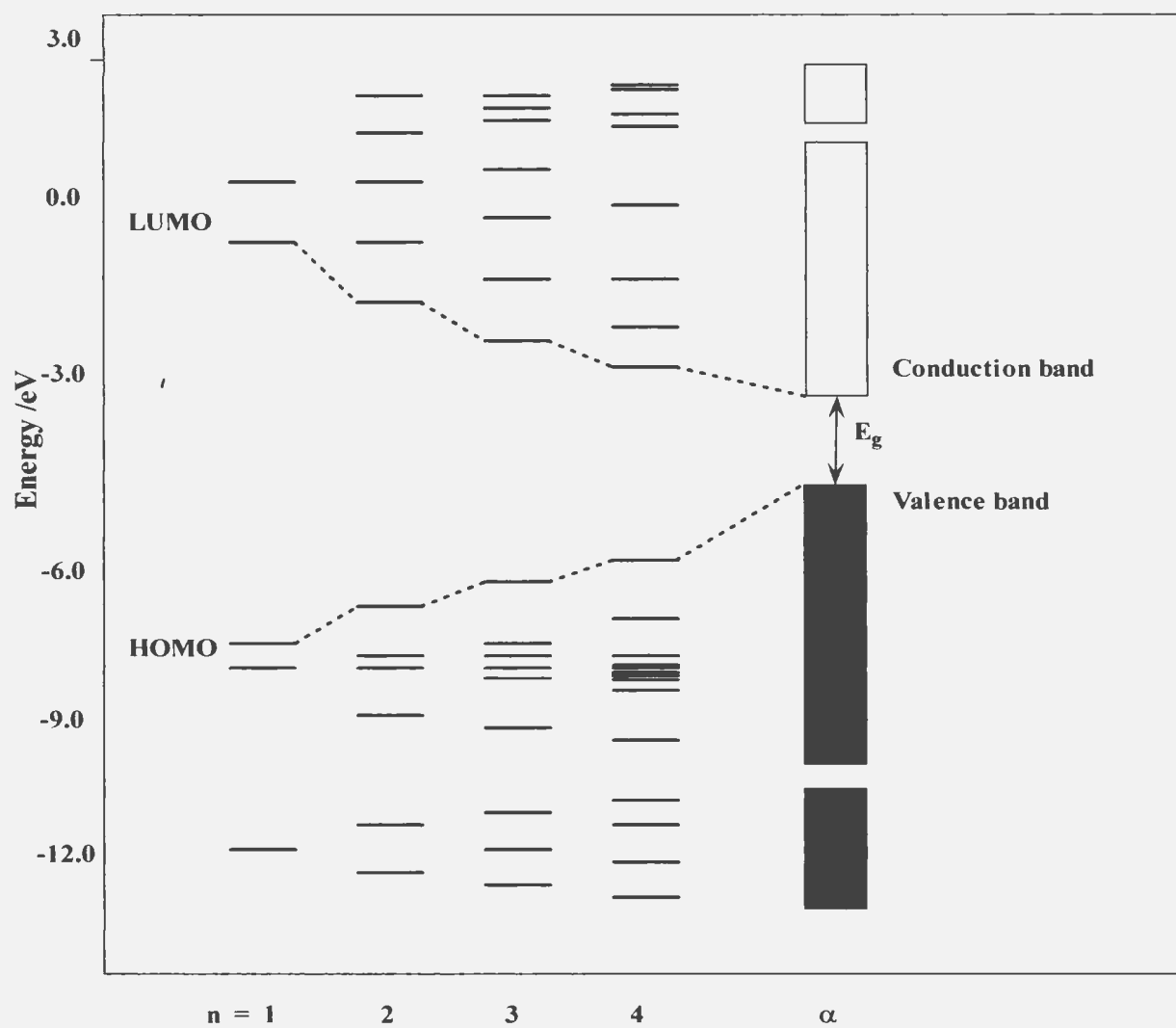
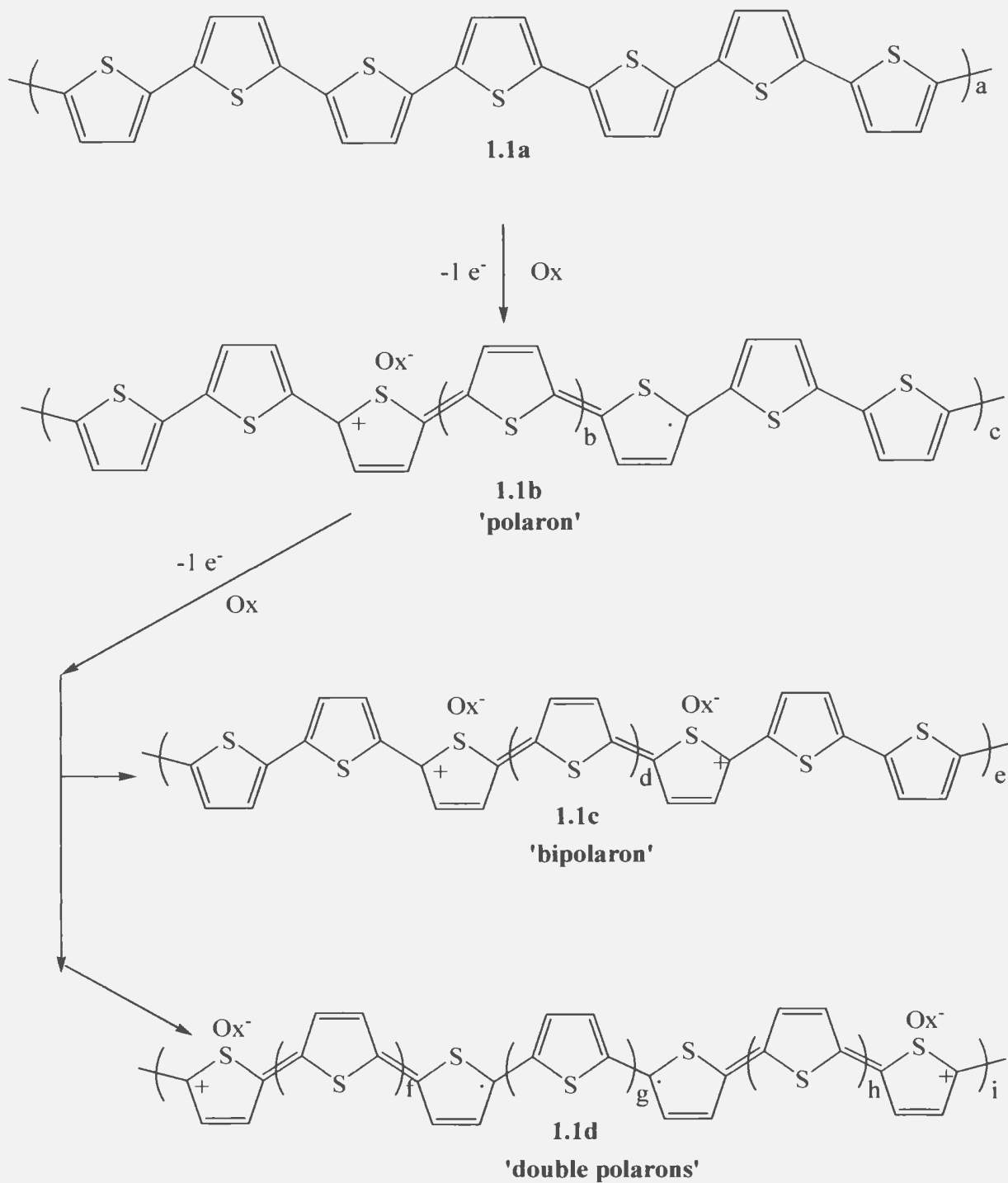


**Fig. 1.1** Development of the band structure of polythiophene from energy levels of the monomer through tetramer of oligo thiophenes to polymeric thiophene [adapted from 31]



**Scheme 1.1.** Structural changes in polythiophene upon doping with a suitable oxidant.

Similar states are formed when the polymer is reduced (n-doped), but the energy levels are below the conduction band. Both polarons and bipolarons are mobile and can move along the polymer chain in an electric field, and thus conduct electric current.

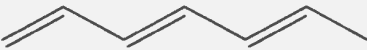
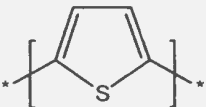
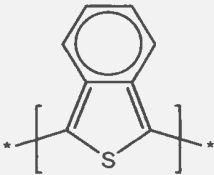
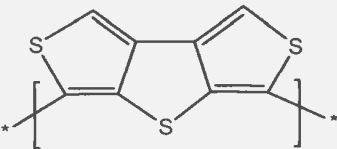
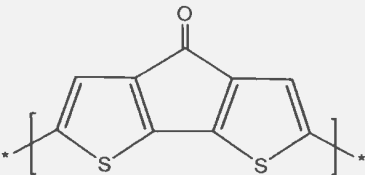
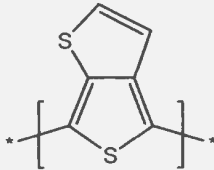
### 1.3 Strategies for Band Gap Engineering

The band gap of a polymer is a measure of its ability to show intrinsic conductivity [1]. The synthesis of low band gap polymers is a research issue in recent investigations for the reason that these materials would conduct without the need for doping [32-35]. A wide range of low band gap polymers has already been reported [32-35] and the structures of some of the low band gap polymers are shown in **Fig. 1.2**. Selected examples will be presented to illustrate the variety of strategies that have been employed.

For polythiophenes the most effective approach for decreasing  $E_g$  involves the tailoring of the monomer structure in order to increase the quinoid character of the  $\pi$ -conjugated system at the expense of its aromaticity [36-45]. Recently, a new low band gap polymer ( $E_g = 1.2$  eV), poly(5,6-dithiooctyl isothianaphthene) has been synthesized [46].

Another design strategy involves the introduction of electron-withdrawing groups at an  $sp^2$  carbon bridging the 4, 4- positions of a bithienyl precursor [32-35]. This strategy was applied by Ferraris and Lambert [47-50] to produce from cyclopenta[2,1-*b*:3,4-*b'*]bithiophen-4-one the electroactive polymer poly-4-dicyanomethylene-4H-cyclopenta[2,1-*b*:3,4-*b'*]dithiophene, poly(1-1) for which  $E_g$  was reported to be below 1.0 eV.



Name	Structure	Band gap (eV)
Trans-polyacetylene		1.5
Polythiophene		2.1
Polyisothianaphthene		1.0
Poly(dithieno(3,4- <i>b</i> :3',4'- <i>d</i> )-thiophene)		1.0
Poly cyclopenta[2,1- <i>b</i> :3,4- <i>b'</i> ]bithiophen-4-one		1.2
Poly(thieno[3,4- <i>b</i> ]-thiophene)		0.85

**Fig. 1.2** Selected examples of low band gap polymers

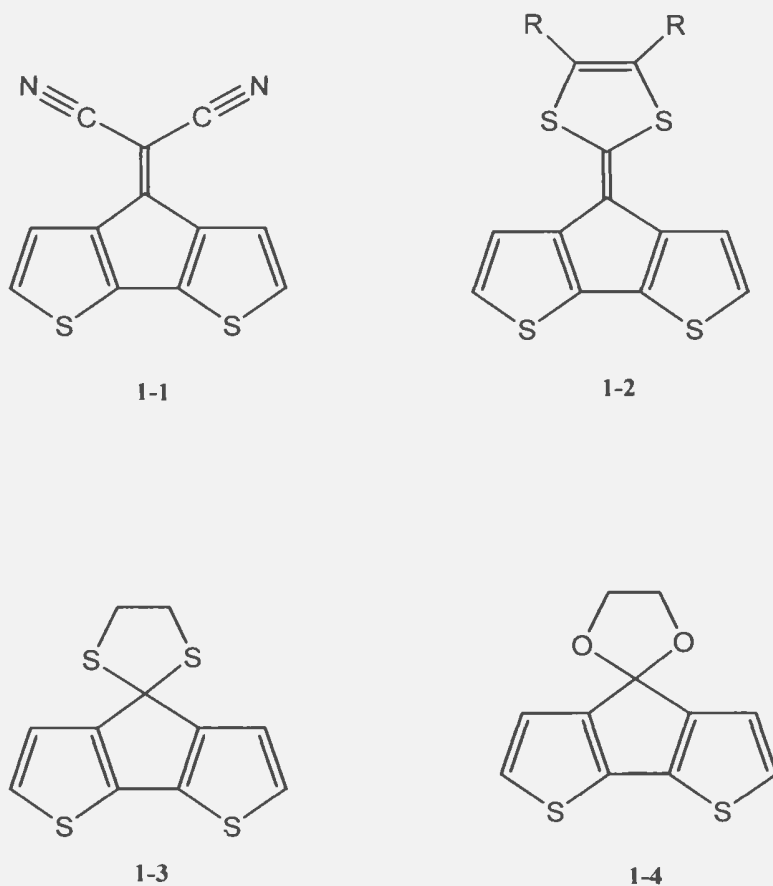


**Fig. 1.3** Examples of bithienyl precursors for low band gap polymers

Introduction of an electron donating group, such as a 1,3-dithiole moiety, at the  $sp^2$  bridging carbon provides the precursor **1-2** (**Fig. 1.3**) and the band gap of poly(**1-2**) was reported to be  $< 1.4$  eV [51]. Poly(**1-3**) with a band gap of 1.4 eV [52] and poly(**1-4**) [53] with a band gap of 0.9 eV have also been categorized as low band gap systems.

Other successful routes in designing low band gap conducting polymers are provided by donor acceptor polymers and copolymers [32-35]. Copolymers can have

tailor made properties depending upon the choice of two semiconducting components, their relative amounts and their arrangement in the polymer chain. The electrochemical copolymerization of electron deficient **1-1** with electron rich EDOT (**1-5**) has resulted in copolymers with very small band gaps [54]. By varying the polymerization potential, the copolymer composition was controlled and the intrinsic conductivities (both p- and n-type) were determined from *in situ* conductivity measurements as a function of potential. Conductivity measurements were carried out by a dual electrode sandwich voltammetric method. Intrinsic conductivities of the copolymers were significantly higher than for their homopolymers [54]. Estimated band gaps from intrinsic conductivities ranged from 0.33 to < 0.16 V. Also the band gaps for the EDOT rich copolymers were found to be ca. zero eV [54].

Recently, a variety of new thiophene based low band gap polymers were synthesized by electrochemical polymerizations of comonomers (**1-6**; **1-7**; **1-8**) [55]. Band gaps of poly-(**1-6**), poly-(**1-7**) and poly-(**1-8**) were found to be 1.3 eV, 0.8 eV and 1.2 eV, respectively.

Substitution or fusion and ladder polymerization have also been successful in the design of low band gap polymers [56-60].

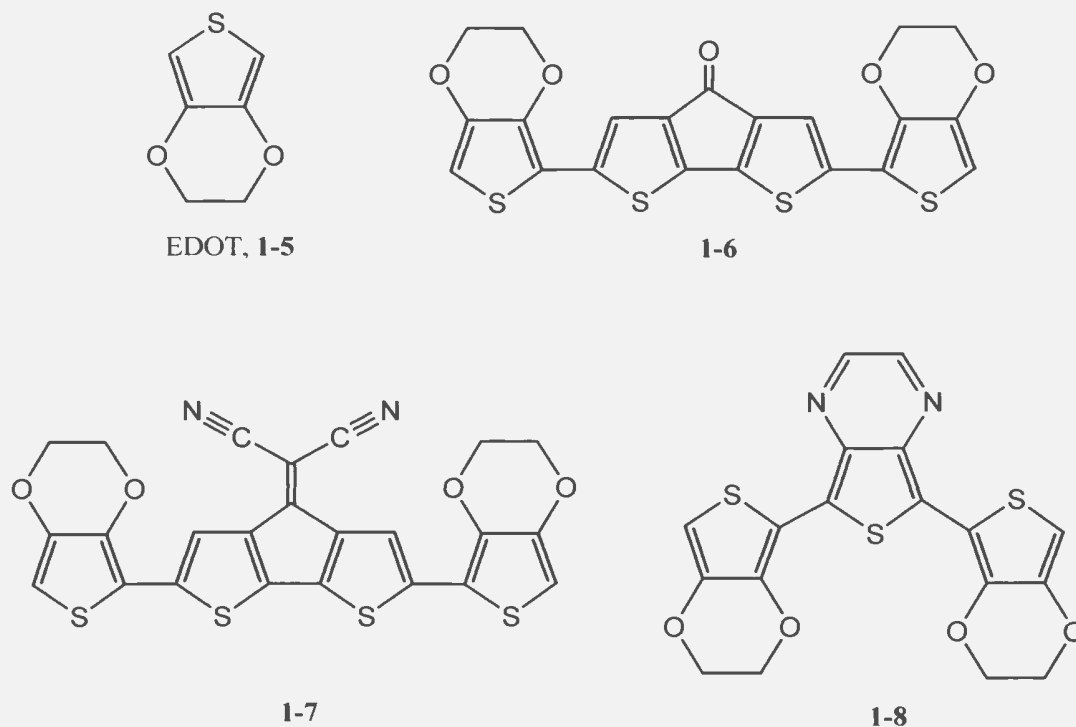


**Fig. 1.4.** 3,4-Ethylenedioxythiophene and donor acceptor comonomers

#### 1.4 Electrochemistry of Conducting Polymers

The electrochemistry of conducting polymers is carried out in both aqueous and non-aqueous electrolytes. The working electrode is typically a conducting polymer film on a conductive electrode substrate such as platinum, glassy carbon or a transparent indium-tin oxide (ITO)/glass electrode. These conducting polymer films are directly prepared on (electrochemically) or cast onto the electrode. Conducting polymer film thicknesses can vary from a few nm to mm. When a potential is applied to the conducting polymer, it can undergo oxidation or reduction. Counter ions flow from the electrolyte to

compensate the resulting charge. Thus the resulting doped polymer is a salt, containing charge balancing counter ions.

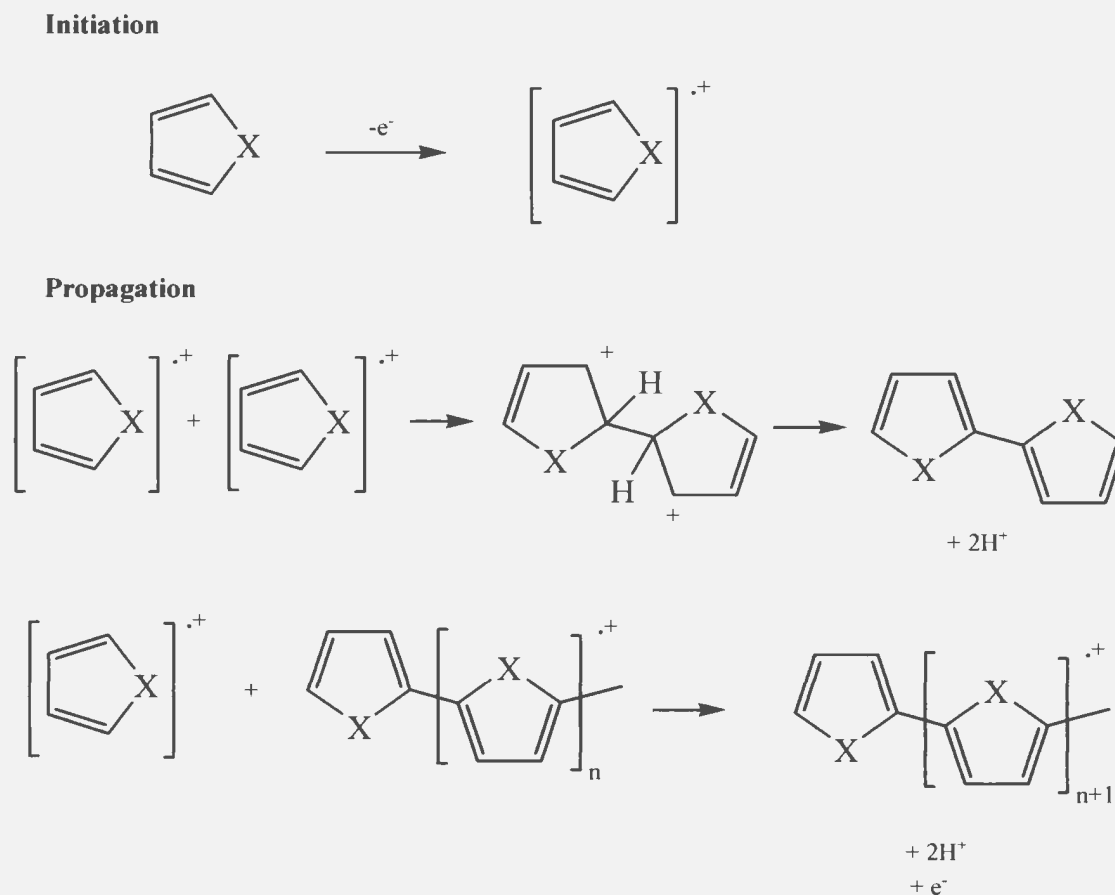
#### **1.4.1 Electrochemical Synthesis of Conducting Polymers**

Electrochemical polymerization presents several advantages such as speed, absence of catalyst, control of film thickness by the deposition charge, and direct production of the polymer in the oxidized conducting form [32, 61-63]. Electrochemical polymerizations can be performed by potentiostatic (constant potential), galvanostatic (constant current) or potential cycling methods [64-66]. A potentiostatic deposition mode generally yields polymer with the most consistent morphology. Galvanostatic deposition can be used when control of charge (e.g. for thickness) is desired but in some cases it has produced polymers of poorer morphology and conductivity. Repeated potential cycling, typically to a few hundred mV beyond the monomer oxidation potential, is one of the widely used methods. This mode of polymerization yields (stable) polymer films almost comparable to potentiostatic deposition. Another attractive feature of this method is that polymerizations can be monitored by using cyclic voltammetry. In this way, some useful mechanistic information can be obtained instantly, which can be applied to the interpretation of the electrochemical behavior of new conducting polymers [64-66].

Typical monomer concentrations for electrochemical polymerization range from 1 mM to 1 M. Electrolyte concentrations may range from 2 to 1000 times more than the monomer concentration. Further, the optimization of the electrosynthesis conditions (concentration of reagents, working electrode rotation) has been carried out [67-76]. Such

investigations have led to significant progress in the control of the structural definition and electrical properties of some conducting polymers [67-76].

The mechanism of oxidative polymerization [77] is illustrated in **Scheme 1.2**.



**Scheme 1.2.** Mechanism of the electrochemical polymerization

The reaction pathway involves:

1. The initial step, radical generation, via electrochemical oxidation.
2. Propagation via a) radical-radical recombination; b) loss of two protons from the dication intermediate species, generates the dimer; c) electrochemical oxidation of the

dimer, generates another oligomer radical; d) combination of this or other similar oligomer radicals with monomer radicals and repetition of steps 2b and 2c, builds up the polymer.

3. Termination via exhaustion of reactive radical species in the vicinity of the electrode or by predetermined processes (manual settings to stop the polymerization process).

Nearly all electrochemical polymerizations of conducting polymers (e.g. polythiophene, polypyrrole, polyaniline) appear to follow the pathway illustrated in Scheme 1.2 [78-80]. Once the initiating electrochemical potential is applied for an electrochemical polymerization, the population of radical cations is likely to far exceed that of neutral monomer in the vicinity of the electrode surface. That is, a generated radical cation is more likely to be surrounded by other radical cations than by neutral monomers or oligomers. The cause for this is the rapid electron transfer kinetics for electrooxidation of monomer, in comparison with the slower diffusion of monomer from the bulk of the reaction medium to the electrode [71-73]. Thus, due to a rapid depletion of monomer concentration at the electrode, a radical-radical recombination was evidenced to dominate the polymerization process over the grafting process (or radical monomer combination) [71, 73, 81-82].

#### **1.4.2 Cyclic Voltammetry of Conducting Polymers**

The basic electrochemical properties of a conducting polymer film can be obtained from cyclic voltammetry (CV) which involves measurement of the current (I) resulting from application of a cyclic potential (E) scan to the conducting polymer, with a fixed scan rate. In the example shown in **Fig. 1.5**, the initial potential (0.0 V) applied at

point a was chosen to avoid any electrolysis of the conducting polymer film before the scan was initiated. The potential was initially scanned in the positive direction. When the potential became sufficiently positive (+0.8 V) to cause oxidation of the conducting polymer (p-doping), an anodic current (indicated at b) began to flow. On scanning to high potentials, the anodic current increased rapidly and peaked at point c (1.2 V). In the reverse scan, a dedoping peak current was observed at point d (1.3 V) and the current approached zero after the dedoping process. Similarly, when the potential was scanned in the negative direction, a cathodic current (n-doping) began to flow at b' (-1.2 V) and peaked at point c' (-1.3 V). In the reverse scan the subsequent dedoping process took place with a peak potential at d' (-1.2 V).

Another element to note in the CV of a conducting polymer is that every conducting polymer has an electrochemical 'window' within which the doping/dedoping (redox) process is reproducible to a large extent, and beyond which oxidative or reductive decomposition of the conducting polymer occurs [77]. To avoid such decompositions, the potential scans were reversed at +1.5 V and -1.5 V during the p-doping and n-doping processes, respectively, in Fig. 1.5. The potentials at point's b and b' are termed p-doping and n-doping onset potentials, respectively, which indicate the injection of charges to the neutral polymer in its ground state. The potentials at c and d are called p-doping and undoping peak potentials. Whereas, potentials at c' and d' are n-doping and undoping peak potentials. Formal potentials ( $E^{\circ}$ ) can be defined as the midpoint between c and d, c' and d'.



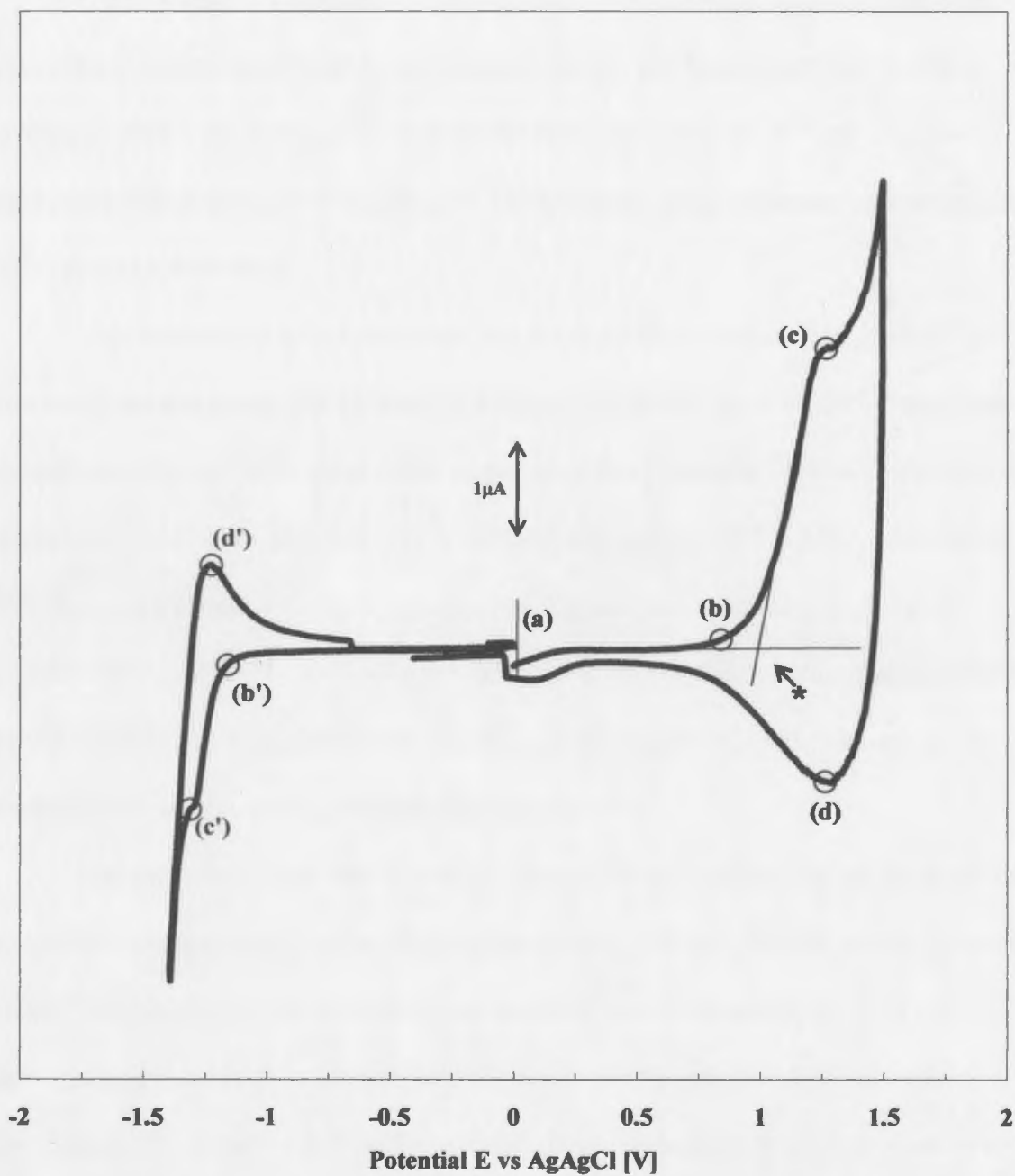


**Fig. 1.5** Cyclic voltammogram at 100 mV/s in  $\text{CH}_3\text{CN}/0.1\text{M Bu}_4\text{NPF}_6$  of poly(ThFI) (Structure 8-5, Chapter 8) on a platinum electrode; \* denotes the graphical estimate of onset potential

### 1.4.3 Impedance Spectroscopy

In this method, a constant amplitude voltage of a given frequency is applied across the conducting polymer in an electrochemical cell. The current that results is monitored via a lock-in amplifier which detects the in-phase and  $90^\circ$  out-of-phase impedance components, which correspond respectively to the resistance and capacitance of the polymer sample [83].

The impedances of polymers such as polypyrrole, polythiophene, polyaniline, polyacetylene and many copolymers have been studied. The aspects of investigations include modeling of the ac impedance response of these materials [83-88], the separation of ionic and electronic contributions to the total conductivity [83, 89-90], overdoping [91], the relative contribution of Faradaic and capacitive components to the total measured charge [92-93], the computation of the diffusion coefficients associated with the oxidation of these polymers and the transport of dopant ions [94, 95], and *in situ* conductance changes during polymer film growth [96].

The impedance response of a conducting polymer deposited on an electrode can be modeled using the equivalent circuit shown in **Fig. 1.6** [86, 83, 97], where  $R_E$  and  $R_I$  are the distributed polymer electronic and ionic resistances respectively  $R_s$  is the uncompensated solution resistance, and  $C_F$  represents the polymer film's Faradaic capacitance. A typical Nyquist plot (complex plane impedance) is characterized by a  $45^\circ$  Warburg-type line followed by a straight line response vertical to the real impedance axis, from which  $R_E$  and  $R_I$  (**Fig 1.7**) can be calculated by using the following two equations.

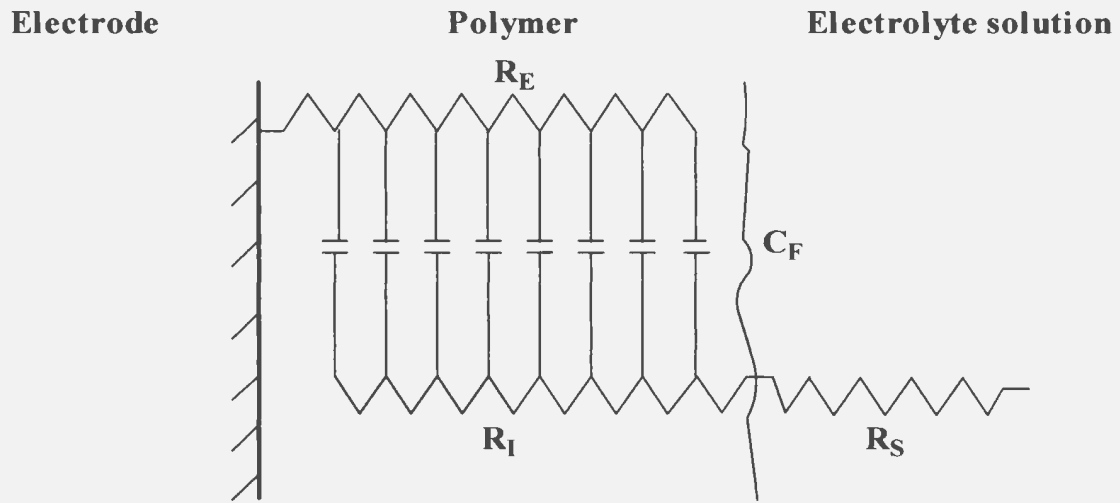


**Fig 1.6** Circuit for a finite transmission line in series with an uncompensated solution resistance

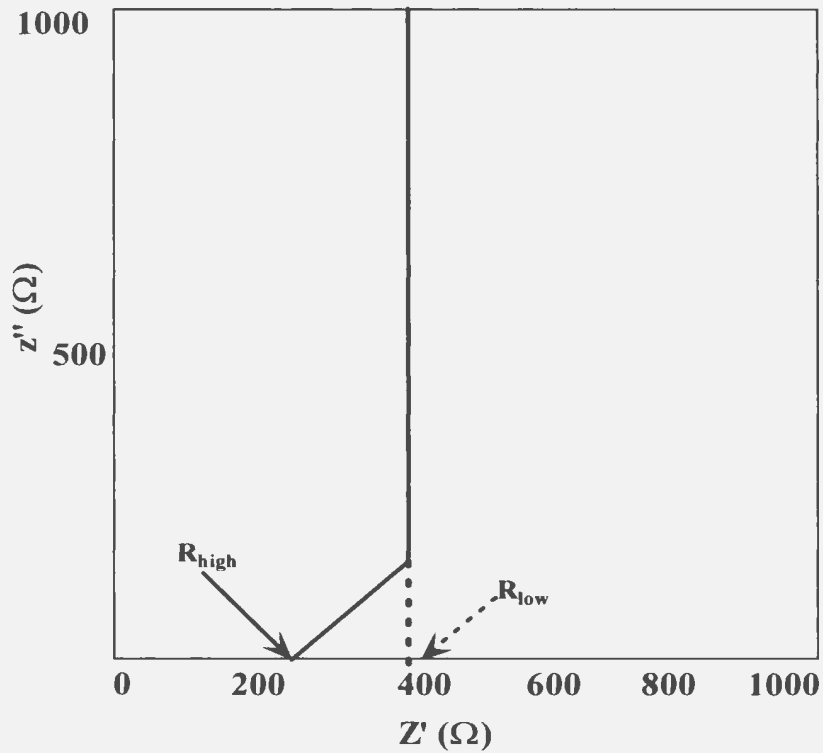


**Fig. 1.7** Representation of an ideal complex plane impedance plot

$$1/R_{\alpha} = 1/R_E + 1/R_I \quad (1.1)$$

$$R_{\Sigma} = R_E + R_I \quad (1.2)$$

Where  $R_{\alpha}$  is given by the subtraction of  $R_S$  from the intercept at high frequency in the Nyquist plot ( $R_{\alpha} = R_{\text{high}} - R_S$ ), and  $R_{\Sigma}$  is obtained by extrapolation of the linear portion at low frequency of the Nyquist plot to the real axis ( $R_{\Sigma} = 3(R_{\text{low}} - R_S)$ ).

#### 1.4.4 UV-VIS-NIR Spectroelectrochemical Measurements

Information on electrochromic properties of conducting polymers can be obtained from spectroelectrochemistry, an *in situ* or sometimes *ex situ* measurement of the transmission mode (widely used) UV-Vis-NIR spectrum of the conducting polymer at various applied potentials [1, 110]. Spectroelectrochemistry of pyrrole and thiophene derivatives [109-110] and many other conducting polymers [1] has been investigated. For most cases, at zero or low doping levels, absorption bands occur in the near UV region, and at high doping levels, a broad band (due to mid gap transitions) stretching from the far visible (ca. 0.6  $\mu$ ) to the near IR (up to 2.5  $\mu$ ) has been identified. High absorption in the near IR region is a sign of charge carrier mobility and also can be associated with high conductivity of a polymer [109-110].

#### 1.5 Evaluation of Band Gaps

The experimental determination of band gaps can be performed by electrochemistry (cyclic voltammetry (CV)), electronic absorption (UV-Vis-NIR) spectroscopy and conductivity measurements.

### 1.5.1 Cyclic Voltammetry

The basic theories of cyclic voltammetry of dissolved redox species cannot easily be transferred to a conducting polymer film formed on an electrode. The frequently used method of evaluating the formal potential of a redox reaction by taking the average of its anodic and cathodic peaks does not necessarily apply to conducting polymers. Normally, broad, distorted and asymmetric voltammograms are seen for conducting polymers [77, 98]. Dopant ion diffusion and the variable chain lengths of conjugated segments of polymers are some of the factors which influence the shape of the voltammogram. Since conjugated segments of polymers with different lengths (or different chain length oligomers) have different redox potentials, the cyclic voltammogram is normally comprised of a distribution of redox potentials. Therefore a single redox wave would not be expected.

The relationship between onset potentials and the density of states is illustrated in **Fig 1.8**. A density of states distribution (a more precise energy level distribution) of a polymer film [99] as a function of doping level is shown on the right hand side of Fig 1.8. Here, the energy levels are plotted as a function of their relative population. The band gap is clearly visible as a region of no orbital population. In approximately the center of this gap is the Fermi level, reflecting an equilibrium potential that represents the chemical

potential of the system, and which changes with oxidation state (doping) of the conducting polymer.

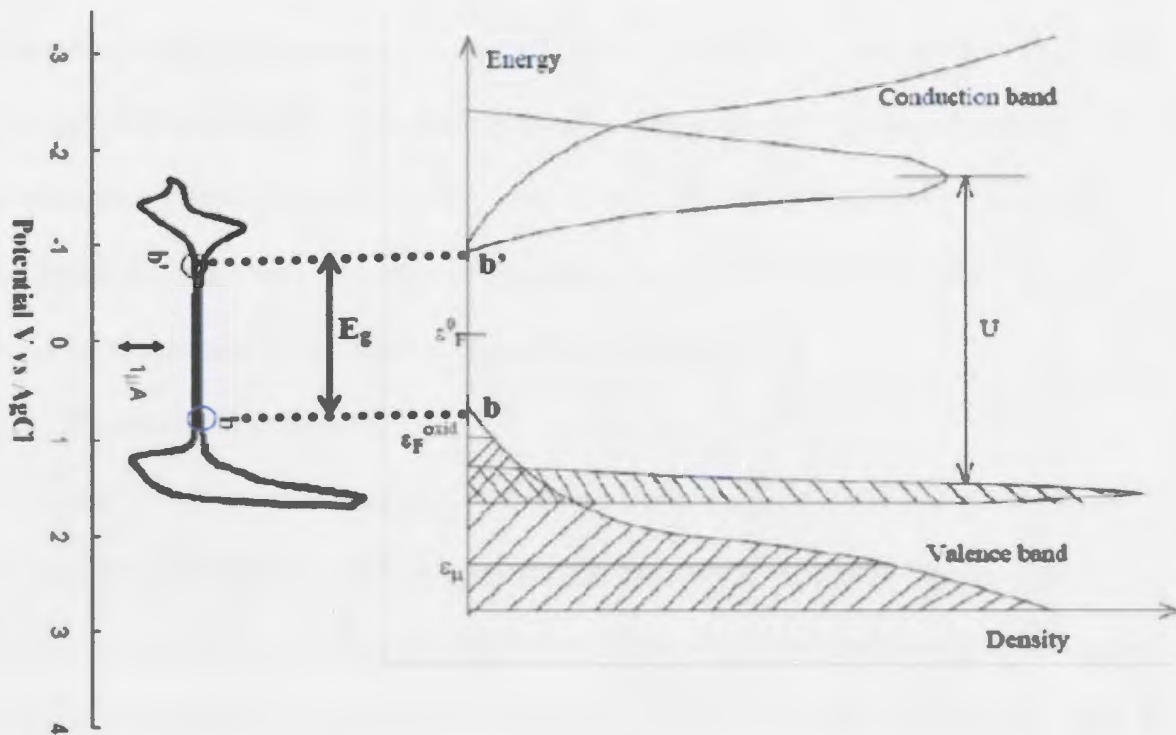


**Fig 1.8** Relationship between electrochemically measured band gap ( $E_g$ ) (experimental result, chapter 8) and density of states (adapted from Ref. [99])

On the left hand side of Fig 1.8, p- and n-doping of a CP film (poly(ThFl); experimental data from this project, see chapter 8) with circled onset potentials b and b' are shown. p-Doping onset (circled point b) and n-doping onset potentials (circled point b'), as defined earlier, indicate the injection of charges into the neutral polymer in the ground state, and should directly correspond to the highest energy states of redox sites as

indicated in Fig 1.8. Point b should correspond to the top of the valence band, whereas point b' to the bottom of the conduction band. So the band gap can be equated to the difference between the onset of oxidation ( $E_{\text{onset}}^{\text{ox}}$ ) and the onset of reduction ( $E_{\text{onset}}^{\text{red}}$ ).

Onset potentials have commonly been evaluated as the crossing point of lines through the background current and steepest part of the peak, as illustrated by the arrow for  $E_{\text{onset}}^{\text{ox}}$  in Fig 1.5 [100]. This method is not entirely accurate because it defines a point that is clearly beyond the onset point. However, it is difficult to objectively define an onset point any other way. A sound methodology for using CV to determine onset or band edge potentials has not been adequately established.

### 1.5.2 Electronic Spectroscopy

In a UV-Vis-NIR spectrum, the onset on the low energy side of the absorption spectrum gives a value for the band-gap. Absorption of UV-Vis-NIR light is typically recorded as broad absorption peaks and not as single, sharp lines representing absorption over an extremely narrow energy range. The absorption curves are broadened because the electronic levels have vibrational levels superimposed on them [101]. Most molecules exist mainly in their ground vibrational state at room temperature. However, excitation can occur to any of the excited state's vibrational levels, so that the absorption due to the electronic transition consists of a large number of lines. In practice, the lines overlap so that a continuous band is observed. Hence the shape of an absorption band is determined by the spacing of the vibrational levels and by the distribution of the total band intensity over the vibrational subbands. For simplicity the potential energy diagram

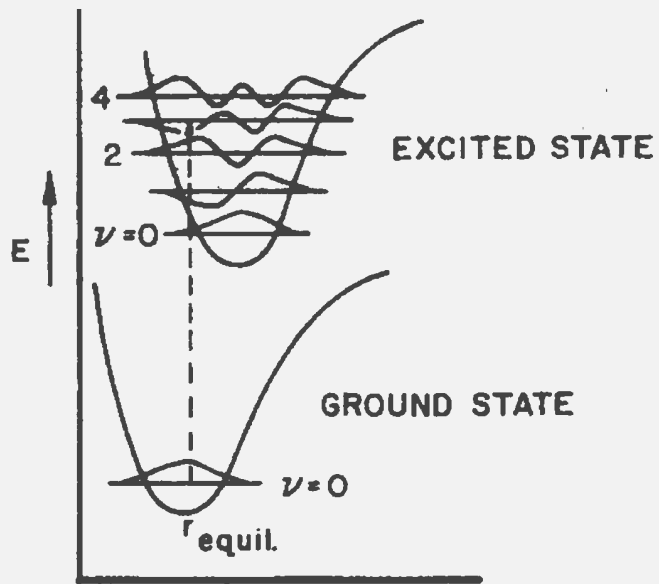


**Fig. 1.9a** Potential energy diagram for a diatomic molecule illustrating Franck-Condon excitation

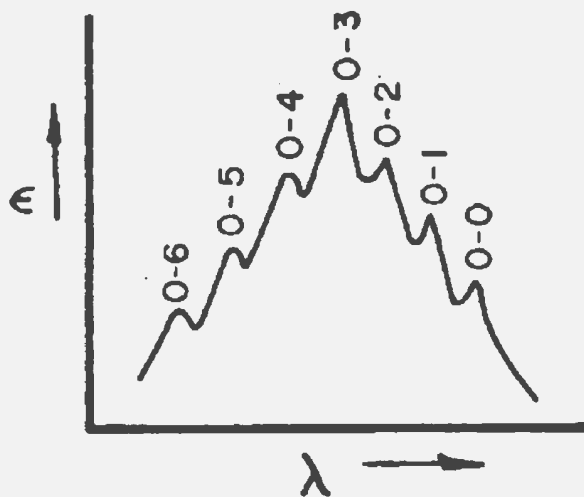


**Fig. 1.9b** Intensity distribution among vibronic bands as determined by the Franck-Condon principle.



for a diatomic molecule illustrating Franck-Condon excitation and intensity distribution among vibronic bands is shown in **Fig 1.9a** and **b** respectively [101].

Figure 1.9b shows the vibrational-electronic spectrum corresponding to Fig 1.9a, with the 0-3 band (from  $\nu=0$  in the ground state to  $\nu=3$  in the excited state) the most intense peak. The other transitions, including the 0-0 band, have significant probabilities. This is because even in the ground electronic state (zeroth vibrational level), the internuclear distance is described by a probability distribution (Fig. 1.9a). Therefore, transitions may originate over a range of  $r$  values so that more than one band originating from  $\nu=0$  may be observed.

The commencement of the absorption on the low energy end which corresponds to the 0-0 transition is the accurate method to calculate the optical band gap. To make the conversion of nanometers to electron volts, one can use the Plank's equation (equation 1.3)

$$E=h\nu=hc/\lambda \quad (1.3)$$

In this equation,  $E$  is the energy (in J),  $h$  is the Planck constant ( $6.626 \times 10^{-34}$  Js),  $c$  is the speed of light ( $3 \times 10^8$  m/s),  $\nu$  is the frequency in Hz and  $\lambda$  is the wavelength in nm. Knowing that 1 eV equals  $1.602 \times 10^{-19}$  J, calculations can be made for the conversion leading to the simple conversion equation (1.4)

$$E \text{ (eV)} = 1240.8 / \lambda \text{ (nm)} \quad (1.4)$$

### 1.5.3 Conductivity

A third method derives the band gap from the evolution of the conductivity. The conductivity is related to the band gap by an Arrhenius-like equation,  $C_{p, \text{intrinsic}} \sim 4.2 \times 10^{-5} \exp(-E_g/2kT)$ , where  $k$  is the Boltzmann constant ( $1.381 \times 10^{-23} \text{ JK}^{-1}$ ). The band gap calculated by this method for a conducting polymer agrees well with the optical band gap [54].

### 1.6 Techniques for Electronic Conductivity Measurement

The basic techniques for measurement of conductivity derive from Ohms law ( $E = IR$ ; where  $E$  is the potential difference,  $I$  the current, and  $R$  the resistance). Between two planes spaced at a distance  $d$  and with an area  $A$ , the resistivity is expressed as

$$\rho = \{E/I\} \times \{A/d\} \quad (1.5)$$

Thus knowing the electrode area, the separation distance, the current flowing and the potential difference between two planes, the resistivity can be computed. The conductivity (denoted  $\sigma$ ), in units of  $\Omega^{-1}\text{-cm}^{-1}$  or Siemens (S)  $\text{cm}^{-1}$  is then its reciprocal.

Ex-situ techniques such as two probe and four probe methods can be used to measure the conductivities of conducting polymers [102-104]. However, these techniques cannot easily be used to probe the variation of conductivity with doping level. In-situ techniques such as two parallel band electrode voltammetry [105], dual electrode

sandwich voltammetry [106,107], rotating disk voltammetry [106] and AC impedance spectroscopy [108] have been used to study the variation of conductivity with potential. Of these methods, dual electrode sandwich voltammetry and AC impedance spectroscopy (discussed in section 1.4.3) are advantageous because they can cover a large conductivity range ( $10^{-9}$  to  $1 \text{ S cm}^{-1}$ ).

### **1.6.1 Dual Electrode Sandwich Voltammetry**

The technique of dual electrode voltammetry uses a sandwich configuration [106,107] where vapor deposition of a thin porous metal (Au) film is used over a polymer-coated Pt disk electrode. The porous electrode is contacted by the solvent. The gold film also covers an adjacent Pt disk that affords potential control at the polymer/solution interface. With the electrode immersed in an electrolyte solution, a bipotentiostat (potentiostat with two working electrodes) is used to maintain a small constant potential difference (10 mV) across the polymer film and the applied potential at the two electrodes is simultaneously scanned, slowly (10 mV/s) to maintain steady state conditions. The voltammogram thus obtained can be converted to a conductivity vs. potential plot using equation 1.5.

### **1.7 Goals of this Work**

The core objective of the project was to design and synthesize new thiophene and fluorene based low band gap conducting materials and investigate their structure property relationships. The following strategies were applied:

- Electropolymerization of a bridged bithiophene and copolymerization of EDOT with a bridged bithiophene. Characterization of their properties by cyclic voltammetry, UV-Vis- NIR, FTIR, mass spectrophotometry, spectroelectrochemistry, and *in situ* conductivity measurements
- Electropolymerization of a bridged bithiophene under hydrodynamic conditions and characterization of polymers and copolymers by scanning electron microscopy, cyclic voltammetry and electrochemical impedance spectroscopy
- Synthesis of a variety of fluorene derivatives and homopolymerization of fluorene derivatives and characterization of copolymers by voltammetric, spectroscopic and *in situ* conductivity measurements

#### References:

1. Skotheim, T. A.; Elsenbaumer, R. L.; Reynolds, J. R. (Eds.), *Handbook of Conducting Polymers* Marcel Dekker, New York, **1998**.
2. Bradley, D. D. C. *IEEE Transactions on Electron Devices* **1991**, *38*, 2688.
3. Tessler, N.; Pinner, D. J.; Ho, P. K. H. *Opt. Mater.* **2001**, *17*, 155.
4. Kim, W.; Palilis, L. C.; Uchida, M.; Kafafi, Z. H. *Chem. Mater.* **2004**, *16*, 4681.

5. Tseng, R. J.; Huang, J.; Ouyang, J.; Kaner, R. B.; Yang, Y. *Nano Lett.* **2005**, *5*, 1077.
6. Boroumand, F. A.; Fry, P. W.; Lidzey, D. G. *Nano Lett.* **2005**, *5*, 67.
7. Peng, C.-Y.; Kalkan, A. K.; Fonash, S. J.; Gu, B.; Sen, A. *Nano Lett.* **2005**, *5*, 439.
8. Bloom, C. J.; Elliott, C. M.; Schroeder, P. G.; France, C. B.; Parkinson, B. A. *J. Am. Chem. Soc.* **2001**, *123*, 9436.
9. Nigrey, P. J.; MacDiarmid, A. G.; Heeger, A. J. *Chem. Commun.* **1979**, 594.
10. Pruss, A.; Beck, F. *J. Electroanal. Chem.* **1984**, *172*, 281.
11. MacDiarmid, A. J.; Mu, S. L.; Somasiri, N. L. D. ; Wu, W. *Mol. Cryst. Liq. Cryst.* **1985**, *121*, 187.
12. Jones, E. T. T.; Chyan, O. M.; Wrighton, M. S. *J. Am. Chem. Soc.* **1987**, *109*, 5526.
13. Burroughes, J. H.; Bradley, D. D. C.; Brown, A. R.; Marks, R. N.; Friend, R. H.; Burn, P. L.; Holmes, A. B. *Nature* **1990**, *347*, 539.
14. Helfrich, W.; Schneider, W. G. *J. Chem. Phys.* **1966**, *44*, 2902.
15. Lohmann, F.; Mehl, W. *J. Chem. Phys.* **1969**, *50*, 500.
16. Basurto, J.; Burshtein, Z. *Mol. Cryst. Liq. Cryst.* **1975**, *31*, 211.
17. Kojima, H.; Ozawa, A.; Takahashi, T.; Nagaoka, M.; Homma, T.; Nagatomo, T.; Omoto, O. *J. Electrochem. Soc.* **1997**, *144*, 3628.
18. Wightman, R. M. *Science* **1988**, *240*, 415.
19. Chidsey, E. D.; Murray, R. W. *Science* **1986**, *231*, 25.

20. Hoa, D. T.; Kumar, T. N. S.; Punekar, N. S.; Srinivasa, R. S.; Lal, R.; Contractor, A. Q. *Anal. Chem.* **1992**, *64*, 2645.
21. Wang, Z.; Zhang, J.; Xing, R.; Yuan, J.; Yan, D.; Han, Y. *J. Am. Chem. Soc.* **2003**, *125*, 15278.
22. Walcarius, A. *Chem. Mater.* **2001**, *13*, 3351.
23. Lee, C.-W.; Kim, Y.-B.; Lee, S.-H. *Chem. Mater.* **2005**, *17*, 366.
24. Dhanabalan, A.; van Dongen, J. L. J.; van Duren, J. K. J.; Janssen, H. M.; van Hal, P. A.; Janssen, R. A. J. *Macromolecules* **2001**, *34*, 2495.
25. Hoeben, F. J. M.; Jonkheijm, P.; Meijer, E. W.; Schenning, A. P. H. J. *Chem. Rev.* **2005**, *105*, 1491.
26. Li, X.-G.; Huang, M.-R.; Duan, W.; Yang, Y.-L. *Chem. Rev.* **2002**, *102*, 2925.
27. Grabowski, Z. R.; Rotkiewicz, K.; Rettig, W. *Chem. Rev.* **2003**, *103*, 3899.
28. Schwab, P. F. H.; Smith, J. R.; Michl, J. *Chem. Rev.* **2005**, *105*, 1197.
29. Gonzalez, M.; Segura, J. L.; Seoane, C.; Martin, N.; Garin, J.; Orduna, J.; Alcala, R.; Villacampa, B.; Hernandez, V.; Lopez Navarrete, J. T. *J. Org. Chem.* **2001**, *66*, 8872.
30. Guldi, D. M.; Luo, C.; Swartz, A.; Gomez, R.; Segura, J. L.; Martin, N.; Brabec, C.; Sariciftci, N. S. *J. Org. Chem.* **2002**, *67*, 1141.
31. Salzner, U.; Lagowski, J. B.; Pickup, P. G.; Poirier, R. A. *Synth. Met.* **1998**, *96*, 177.
32. Havinga, E. E.; ten Hoeve, W.; Wynberg, H. *Synth. Met.* **1993**, *55*, 299.
33. Roncali, J. *Chem. Rev.* **1997**, *97*, 173.

34. van Mullekom, H. A. M.; Vekemans, J. A. J. M.; Havinga, E. E.; Meijer, E. *W. Mater. Sci. Eng., R* **2001**, *32*, 1.
35. Ajayaghosh, A. *Chem. Soc. Rev.* **2003**, *32*, 181.
36. Wudl, F. ; Kobayashi, M. ; Heeger, A. J. *J. Org. Chem.* **1984**, *49*, 3381.
37. Wudl, F.; Kobayashi, M.; Colaneri, N.; Boysel, M.; Heeger, A. J. *Mol. Cry. Liq. Cry.* **1985**, *118*, 195.
38. Kobayashi, M.; Colaneri, N.; Boysel, M.; Wudl, F.; Heeger, A. J. *J. Chem. Phys.* **1985**, *85*, 5717.
39. Colaneri, N.; Boysel, M.; Wudl, F.; Heeger, A. J.; Wudl, F. *Synth. Met.* **1986**, *14*, 45.
40. Yashima, H.; Kobayashi, M.; Lee, K. B.; Chung, T. C.; Heeger, A. J.; Wudl, F. *J. Electrochem. Soc.* **1987**, *134*, 46.
41. Dale, S. M.; Glide, A.; Hillman, A. R. *J. Mater. Chem.* **1992**, *2*, 99.
42. Bredas, J. L.; Heeger, A. J.; Wudl, F. *J. Chem. Phys.* **1986**, *85*, 4673.
43. Pomerantz, M.; Chaolner, B.; Harding, L. O.; Tseng, J. J.; Pomerantz, W. J. *Synth. Met.* **1993**, *55*, 960.
44. Nayak, K.; Marynick, D. S. *Macromolecules* **1990**, *23*, 2237.
45. King, G.; Higgins, S. J. *Chem. Commun.* **1994**, 825.
46. Goris, L.; Loi, M. A.; Cravino, A. ; Neugebauer, H. ; Saricifici, N. S. ; Vanderzande, D. *Synth. Met.* **2003**, *138*, 249.
47. Ferraris, J. P.; Lambert, T. L.; Rodriguez, S. U.S. Patent 5, 510, 438, 1996.
48. Lambert, T. L.; Ferraris, J. P. *Chem. Commun.* **1991**, 752.

49. Ferraris, J. P.; Lambert, T. L. *Chem. Commun.* **1991**, 1268.
50. Ferraris, J. P.; Henderson, C.; Torres, D.; Meeker, D. *Synth Met.* **1995**, *72*, 147.
51. Kozaki, M.; Tanaka, S.; Yamashita, Y. *J. Org. Chem.* **1994**, *59*, 442.
52. Michael, U.; Gronowitz, S. *Chem. Scr.* **1973**, *4*, 126.
53. Brisset, H.; Gautier, C.; Gorgues, A.; Jubault, M.; Roncali, J. *J. Chem. Soc., Chem. Commun.* **1994**, 1305.
54. Huang, H.; Pickup, P. G. *Chem. Mater.* **1998**, *10*, 2212.
55. Berlin, A.; Zotti, G.; Zecchin, S.; Schiavon, G.; Vercelli, B.; Zanelli, A. *Chem. Mater.* **2004**, *16*, 3667.
56. Mintimire, J. W.; White, C. T.; Elert, M. L. *Synth. Met.* **1986**, *16*, 235.
57. Bredas, J. L. *J. Chem. Phys.* **1985**, *82*, 3808.
58. Bredas, J. L.; Chance, R. R.; Silbey, R. *Phys. Rev.* **1982**, *70*, 1132.
59. Bozovic, I. *Phys. Rev. B.* **1985**, *32*, 8136.
60. Bakhshi, A. K.; Ladik, J. *Synth. Met.* **1989**, *30*, 115.
61. Waltman, R. J.; Bargon, J. *Tetrahedron* **1986**, *64*, 76.
62. Chandler, G. K.; Pletcher, D. *Spec. Period Rep. Electrochem.* **1985**, *10*, 117.
63. Heinze, J. *Top. Curr. Chem.* **1990**, *152*, 1.
64. Roncali, J.; Guy, A.; Lemaire, M.; Garreau, R.; Hoa, H. A. *J. Electroanal. Chem.* **1991**, *312*, 277.
65. Roncali, J.; Garnier, F. *J. Phys. Chem.* **1988**, *92*, 833.



66. Kanatzidis, M. G. ; Marcy, H. O. ; McCarthy, W. J. ; Kannewurf, C. R. ; Marks, T. J. *Solid State Ionics* **1989**, *32*, 594.
67. Roncali, J.; Garnier, F. *New. J. Chem.* **1986**, *4*, 237.
68. Sato, M.; Tanaka, S.; Kaeriyama, *Synth. Met.* **1986**, *14*, 279.
69. Yassar, A.; Roncali, J.; Garnier, F. *Macromolecules* **1989**, *22*, 804.
70. Roncali, J.; Yassar, A.; Garnier, F. *Chem. Commun.* **1988**, 581.
71. Otero, F.; Rodriguez, J. *J. Electroanal. Chem.* **1991**, *310*, 219.
72. Zhao, S. Z.; Pickup, P. G. *J. Chem. Soc., Faraday Trans.* **1994**, *90*, 3097.
73. Lang, P.; Chao, F.; Costa, M.; Lheritier, E.; Garnier, F. *Phys. Chem.* **1988**, *92*, 1528.
74. Raymond, D. E.; Harrison, J. D. *J. Electroanal. Chem.* **1993**, *361*, 65.
75. Lin, Y.; Wallace, G. G. *Electrochim. Acta* **1994**, *39*, 1409.
76. Fermin, D. J.; Scharifker, B. R. *J. Electroanal. Chem.* **1993**, *357*, 273.
77. Pickup, P. G. *In Modern Aspects of Electrochemistry* Convey, B. E.; Bockris, J. O'M.; White, R.E., Eds.; Plenum: New York, **1999**, *33*, 549.
78. Waltman, R. J.; Bargon, J. *Can. J. Chem.* **1986**, *64*, 76.
79. Genies, E. M.; Boyle, A.; Lapkowski, M.; Tsintavis, C. *Synth. Met.* **1990**, *36*, 139.
80. Syed, A. A.; Dinesan, M. K. *Talanta* **1991**, *38*, 815.
81. Andrieux, C. P.; Audebert, P.; Hapiot, P. ; Saveant, J. M. *J. Phys. Chem.* **1991**, *95*, 10158.

82. Audebert, P.; Catel, J. M.; Lecousturmer, G.; Duchenet, V.; Hapiot, P. J. *Phys. Chem.* **1995**, *99*, 11923.
83. Pickup, P. G. *J. Chem. Soc., Faraday Trans.*, **1994**, *86*, 3631.
84. Albery, W. J.; Chen, Z.; Horrocks, B. R.; Mount, A. R. Wilson, P. J.; Bloor, D.; Monkman, A. T.; Elliott, C. M. *Faraday Discuss. Chem. Soc.* **1989**, *88*, 247.
85. Albery, W. J.; Mount, A. R. *J. Electroanal. Chem.* **1991**, *350*, 3.
86. Albery, W. J.; Mount, A. R. *J. Chem. Soc. Faraday Trans.* **1994**, *90*, 1115.
87. Tanguy, J. *Synth. Met.* **1991**, *41*, 2991.
88. Fletcher, S. *J. Electroanal. Chem.* **1992**, *337*, 127.
89. Ren, X.; Pickup, P. G. *J. Electroanal. Chem.* **1992**, *139*, 2097.
90. Ren, X.; Pickup, P. G. *Electrochim. Acta* **2001**, *46*, 4177.
91. Tanguy, J.; Mermilliod, N. *Synth. Met.* **1987**, *21*, 129.
92. Tanguy, J.; Mermilliod, N.; Hoclet, M. *J. Electroanal. Chem.* **1987**, *134*, 795.
93. Tanguy, J.; Mermilliod, N.; Hoclet, M. *Synth. Met.* **1987**, *18*, 7.
94. Penner, R. M.; Martin, C. R. *J. Phys. Chem.* **1989**, *93*, 984.
95. Desloius, C.; Musiani, M. M.; Tribollet, B. *J. Phys. Chem.* **1994**, *98*, 2936.
96. Kankare, J.; Kupila, E. L. *J. Electroanal. Chem.* **1992**, *322*, 167.
97. Tanguy, J.; Hoclet, M. *Synth. Met.* **1989**, *28*, 145.
98. Ren, X.; Pickup, P. G. *J. Electroanal. Chem.* **1994**, *365*, 289.
99. Scott, J. C.; Pfluger, P.; Krounbi, T.; Street, G. B. *Phys. Rev. B* **1983**, *28*, 2140.

100. Meng, H.; Wudl, F. *Macromolecules* **2001**, *34*, 1810.
101. Lambert, J. B. et al. *Organic Structural Spectroscopy* Prentice-Hall, Inc. New Jersey **1998**.
102. van der Pauw, L. J. *Philips Tech. Rev.*, **1958**, *20*, 220.
103. Montgomery, H. C. *J. Appl. Phys.* **1971**, *42*, 2971.
104. Logan, B. F.; Rice, S. O.; Wick, R. F. *J. Appl. Phys.* **1971**, *42*, 2975.
105. Schiavon, G.; Sitran, S.; Zotti, G. *Synth. Met.* **1989**, *32*, 209.
106. Pickup, P. G.; Kutner, W.; Leidner, C. R.; Murray, R. W. *J. Am. Chem. Soc.* **1984**, *106*, 1991.
107. Ochmanska, J.; Pickup, P. G. *J. Electroanal. Chem.* **1991**, *297*, 211.
108. Ren, X.; Pickup, P. G. *J. Electroanal. Chem.* **1997**, *420*, 251.
109. Furukawa, Y.; Tazawa, S.; Fuji, Y.; Harada, I. *Synth. Met.* **1988**, *24*, 329.
110. Mastragostino, M. *Applications of Electroactive Polymers*, Chapman & Hall, New York. **1993**, *7*, 223.

## *Chapter 2*

### **Experimental Section**

#### **2.1 Chemicals and Reagents**

Unless otherwise stated, all commercial chemicals and solvents were used as received without further purification.

#### **2.2 Electrochemical Synthesis and Studies**

A Pine Instruments RDE-4 Potentiostat and a conventional three-electrode cell were used for electrochemical experiments, which included electropolymerization and electrochemical characterization of polymers. Working electrodes were either platinum discs ( $5.2 \times 10^{-3} \text{ cm}^2$  or  $1.2 \times 10^{-4} \text{ cm}^2$ ) sealed in glass or indium tin oxide coated glass ( $10 \Omega/\text{square}$ , Donnelly Corp.) A copper wire was used as the counter electrode and Ag/AgCl as the reference electrode. In all cases, the electrolyte concentration was either 0.01 M or 0.1 M.

Unless otherwise stated, for all the electrochemical studies normally 100 mV/s was employed as the potential scan rate. Before each experiment, the solution was purged with argon and the electrochemical studies were performed under argon. All

polymerizations were carried out at ambient temperature ( $22 \pm 2$  °C). Polymer films were rinsed with acetone and dried in air before further experiments.

### 2.3 Rotating Disc Voltammetry

The electrodes used in these experiments consisted of a platinum disc of diameter 1.0 mm ( $A= 0.0078$  cm<sup>2</sup>) sealed in a Teflon case. Electrode rotation was performed with a Pine Instruments ASR Analytical Rotator. A Pine RDE-4 Potentiostat controlled the potential in a three-compartment cell. The hydrodynamic flow pattern resulting from rapid rotation of the disk moves liquid horizontally out and away from the center of the disk with a consequent upward axial flow to replenish liquid at the surface as shown by the arrows in **Fig 2.1** [1].

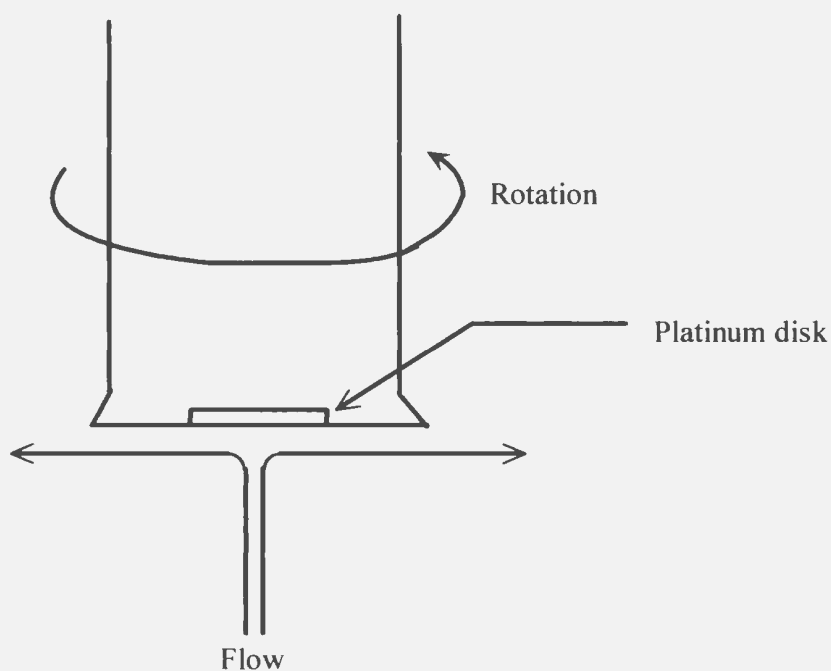


**Fig. 2.1** Rotating disk electrode with hydrodynamic flow pattern

## 2.4 Dual Electrode Sandwich Voltammetry

Fig. 2.2 shows the schematic structure of a dual electrode assembly for *in situ* conductivity measurement. One of the platinum disc (area  $5.2 \times 10^{-3} \text{ cm}^2$ ) was electrochemically coated with a polymer film, then rinsed with acetone and later dried in air before gold vacuum deposition.

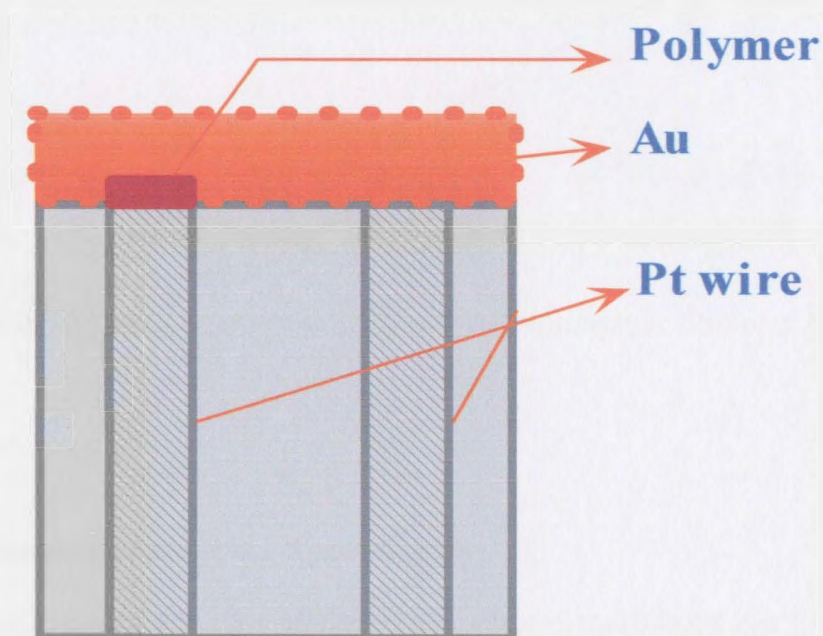


**Fig. 2.2** Schematic dual-electrode used in the measurement of conductivity against potential

Gold films were vapour deposited on dual electrode assemblies with an Edward's model 4 coating unit, in a vacuum below  $10^{-3}$  torr. Electrical contact to the gold film was made by an adjacent platinum disk. By this way, the active conducting polymer film is sandwiched between two working electrodes. A bipotentiostat (a potentiostat with two working electrodes) was employed for monitoring conductivity of the polymer films as a function of applied potential. The applied potential at the two electrodes is simultaneously scanned; slowly (10mV/s) to maintain steady state conditions, and a small constant potential difference, 10 mV, is maintained between the two electrodes. The current flowing between them is monitored to yield the *in situ* resistivity and hence conductivity from equation 2.1 [2-3].

$$\sigma = \frac{I \times d}{\Delta E_{\text{Pt-Au}} \times A} \quad \dots (2.1)$$

Where I is the measured current, d is the thickness of the polymer film and A is the electrode area.

## 2.5 Electrochemical Impedance Spectroscopy

Electropolymerized films, on platinum disc electrodes ( $0.0078 \text{ cm}^2$ ), were allowed to soak in the appropriate electrolyte solution, which had been degassed with argon for 10 minutes prior to the electrochemical experiments. A blanket of argon was used to exclude oxygen and atmospheric water. A single cyclic voltammetric sweep was performed before and after impedance investigation in order to determine the  $E_{1/2}$  value and later to

check the stability of the active polymeric film. Impedance data was collected at room temperature using a Solatron 1250 frequency response analyzer and a Solatron 1286 potentiostat/galvanostat under the control of ZPlot software. The perturbation amplitude was 5 mV.

## **2.6 UV-VIS-NIR Spectroscopy**

UV-vis-NIR spectra were recorded with a Cary 5E spectrometer. The polymer film was deposited onto a narrow slide of ITO coated glass. The slide was then positioned inside a standard 1 cm quartz cuvette together with a Pt wire counter electrode and a reference electrode consisting of a Pt wire in a thin glass tube packed with polypyrrole [4] and Nafion for spectroelectrochemistry experiments. The potential of this reference electrode was stable during experiments at 0.36 V vs Ag/AgCl. A spectrum of the same cell with a bare ITO electrode was subtracted from all spectra to correct for the absorbance of the cell, ITO electrode and electrolyte solution.

## **2.7 FT-IR Spectroscopy**

Electrochemically undoped polymer films (ca. 1 mg) were scraped from ITO electrodes, and pressed into pellets with KBr (150 mg). Chemically polymerized samples were drop casted onto an optical grade silicon disc (25 x 2 mm, Nicodom Ltd.). For both the cases spectra were recorded using a Mattson Polaris spectrometer extending into the near and far infrared regions.



## 2.8 Scanning Electron Microscopy

Measurements were performed with a Hitachi S-570 scanning electron microscope. Calibration relationships were obtained from scanning electron microscopy of polymer films either on a Pt wire or Pt disc, which will be discussed under appropriate sections in the following chapters.

## 2.9 Elemental Analysis

Elemental analyses were performed by Canadian Microanalytical Services, 207-8116 Alexander Road, RR #7, Delta, BC, V4G 1G7

## 2.10 NMR Spectroscopy

Nuclear magnetic resonance (NMR) spectra were acquired on a Bruker instrument at 500 MHz ( $^1\text{H}$  NMR). Samples were dissolved in deuterated chloroform and filtered before further investigations.

### References:

1. Kissinger, P. T.; Heineman, W. R. *Laboratory Techniques in Electro-analytical Chemistry* New York, Marcel Dekker, Inc. **1996**.
2. Mao, H.; Pickup, P. G. *J. Am. Chem. Soc.* **1990**, *112*, 1776.
3. Ochmanska, J.; Pickup, P. G. *J. Electroanal. Chem.* **1991**, *297*, 211.
4. Qi, Z.; Pickup, P. G. *Chem. Mater.* **1997**, *9*, 2934.

**Chapter 3** *Chem. Mater.*, 2003, **15**, 1918 -1923.

**$\Delta^{4,4'}$ -Dicyclopenta[2,1-*b*:3,4-*b'*]dithiophene. A Conjugated Bridging Unit for Low Band Gap Conducting Polymers**

**Kavithaa Loganathan<sup>1</sup>, Eduardo G. Cammisa<sup>2</sup>, Brent D. Myron<sup>3</sup>, and**

**Peter G. Pickup<sup>4</sup>**

**Abstract:**

$\Delta^{4,4'}$ -Dicyclopenta[2,1-*b*:3,4-*b'*]dithiophene has been prepared from cyclopenta[2,1-*b*:3,4-*b'*]bithiophen-4-one and its electrochemical and spectroscopic properties have been characterized. Its low HOMO-LUMO gap and facile electrochemical polymerization make it an attractive building block for low band gap conducting polymers. Films of poly-( $\Delta^{4,4'}$ -dicyclopenta[2,1-*b*:3,4-*b'*]dithiophene) on electrodes have been characterized by cyclic voltammetry, electronic absorption spectroscopy, IR spectroscopy, and in situ conductivity measurements. The spectroscopic and electrochemical results confirm the formation of a polymeric material with long conjugation length and low band gap (ca. 0.5 eV). The intrinsic conductivity is consistent with this band gap.

<sup>1</sup>This author contributed the experimental part for Figures 3.1 to 3.7 and data interpretation, and wrote the first draft of the manuscript.

<sup>2</sup>This author contributed the synthesis of compound 3-3.

<sup>3</sup>This author contributed the experimental part for Figures 3.8.

<sup>4</sup>This author contributed data interpretation and preparation of the final form of the manuscript.

### 3.1 Introduction

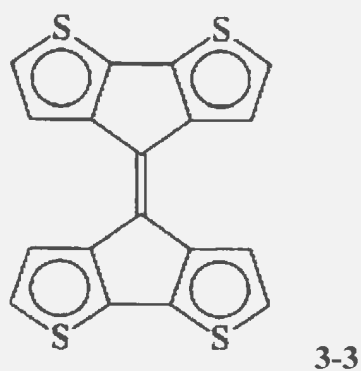
Among conducting polymers, polythiophene is particularly attractive because of its high conductivity and good environmental stability in both its p-doped and undoped states [1-3]. Furthermore, its structural versatility has made possible the development of numerous thiophene-based polymers with various desired properties, such as high stability [4], superior conductivity [3], processability [5], solubility [6-8], and low band gap [9, 10]. To achieve polythiophene of high quality, in addition to the careful optimization of electrosynthesis conditions from the thiophene monomer [11-14], oligomers, particularly 2,2'-bithiophene and 2,2':5',2' '-terthiophene, have been employed as precursors [15-18]. Owing to the lower oxidation potentials and exclusive  $\alpha$ - $\alpha'$  linkages in these precursors, polybithiophene and polyterthiophene are expected to be closer to the ideal polythiophene structure than materials prepared from thiophene itself [15]. Substantial work on comparative studies of the electrochemical and spectroscopic properties of polymers synthesized from thiophene, bithiophene, and terthiophene has been reported [1,15].

Conducting polymers prepared from bithiophene precursors with electron-withdrawing groups at an  $sp^2$ -carbon bridging the  $\beta$  and  $\beta'$  positions form an interesting branch of conducting polymers with reduced band gaps ( $E_g < 1.5$  eV) [10-19]. For example, cyclopenta[2,1-*b*:3,4-*b'*]bithiophen-4-one (**3-1**) produces a polymer with a band gap of ca. 1.2 eV [20] and poly(4-dicyanomethylene-cyclopenta[2,1-*b*:3,4,*b'*]bithiophene)

(**3-2**) has one of the lowest band gaps (ca. 0.8 eV) [21] reported to date for a thiophene-based system.



The linking of two bridged bithiophene moieties by a double bond, as in  $\Delta^{4,4'}$ -dicyclopenta[2,1-*b*:3,4-*b'*]-dithiophene (structure **3-3**) [22-23], represents an intriguing extension of this group of polythiophenes. We report here that **3-3** can be electrochemically polymerized to produce low band gap materials with substantial conductivity. Films of poly-**3-3** on electrodes have been characterized by cyclic voltammetry, infrared spectroscopy, electronic absorption spectroscopy, and in situ conductivity measurements.



The attraction of **3-3** over other cyclopentadithiophenes that have been reported is that its four thiophene rings allow it to cross-link conjugated systems in a well-defined way, with conjugation in two dimensions. It may therefore be an attractive building block for molecular electronic systems in which it can act as a four-way electronic junction.

## 3.2 Experimental Section

### 3.2.1 Chemicals and Electrodes

Nitrobenzene (Aldrich, 99.93+ AnalaR grade), acetonitrile (Aldrich, 99.93+% Biotech grade), Bu<sub>4</sub>NPF<sub>6</sub> (Fluka, electrochemical grade), and other chemicals were used as received. Working electrodes were either Pt disks ( $5.2 \times 10^{-3}$  cm<sup>2</sup> or  $1.2 \times 10^{-4}$  cm<sup>2</sup>) sealed in glass or indium/tin oxide coated glass (10  $\Omega$ /square, Donnelly Corp.).

### 3.2.2 Synthesis of 3-3

A solution of cyclopenta[2,1-*b*:3,4-*b'*]dithiophene-4-one [24] (202 mg, 1.04 mmol) and Lawesson's reagent (1.30 g, 3.12 mmol) in dry benzene was refluxed for 12 h under a nitrogen atmosphere. The reaction mixture was cooled and the solvent was then removed by rotary evaporation affording a solid, which was purified by column chromatography (silica gel, hexane:dichloromethane 9:1) to give a dark brown solid (40 mg, 0.11 mmol, 22%). mp 237-240 °C (dec). <sup>1</sup>H NMR (300 MHz, CDCl<sub>3</sub>):  $\delta$ 7.52 (d,  $J$  = 5.0 Hz, 4H), 7.10 (d,  $J$  = 5.0 Hz, 4H). <sup>13</sup>C NMR (75 MHz, CDCl<sub>3</sub>):  $\delta$ 144.7, 140.9, 125.2, 124.4, 121.4. MS  $m/z$  (%) 352 (M<sup>+</sup>, 100), 320 (7), 307 (13), 176 (14). HRMS: calculated for C<sub>18</sub>H<sub>8</sub>S<sub>4</sub>, 351.95089; found, 351.94977.

### 3.2.3 Polymerization of 3-3

Films of poly-3-3 were formed on electrodes by the anodic electrochemical polymerization of 3-3 (ca. 2-5 mM) in nitrobenzene containing 0.01 M Bu<sub>4</sub>NPF<sub>6</sub>. Typically, films were formed by cycling the potential between 0 and +1.5 V at 100 mV s<sup>-1</sup>. All polymerizations and electrochemical experiments were carried out at ambient temperature (22 ± 2 °C). Polymer films were rinsed with acetone and dried in air before further experiments.

Electrospray mass spectroscopy of one sample that had been dissolved in a 1:3 mixture of *N*-methylpyrrolidone and DMF at 70 °C and then diluted with acetonitrile showed peaks at  $m/z = 2466$  ( $n = 7$ ), 2114, and 1516, as well as peaks at 1058 and 706, corresponding to the trimer and dimer, respectively. This indicates that a polymeric material is formed during the anodic deposition of films of 3-3.

### 3.2.4 Polymer Film Thickness

The thickness of a film of poly-3-3 deposited on a 0.0127-cm diameter Pt wire was estimated by scanning electron microscopy from the increase in diameter. This provided a relationship of 1.6 μm cm<sup>2</sup> C<sup>-1</sup> between film thickness and voltammetric charge that was used to estimate the thicknesses of all other films.

### 3.2.5 Conductivity Measurements

A thin film of poly-**3-3** deposited on a Pt disk electrode was coated with gold by vacuum deposition, and dual working electrode experiments were performed with a Pine Instruments RDE4 bi-potentiostat in a four-electrode cell containing acetonitrile + 0.01 M Bu<sub>4</sub>NPF<sub>6</sub> [25]. In one type of experiment, the potentials of both the underlying Pt electrode and the gold film were slowly scanned (10 mV s<sup>-1</sup>) relative to the reference electrode, with a 10-mV potential difference maintained between them. The resistance of the polymer film at each potential during the scan was calculated from the current by applying Ohm's law. In a second type of experiment, the potential of the gold film was held at 0 V vs SSCE while the potential of the underlying Pt disk was scanned. The resistance at each potential was calculated from the current (*i*) using  $R = s/i$ , where *s* is the slope of a plot of log(*i*) vs *E* [26]. Conductivity vs potential plots obtained by these two methods agreed well at high doping levels (-0.7 V < *E* < 0.4 V) but diverged in the intermediate potential range where the current in the first type of experiment (fixed Δ*E* = 10 mV) became too small to measure accurately. The higher potential differences across the film in the second type of experiment (and thus higher currents) allowed us to extend the measurements to lower conductivities.

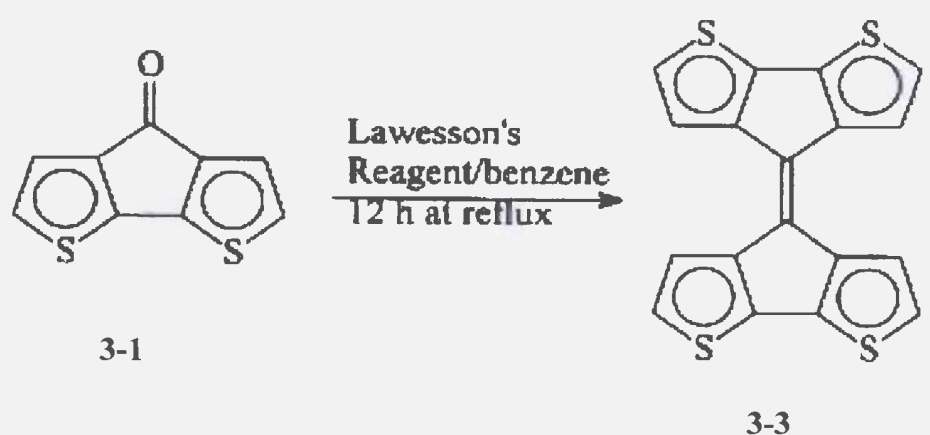
### 3.3 Results and Discussion

#### 3.3.1 Monomer Synthesis

Compound **3-3** was obtained in 22% yield by treating cyclopenta[2,1-*b*:3,4-*b'*]-dithiophene-4-one (**1-1**) with 3 equiv of Lawesson's reagent under a nitrogen atmosphere (12 h reflux in benzene) (**Scheme 3.1**). Our original intention here was to prepare

cyclopenta[2,1-*b*:3,4-*b'*]dithiophene-4-thioiketone, which has been predicted to form a low band gap polymer with good n-type conductivity [27]. However, this compound was not detected in the reaction mixture. The formation of **3-3** was expected since a similar dimer is obtained from fluorenone, in addition to the thioiketone [28].

**Scheme 3.1**



### 3.3.2 Electrochemistry of the Monomer and Electrochemical Polymerization

**Fig. 3.1** shows cyclic voltammograms for the reduction and oxidation (first two cycles) of **3-3** at a Pt electrode. The cathodic cycle was performed first to avoid contamination of the electrode surface by the polymer formed during anodic cycling.

Reduction of **3-3** occurs at a peak potential of ca. -1.1 V and is preceded by a small pre-peak at ca. -0.9 V. During the first anodic cycle, oxidation waves are observed at peak potentials of +1.12 and +1.37 V. In the reverse scan, there is a reduction wave at ca. +0.80 V that can be attributed to the undoping (reduction) of polymeric material



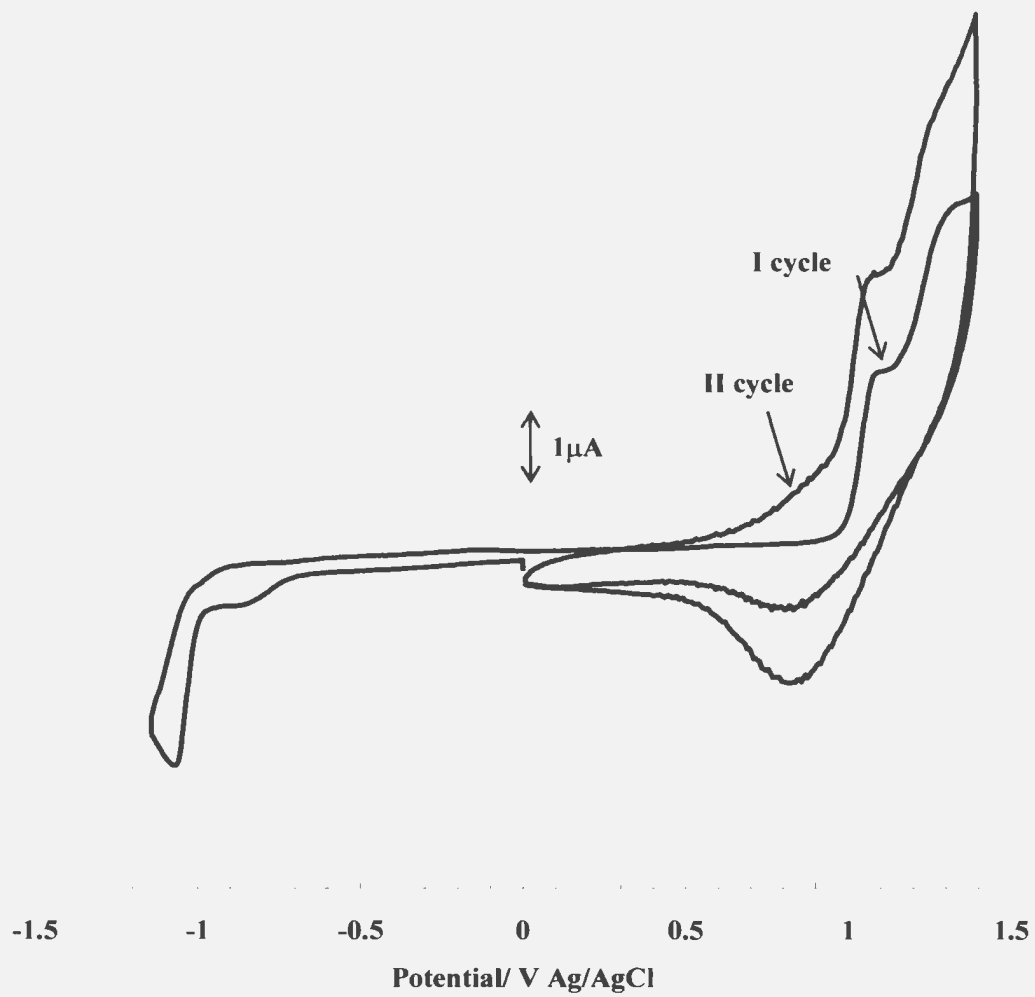


**Fig. 3.1** Cyclic voltammograms ( $100 \text{ mV s}^{-1}$ ) of **3-3** ( $<1 \text{ mM}$ ) in acetonitrile containing  $0.01 \text{ M Bu}_4\text{NPF}_6$ .

deposited on the electrode during the forward scan (see below). In the second cycle, both the oxidation and reduction currents are increased compared to the first cycle, and a new anodic wave appears at a lower potential (ca. +0.9 V). These observations are typical of conducting polymer formation on the electrode surface [29].

Compared to bithiophene, which exhibits a formal potential for oxidation of ca. +1.3 V vs SCE [15], **3-3** is significantly more easily oxidized ( $E^{\circ'} \sim 1.16$  V vs SCE). Thus, the bridging group at the 3-3' positions of the bithiophene unit in **3-3** is seen to increase the energy level of the HOMO. This is in contrast to the effects of the ketone and dicyanoethene bridging groups of **3-1** and **3-2**, which have little influence on the HOMO energy of bithiophene [21]. The electron-withdrawing effects of these groups may offset any increase in the HOMO energy that would be caused by the bridging group, although it is more likely that the increase in HOMO energy in **3-3** is due to its delocalization over the two linked bithiophene units. Indeed, the two oxidation waves observed for **3-3** in Fig. 3.1 indicate that the two bithiophene units are oxidized sequentially and that there are strong electronic interactions between them.

The formal potential for reduction of **3-3** (ca. -1.1 V) is much less negative than for bithiophene (-2.2 V vs SCE) and between the values of -1.2 and -0.8 V for **3-1** and **3-2**, respectively [21]. Thus, the substantial lowering of the LUMO energy produced by the  $sp^2$ -bridging group is observed even in the absence of an electron-withdrawing substituent.

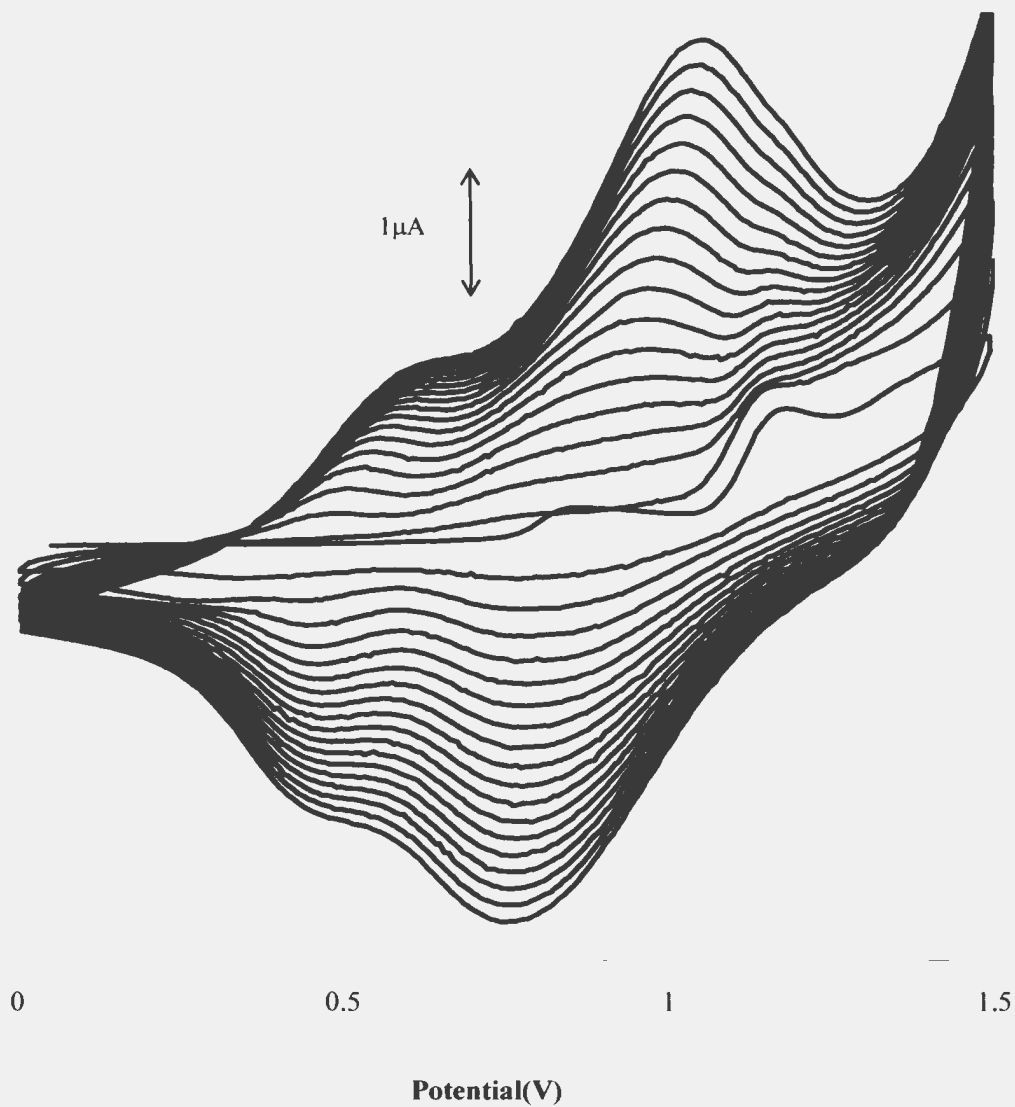


**Fig. 3.2** Cyclic voltammograms ( $100 \text{ mV s}^{-1}$ ) recorded during the formation of a poly(3-3) film on a Pt electrode under potential cycling conditions from 5 mM 3-3 in nitrobenzene containing 0.01 M  $\text{Bu}_4\text{NPF}_6$ . Currents increased during cycling.

From the difference in the peak potentials for oxidation and reduction of **3-3**, its electrochemical HOMO-LUMO gap can be estimated to be ca. 2.2 eV. Both the HOMO and LUMO shifts of **3-3** relative to bithiophene lead to a reduction in the HOMO-LUMO gap and make **3-3** one of the lowest HOMO-LUMO gap precursors for conducting polymers reported to date.

Poly-**3-3** films were prepared for further characterization by the potential cycling method, as illustrated in **Fig. 3.2** (see Experimental Section for details). Since **3-3** is not very soluble in acetonitrile (solubility <1 mM), its electrochemical polymerization was performed in nitrobenzene. Continuous potential cycling between 0 and +1.5 V results in a steady increase in the polymer waves at ca. +0.55 and +0.9 V. Following such experiments, a brown film is observed coating the electrode.

Constant potential and constant current polymerization were also tried, but both failed to produce sustained growth of good quality films. At constant potential, the polymer growth rate decayed rapidly with time, while at constant current the potential rapidly rose to values that caused oxidative degradation of the film.

### **3.3.3 Electronic Absorption Spectroscopy**

UV-vis absorption spectroscopy of **3-3** (**Fig. 3.3**, curve A) was carried out in acetonitrile. **3-3** exhibits a strong  $\pi$ - $\pi^*$  absorption with a maximum at 380 nm (3.26 eV) and an onset of ca. 440 nm (2.8 eV). These values indicate that the HOMO-LUMO gap for **3-3** is ca. 0.8 eV lower than that of bithiophene ( $\lambda_{\text{max}} = 302$  nm (4.1 eV) [30]). This is

somewhat lower than the difference of 1.3 eV (2.2 eV for **3-3** and 3.5 eV for bithiophene) estimated by cyclic voltammetry.

Also shown in Fig. 3.3 (curve B) is an electronic absorption spectrum of a poly-**3-3** film that had been electrochemically deposited on an indium/tin oxide coated glass slide and then held at 0 V for 2 min to ensure that it was in the undoped state. From the onset of absorption of  $>1600$  nm, a band gap of  $<0.8$  eV is obtained. This band gap is much lower than that of polythiophene (2.2 eV) [10] and comparable to that of poly-**3-2**, making poly-**3-3** one of the lowest band gap conducting polymers reported to date.

The very low onset of absorption of poly-**3-3** indicates that it is a highly conjugated material. On the basis of both experimental and theoretical studies of polythiophenes and other conjugated polymers, it is known that there is a linear correlation between the position of the electronic absorption band and the inverse of the conjugation length of the polymer [31]. The slope of  $\pi$ - $\pi^*$  energy gaps vs  $1/n$  (where  $n$  is the number of rings in the conjugated chain) is similar for thiophene (3.9 eV) and pyrrole (3.7 eV). We can reasonably use these values (in this case the thiophene value) to estimate conjugation lengths in new materials. From the onset of the absorbance of poly-**3-3** ( $<0.8$  eV from Fig. 3.3, curve B) and the onset of absorption of **3-3** (2.8 eV from Figure 3.3, curve A,  $n_{3-3} = 2$ ), the conjugation length ( $n_{\text{pol}} = 3.9 / (3.9/n_{3-3} + \Delta E_{\text{pol}} - \Delta E_{3-3})$ ) is found to be infinite. In other words, the decrease in band gap in going from **3-3** to poly-**3-3** is within experimental error of the decrease observed on going from bithiophene to polythiophene of effectively infinite conjugation length. In practical terms, this means

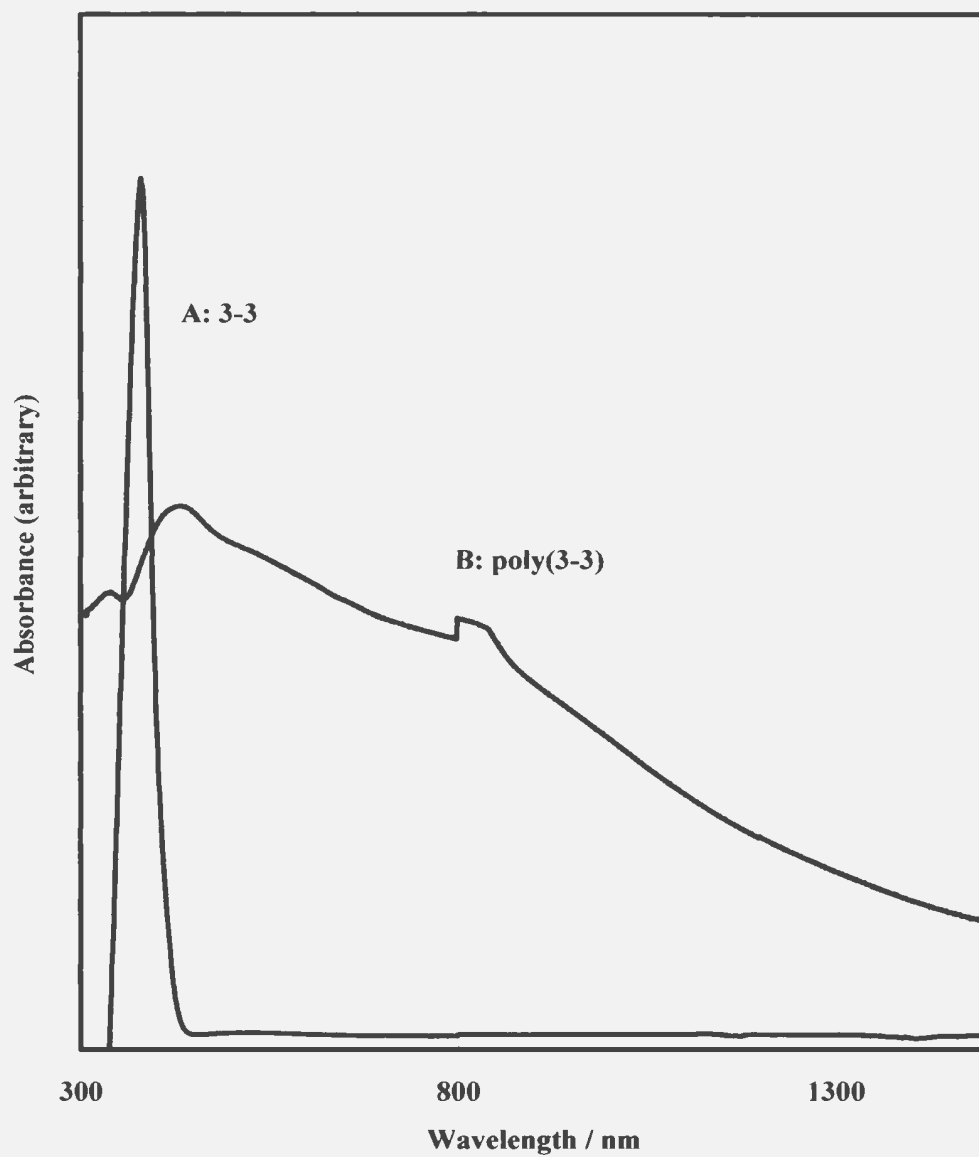


**Fig. 3.3** Electronic absorption spectra of 3-3 in acetonitrile and a poly(3-3) film on an indium/tin oxide electrode.

that it can reasonably be concluded that  $n_{\text{pol}}$  for poly-**3-3** is  $>20$ .

If, on the other hand, the peak absorbances from Fig. 3.3 are used in this calculation (3.26 eV for **3-3** and 3.02 eV for poly-**3-3**), the conjugation length appears to be only 2.3 (1.1 repeat units of **3-3**). This indicates that a wide range of conjugation lengths are present in the film, and this is consistent with the way in which **3-3** would be expected to polymerize (**Fig. 3.4**). Thus, extended polymerization at the 5-positions of rings A and B (defined as the more extensively coupled bithiophene segment of each monomer unit) would be expected to produce highly conjugated chains, while growth of side chains at rings C and/or D would be expected to be sterically restricted, producing shorter conjugated chains. The prominence of the peak at 410 nm in the spectrum of poly-**3-3** (**Fig. 3.4**) suggests that the polymer is primarily linear and that most of the pendent segments (rings C and D) are monomeric (i.e.,  $R_C = R_D = H$ ).

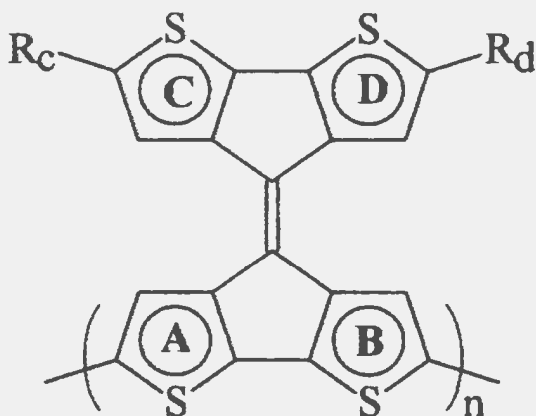


**Fig. 3.4** Expected structure of poly(**3-3**)

The electronic absorption spectrum of poly(**3-3**) provides very strong evidence that electrochemical oxidation of **3-3** does indeed produce a highly conjugated polymer on the electrode surface. It can be inferred from the spectrum that the monomer unit remains intact in the polymer, that the linkages are predominantly at the 5-positions, and that the polymer is not highly defective. If any of these conclusions were not true, it would be impossible to reasonably explain the strong absorbance of poly(**3-3**) extending to wavelengths above 1500 nm.

### 3.3.4 IR Spectroscopy

**Fig. 3.5** shows IR spectra of **3-3** and poly(**3-3**). The spectra are broadly similar, indicating that the polymer has similar structural features to the monomer. However, there are significant differences that are consistent with the expected mode ( $\alpha$ - $\alpha'$ ) of polymerization [32]. The new band at  $1195\text{ cm}^{-1}$  can be assigned to inter-ring C-C bonds between monomer units and is consistent with coupling at the  $\alpha$ -positions. The common band at  $667\text{ cm}^{-1}$  is probably the "out-of-plane" mode of the  $\text{C}_{\alpha}\text{-H}$  bonds [32]. Its decrease in relative intensity with polymerization is again consistent with  $\alpha$ - $\alpha'$  coupling. The new intense band at  $840\text{ cm}^{-1}$  in the polymer is due to the dopant ion,  $\text{PF}_6^-$ .

The absence of any strong bands in the  $1700\text{-}1800\text{-cm}^{-1}$  region for the polymer indicates that there has not been significant overoxidation during its synthesis. Overoxidation would lead to nucleophilic attack of water at the  $\beta$ -positions of the thiophene rings and the creation of carbonyl defects [33].



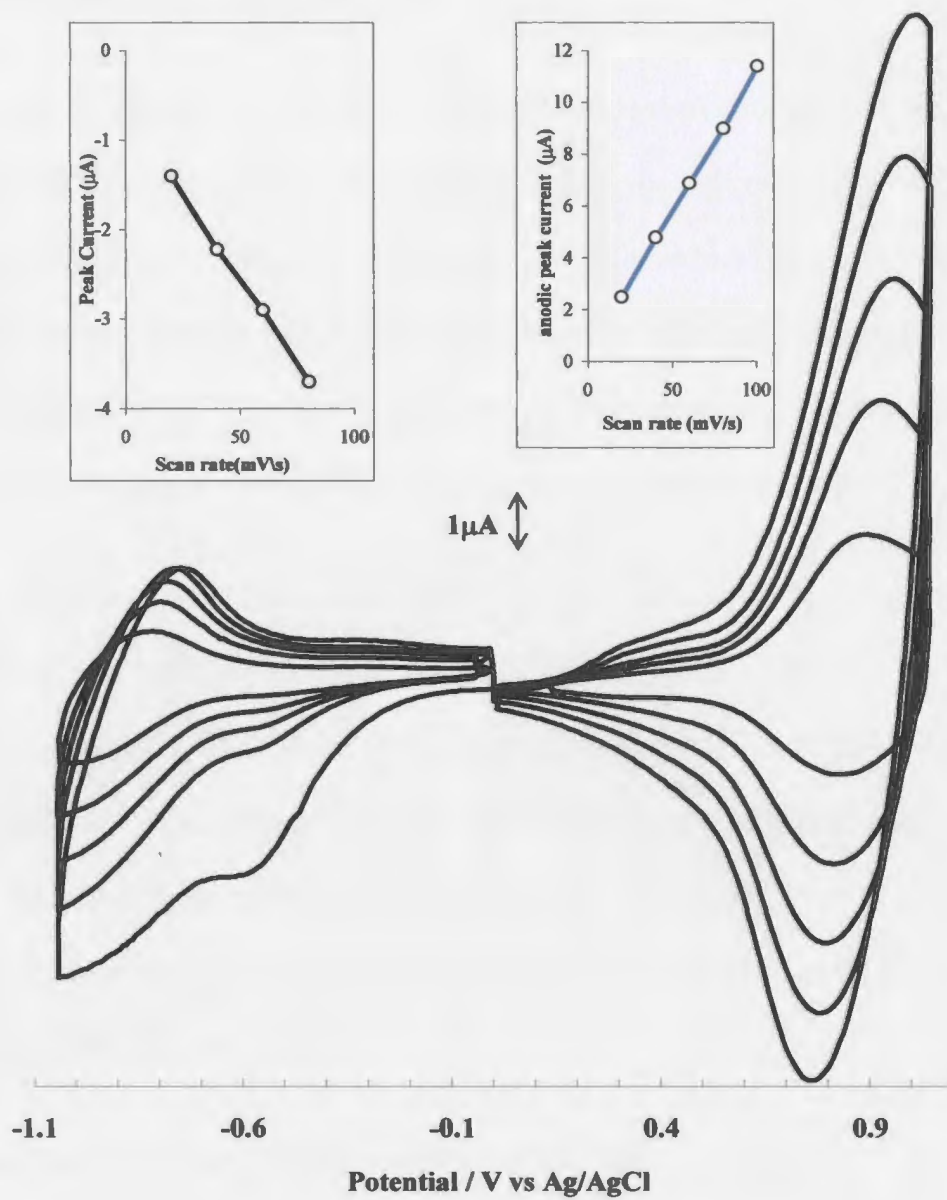


Fig. 3.5 IR Spectra (KBr disks) of 3-3 and poly(3-3)

### 3.3.5 Electrochemistry of Poly (3-3) Films

Cyclic voltammograms of a poly(3-3) coated Pt electrode at various sweep rates in monomer-free acetonitrile containing 0.01 M Bu<sub>4</sub>NPF<sub>6</sub> are shown in **Fig. 3.6**. p-Doping of the polymer film is observed as a reversible wave in the 0 to +1.10 V region, while n-doping appears as a broader and less reversible wave in the 0 to -1.1 V region. Peak currents for both waves increase approximately linearly with increasing potential sweep rate (see insets in Fig. 3.6), indicating that they correspond to rapid surface processes.

The formal potentials for the main p-doping and n-doping processes, from **Fig. 3.6**, are ca. +0.9 and -0.9 V, respectively. The difference of  $\Delta E_{\text{pol}} \sim 1.8$  eV corresponds to a conjugation length ( $n_{\text{pol}} = 3.9/(3.9/n_{3-3} + \Delta E_{\text{pol}} - \Delta E_{3-3})$  with  $\Delta E_{3-3} \sim 2.2$  eV) of ca. 2.5, which is consistent with the value obtained from the peak in the electronic absorption spectrum. The onsets of p-doping and n-doping are ca. +0.2 and -0.3 V, respectively, corresponding to a band gap of ca. 0.5 eV and a conjugation length of ca. 16, which is consistent with the result from the onset of electronic absorption. Given the difficulty of accurately determining onset potentials and wavelengths, the agreement with the optical band gap (<0.8 eV) is good. Thus, both the optical and electrochemical results indicate that poly(3-3) consists of reasonably long conjugated chains, with shorter side chains. There are also likely to be some cross-links, but their existence (or not) cannot be established from the optical and electrochemical data.



**Fig. 3.6** Cyclic voltammograms ( $10\text{-}100\text{ mV s}^{-1}$ ) of a poly(3-3) coated Pt electrode in acetonitrile containing  $0.01\text{ mol dm}^{-3}\text{ Bu}_4\text{NPF}_6$

### 3.3.6 In Situ Conductivity Measurements

In situ conductivity measurements were made by a dual-electrode sandwich technique in which a porous gold film evaporated over a polymer film on a Pt electrode acts as a second electronic contact [25]. **Fig. 3.7** shows cyclic voltammetry of a film used in one such experiment, together with a plot of conductivity vs potential obtained from dual-electrode voltammetry. The range of the initial voltammogram was restricted to avoid possible degradation of the film before the conductivity measurements.

In **Fig. 3.7**, the p-type conductivity of the polymer rises to a maximum of ca.  $1.4 \times 10^{-5} \text{ S cm}^{-1}$  at +0.98 V. On the reverse scan, the conductivity peak occurs at approximately the same potential, but is 25% lower, indicating some instability of the film at high potential. The n-type conductivity, observed in the negative scan, is ca. 10 times smaller than the p-type conductivity, peaking at  $1.2 \times 10^{-6} \text{ S cm}^{-1}$  at ca. -1.1 V. This is consistent with the high p-type/n-type conductivity ratios observed for poly(3-methylthiophene) [34] and poly (**3-2**) [35].

The conductivity of poly(**3-3**) is much lower than those observed for polythiophene and poly(**3-2**), which have reported maximum p-type conductivities of 0.1 and  $0.6 \text{ S cm}^{-1}$  [35,36], respectively. Since the doping levels of all three polymers are similar, the mobility of charge carriers must be very low in poly(**3-3**). This may be due to a greater rigidity in the polymer, due to cross-linking, which would inhibit interchain

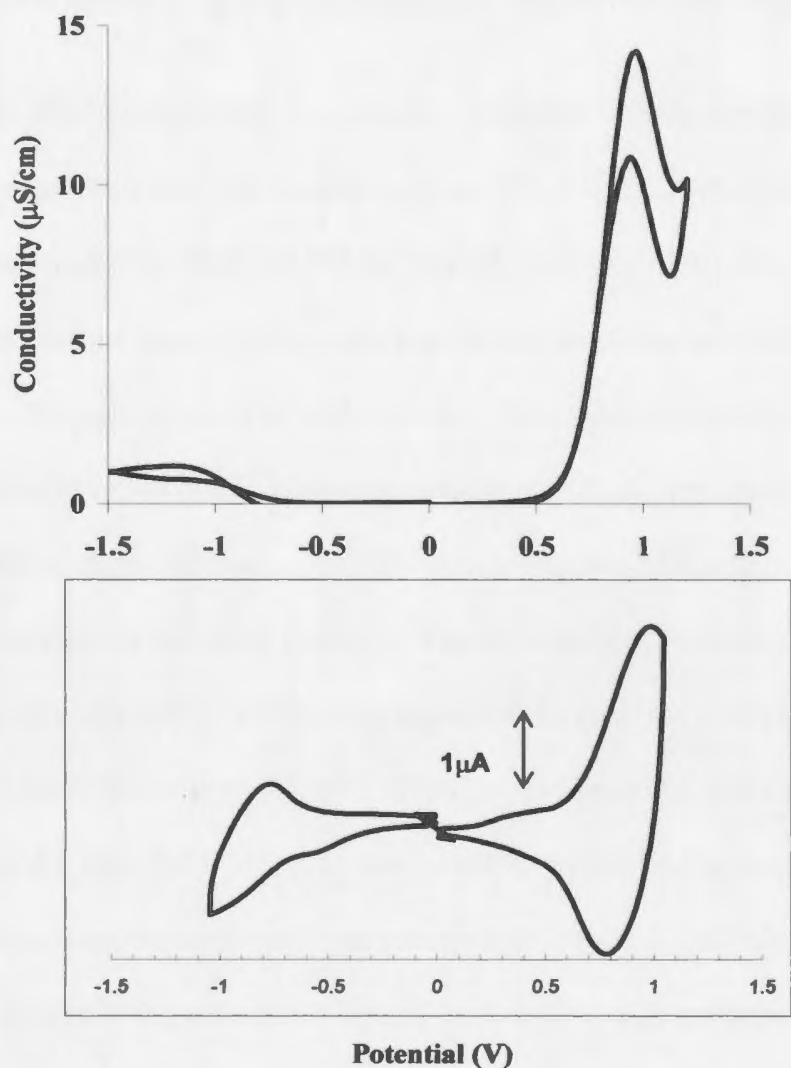


**Fig. 3.7** Cyclic voltammograms ( $100 \text{ mV s}^{-1}$ ) and in situ conductivity as a function of potential (in acetonitrile containing  $0.01 \text{ mol dm}^{-3} \text{ Bu}_4\text{NPF}_6$ ) for a poly(3-3) film sandwiched between Pt disk electrode and a porous gold film. Conductivity data were obtained with a fixed  $10 \text{ mV}$  potential difference between the Pt and Au contacts to the film.

electron hopping. It may also be due to a larger average interchain distance caused by the larger size of the monomer unit and inefficient packing of the branched polymer chains.

Log plots of conductivity vs potential, obtained from an experiment in which the potential of the gold contact was maintained at 0 V (vs SSCE) while the potential of the Pt disk was scanned (from 0 to +0.9 V and then from 0 to -1.0 V), are shown in **Fig. 3.8** (the somewhat higher conductivities observed in this experiment relative to those in **Fig. 3.7** are within the normal range of variation seen for electrochemically prepared films). The approximately exponential increases in conductivity as the polymer is p-doped (i.e., as the potential is increased from ca. -0.05 V) or n-doped (decreasing potential) are typical of conjugated polymers [35,37,38]. The intercepts of lines through these two regions of the log plot in Fig. 3.8 give an approximate measure of the polymer's intrinsic conductivity [35]. The value of  $2 \times 10^{-10} \text{ S cm}^{-1}$  is similar to the intercept ( $1.0 \times 10^{-9} \text{ S cm}^{-1}$ ) obtained for poly(**3-2**) [35], a similar polymer with a similar band gap (0.8 eV). In that case the intercept method used here (because we could not obtain accurate conductivity values in the potential range of ca.  $\pm 0.1 \text{ V}$ ) underestimates the intrinsic conductivity by about an order of magnitude, and so the intrinsic conductivity of poly(**3-3**) is probably closer to  $10^{-9} \text{ S cm}^{-1}$ .

The band gap ( $E_g$ ) of poly(**3-3**) was estimated from the conductivity data using the equation for thermal excitation of a semiconductor,  $C_{p,\text{intrinsic}} \sim 4.2 \times 10^{-5} \exp(-E_g/2kT)$  [39]. This method has been shown to be accurate for poly(**3-2**) [35] and copolymers of **3-2** with 3,4-ethylenedioxythiophene [40]. The concentration of thermally excited p-type

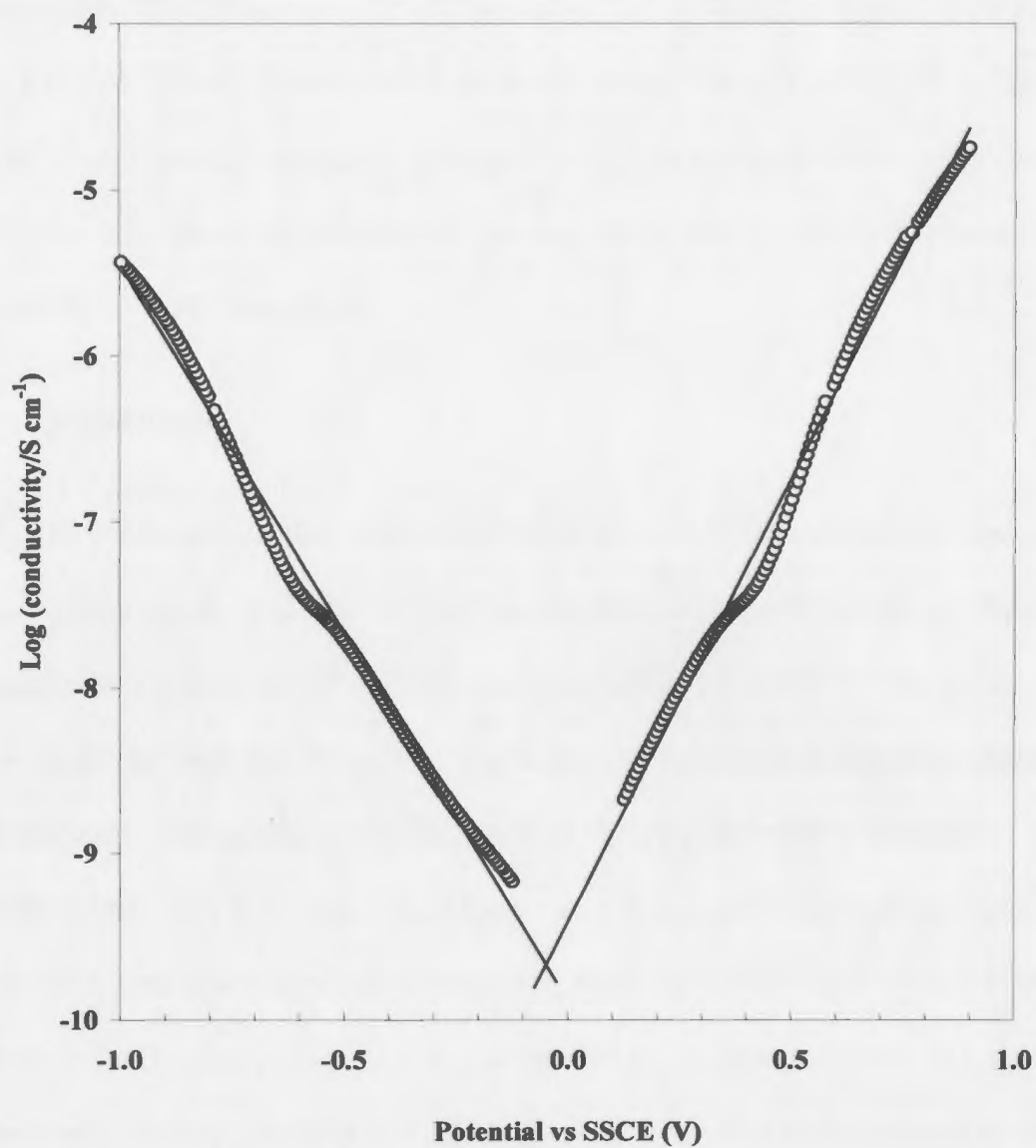


**Fig. 3.8** Log plot of in situ conductivity as a function of potential (in acetonitrile containing  $0.01 \text{ mol dm}^{-3} \text{ Bu}_4\text{NPF}_6$ ) for a poly-(3-3) film sandwiched between a Pt disk electrode and a porous gold film. The gold film was maintained at 0 V vs SSCE in this experiment.

charge carriers,  $C_{p,\text{intrinsic}}$ , was estimated to be ca.  $10^{-8}$  mol  $\text{cm}^{-3}$  from the ratio of the intrinsic conductivity ( $\sigma_{\text{intrinsic}} \sim 2 \times 10^{-10}$  S $^{-1}$   $\text{cm}^{-1}$ ) to the maximum p-type conductivity ( $\sigma_{p,\text{max}} = 1.8 \times 10^{-5}$  S  $\text{cm}^{-1}$ ) and an estimated maximum p-doping level ( $C_{p,\text{max}}$ ) of ca.  $10^{-3}$  mol  $\text{cm}^{-3}$  (i.e.,  $C_{p,\text{intrinsic}} \sim \sigma_{\text{intrinsic}} C_{p,\text{max}} / \sigma_{p,\text{max}}$ ) [35]. This analysis yields a band gap of ca. 0.4 eV, which is consistent (within experimental error) with the electrochemical (0.5 eV) and optical (<0.8 eV) band gaps.

### 3.4 Conclusions

The conjugated bridge between the bithiophene units in structure **3-3** causes a substantial lowering of the HOMO-LUMO gap relative to bithiophene and significant decreases relative to other bridged bithiophenes, such as **3-1** and **3-2**. This in turn leads to a lowering of the band gap of the conjugated polymer formed by electrochemical polymerization. The band gap of poly(**3-3**) is ca. 0.5 eV, while the band gaps of polybithiophene, poly(**3-1**), and poly(**3-2**) are ca. 2.2, 1.2, and 0.8 eV, respectively. Unfortunately, the lower band gap of poly(**3-3**) does not translate into a higher intrinsic conductivity, relative to poly(**3-2**), because the mobility of charge carriers is lower. Nevertheless, the very low HOMO-LUMO gap of **3-3** together with its four linkable thiophene terminals may make it a useful component for cross-linking low band gap systems and of value as a building block for molecular electronic systems.



## References

1. Roncali, J. *Chem. Rev.* **1992**, *92*, 711.
2. Schopf, G.; Kossmehl, G. *Polythiophenes-Electrically Conductive Polymers*; Series: Advances in Polymer Science, 129; Springer-Verlag: Berlin, 1997.
3. McCullough, R. D. *Adv. Mater.* **1998**, *10*, 93.
4. Groenendaal, B. L.; Jonas, F.; Freitag, D.; Pielartzik, H.; Reynolds, J. R. *Adv. Mater.* **2000**, *12*, 481.
5. Leclerc, M.; Faid, K. *Adv. Mater.* **1997**, *9*, 1087.
6. Bryce, M. R.; Chissel, A.; Kathirgamanathan, P.; Parker, D.; Smith, N. R. M. *Chem. Commun.* **1987**, 466.
7. Patil, A. O.; Ikenoue, Y.; Wudl, F.; Heeger, A. J. *J. Am. Chem. Soc.* **1987**, *109*, 1858.
8. Guay, J.; Diaz, A. F.; Bergeron, J. Y.; Leclerc, M. *J. Electroanal. Chem.* **1993**, *361*, 85.
9. Pomerantz, M. In *Handbook of Conducting Polymers*, 2nd ed.; Skotheim, T. A., Elsenbaumer, R. L., Reynolds, J. R., Eds.; Marcel Dekker: New York, 1998; pp 277-310.
10. Roncali, J. *Chem. Rev.* **1997**, *97*, 173.
11. Roncali, J.; Garnier, F. *New J. Chem.* **1986**, *4-5*, 237.
12. Hotta, S. *Synth. Met.* **1988**, *22*, 103.
13. Barsch, U.; Beck, F.; Hambitzer, G.; Holze, R.; Lippe, J.; Stassen, I. *J. Electroanal. Chem.* **1994**, *369*, 97.

14. Li, C.; Shi, G. Q.; Xue, G.; Jin, S.; Yu, B.; Yang, S. J. *J. Polym. Sci., Part B: Polym. Phys.* **1995**, *33*, 2199.
15. Roncali, J.; Garnier, F.; Lemaire, M.; Garreau, R. *Synth. Met.* **1986**, *15*, 323.
16. Hillman, A. R.; Swann, M. J. *Electrochim. Acta* **1988**, *33*, 1303.
17. Rasch, B.; Vielstich, W. *J. Electroanal. Chem.* **1994**, *370*, 109.
18. Eales, R. M.; Hillman, A. R. *J. Electroanal. Chem.* **1988**, *250*, 219.
19. Ferraris, J. P.; Lambert, T. L.; Rodriguez, S. U.S. Patent 5,510,438, 1996.
20. Lambert, T. L.; Ferraris, J. P. *Chem. Commun.* **1991**, 752.
21. Ferraris, J. P.; Lambert, T. L. *Chem. Commun.* **1991**, 1268.
22. Cammisa, E. G. M.Sc. Dissertation, Memorial University of Newfoundland, St. John's, Canada, 2000.
23. Ebron, V. H.; Michelini, L. I.; Miles, R. B.; Loveday, D.; Mudigonda, D.; Ferraris, J. P. *Polym. Mater. Sci. Eng.* **2002**, *86*, 4.
24. Lucas, P.; El Mehdi, N.; Ho, H. A.; Belanger, D.; Breau, L. *Synthesis* **2000**, *45*, 1253.
25. Pickup, P. G.; Kutner, W.; Leidner, C. R.; Murray, R. W. *J. Am. Chem. Soc.* **1984**, *106*, 1991.
26. Mao, H.; Pickup, P. G. *Chem. Mater.* **1992**, *4*, 642.
27. Salzner, U. *J. Mol. Model.* **2000**, *6*, 195.
28. Scheibye, S.; Shabana, R.; Lawesson, O.; Romming, C. *Tetrahedron* **1982**, *38*, 993.

29. Pickup, P. G. In *Modern Aspects of Electrochemistry*; Conway, B. E., Bockris, J. O'M., White, R. E., Eds.; Plenum: New York, 1999; Vol. 33, pp 549-597.
30. Krische, B.; Zagorska, M.; Hellberg, J. *Synth. Met.* **1993**, *58*, 295.
31. Salzner, U.; Lagowski, J. B.; Pickup, P. G.; Poirier, R. A. *J. Phys. Chem.* **1998**, *102*, 2572.
32. Louarn, G.; Buisson, J. P.; Lefrant, S.; Fichou, D. *J. Phys. Chem.* **1995**, *99*, 11399.
33. Pud, A. A. *Synth. Met.* **1994**, *66*, 1.
34. Crooks, R. M.; Chyan, O. M. R.; Wrighton, M. S. *Chem. Mater.* **1989**, *1*, 2.
35. Huang, H.; Pickup, P. G. *Acta Polym.* **1997**, *48*, 455.
36. Ofer, D.; Crooks, R. M.; Wrighton, M. S. *J. Am. Chem. Soc.* **1990**, *112*, 7869.
37. Mao, H.; Pickup, P. G. *J. Am. Chem. Soc.* **1990**, *112*, 1776.
38. Ochmanska, J.; Pickup, P. G. *J. Electroanal. Chem.* **1991**, *297*, 211.
39. Bard, A. J.; Faulkner, L. R. *Electrochemical Methods: Fundamentals and Applications*; John Wiley & Sons: New York, 1980.
40. Huang, H.; Pickup, P. G. *Chem. Mater.* **1998**, *10*, 2212.

**Poly ( $\Delta^{4,4'}$ -Dicyclopenta[2,1-b:3,4-b']dithiophene-co-3,4-ethylenedioxythiophene): Electrochemically Generated Low Band Gap Conducting copolymers**

Kavithaa Loganathan<sup>1</sup> and Peter G. Pickup<sup>2</sup>

**Abstract**

A low HOMO-LUMO gap, alkene bridged bis-bithiophene ( $\Delta^{4,4'}$ -dicyclopenta [2,1-b:3,4-b']dithiophene) has been copolymerized with electron rich 3,4-ethylenedioxythiophene, to produce copolymers with reduced band gaps and enhanced conductivities.

Electrochemical band gaps as low as 0.1 eV have been observed, but maximum conductivities were only ca. 0.3 mS cm<sup>-1</sup>. Poor matching of the HOMO energies of the two components, together with cross-conjugation at the alkene bridge appear to limit charge carrier mobilities. These results provide further evidence that the use of donor and acceptor moieties to decrease band gaps leads to materials with decreased charge carrier mobilities due to charge localization.

<sup>1</sup>This author contributed the experimental part for this manuscript and data analysis and wrote the first draft.

<sup>2</sup>This author contributed data analysis and preparation of the final manuscript.

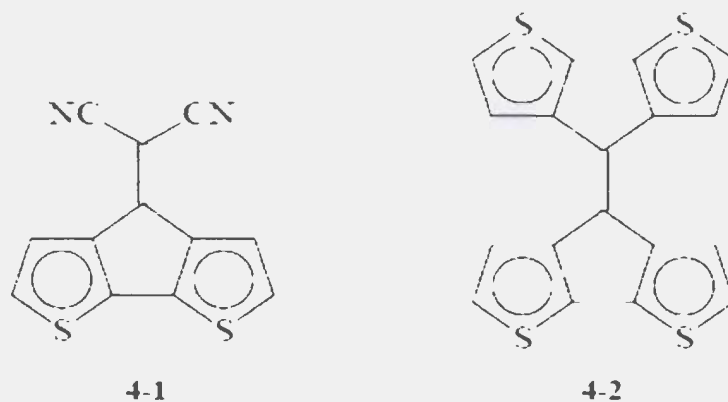
## 4.1 Introduction

After more than twenty years of development, the design of electronically conducting polymers has become a mature and sophisticated science [1-5]. Poly-(3,4-ethylenedioxythiophene) (PEDOT), which has a very low oxidation potential, a stable p-doping process, and high p-type conductivity (up to  $600 \text{ S cm}^{-1}$ ), has emerged as one of the most important conducting polymers [6,7]. When electron rich EDOT is co-polymerized with strong electronic acceptors such as 4-dicyanomethylene-4H-cyclopenta[2,1-b; 3,4-b'] dithiophene (**4-1**) [8], dicyanomethylene fluorene [9, 10], and thieno[3,4-*b*]pyrazine [11], very low band-gap materials are produced.

Band gap engineering [12] has become an important part of the science of conjugated polymers and has been the subject of several reviews [12-14]. The use of alternating donor-acceptor moieties has been a popular and successful approach [12], although it has been argued that decreasing the band gap in this way comes at the expense of decreased conjugation and charge carrier mobilities [15,16]. There is experimental evidence of this in a number of systems [8,17].

We report here on the electrochemical synthesis, characterization and conductivities of a series of copolymers of  $\Delta^{4,4'}$ -dicyclopenta[2,1-b:3,4-b']dithiophene [18,19] (**4-2**) and electron rich EDOT. Thin films of these copolymers have been prepared by oxidative electrochemical polymerization and characterized by cyclic voltammetry, IR spectroscopy, electronic spectroelectrochemistry and dual electrode sandwich voltammetry.

Poly(**4-2**) has a band gap of ca. 0.5 eV [19], which is one of the lowest values that has been reported for an organic polymer. However, the charge carrier mobility in poly(**4-2**) was found to be disappointingly low [19], and its intrinsic conductivity of ca.  $10^{-9}$  S cm<sup>-1</sup> is no higher than that of poly(**4-1**) [20], which has a band gap of ca. 0.8 eV. Monomer **4-2** has therefore been copolymerized with EDOT in order to both lower the band gap of the resulting copolymers, and to increase their p-type charge mobilities and intrinsic conductivities.



## 4.2 Experimental

### 4.2.1 Chemicals and Electrodes

Nitrobenzene (Aldrich, 99.93+ AnalaR grade), acetonitrile (Aldrich, 99.93+% Biotech grade), Bu<sub>4</sub>NPF<sub>6</sub> (Fluka, electrochemical grade) and other chemicals were used as received. Working electrodes were either Pt discs ( $5.2 \times 10^{-3}$  cm<sup>2</sup>) sealed in glass or indium/tin oxide coated glass (ITO, 10 Ω/square, Donnelly Corp.).

#### 4.2.2 IR Spectroscopy

Electrochemically undoped polymer films were scraped from ITO electrodes, and pressed into pellets with KBr.

#### 4.2.3 Spectroelectrochemistry

UV-vis-NIR spectra were recorded with a Cary 5E spectrometer. A film of copolymer was deposited onto a narrow slide of ITO coated glass. The slide was then positioned inside a standard 1 cm quartz cuvette together with a Pt wire counter electrode and a reference electrode consisting of a Pt wire in a thin glass tube packed with polypyrrole and Nafion. The potential of this reference electrode was stable during experiments at 0.36 V vs Ag/AgCl. A spectrum of the same cell with a bare ITO electrode was subtracted from all spectra to correct for the absorbance of the cell, ITO electrode and electrolyte solution.

#### 4.2.4 Conductivity measurements

A thin film of poly(4-2) deposited on a Pt disc electrode was coated with gold by vacuum deposition. Dual working electrode experiments were performed with a Pine Instruments RDE4 bi-potentiostat in a four electrode cell containing acetonitrile +0.1 M Bu<sub>4</sub>NPF<sub>6</sub> [21]. The potentials of both the underlying Pt electrode and the gold film were slowly scanned (10 mV s<sup>-1</sup>) relative to the reference electrode, with a 10 mV potential difference maintained between them. The resistance of the polymer film at each potential during the scan was calculated from the current by applying Ohm's law. Film thicknesses were estimated from the charge (integrated to +1.00 V) under the final voltametric scan during film synthesis, by using the relationship of 37 mC cm<sup>-2</sup> per μm established by

scanning electron microscopy for films the homo- and co- polymers. This relationship was not significantly dependent on composition (from pure poly(4-2) to pure PEDOT), and so an average value was used for all compositions.

### 4.3 Results and Discussion

#### 4.3.1 Synthesis of Poly-(2-co-EDOT) Copolymers

Three copolymers with different compositions were synthesized from EDOT : 4-2 molar ratios of 0.5 (CP1), 1 (CP2), and 2.5 (CP3). Films of copolymers were deposited on platinum disk electrodes by cycling the potential between  $-0.5$  and  $1.4$  V at a scan rate of  $100 \text{ mV s}^{-1}$  in nitrobenzene containing  $0.1 \text{ M Bu}_4\text{NFP}_6$ . The solution was degassed with Ar for 5 min before polymer synthesis. Peak currents increased on successive cycles reflecting the formation of a conducting polymer. Copolymer films were rinsed with acetone and dried in air before further experiments.

**Fig. 4.1a** shows typical multisweep cyclic voltammograms of a mixture of 4-2 (2 mM) and EDOT (1 mM). During the first anodic cycle, oxidation waves were observed at peak potentials of  $1.01$  and  $1.26$  V. In the reverse scan, there was a reduction wave at ca.  $0.65$  V with a shoulder at  $-0.16$  V that can be attributed to the undoping of polymeric material deposited on the electrode during the forward scan. Continuous potential cycling between  $-0.5$  and  $1.4$  V resulted in a steady increase in the polymeric waves and formation of a brown film on the Pt electrode. Multisweep voltammograms of CP2 formation are illustrated in Figure 4.1b. During the first cycle, as the potential was scanned forward, oxidation waves were observed at  $1.03$  and  $1.29$  V.



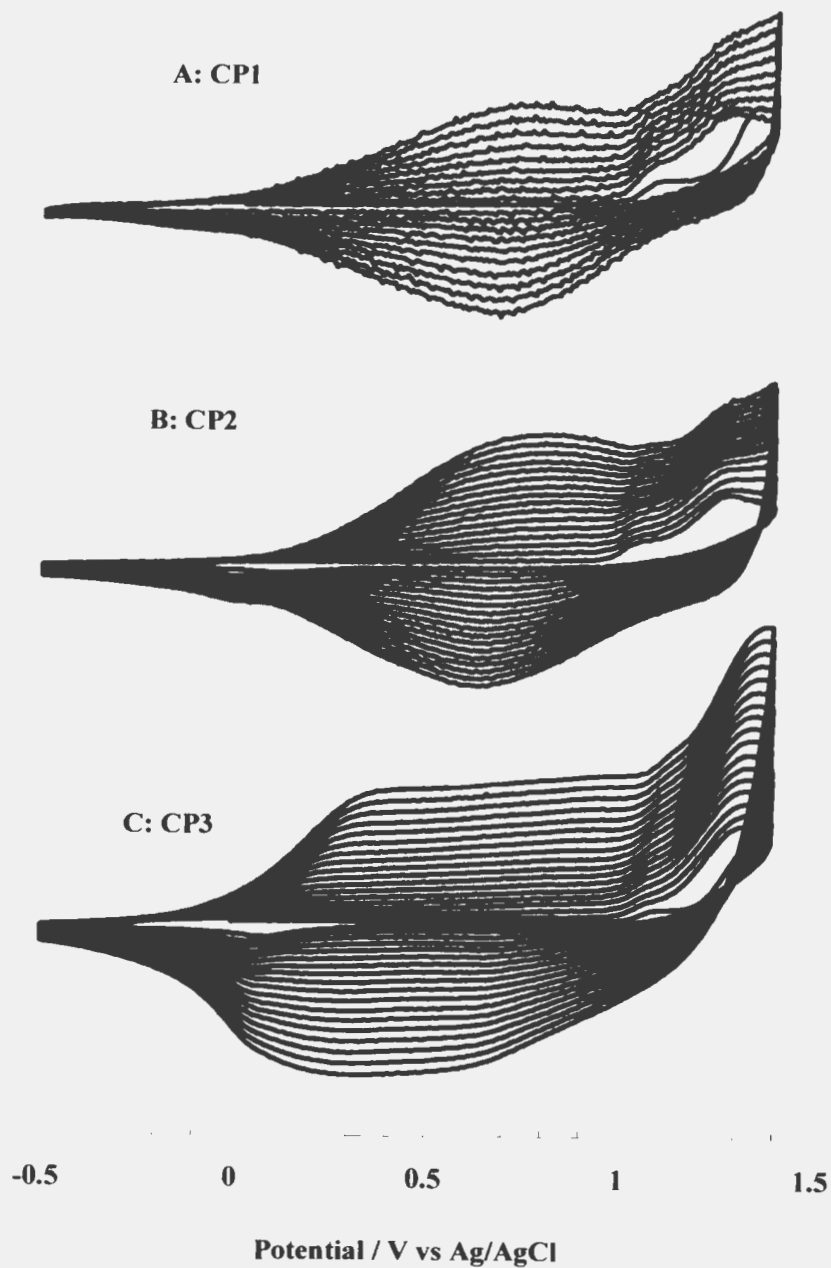


**Fig. 4.1** Multisweep cyclic voltammograms (100 mV/s) at a Pt electrode ( $0.0052 \text{ cm}^2$ ) of mixtures of **4-2** (2 mM) and EDOT (**A** 1 mM; **B** 2 mM; **C** 5 mM) in nitrobenzene containing 0.1 M  $\text{Bu}_4\text{NPF}_6$ . The current has been multiplied by a factor of five in **A** to facilitate comparison. Peak anodic currents on the last cycle shown were 3.0 (**A**), 20 (**B**), and 27  $\mu\text{A}$  (**C**).

In the reverse scan, there was a reduction wave with a main current peak at 0.60 V and a small shoulder at 0.0 V, both of which are due to the undoping of the polymer deposited on the electrode during the forward scan. The reduction current at 0.0 V was higher than observed for CP1, which indicates that more EDOT was incorporated into the copolymer.

Figure 4.1c shows a typical sequence of voltammograms for the electrochemical generation of a CP3 film on the Pt electrode. The broad cathodic and anodic waves, which extend to lower potentials than those for CP1 and CP2, indicate that a large amount of EDOT was incorporated into CP3.

### 4.3.2 IR Spectra

IR spectra of samples of the three copolymers and two homopolymers are shown in **Fig. 4.2**. The most notable differences between the spectra of poly(**4-2**) and PEDOT are the absorbances at 1265 ( $C_{\beta}-C_{\beta}$ ) and 1400  $\text{cm}^{-1}$  ( $C_{\alpha}=C_{\beta}$ ) for poly(**4-2**), the absorbances at 505 and 1060  $\text{cm}^{-1}$  (C-O) [22] for PEDOT, and the lower intensity and broadness of the  $\text{PF}_6^-$  band at ca. 840  $\text{cm}^{-1}$  in the PEDOT spectrum. Monomer **4-2**, also exhibits a  $C_{\alpha}=C_{\beta}$  band at 1400  $\text{cm}^{-1}$  [19], while the corresponding band for PEDOT is at ca. 1500  $\text{cm}^{-1}$  [8,22], making the 1400  $\text{cm}^{-1}$  band a clear marker for **4-2** moieties in the copolymers. Similarly the 1060  $\text{cm}^{-1}$  C-O stretch is a marker for EDOT. The ratio of the absorbance at 1060  $\text{cm}^{-1}$  to that at 1400  $\text{cm}^{-1}$  should provide an approximate measure of the EDOT content of the copolymer. Values of 0.48, 0.41, 0.86, 1.6, and 6.4

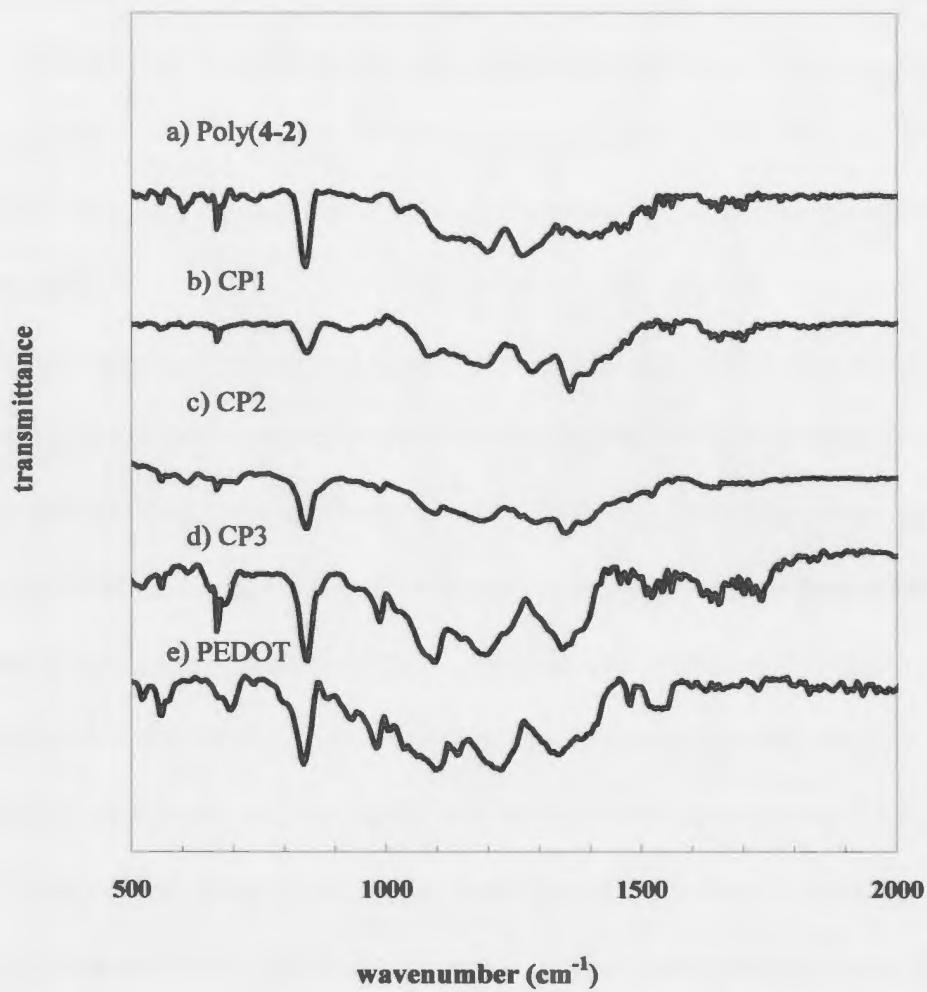


**Fig. 4.2** IR spectra (KBr discs) of a) poly(4-2), b) CP1, c) CP2, d), CP3, e) poly-EDOT

were obtained for poly(4-2), CP1, CP2, CP3, and PEDOT, respectively. These values indicate that the EDOT content of the copolymers increased in the order CP1 < CP2 < CP3, which is consistent with the 4-2 : EDOT ratios used for their synthesis and the electrochemical results. However, use of these ratios as quantitative measures of the copolymer compositions is unwise because copolymerization causes changes in vibrational frequencies that are not taken in to account here. The  $A_{1060}/A_{1400}$  ratio for CP1 indicates that the low EDOT content of this copolymer is not detectable by IR spectroscopy. Indeed the spectrum of this copolymer is not significantly different from that of poly(4-2).

That the copolymers are not simply mixtures of the two homopolymers can be demonstrated by comparing the spectra of the copolymers with weighted sums of the spectra of the homopolymers as illustrated for CP3 in **Fig. 4.3**. The weighting was chosen to match the absorbances at 1060 and 1400  $\text{cm}^{-1}$  in both spectra. There are many notable differences between the spectrum of the copolymer, and the composite spectrum, indicating that 4-2 and EDOT form a true copolymer during electrochemical polymerization of mixed monomer solutions. A similar comparison for CP2 (not shown) revealed similar differences. Most notably there was a shift of a strong band at ca. 1300  $\text{cm}^{-1}$  in the composite spectrum to ca. 1350  $\text{cm}^{-1}$  in the copolymer spectrum, as also seen in **Fig. 4.3**.

### 4.3.3 Electrochemistry of Copolymers

**Fig. 4.4** shows cyclic voltammograms of a CP1 film together with a voltammogram for a poly(4-2) film. The main oxidation and reduction peaks in the

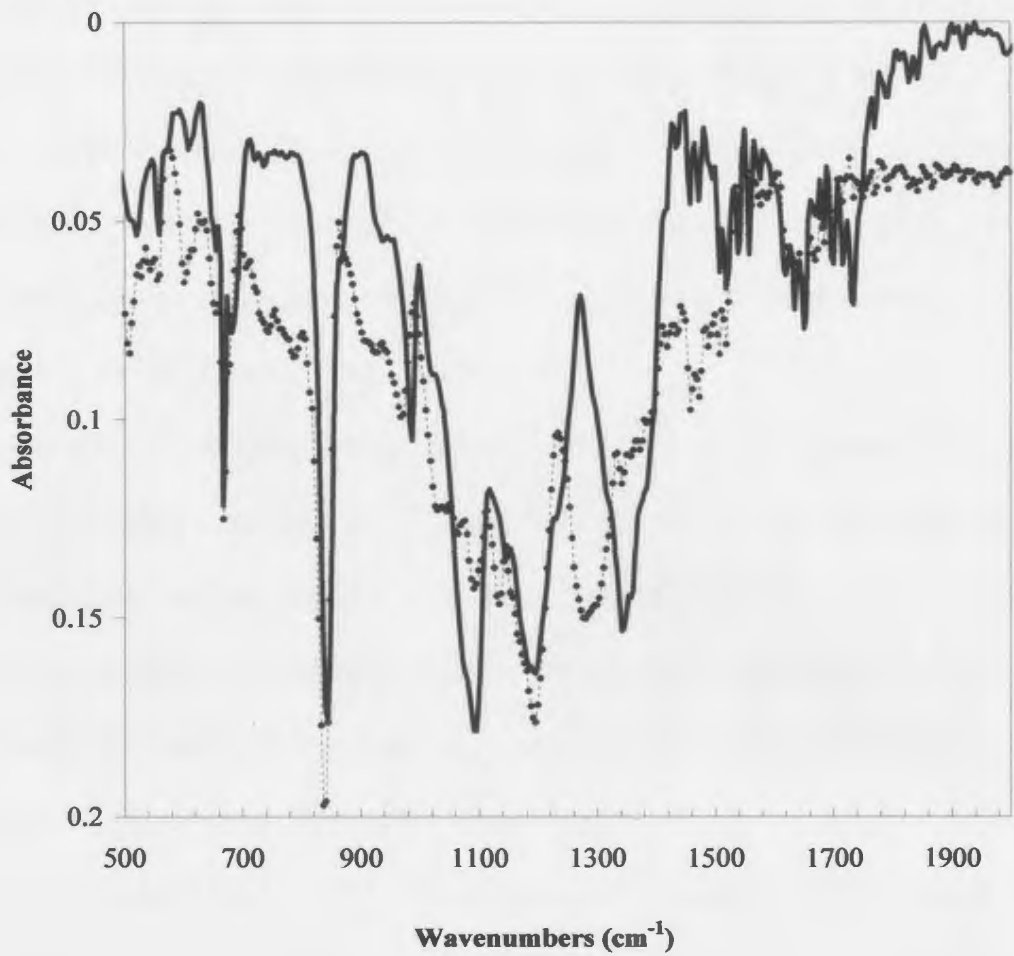


**Fig. 4.3** Comparison of an IR spectrum of CP3 (solid line) with a composite spectrum obtained by adding the spectra (absorbances) of poly(4-2) and PEDOT in a ratio of 0.75:1 (i.e.  $A_{comp} = 0.9A_{poly(4-2)} + 1.2A_{PEDOT}$ ).

voltammogram of CP1 are at similar positions to those of poly(**4-2**), indicating dominance of the electrochemistry by **4-2**, which is the main component of this copolymer. However, the presence of EDOT sites is clearly shown by the prepeaks at 0.00 and 0.50 V, and the enhanced p-doping and undoping charges in the -0.2 to +0.8 V potential region. Because of their high HOMO energies, EDOT rich segments of the copolymer are more easily oxidized than segments rich in **4-2**. It is interesting that cyclic voltammetry reveals the presence of EDOT very clearly, while IR spectroscopy was insensitive to the presence of EDOT in CP1.

The main p-doping/undoping peaks for CP1 were at similar potentials to those for poly(**4-2**), indicating that CP1 had a high **4-2** to EDOT ratio. The slight negative potential shift in the copolymer indicates a small influence of EDOT on the doping of **4-2**-rich segments of the copolymer. A further notable difference between the p-doping/undoping of CP1 and that of poly-**4-2** is the significantly smaller anodic vs. cathodic peak separation, which indicates faster redox kinetics in CP1.

n-Doping/undoping of CP1 occurred at similar potentials as for poly(**4-2**) (Fig. 4.4). The formal potentials (average of the cathodic and anodic peak potentials) were ca. -0.89 V and -0.87 V, respectively. As with p-doping/undoping, the peak separation for n-doping/undoping was smaller for the copolymer film than for poly(**4-2**), indicating faster kinetics. Curiously, the n-doping waves for CP1 were much larger than for poly(**4-2**), even though the main p-doping peaks were approximately the same height, reflecting similar amounts of **4-2** in each film. Since EDOT units are not expected to contribute to n-doping in this potential range [8,16], the smaller currents for poly(**4-2**) would appear to

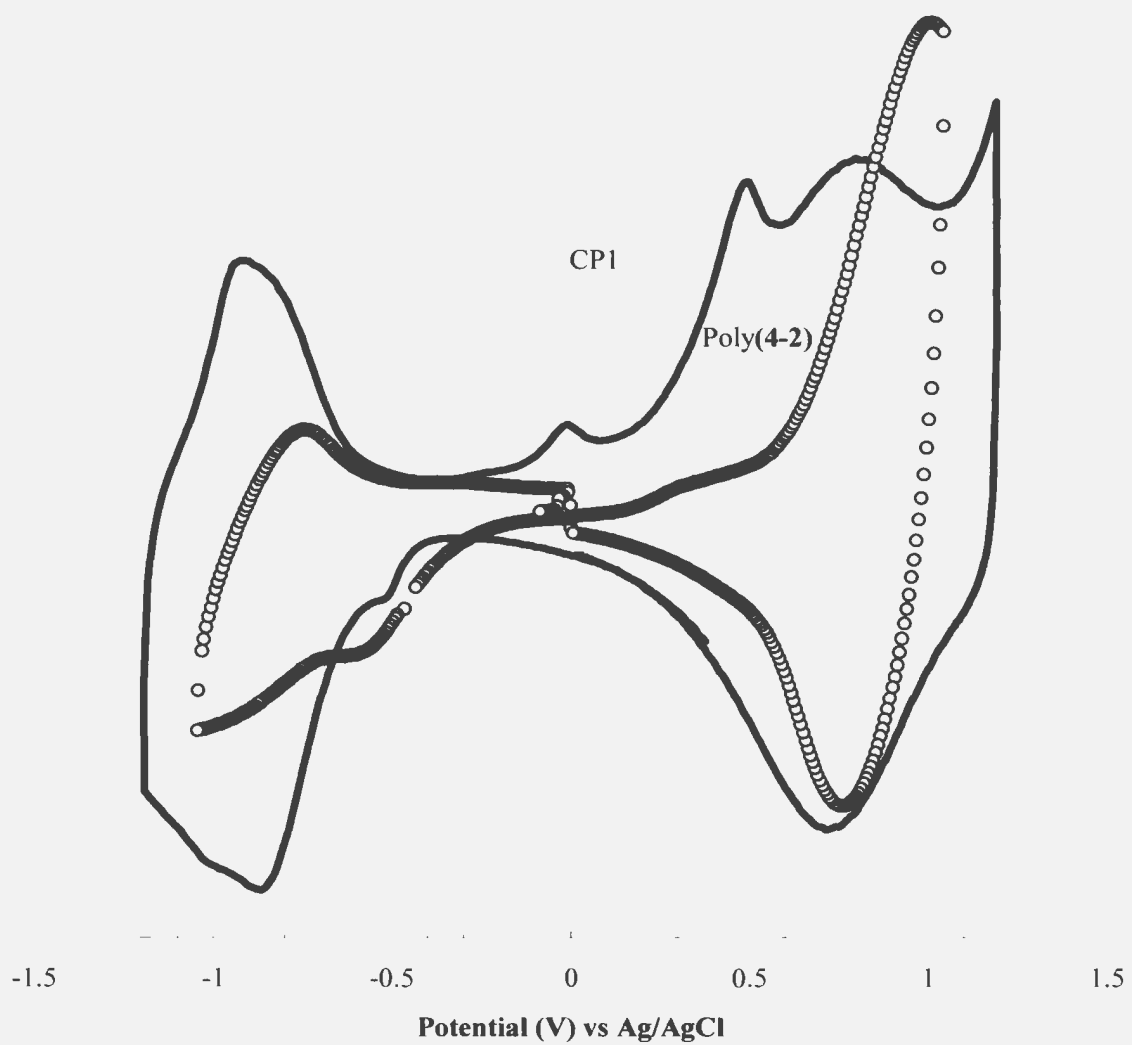


**Fig. 4.4** Cyclic voltammograms at 100 mV/s for films of CP1 and poly(4-2) on Pt in acetonitrile containing 0.1 M  $\text{Bu}_4\text{NFP}_6$

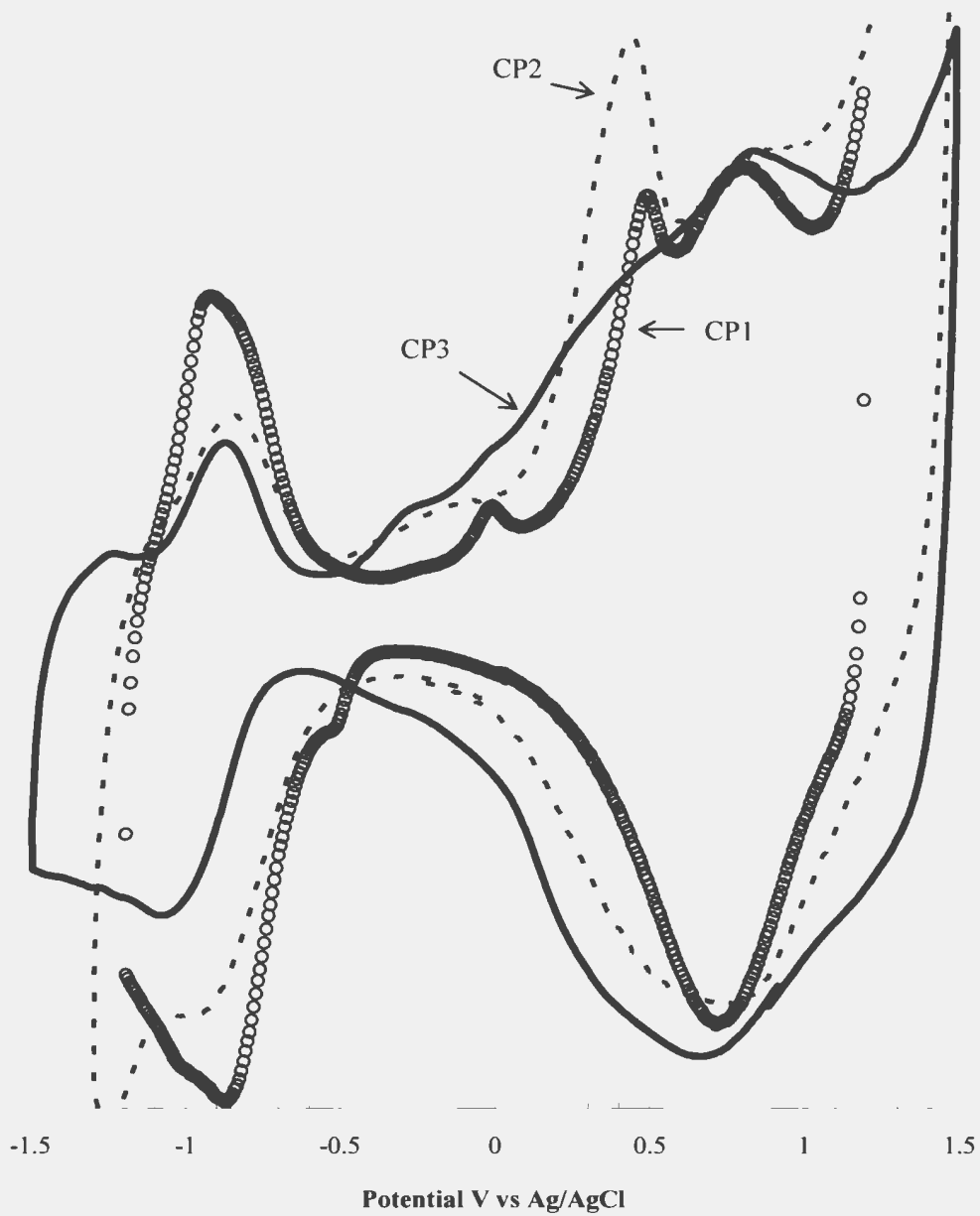


**Fig. 4.5** Comparison of cyclic voltammograms of (a) CP1, (b) CP2 and (c) CP3 in acetonitrile containing 0.1 M  $\text{Bu}_4\text{NPF}_6$  Scan rate: 100 mV/s



be due to kinetic effects. Thus, a small amount of EDOT is seen to dramatically enhance to n-dopability of poly(4-2).

**Fig. 4.5** shows a comparison of the cyclic voltammograms of three different copolymers. The voltammogram of CP2 shows an earlier prepeak than CP1, at ca. -0.1 V, an enhanced prepeak at 0.45 V and enhanced currents in the -0.5 to 0.5 V region, which are all consistent with a higher proportion of electron-rich EDOT. Furthermore, the p-doping/undoping to n-doping/undoping charge ratio is larger for CP2 than for CP1, again indicating a higher EDOT content, since EDOT does not contribute a significant n-doping charge in the potential region investigated [8]. These trends continue from CP2 to CP3, reflecting the even higher EDOT content in CP3. In addition, the anodic prepeaks merge into a broad p-doping envelope, indicating better connectivity of EDOT-rich segments of the copolymer. The positions and shapes of the n-doping/undoping peaks are similar for all three copolymers and poly(4-2), indicating that n-doping sites are localized on the 4-2 moieties. The slight negative shift of the n-doping peak with increasing EDOT content may be kinetic in origin, or may reflect a slight influence due to electron donation from the EDOT moieties.

The electrochemical processes of the copolymers were reversible and very stable over many scans. Both the p-doping and n-doping currents increased linearly with scan rate, indicating fast kinetics and the absence of diffusion controlled processes.

The lowering of the onset of p-doping of the copolymers with increasing EDOT content implies that the presence of EDOT increases the energy of the top of the valance band (HOMO energy). The changes in the onset of n-doping are smaller (except for

CP3), indicating that the bottom of the conduction band (LUMO) is less sensitive to the presence of EDOT. As a consequence, the electrochemical band-gaps of the copolymers are less than that of poly(4-2). The electrochemical band gaps (differences between the onsets of p- and n-doping) are difficult to accurately quantify, but can be estimated to be ca. 0.5 eV for poly(4-2) and ca. 0.3, 0.1, and 0.2 eV, for CP1, CP2, and CP3, respectively.

It has recently been advocated [17] that electrochemical band gaps should be estimated from standard potentials ( $E^0$ ) rather than onset potentials, and this would significantly increase the estimated band gaps for both poly(4-2), and the copolymers (and most of the other polymers reported in the literature). It would also indicate that poly(4-2) and the copolymers have similar band gaps. This would be at odds with the very different voltammograms observed in Fig. 4.5, which clearly indicate that substantial p-doping occurs at lower potentials in the copolymers. The problem here is that voltammetric wave shapes are not Nernstian, and that the voltammetric peaks do not provide accurate estimates of  $E^0$ . This is a general problem in the area of conducting polymers, and in our opinion the use of peak potentials is more misleading than the use of current onsets. We also favour the use of onset potentials because they reflect more accurately the formal potentials of the most easily oxidized or reduced chain segments, which are most representative of the ideal polymer.

#### 4.3.4 Spectroelectrochemical Studies of Copolymers

**Fig. 4.6** shows UV-vis-NIR absorption spectra of undoped CP1, CP2 and CP3 films. These spectra were obtained at controlled potential in a spectroelectrochemical

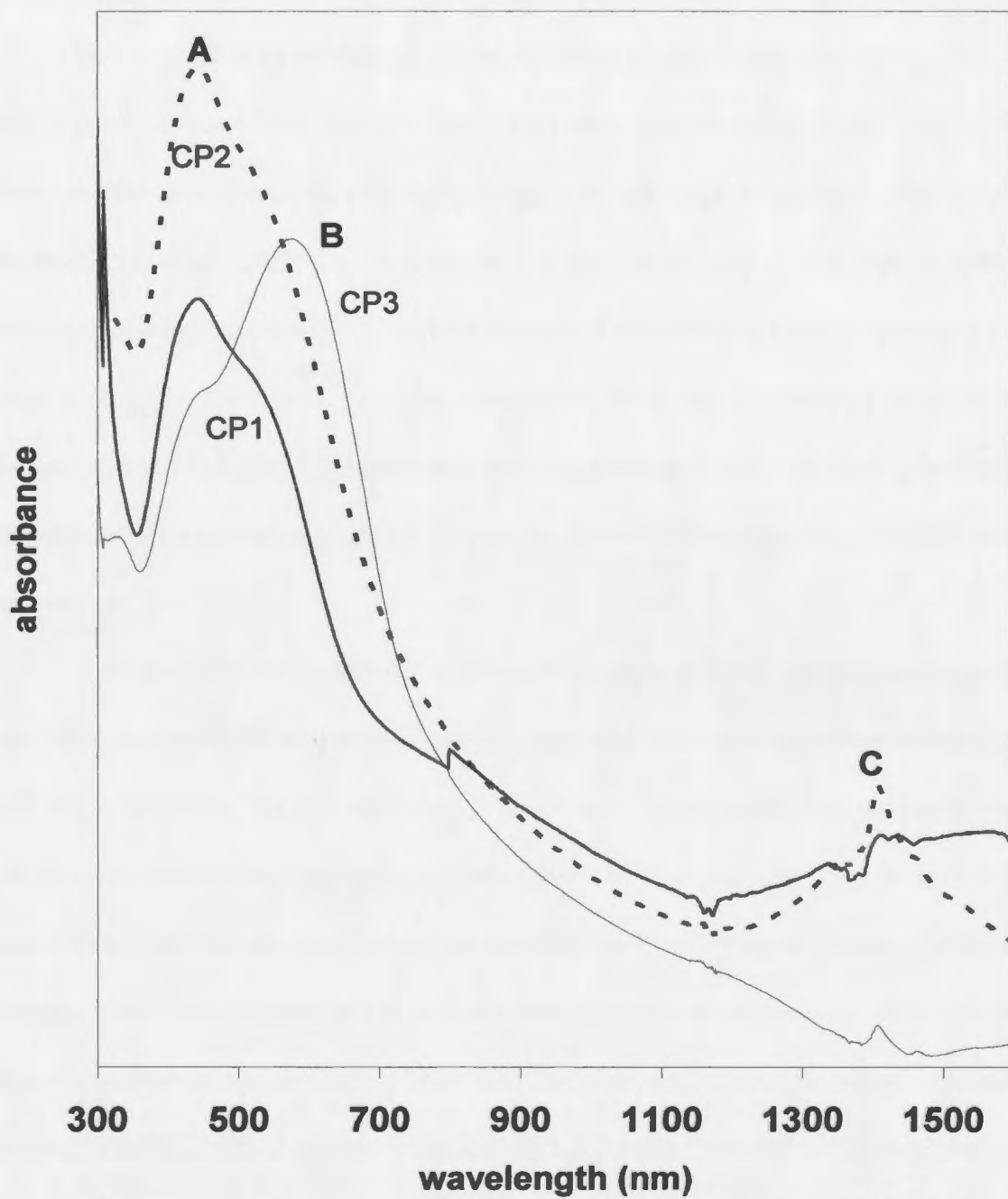


**Fig.4.6** Electronic absorption spectra of CP1, CP2, and CP3 films on ITO electrodes at controlled potential (-0.3 V, -0.3 V, and -0.5 V, respectively) in acetonitrile containing 0.1 M  $\text{Bu}_4\text{NPF}_6$

cell. The potential in each case was set at the current minimum in the voltammogram of the copolymer.

All three spectra exhibit a peak or shoulder at ca. 440 nm and a peak or shoulder at 512 nm (CP1) to 572 (CP3) nm. These have been designated as A and B in the figure. From their relative intensities in the three spectra, and from comparison with spectra of the homopolymers [19,23], peak A appears to arise from units of **4-2** in the copolymer, while peak B appears to arise from EDOT units. The invariance of the wavelength of peak A suggests that this is a localized transition, while the variation of the position of B indicates delocalization. This transition shifts to lower energy as the EDOT content of the copolymer is increased, consistent with an increase in the average oligo-EDOT segment length.

CP1 and CP2 also exhibit a significant absorption band (C) at long wavelengths (ca. 1550 nm and 1400 nm, respectively). There may be a corresponding absorption for CP3 at ca. 1600 nm, but it is too weak to be certain. These bands may be due to HOMO-LUMO transitions or trapped p-type charge carriers. To investigate this, spectra were recorded at more positive potentials, corresponding to p-doping of the copolymers. Results for CP3 are shown in **Fig. 4.7**. As the potential was increased, peak B decreased and a new absorption grew at ca. 1400 nm. The decrease in peak B is consistent with p-doping of EDOT rich segments of the copolymer, while the 1400 nm absorption can be assigned to transitions to interband polaron or bipolaron levels. Similar changes were observed for CP1 and CP2. In all three copolymers, the 440 nm absorbance (peak A) did

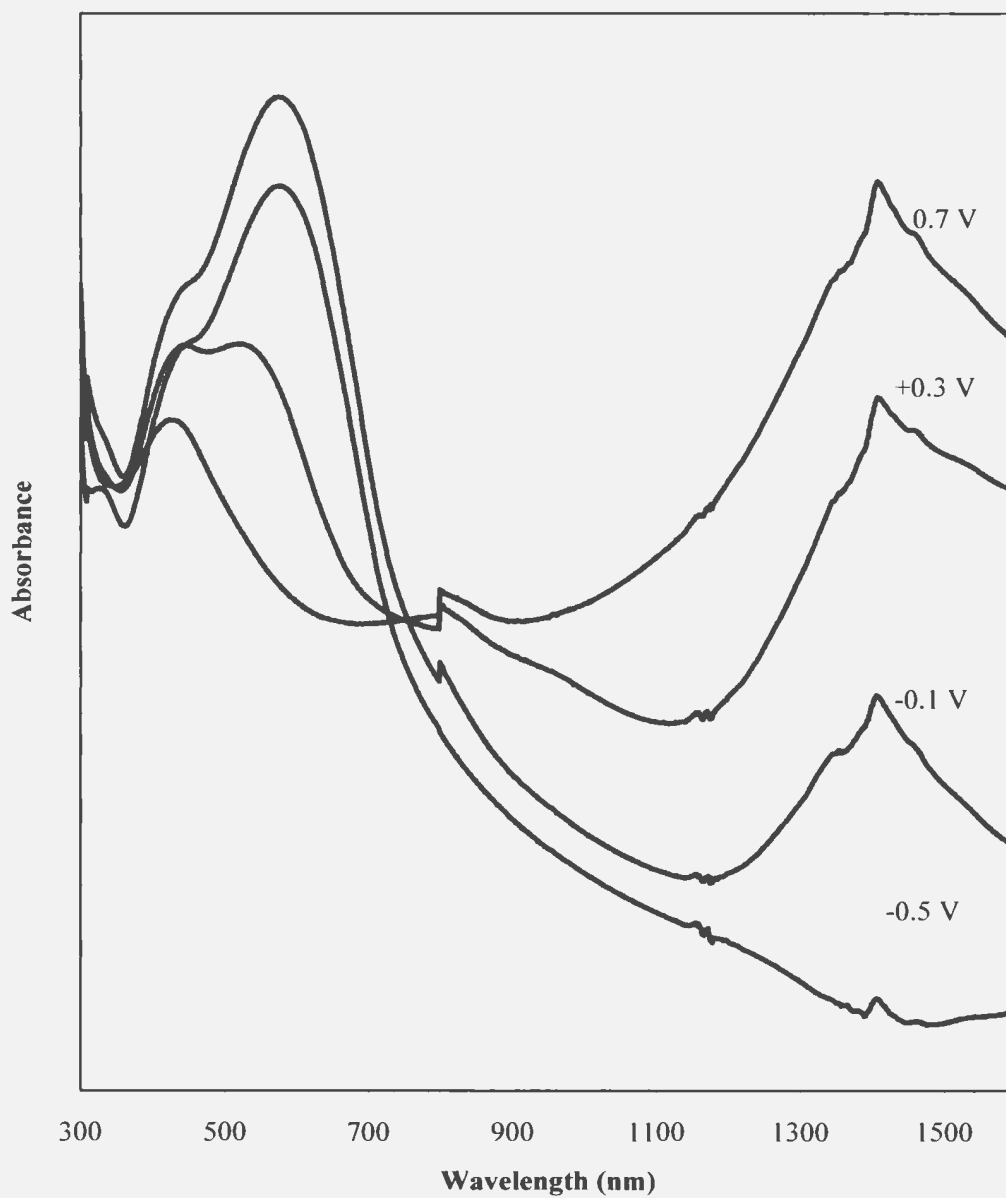


**Fig. 4.7** Electronic absorption spectra of a CP3 film on an ITO electrode at potentials of -0.5, -0.1, +0.3 and +0.7 V in acetonitrile containing 0.1 M  $\text{Bu}_4\text{NFP}_6$ .

not vary significantly in intensity or position with p-doping, indicating that it is due to a transition localized on the bridging double bond of **4-2**.

The spectra in Figs. 4.6 and 4.7 are consistent with the low band gaps indicated by the electrochemistry of the copolymers, since the expected HOMO-LUMO transitions would be below the solvent cut-off of ca. 1600 nm (0.8 eV). Based on the estimated electrochemical band gaps, absorption onsets should be at ca. 4300 nm for CP1, and higher for CP2 and CP3. The absence of clear HOMO-LUMO transitions in the accessible wavelength range provides evidence that these are indeed very low band gap materials.

#### **4.3.5 In Situ Conductivity Measurements**

Electronic conductivities of copolymer films were measured as a function of potential in acetonitrile containing 0.1 M  $\text{Bu}_4\text{NFP}_6$  by using the dual electrode sandwich technique [21]. Maximum p-type conductivities were  $0.034 \pm 0.011 \text{ mS cm}^{-1}$  for CP1,  $0.044 \pm 0.017 \text{ mS cm}^{-1}$  for CP2, and  $0.30 \pm 0.14 \text{ mS cm}^{-1}$  for CP3. These values are averages and standard deviations for two films of each copolymer, and include an estimate of the uncertainty in the film thicknesses. The order of these maximum conductivities, which increase with increasing EDOT content, is consistent with the expectation that p-type conductivity is dominated by the EDOT moieties. This conclusion is further supported by the potential dependencies of the conductivities shown in **Fig. 4.8**. For clarity, and to stress the potential dependence, the data in Fig. 4.8 have been normalized with respect to each film's maximum conductivity. It can be seen that the

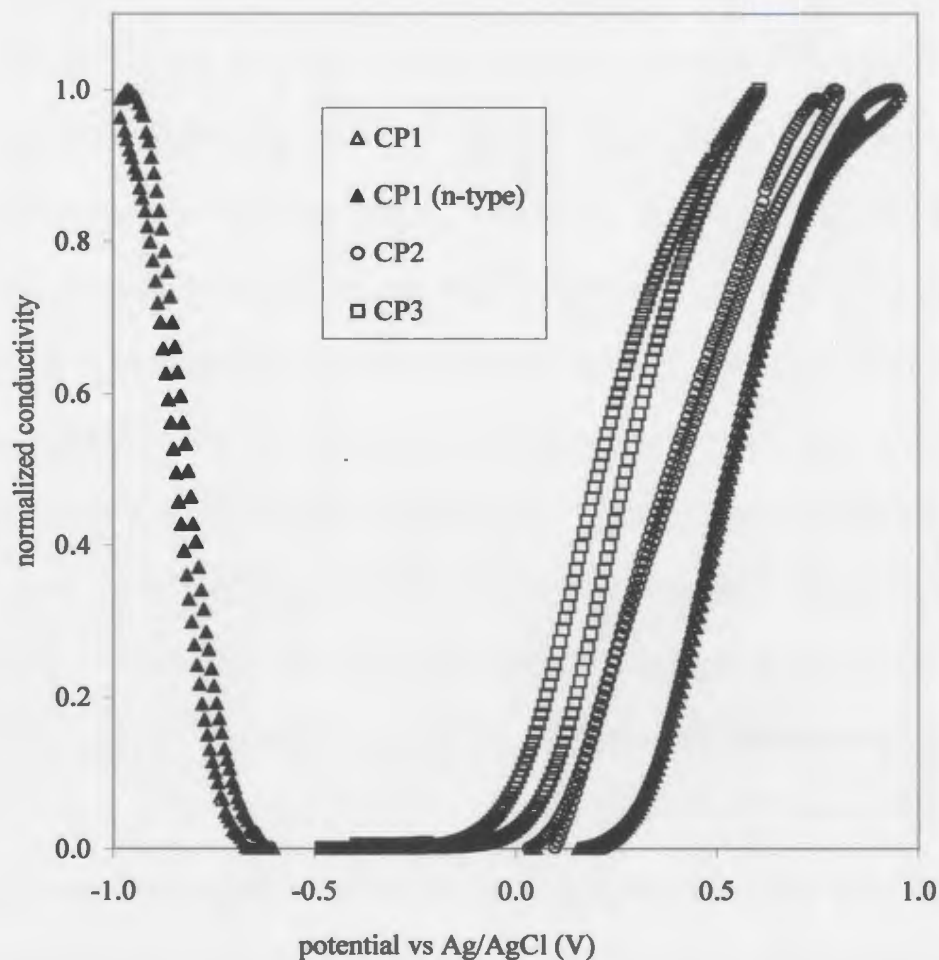


**Fig.4.8** Normalized conductivities of copolymer films as a function of potential in acetonitrile containing 0.1 M  $\text{Bu}_4\text{NFP}_6$ . Both p-type (potentials  $> -0.3$  V), and n-type (potentials  $< -0.5$  V) conductivities were observed for CP1 (open and solid triangles, respectively), while only p-type conductivity was observed for CP2 (open squares) and CP3 (open circles).

onset of p-type conductivity moves to lower potentials as the EDOT content of the copolymer is increased, again indicating dominance by these moieties.

The p-type conductivities of the copolymers are higher than the maximum value of  $14 \mu\text{S cm}^{-1}$  reported for the poly(**4-2**) homopolymer [19], but much lower than the p-type conductivity of  $0.6 \text{ S cm}^{-1}$  measured for PEDOT by the same method [8]. Since the doping levels of all three copolymers and two homopolymers are similar, the mobility of charge carriers must depend strongly on the EDOT content of the (co)polymer. Clearly, interruption of EDOT conjugation by **4-2** severely restricts charge carrier mobility. This is not surprising in light of the poor matching of the HOMO energies of the two monomer units. However, the effect is more pronounced than was observed in copolymers of EDOT with **4-1**. The difference may be that **4-2** also causes branching of the copolymer and gives cross-conjugated linkages with poor conjugation through its central double bond.

Only one of the copolymer films tested exhibited measurable n-type conductivity and this data is included in Fig. 4.8. It has been normalized with respect to the maximum value of  $2.0 \mu\text{S cm}^{-1}$ . This is close to the maximum n-type conductivity of  $1.2 \mu\text{S cm}^{-1}$  reported for the poly(**4-2**) homopolymer, indicating dominance of n-type conductivity by **4-2** [19]. Localization of the n-type charge carriers on the **4-2** moieties is responsible for the low n-type conductivity relative to the p-type conductivity [19], which was  $34 \mu\text{S cm}^{-1}$  for this particular copolymer film. n-Type conductivities for the other copolymers may have been as high as  $1 \mu\text{S cm}^{-1}$ , but could not be measured due to large background currents.



#### 4.4 Conclusions

Copolymerization of **4-2** with EDOT produces materials with reduced electrochemical band gaps, enhanced conductivities and faster electrochemical kinetics. However, poor conjugation of the resulting materials leads to low charge carrier mobilities and conductivities relative to the poly-EDOT homopolymer. The donor-acceptor method for band gap reduction is again shown to be effective, but at the expense of charge carrier mobility. Thus, the expected gains in intrinsic conductivity with band gap reduction have not been realized. This is consistent with theoretical analysis which indicates that the use of donor and acceptor units to decrease the band gap of polythiophenes will lead to decreased delocalization of orbitals and lower charge carrier mobilities [15,16]. It is not clear how, or whether, this limitation can be resolved.

#### Acknowledgements

This work was supported by the Natural Sciences and Engineering Research Council of Canada and Memorial University.

#### References

1. Hall, N. *Chem. Commun.* **2003**, 1.
2. Shirakawa, H., *Angew. Chem. Int. Ed. Engl.* **2001**, *40*, 2574.
3. Nalwa, H. S. Ed., *Handbook of Advanced Functional Molecules and Polymers*, **2001**, vol. 1-4 (Gordon & Breach).
4. MacDiarmid, A.G. *Angew. Chem. Int. Ed.* **2001**, *40*, 2581.
5. Heeger, A. J. *Angew. Chem. Int. Ed.* **2001**, *40*, 2591.

6. Groenendaal, L.; Jonas, F.; Freitag, D.; Pielartzik, H.; Reynolds, J. R. *Advan. Mater.* **2000**, *12*, 481.
7. Groenendaal, L.; Zotti, G.; Aubert, P. H.; Waybright, S. M.; Reynolds, J. R. *Advan. Mater.* **2003**, *15*, 855.
8. Huang, H.; Pickup, P. G. *Chem. Mater.* **1998**, *10*, 2212.
9. Rault-Berthelot, J.; Raoult, E. *Adv. Mat. Opt. Elect.* **2000**, *10*, 267.
10. Rault-Berthelot, J.; Raoult, E.; Le Floch, F. *J. Electroanal. Chem.* **2003**, *546*, 29.
11. Akoudad S.; Roncali, J. *Chem. Commun.* **1998**, 2081.
12. van Mullekom, H. A. M.; Vekemans, J. A. J. M.; Havinga, E. E.; Meijer, E. W. *Mater. Sci. Eng.* **2001**, *32*, 1.
13. Roncali, J. *Chem. Rev.* **1997**, *97*, 173.
14. Pomerantz, M. in *Handbook of Conducting Polymers*, 2nd ed., T.A. Skotheim, R.L. Elsenbaumer, and J.R. Reynolds, Eds. (Marcel Dekker, New York, **1998**), pp. 277-310.
15. Salzner, U. *J. Phys. Chem. B.* **2002**, *106*, 9214.
16. Salzner U.; Kose, M. E.; *J. Phys. Chem. B.* **2002**, *106*, 9221.
17. Berlin, A.; Zotti, G.; Zecchin, S.; Schiavon, G. ; Vercelli, B. ; Zanelli, A. *Chem. Mater.* **2004**, *16*, 3667.
18. Ebron, V. H.; Michelini, L. I.; Miles, R. B.; Loveday, D.; Mudigonda, D.; Ferraris, J. P. *Polymeric Materials: Science and Engineering* **2002**, *86*, 4.
19. Loganathan, K.; Cammisa, E. G.; Myron, B. D.; Pickup, P. G. *Chem. Mater.* **2003**, *15*, 1918.

20. Huang, H.; Pickup, P. G. *Acta Polymerica* **1997**, *48*, 455.
21. Pickup, P. G.; Kutner, W.; Leidner, C.R.; Murray, R.W. *J. Amer. Chem. Soc.* **1984**, *106*, 1991.
22. Kvarnstrom, C.; Neugebauer, H.; Blomquist, S.; Ahonen, H. J.; Kankare, J.; Ivaska, A. *Electrochim. Acta.* **1999**, *44*, 2739.
23. Dietrich, M.; Heinze, J.; Heywang, G.; Jonas, F. *J. Electroanal. Chem.* **1994**, *369*, 87.

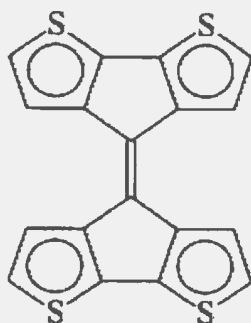
## *Chapter 5*

### **The Influence of Electrode Rotation on Morphologies and Conductivities of Poly-( $\Delta^{4,4'}$ -Dicyclopenta[2,1-b:3,4-b']dithiophene)**

Electrochemical polymerization has become a widely used procedure for quick generation of conducting polymers [1]. Many investigations have been performed on the mechanism of the electrochemical polymerization and deposition of thiophene based conducting polymers [2-6]. Techniques such as voltammetry [7-18], chronoamperometry [19-21], impedance [8, 10], microscopy [22-24], and spectroscopy [25-27] have been applied for such investigations. Studies on interfacial reactions [7-8, 28-29] have shown that polymer deposition usually takes place through two simultaneous processes. They are propagation at the ends of polymer chains in the polymer matrix and the precipitation of oligomeric/polymeric species from solution onto the electrode surface.

The nature of conducting polymer films plays a major role in materials selection for many conducting polymer based applications. For example porous materials are most suitable for applications in batteries and electrocatalysis, while compact films would generally be preferable in analytical applications (e.g. ion selective sensors) [1, 8]. Tuning electrical properties such as conductivity via the morphology of electrodeposited conducting polymers is an emerging research area and such investigations have been successful for poly(3-methylthiophene) [8].

The rotating disk voltammetric method has been employed to control the morphologies of polythiophene and poly(3-methylthiophene). Otero and coworkers [7] have proposed a model of interfacial reactions by studying electrodeposition of polythiophene under stationary and stirred conditions. Zhao and Pickup [8] have performed such investigations with poly(3-methylthiophene) and found that precipitation causes uneven film deposition under stationary conditions. Their study has also proved that at higher electrode rotation rates, propagation at the ends of polymer chains in the polymer matrix leads to a more compact film. Electrochemical impedance spectroscopy was used to probe the effect of electrode rotation on the morphology and conductivity of poly(3-methylthiophene) [8]. However, investigations on thiophene derivatives have also shown that the deposition mechanism can depend on the nature of the monomer [8]. This prompted us to investigate the interfacial reactions during polymerization of bridged bithiophene (**5-1**) which can cross link conjugated systems in a well defined way with conjugation in two dimensions.



**5-1**

Similar investigations were performed on copolymers of **5-1** with EDOT, and the effect of working electrode rotation, during the polymer growth, on the conductivities of poly(**5-1**) and its copolymers are reported in this chapter.

## **5.1 Effect of Electrode Rotation on Polymer Growth**

### **5.1.1 Electrochemical Polymerization of Dicyclopenta[2,1-*b*:3,4-*b'*]dithiophene**

**Figure 5.1** shows a comparison of multisweep cyclic voltammograms for the electrochemical polymerizations of dicyclopenta[2,1-*b*:3,4-*b'*]dithiophene (**5-1**) in nitrobenzene containing 0.1 M Bu<sub>4</sub>NPF<sub>6</sub> at electrode rotation rates of 0 rpm, 400 rpm, 800 rpm and 1200 rpm. Experiments were carried out at a scan rate of 100 mV s<sup>-1</sup> and a constant polymerization time was maintained to see the effect of electrode rotation rate on polymer growth. Continuous potential scanning between 0 and 1.5 V resulted in a steady increase in the anodic peak current at ca. 0.8 V in all four experiments.

### **5.1.2 Morphology of Polymer Films**

**Figure 5.2** shows scanning electron microscopy images of poly-(**5-1**) films prepared at stationary (a) and rotating [(b) 400, (c) 800 and (d) 1400 rpm] platinum electrodes in nitrobenzene. Polymerization conditions such as oxidation potential,

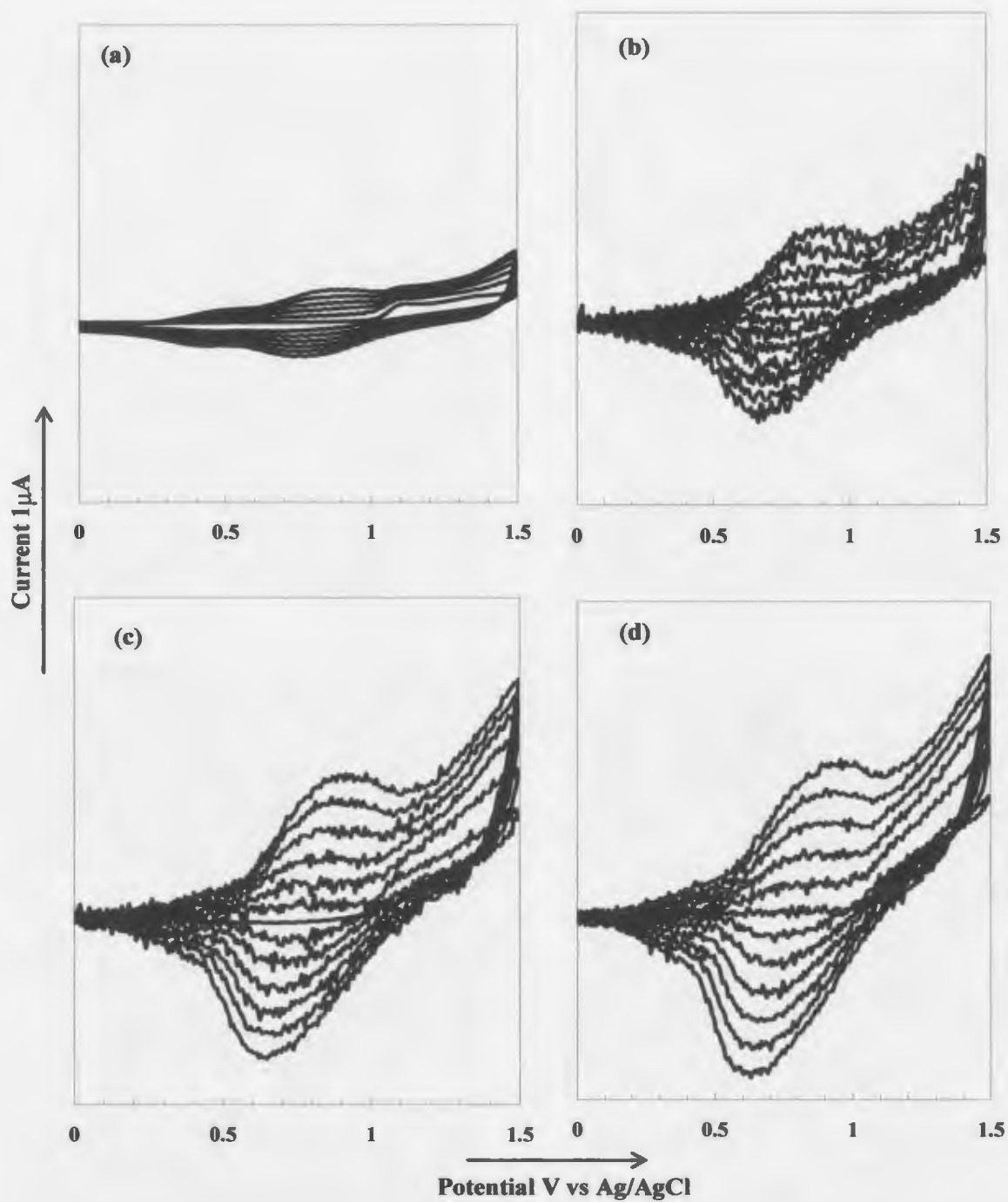


**Fig. 5.1** Repetitive sweep polymerizations of 2 mM 5-1 at rotation rates of (a) 0 rpm, (b) 400 rpm, (c) 800 rpm, (d) 1200 rpm

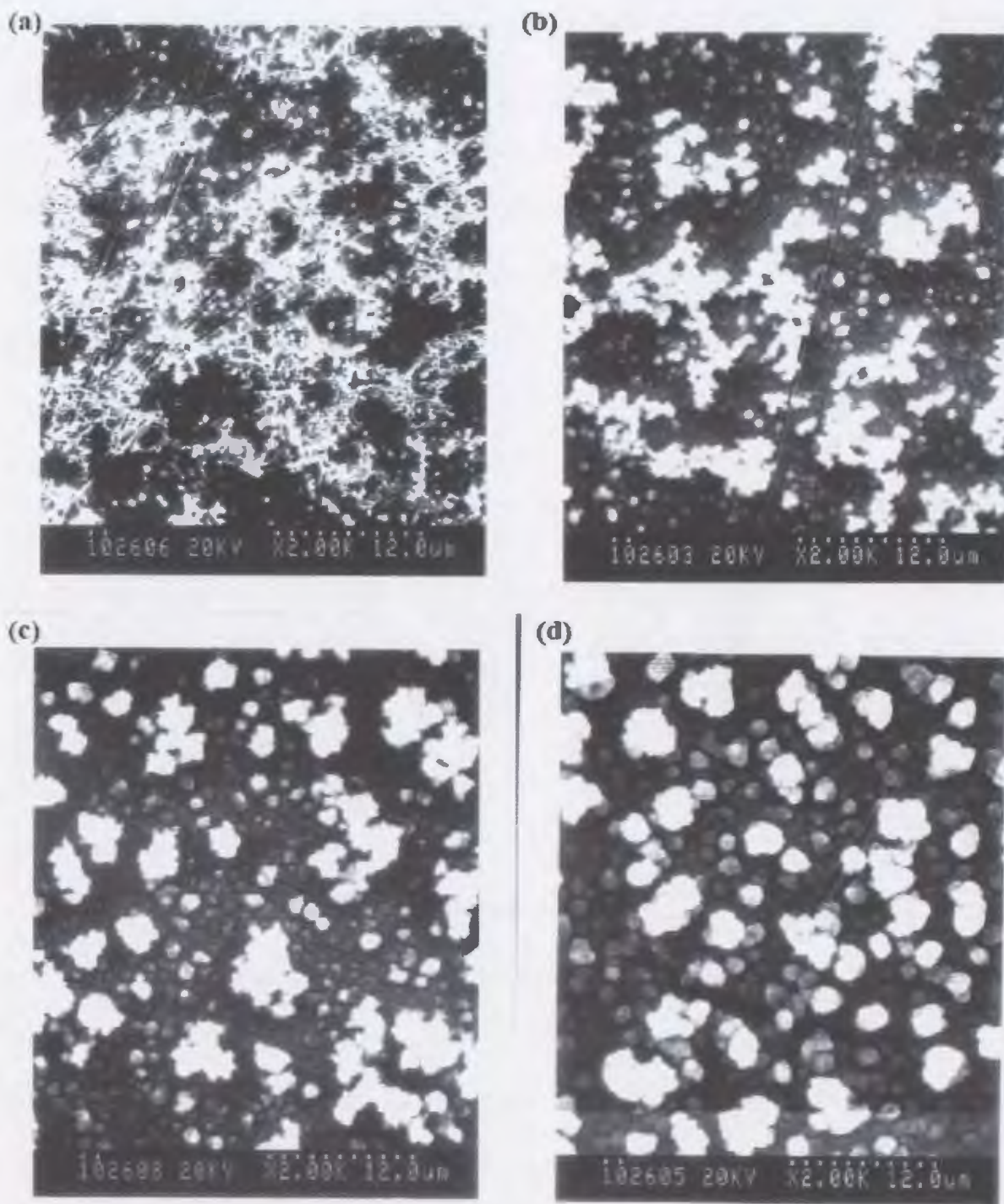


**Fig. 5.2** Scanning electron micrographs of poly-(5-1) films deposited on stationary (a) or rotating [(b) 400 rpm (c) 800 rpm (d) 1200 rpm] Pt electrodes



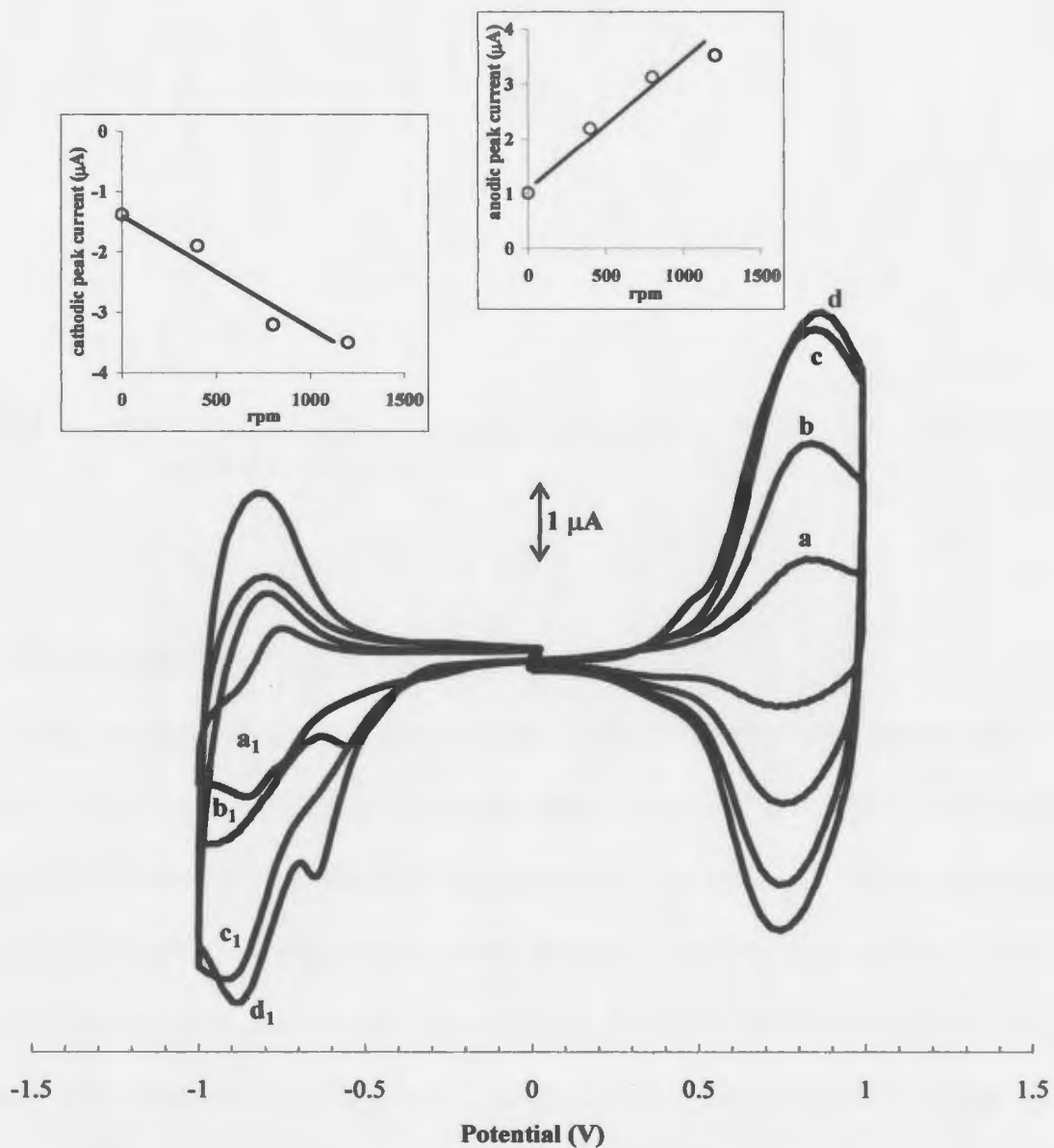
electrolyte concentration and polymerization time were kept constant for all the films to see dominance of the effect of electrode rotation on structural variations.

Image (a) shows a web-like *fibrillar* structure with some fine *globular* regions. Image (b) shows less abundant, but denser *fibrillar* structures and *globular* structures with larger particle sizes. The transition from *fibrillar* to *globular* structure is more obvious when comparing images (b) and (c). Image (d) shows the largest globular structures with no fibrils. The diameter of the *globular* particles of poly-(5-1), synthesized by electrode rotation at 1200 rpm range from 1.5  $\mu\text{m}$  to 3.5  $\mu\text{m}$ . Each particle appears to be an aggregation of smaller spheres. Based on these morphologies (shown in Fig 5.2 a-d), poly-(5-1) will be named as poly-(0); poly-(400); poly-(800) and poly-(1200) in the following sections.

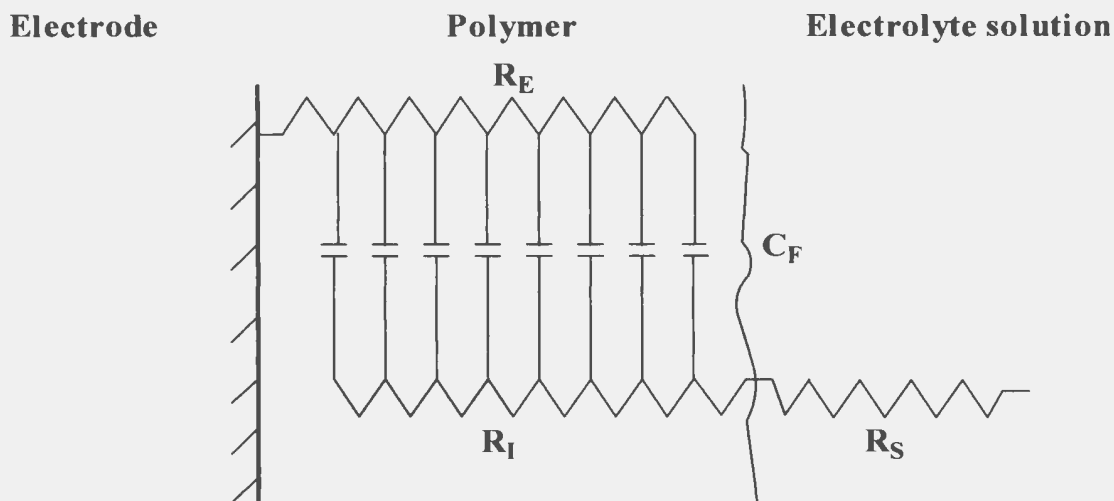
## 5.2 Characterization of the Films

### 5.2.1 Cyclic Voltammetry

**Fig. 5.3** shows cyclic voltammograms in monomer free  $\text{Bu}_4\text{NPF}_6\text{-CH}_3\text{CN}$  for the poly(5-1) films prepared in the experiments in Fig. 5.1. p-Doping of the polymer films was observed as reversible waves in the 0 to +1.0 V region, while n-doping appeared as broader and less reversible waves in the 0 to -1.0 V region. Peak currents for both waves increased approximately linearly with increasing electrode rotation rate (insets in Fig. 5.3). The formal potentials for the main p-doping and n-doping processes were ca. + 0.8 V and - 0.85 V, respectively. The doped polymer films were preserved under a nitrogen atmosphere for impedance analyses.



**Fig. 5.3** Cyclic voltammograms in acetonitrile containing 0.1 M  $\text{Bu}_4\text{NPF}_6$  of the poly-(5-1) films prepared in the polymerizations depicted in Fig. 5.1. Insets show variations of cathodic and anodic peak currents with electrode rotation rates.



**Scheme 5.1** Circuit for a finite transmission line in series with an uncompensated solution resistance

### 5.2.2 Electrochemical Impedance Spectroscopy

**Fig. 5.4** illustrates impedance plots (at 0.8 V) for platinum electrodes coated with poly-(5-1), and corresponding to the p-doped films shown in Fig 5.3, in 0.1 M  $\text{Bu}_4\text{NPF}_6$ -acetonitrile solution under a nitrogen atmosphere. The poly-(0), poly-(400), poly-(800) and poly-(1200) films all exhibited the same constant high frequency resistance ( $R_h$ ) but their low frequency resistances ( $R_l$ ) were different. From the differences between the low frequency intercepts and high frequency intercepts (illustrated as  $R_l$  and  $R_h$  in Fig. 5.4), resistances ( $3(R_l - R_h)$ ) for poly-(0), poly-(400), poly-(800) and poly-(1200) were calculated to be 756, 726, 351, and 210  $\Omega$ , respectively.

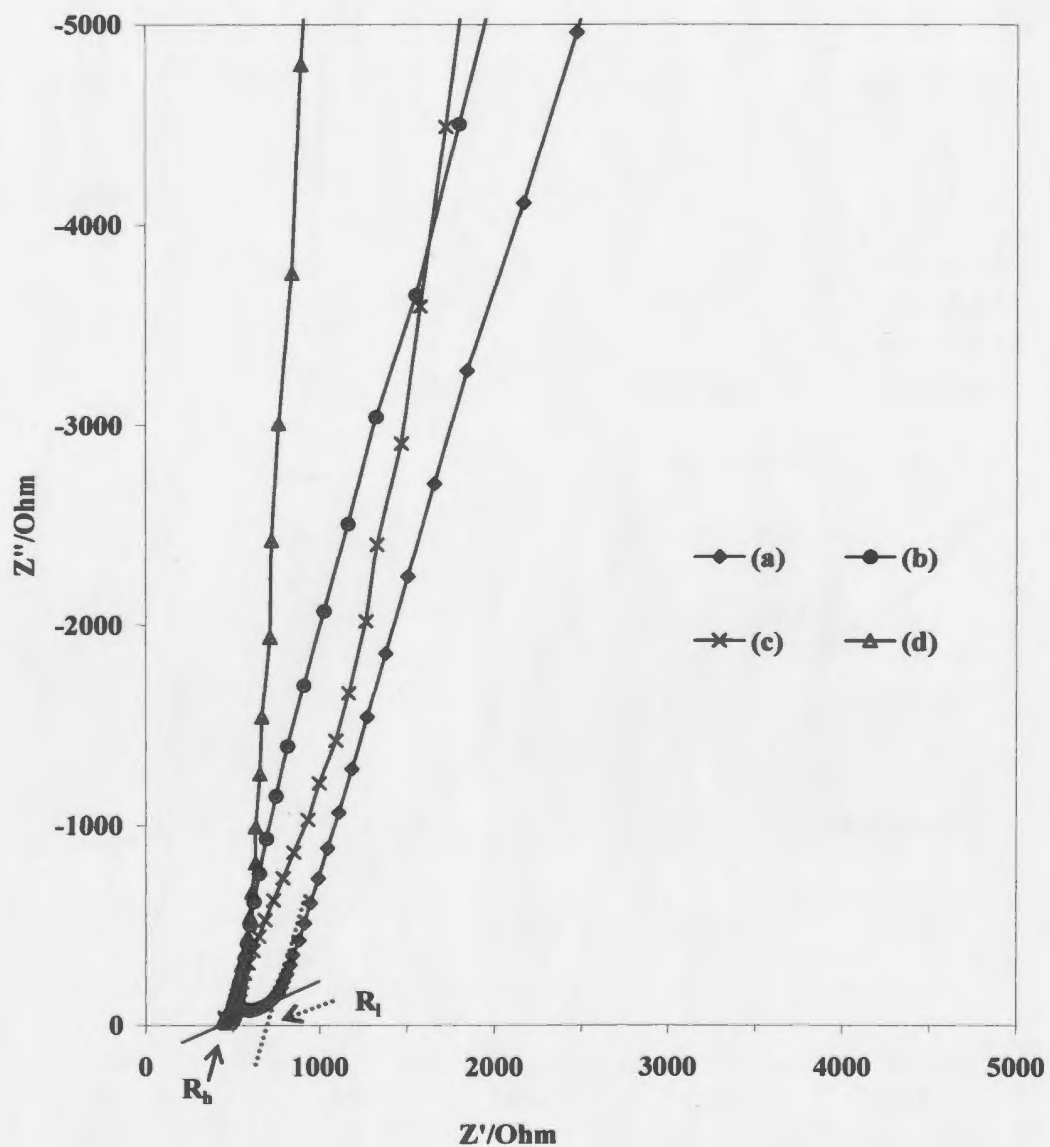


Fig. 5.4. Impedance plots for Pt electrodes coated with poly(5-1) in 0.1 M  $\text{Bu}_4\text{NPF}_6\text{-CH}_3\text{CN}$ . Film thicknesses: (a) poly-(0), 0.3  $\mu\text{m}$ ; (b) poly-(400), 0.8  $\mu\text{m}$ ; (c) poly-(800), 1.3  $\mu\text{m}$ ; (d) poly-(1200), 1.4  $\mu\text{m}$ .

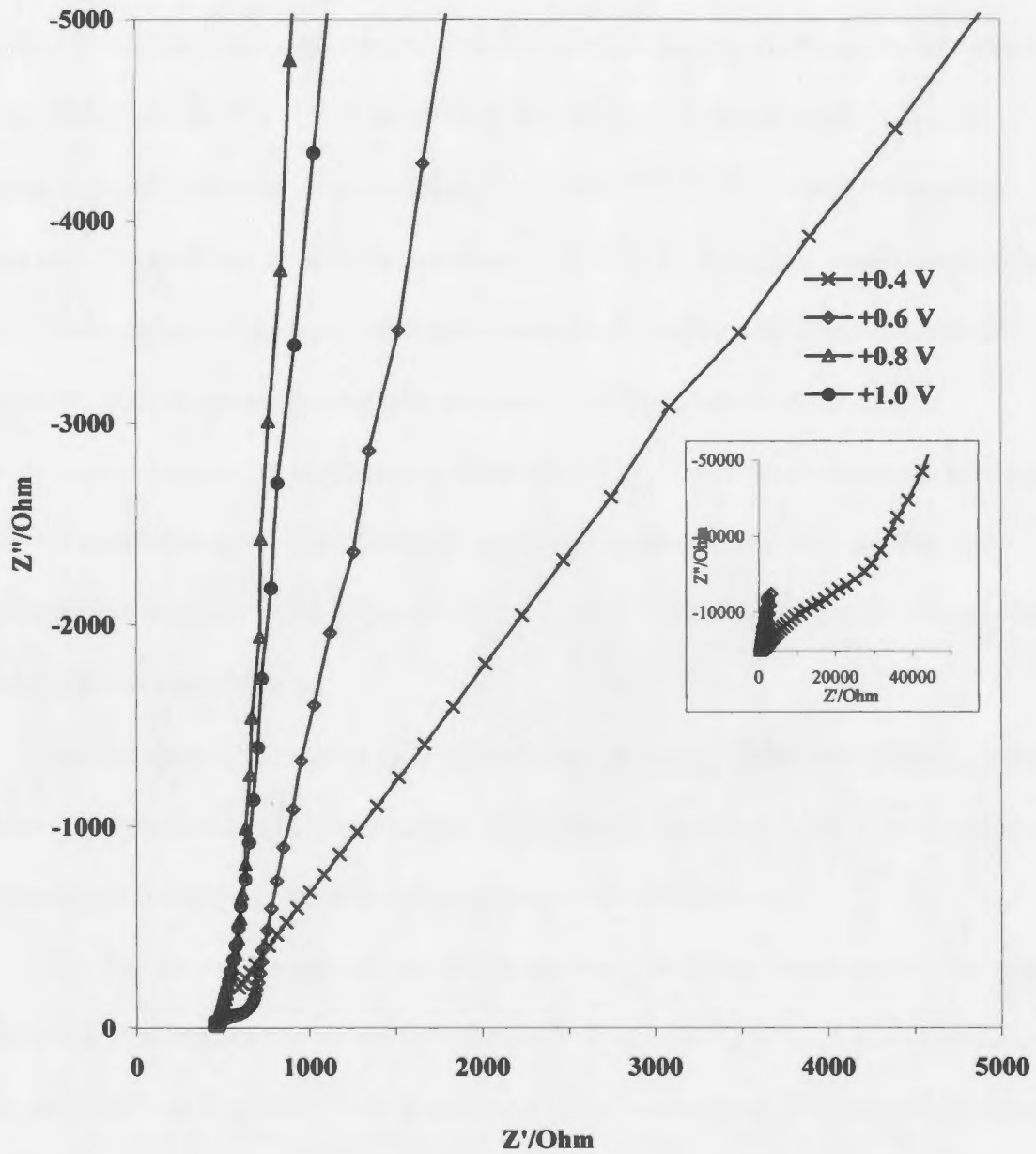


Fig. 5.5 Impedances of p-doped poly-(1200) in 0.1 M  $\text{Bu}_4\text{NPF}_6$  acetonitrile solution

**Fig. 5.5** shows impedance plots at various p-doping potentials for poly-(1200), a polymer film synthesized under hydrodynamic conditions (at a working electrode rotation rate of 1200 rpm). At 0.4 V, the impedance plot shows a partial semicircle in the Warburg type ( $45^\circ$ ) region which extends to ca. 30,000  $\Omega$  followed by a steeper low frequency region. When heavily doped (from +0.6 V to +1.0 V), the response exhibits a ca.  $45^\circ$  Warburg type region in addition to a nearly vertical low frequency capacitive impedance. This response is generally observed for a film behaving as a finite transmission line which is illustrated in **Scheme 5.1** [9]. From the differences between the low frequency intercepts and high frequency intercepts of the plots in Fig. 5.5, resistances for the poly-(1200) film at +0.6 V, +0.8 V, +1.0 V were calculated to be 666, 246 and 189  $\Omega$ , respectively.

The circuit in Scheme 5.1 should give a  $45^\circ$  Warburg type response and a low frequency (vertical) limiting capacitance. Deviations from the  $45^\circ$  and vertical slopes in the experimental data are due to inhomogeneity of the films [10].

**Fig. 5.6** shows capacitance vs. real impedance plots that correspond to the data in Fig 5.4. The real impedance for poly-(0) was slightly higher than those obtained for poly-(400), poly-(800) and poly-(1200). In addition the low frequency (limiting) capacitance increased as we see from films poly-(0) to poly-(1200). **Fig. 5.7** shows capacitances vs. real impedances for n-doped poly-(400) and poly-(1200) films. Poly-(1200) exhibited a higher low frequency (limiting) capacitance than poly-(400).

**Fig. 5.8** shows estimated conductivities (*in situ*) as a function of potential for the poly-(1200) film. The p-type conductivity was high at +1.0 V and it decreased as the

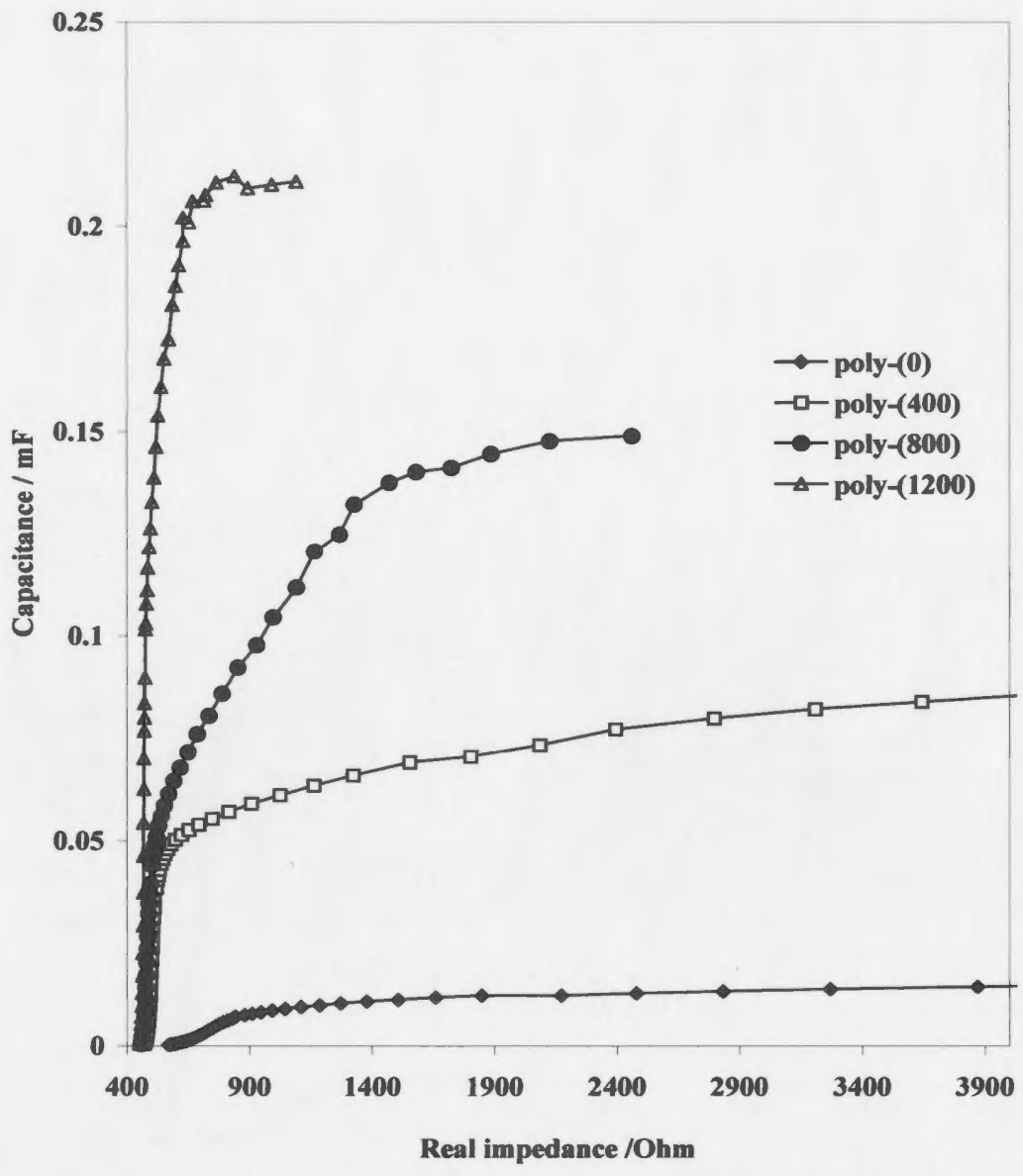


Fig. 5.6 Capacitance vs real impedance plots for p-doped (+0.8 V) poly-(5-1) films.

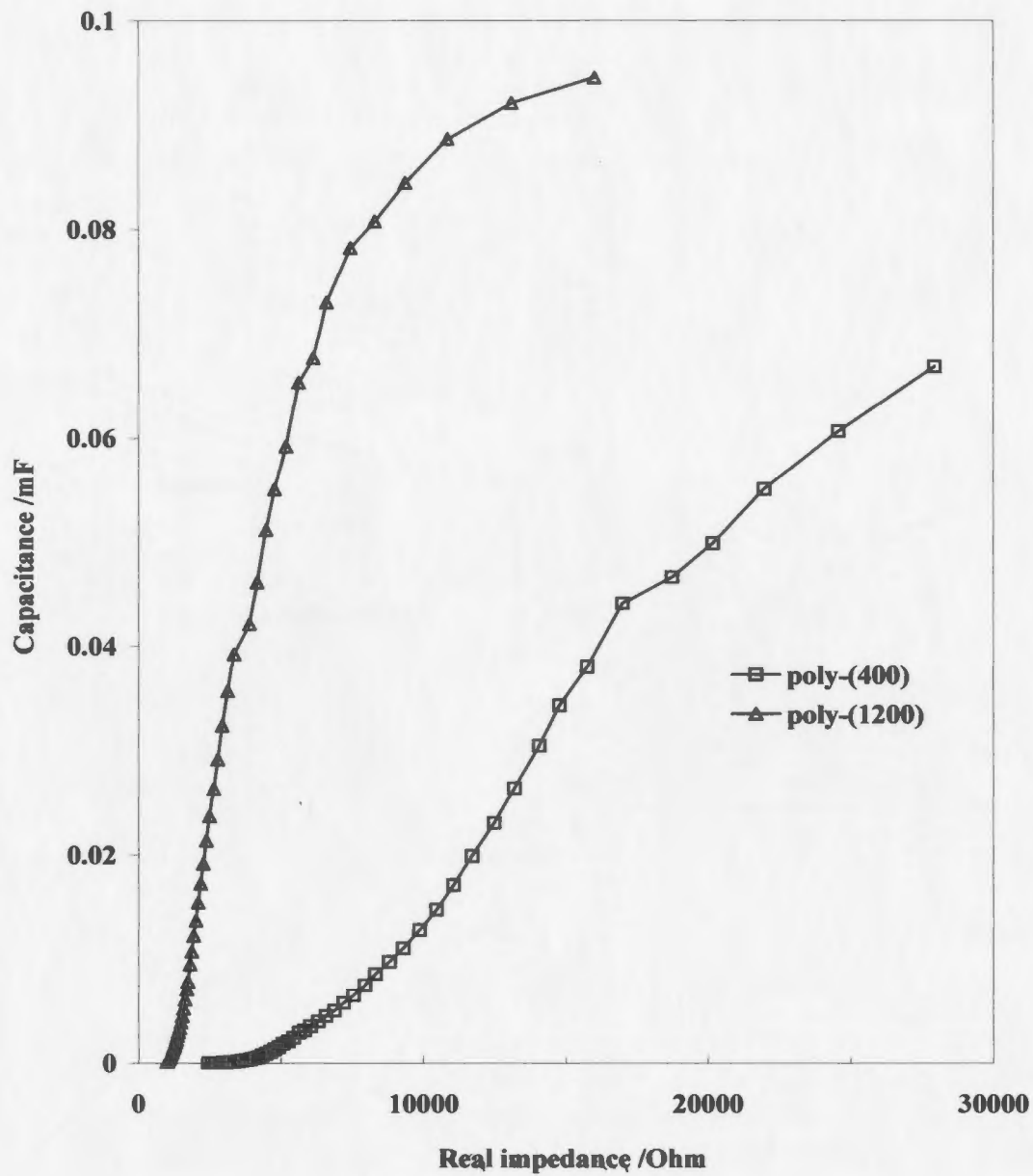
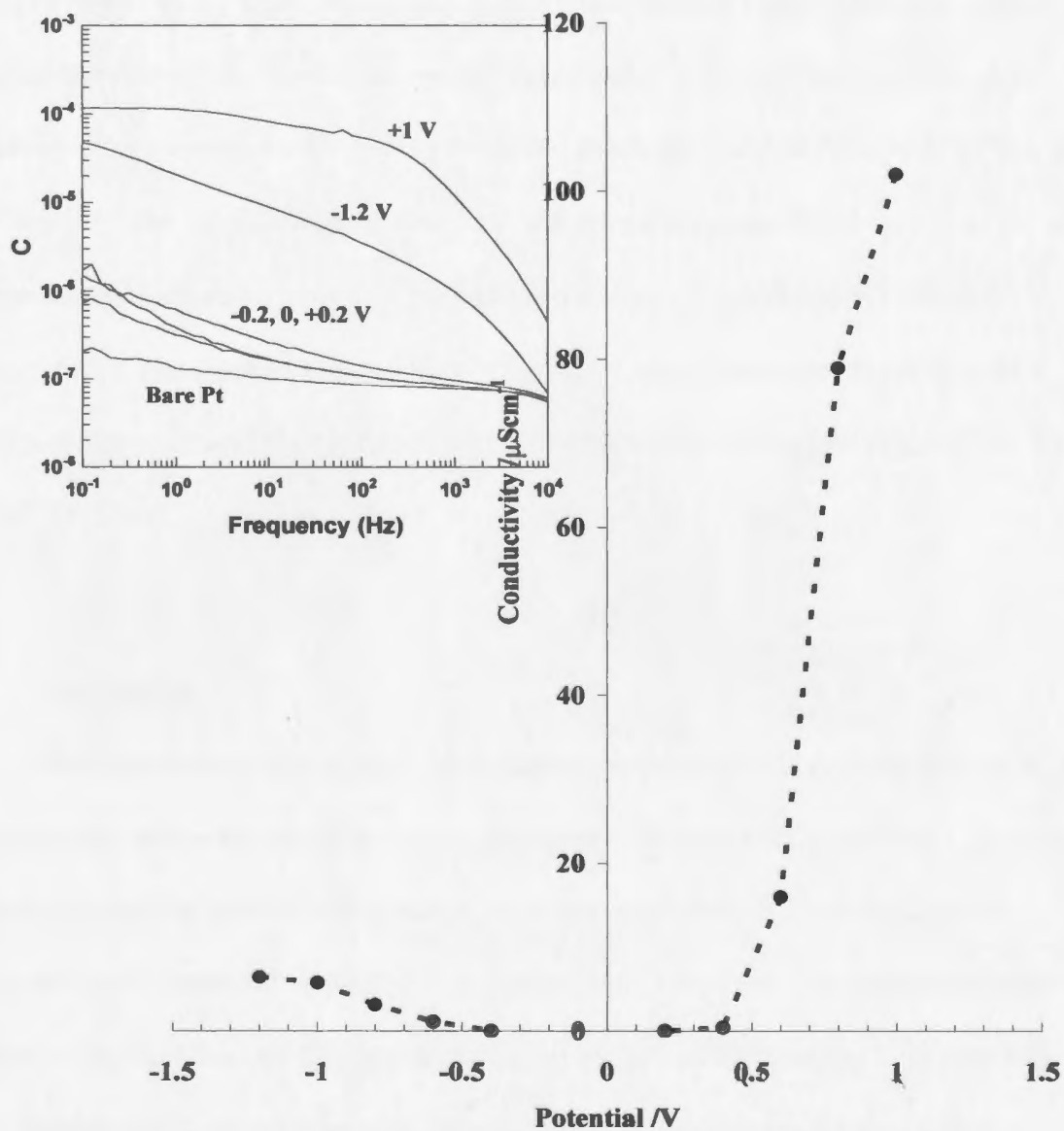


Fig. 5.7 Capacitance vs real impedance plots for n-doped (-0.8 V) poly(5-1) films





**Fig. 5.8** *In situ* conductivity (calculated from AC impedance data) as a function of potential for poly-(1200). Inset shows capacitance vs frequency profiles

doping level was decreased. The film acted as an electronic insulator in the region between +0.2 V and -0.2 V, and had a negligible capacitance (see inset of Fig 5.8). However,  $R_h$  was still low (Fig. 5.5), indicating that the film maintained a high ionic conductivity. This justifies the assumption in the following analysis that  $R_i$  is negligible. The n-type conductivities increased with doping level and reached a maximum at -1.2 V. The n-type conductivity was ca. 10 times smaller than the p-type conductivity. Maximum p-type and n-type conductivities for poly-(1200) were estimated to be 102 and 6.7  $\mu\text{S cm}^{-1}$ , respectively. The inset in Fig. 5.8 shows capacitance vs. frequency plots of a bare platinum electrode and the electrode with poly-(1200) at doping potentials of +1.0, +0.2, 0, -0.2, -1.2 V.

### 5.3 Discussion

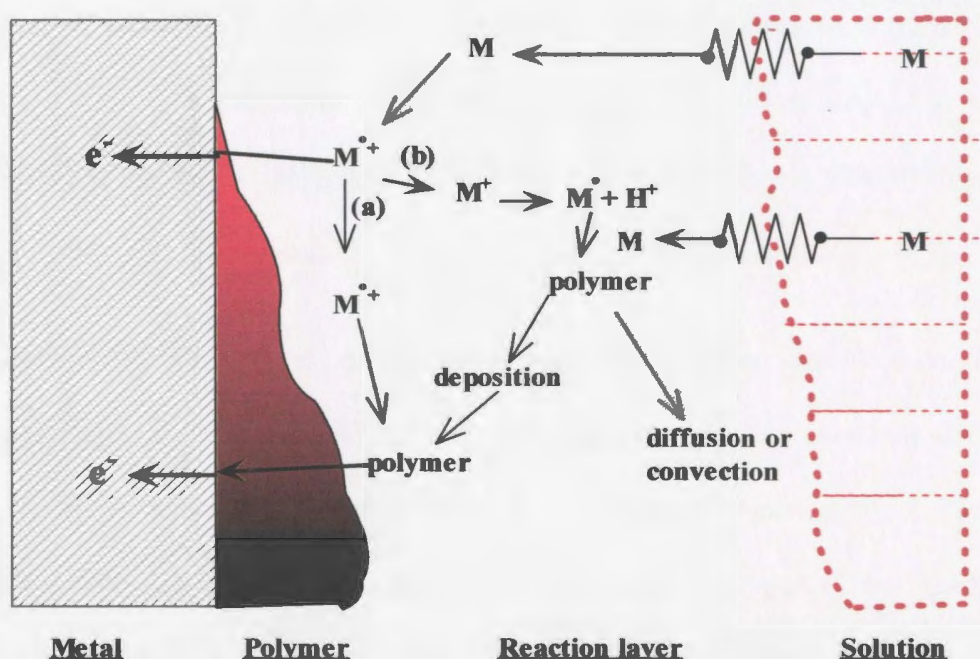
Polymerization by *rotated disk voltammetry* is similar to polymerization by cyclic voltammetry in that the working electrode potential is swept back and forth across the formal potential of a monomer solution. It differs significantly in that the working electrode itself is rotated, typically at speeds of 100-5000 rpm. This rotational motion sets up a well defined flow of solution towards the surface of the rotating disk electrode. The flow pattern is akin to a vortex that literally sucks the solution (and the monomer) towards the electrode. This increases the rate of radical cation formation and increases the rate at which products are transported away from the electrode. Therefore, the application of rotating disk voltammetry during polymer synthesis produces significant changes in the morphological and electrochemical properties of poly-(5-1).

**Table 5.1** Polymerization peak currents and thicknesses of the polymer films prepared at various rotation rates shown in Fig 5.1.

Curve	Rotation rate (rpm)	Peak current		Thickness $\mu\text{m}$
		Anodic (mA/cm <sup>2</sup> )	cathodic (mA/cm <sup>2</sup> )	
a	0	0.709	-0.702	0.32
b	400	1.873	-1.847	0.84
c	800	2.802	-2.789	1.26
d	1400	3.095	-3.287	1.39

**Table 5.2** Electrochemical data for poly-(5-1) films shown in Fig 5.3

		p-doping				n-doping			
$\omega$ / rpm	$Q_{\text{pol}}$ /mC	$E_{\text{p(ox)}}$ /V	$i_{\text{p(ox)}}$ / $\mu\text{A}$	$E_{\text{p(red)}}$ /V	$i_{\text{p(red)}}$ / $\mu\text{A}$	$E_{\text{n(red)}}$ /V	$i_{\text{n(red)}}$ / $\mu\text{A}$	$E_{\text{n(ox)}}$ /V	$i_{\text{n(ox)}}$ / $\mu\text{A}$
0	159	0.85	10.0	0.75	-4.71	-0.91	-13.7	-0.73	3.08
400	357	0.85	21.9	0.75	-14.6	-0.95	-18.8	-0.80	8.42
800	595	0.86	33.6	0.73	-22.8	-0.91	-32.6	-0.80	6.67
1200	664	0.87	35.4	0.72	-27.4	-0.90	-35.0	-0.80	16.8



**Scheme 5.2** A schematic representation of the electrogeneration of a polymer at a rotating disc electrode (adapted from Ref. [7]). Polymerization (a) on grafted species (b) by oligomerization in the reaction layer

**Table 5.1** shows the variation of the polymerization peak currents and thicknesses of the polymer films prepared at various rotation rates. Polymerization charges of 5-1 at various electrode rotation rates were calculated from the final anodic wave by integration from 0 to +1.0 V (**Table 5.2**). Higher polymerization charges and thicknesses were observed at increasing rotation rates.

Polymerizations usually take place via two simultaneous processes: on grafted species (**Scheme 5.2a**) and oligomerization in the reaction layer (**Scheme 5.2b**) [7]. As the electrode rotation rate during the polymer synthesis was increased from 0 to 1200 rpm, both the anodic and cathodic peak currents increased (Fig. 5.1), indicating the

generation of thicker (or denser) films. When the electrode is rotated, the reaction layer is replenished with fresh monomer solution and the monomer moves across the reaction layer via simple molecular diffusion. The diffusion layer is thinner than at 0 rpm and decreases with increasing rpm. Therefore, the flux of monomer increases.

For polythiophene and poly(3-methylthiophene), current densities decreased with increasing rotation rate [7-8]. Moreover the precipitation process dominated for polymerizations [7-8] at stationary electrodes and resulted in uneven films. Changes in grafting processes would have occurred for polythiophene and poly(3-methylthiophene) when the electrode was rotated but would have appeared minor due to the dominance of the precipitation process. The progressive increase in current densities in the present case points to an enhancement of the grafting process under hydrodynamic conditions and it is also clear that the grafting process dominates over the precipitation process under stationary conditions. Further, increasing the rotation rate promotes progressive destruction of the reaction layer with the elimination of oligomers and soluble polymers into the bulk solution. The increase in current density with increasing rotation rate is contrary to the previously proposed model [7]. It should be noted that for polythiophene and poly(3-methylthiophene), 0.1 M solutions were used to probe interfacial reactions [7-8]. Therefore variations of interfacial reaction processes in the present study (with 2mM monomer solution) can be attributed to the concentration effect. It is clear from the SEM images in Fig. 5.2 that polymer synthesized under stationary condition possess crosslinked *fibrillar-globular* structures. Fibrillar formation can occur through precipitation and coalescing of the growing polymer once a critical

**Table 5.3** Capacitances and conductivities from the impedance data for poly-(5-1) coated Pt electrodes shown in Fig.5.3

$\omega$ / rpm	p-doped with $\text{PF}_6^-$ (E= +0.8 V)				n-doped with $\text{Bu}_4\text{N}^+$ (E= -0.8 V)			
	Capacitance /mF	$R_{\text{high}}$ / $\Omega$	$R_{\text{low}}$ / $\Omega$	Conductivity $\mu\text{Scm}^{-1}$	Capacitance /mF	$R_{\text{high}}$ / $\Omega$	$R_{\text{low}}$ / $\Omega$	$\sigma$ $\mu\text{Scm}^{-1}$
0	0.01	479	731	5.86	-	-	-	-
400	0.08	488	730	15.6	67	1531	6951	0.72
800	0.15	466	583	49.9	-	-	-	-
1200	0.21	471	553	79.0	94	1532	2831	4.96

**Table 5.4** Capacitances and conductivities from the impedance data for poly-(1200) coated Pt electrodes illustrated in Fig.5.3d.

	p-Doping potential /V				n-Doping potential /V			
	+1.0	+0.8	+0.6	+0.4	-0.6	-0.8	-1.0	-1.2
C /mF	0.12	0.21	0.11	0.02	0.03	0.09	0.06	0.05
$R_{\text{high}}$ / $\Omega$	464	471	472	440	1179	1174	1173	1184
$R_{\text{low}}$ / $\Omega$	527	553	863	17095	6779	3268	2298	2188
$\sigma$ / $\mu\text{Scm}^{-1}$	102	79	16	0.4	1.1	3.1	5.7	6.4

chain length is reached. Electrode rotation during polymer synthesis suppresses the precipitation process and therefore, a clear *globular* structure is seen for poly-(1200). Thus expansion of polymer nuclei on the electrode surface, supported by observation of a *globular* morphology occurs more rapidly at higher rotation rates than under stationary conditions.

Electrochemical data for poly-(5-1) films from Fig 5.3 are listed in **Table 5.2**. Since peak currents are proportional to the amount of polymer on the electrode, it is clear that more polymer was formed on the rotated electrodes, and that the amount of polymer deposited on the electrode surface increases with increasing rotation rate during preparation.

Capacitances and conductivities at +0.8 V and at -0.8 V for poly-(0), poly-(400), poly-(800) and poly-(1200) films are listed in **Table 5.3**. High frequency resistances at +0.8 V were constant for all poly-(5-1) films. This behavior indicates that the ionic resistance was small for all films. Low frequency resistances decreased with increasing electrode rotation rate during polymerization. Capacitances, which are proportional to the quantity of polymer, increased with increasing rotation rate. Therefore the thicker polymer films, consisting of more polymer, exhibit the lowest resistance. This behavior indicates that the resistance to the motion of electrons across the polymer film was higher for the thinner films. Further, the slopes of capacitance vs. real impedance plots increased with rotation rate (see Fig. 5.6 and Fig. 5.7). Since capacitance is directly proportional to the thickness of the polymer film, the slope of the capacitance vs. real impedance plot is

proportional to the film's conductivity. The increase in conductivities, as we see from poly-(0) to poly-(1200), can be attributed to an enhancement of the grafting process.

Capacitances and conductivities from the impedance data for poly-(1200) at various p – and n-doping potentials are listed in **Table 5.4**. The low frequency capacitance increased with increasing doping potential. The maximum p-type and n-type conductivities for the poly-(1200) film were ca. 102 and ca. 6.6  $\mu\text{Scm}^{-1}$ .

The maximum conductivities estimated, for poly-(0) film, by this method agreed well with those obtained from dual electrode sandwich voltammetry (Chapter 3, section 3.3.6). Maximum p-type and n-type conductivities for poly-(5-1) were 14  $\mu\text{S cm}^{-1}$  and 1.2  $\mu\text{S cm}^{-1}$ , respectively (section 3.3.6) an order of magnitude lower than observed for poly-(1200) film by impedance. Increase in conductivity of poly(1200) film can be attributed to the highly ordered and more denser globular structure. Thus, electrode rotation during polymerization sweeps away the precipitated oligomers near the electrode surface and enhances the grafting process which has a significant positive impact on the film's conductivity.

## **5.4 Characterization of Copolymers of (5-1) and EDOT (CP1, CP2 and CP3)**

### **5.4.1 Cyclic Voltammetry**

Copolymer films CP1, CP2 and CP3 were electrochemically synthesized as described in **Section 4.3** (Chapter 4). **Fig. 5.9** compares doping processes of CP films polymerized under stationary (a) to hydrodynamic conditions of 400- 1200 rpm (b-d). The p and n-doping peak currents increased with increasing electrode rotation rate. The



formal potentials for the main p-doping and n-doping processes of CP1, CP2 and CP3 were ca. +0.89 and -0.87 V; +0.80 and -0.87 V; +0.65 and -1.05 V, respectively. The

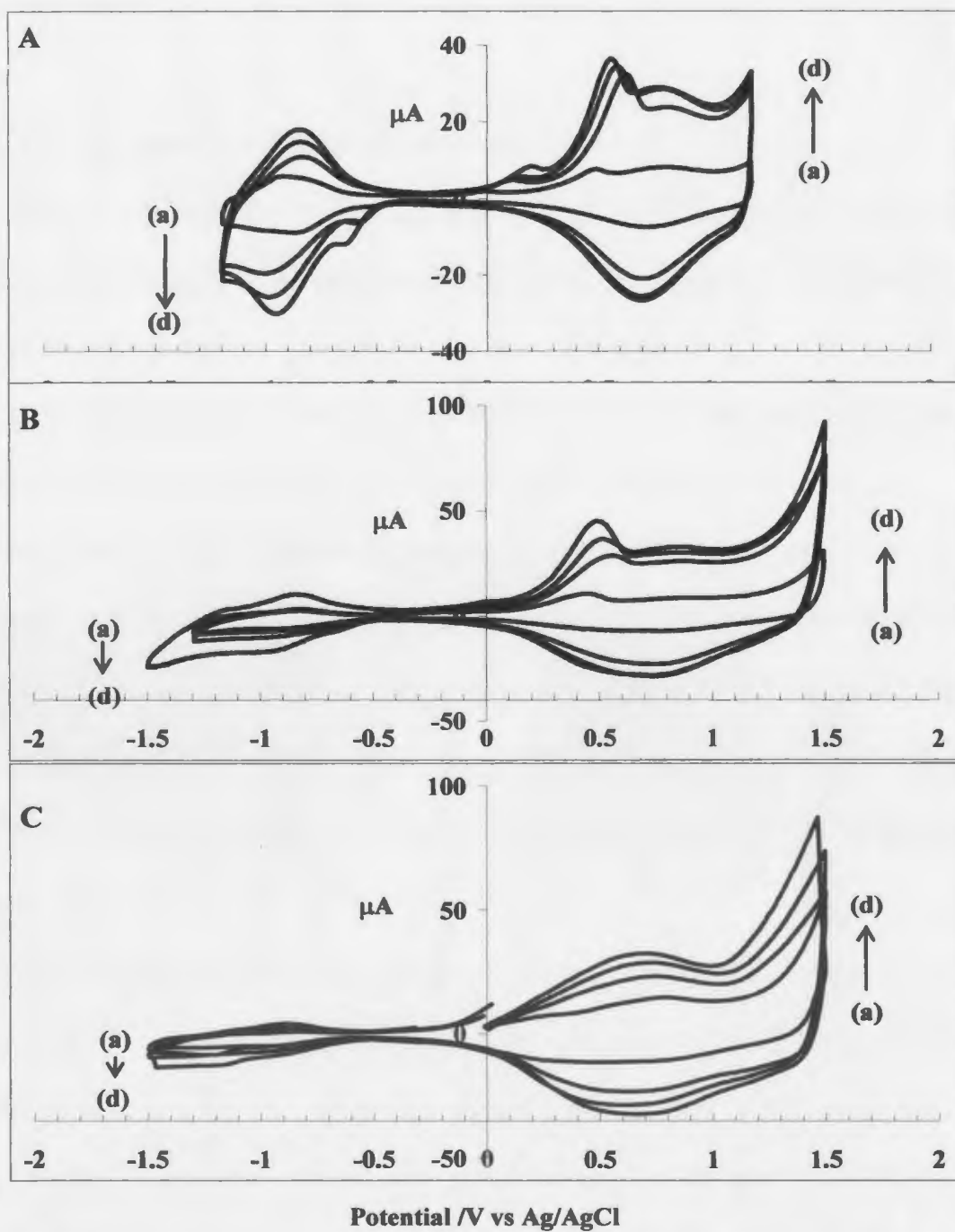


**Fig. 5.9** Cyclic voltammograms (100 mV/s) of A CP1; B CP2; C CP3 coated Pt electrodes in  $\text{Bu}_4\text{NPF}_6\text{-CH}_3\text{CN}$ . (a to d; doping processes of CP films polymerized under stationary to hydrodynamic conditions 400- 1200 rpm)

doped copolymer films were preserved under a nitrogen atmosphere for impedance analyses.

#### 5.4.2 Electrochemical Impedance Spectroscopy

**Fig. 5.10** illustrates impedance plots (at +0.8 V) for platinum electrodes coated with CP1, and corresponding to the p-doped films shown in Fig. 5.9A, in 0.1M Bu<sub>4</sub>NPF<sub>6</sub>-acetonitrile solution under a nitrogen atmosphere. Like poly-(5-1), the CP1-(0), CP1-(400), CP1-(800) and CP1-(1200) films all exhibited the same constant high frequency resistance ( $R_h$ ) but their low frequency ( $R_l$ ) resistances were different. From the differences between the low frequency intercepts and high frequency intercepts resistances for CP1-(0), CP1-(400), CP1-(800) and CP1-(1200) were calculated to be 282, 206, 150, 143  $\Omega$ , respectively. Resistances of CP2-(0), CP2-(400), CP2-(800) and CP2-(1200) (**Fig. 5.11**) were 126, 122, 111, and 36  $\Omega$ , respectively. CP3-(0), CP3-(400), CP3-(800) and CP3-(1200) (**Fig. 5.11**) films exhibited resistances at 193, 30, 26, and 4  $\Omega$ , respectively.

**Fig.5.12** shows capacitance versus real impedance plots for copolymer films CP1, CP2 and CP3 at various rotation rates. It is clear from the experimental data (**Table 5.6**) that films grown at 1200 rpm possess the highest low frequency (limiting capacitance) for both p-type and n-type processes. The p-type limiting capacitance of CP3-(1200) was higher than those observed for CP2-(1200) and CP1-(1200). The n-type limiting capacitance of CP1 film was higher than that of CP2 film. **Fig 5.13** shows capacitance versus potential plots for copolymer films CP1, CP2 and CP3. For CP1 and CP2, the

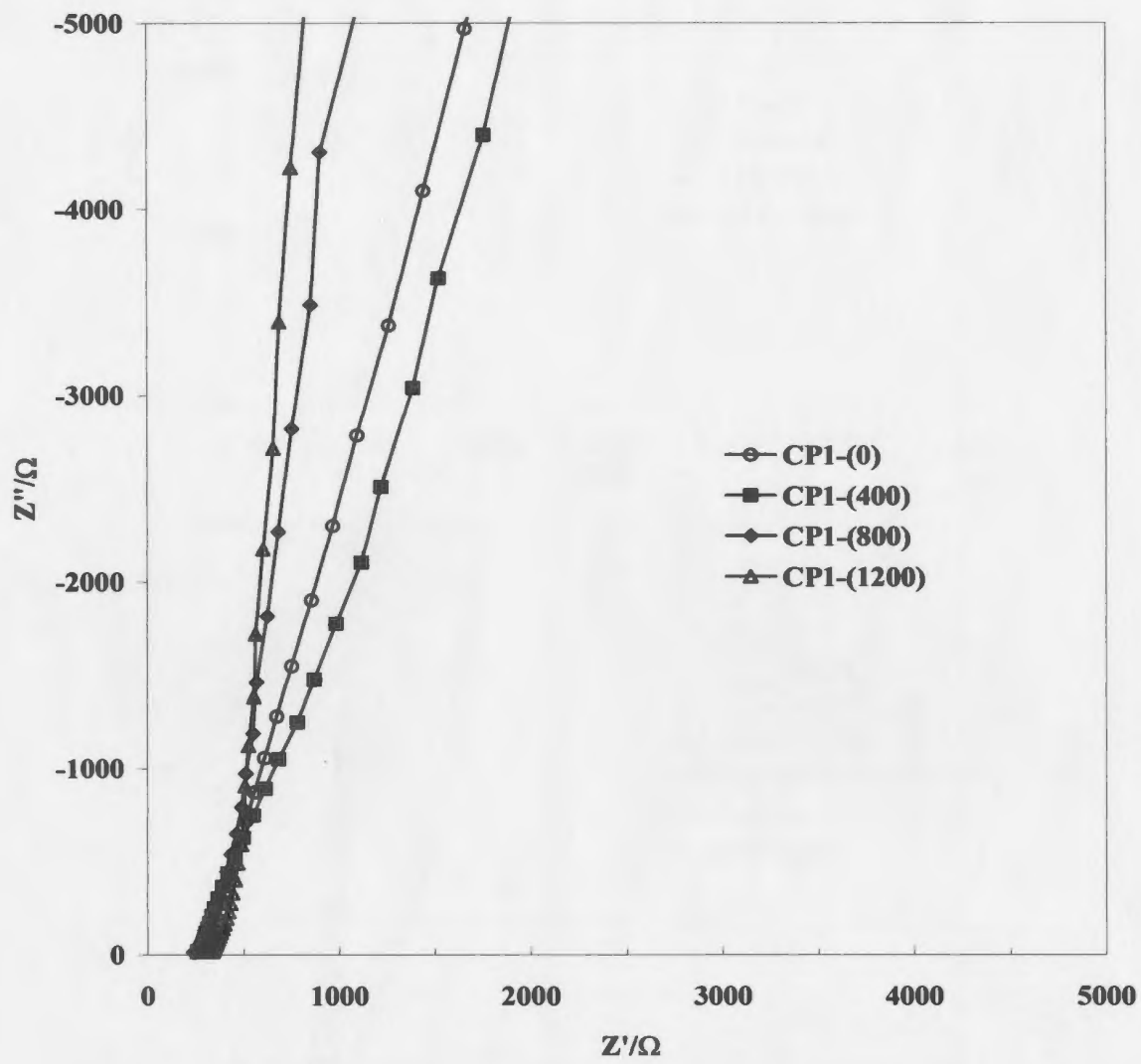


**Fig. 5.10** Impedance plots for Pt electrodes coated with p-doped CP1 in 0.1M  $\text{Bu}_4\text{NPF}_6\text{-CH}_3\text{CN}$  at various electrode rotation rates. Film thicknesses: CP1-(0), 0.35  $\mu\text{m}$ ; CP1-(400), 0.99  $\mu\text{m}$ ; CP1-(800), 1.1  $\mu\text{m}$ ; CP1-(1200), 1.2  $\mu\text{m}$

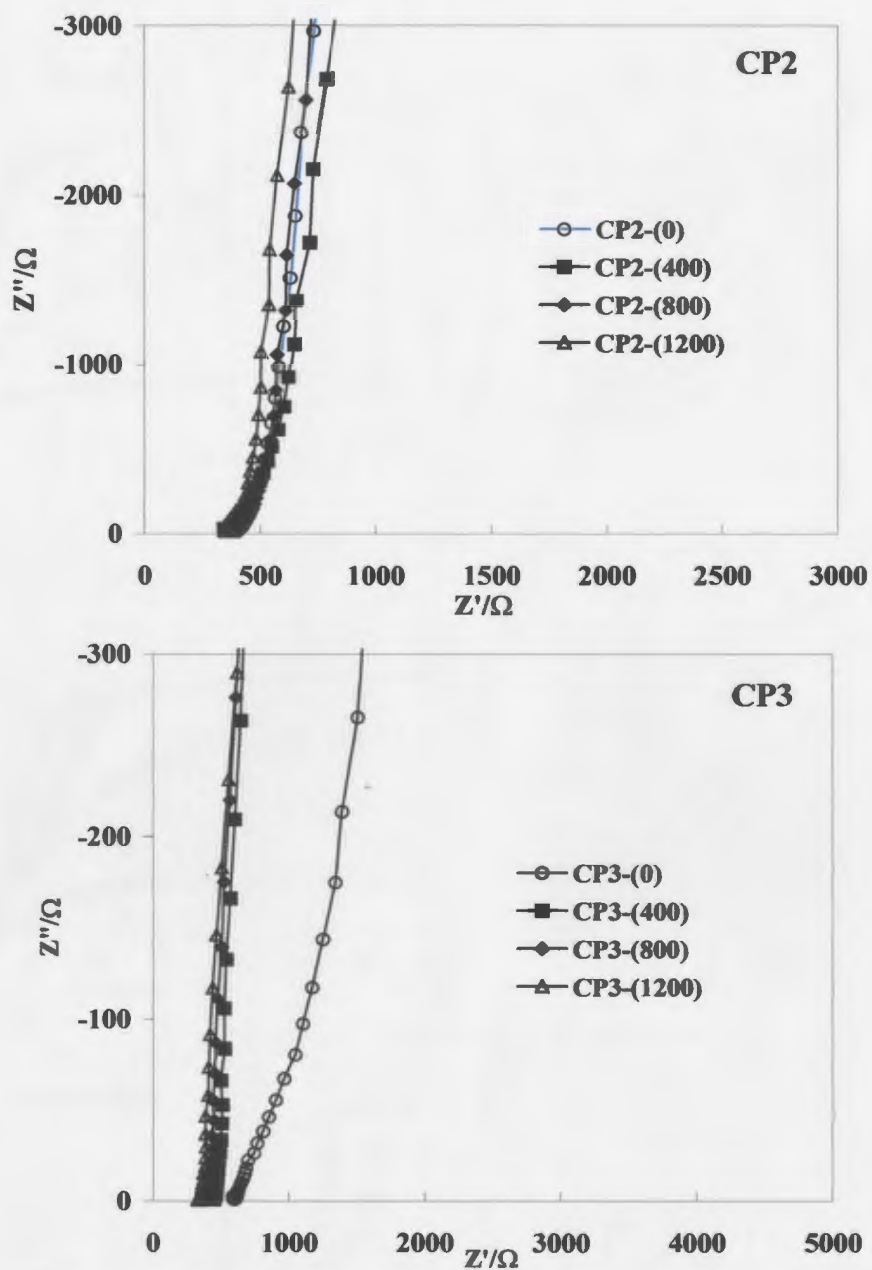


**Fig. 5.11** Impedance plots for Pt electrodes coated with p-doped copolymer films in 0.1M  $\text{Bu}_4\text{NPF}_6\text{-CH}_3\text{CN}$  at various electrode rotation rates. Film thicknesses: CP2-(0), 0.37  $\mu\text{m}$ ; CP2-(400), 1.1  $\mu\text{m}$ ; CP2-(800), 1.4  $\mu\text{m}$ ; CP2-(1200), 1.4  $\mu\text{m}$ ; CP3-(0), 0.60  $\mu\text{m}$ ; CP3-(400), 0.97  $\mu\text{m}$ ; CP3-(800), 1.2  $\mu\text{m}$ ; CP3-(1200), 1.4  $\mu\text{m}$

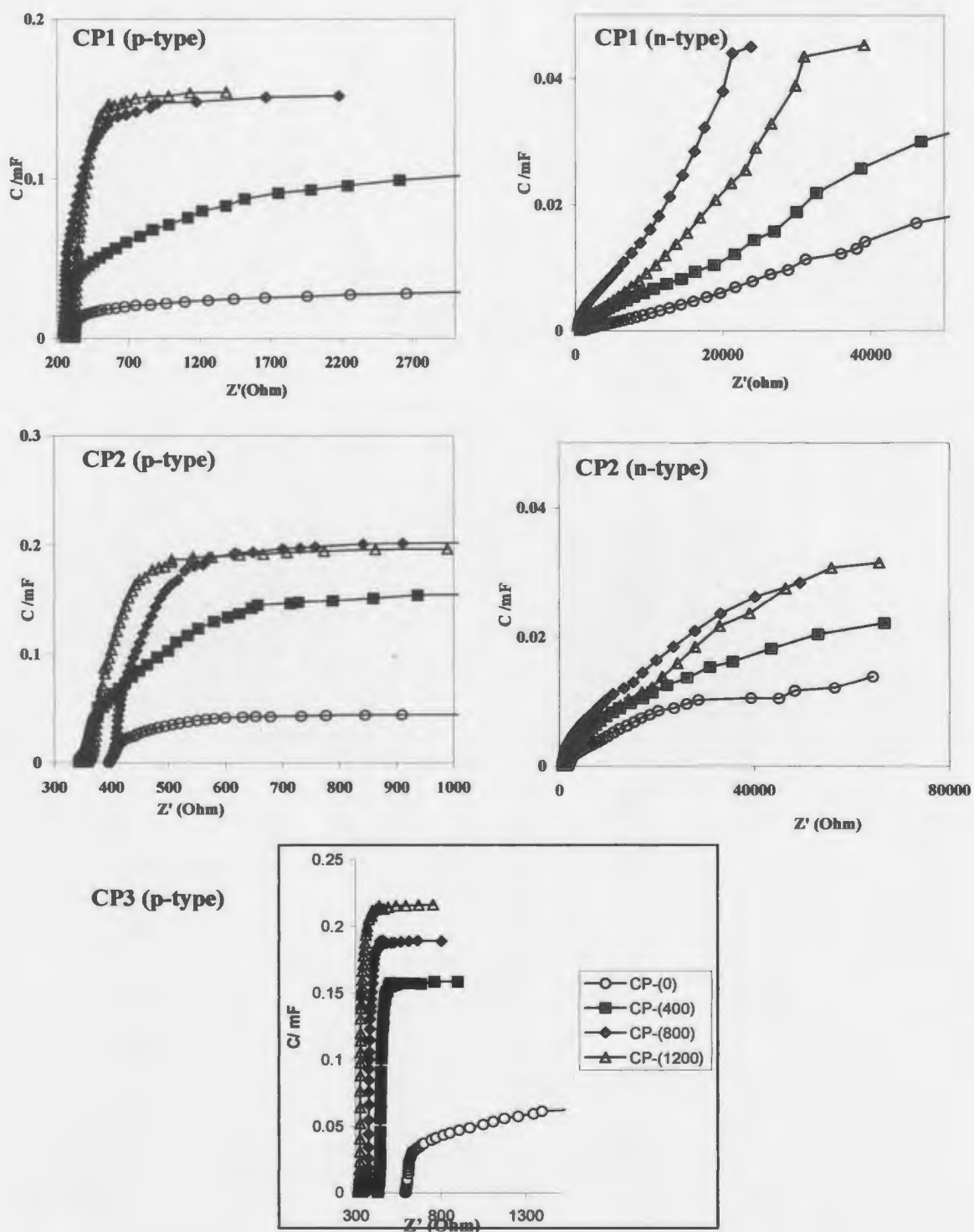


**Fig. 5.12** Capacitance vs. real impedance plots for p-doped (CP1 and CP2 at +0.8 V; CP3 at +0.6 V) and n-doped (-0.9 V) CP films.

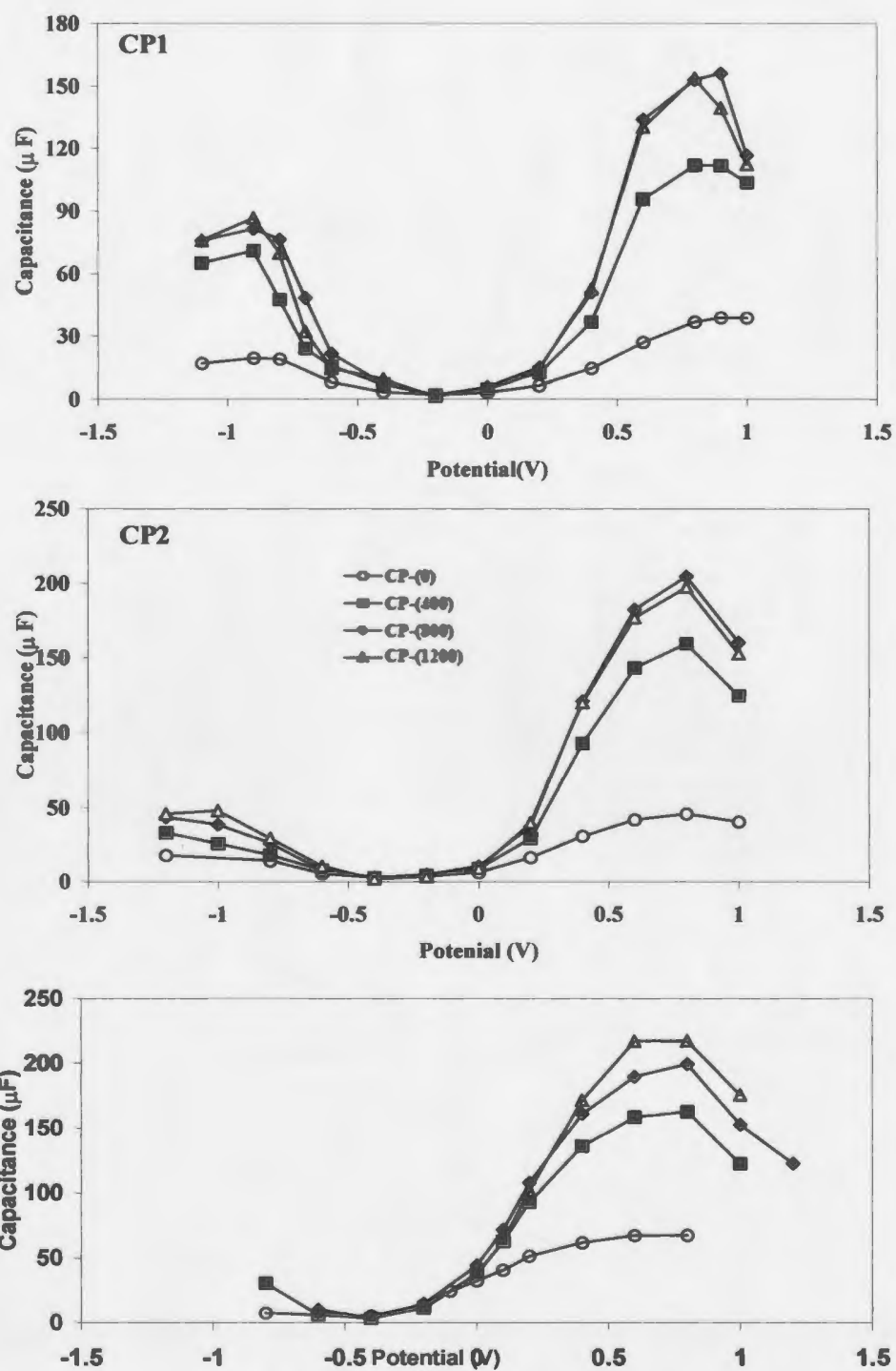


Fig. 5.13 Capacitance vs. potential plots for copolymer films shown in Fig 5.9

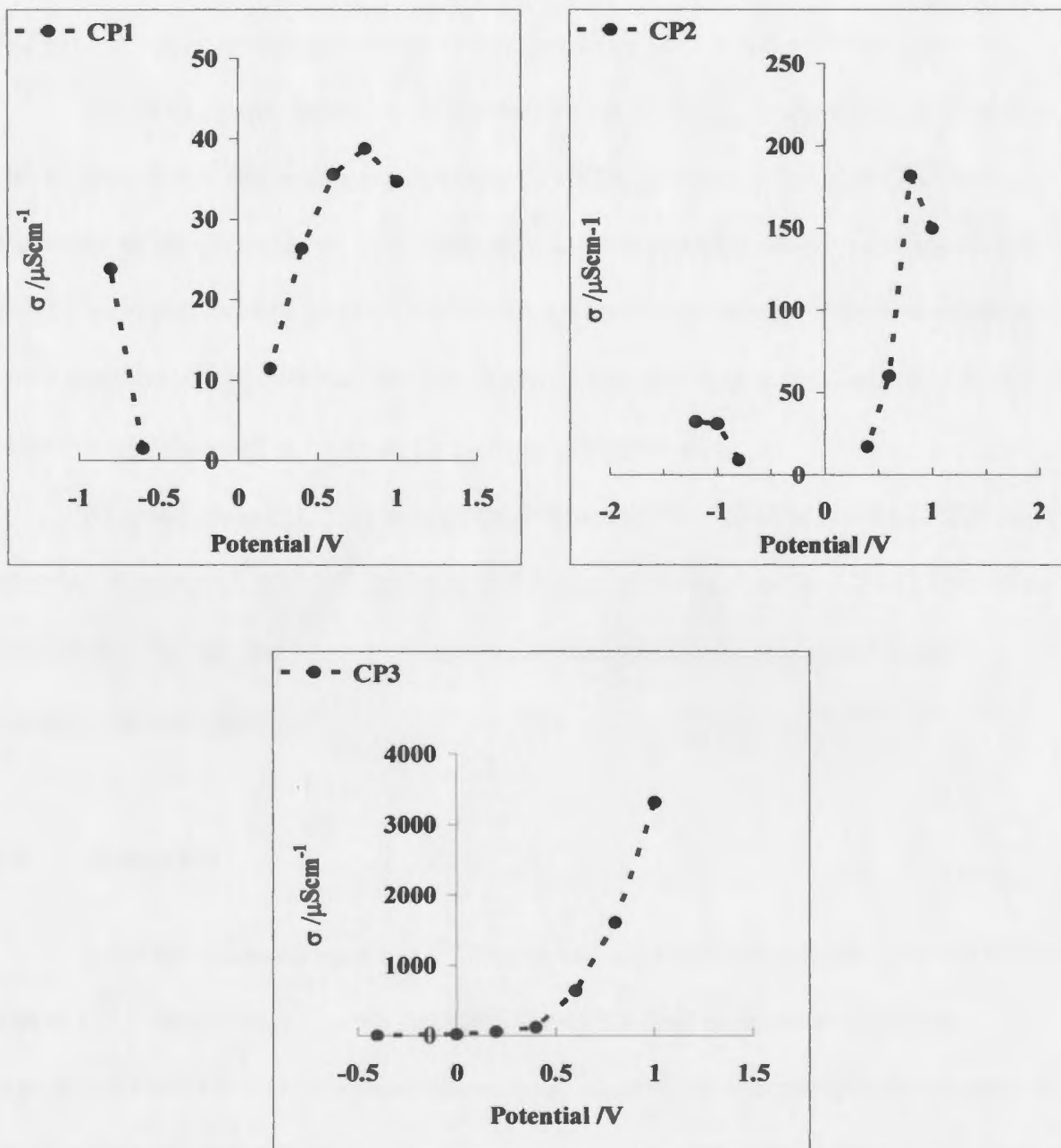


Fig. 5.14 Conductivity vs potential plots of copolymer films polymerized at 1200 rpm



capacitance reaches maximum at ca. +0.8 V for p-doping and ca. -0.9 V for n-doping, and for CP3, the capacitance reaches a maximum at ca. +0.6 V for p-doping process.

**Fig. 5.14** shows estimated conductivities (*in situ*) as a function of potential for CP1-(1200) films. The p-type conductivity of CP1-(1200) was high at +0.8 V and decreased as the doping level was decreased. The n-type conductivities increased with doping level and reached a maximum at -0.8 V. The n-type conductivity was slightly lower than the p-type conductivity. Maximum p-type and n-type conductivities for CP1-(1200) were estimated to be 39 and 24  $\mu\text{Scm}^{-1}$ , respectively.

Also shown in Fig. 5.14 are conductivities of CP2-(1200) and CP3-(1200) as a function of potential. Maximum p-type and n-type conductivities for CP2-(1200) were estimated to be 182 and 32  $\mu\text{Scm}^{-1}$ . CP3-(1200) exhibited the maximum p-type conductivity of 3.3  $\text{mScm}^{-1}$ .

## 5.5 Discussion

Polymerization charges of CP films at various electrode rotation rates are listed in **Table 5.5**. Charges ( $Q_{\text{copol}}$ ) were calculated from the final anodic wave. Higher copolymerization charges and thicknesses were observed at increasing rotation rates. As the electrode rotation rate during copolymer synthesis was increased from 0 to 1200 rpm, both anodic and cathodic peak currents increased (Table 5.5), indicating the generation of thicker (or denser) films. This behavior was similar to that observed for poly-(5-1) films and therefore indicates a greater flux of monomer under hydrodynamic conditions.

**Table 5.5** Electrochemical data for copolymer films shown in Fig 5.9

	$\omega$ / rpm	$Q_{\text{copol}}^*$ /mC	p-doping				n-doping			
			$E_{\text{p(ox)}}$ /V	$i_{\text{p(ox)}}$ / $\mu\text{A}$	$E_{\text{p(red)}}$ /V	$i_{\text{p(red)}}$ / $\mu\text{A}$	$E_{\text{n(red)}}$ /V	$i_{\text{n(red)}}$ / $\mu\text{A}$	$E_{\text{n(ox)}}$ /V	$i_{\text{n(ox)}}$ / $\mu\text{A}$
CP1	0	525	0.80	8.25	0.71	-7.43	-0.87	-8.87	-0.89	5.88
	400	626	0.88	23.1	0.64	-20.0	-1.05	-19.1	-0.77	10.1
	800	815	0.80	28.5	0.69	-25.5	-0.99	-25.5	-0.83	14.9
	1200	898	0.79	28.9	0.68	-26.6	-0.95	-30.1	-0.83	19.6
CP2	0	728	0.83	8.54	0.72	-7.05	-0.98	-7.29	-0.83	3.73
	400	841	0.80	27.9	0.69	-22.7	-0.99	-9.41	-0.82	3.26
	800	960	0.80	35.0	0.69	-28.2	-0.99	-13.0	-0.82	4.70
	1200	998	0.79	31.6	0.65	-27.6	-0.99	-16.8	-0.84	10.4
CP3	0	751	0.79	14.8	0.69	-11.0	-1.10	-5.39	-0.86	0.80
	400	868	0.74	23.4	0.62	-23.2	-1.20	-8.56	-0.90	3.08
	800	1020	0.73	28.8	0.62	-28.6	-1.27	-8.76	-0.87	4.21
	1200	1024	0.70	32.5	0.64	-32.2	-1.18	-12.6	-0.89	4.23

\* integrated to +1.25 V

**Table 5.6** Capacitances and resistances from the impedance data for copolymer film coated Pt electrodes shown in Fig.5.9

		p-doped (at +0.8 V ) with PF <sub>6</sub> <sup>-</sup>				n-doped (at -0.8 V )with Bu <sub>4</sub> N <sup>+</sup>			
	$\omega$ / rpm	C /mF	R <sub>high</sub> /Ω	R <sub>low</sub> /Ω	$\sigma$ μScm <sup>-1</sup>	C /mF	R <sub>high</sub> /Ω	R <sub>low</sub> /Ω	$\sigma$ μScm <sup>-1</sup>
CP1	0	0.04	240	522	5.8	0.02	559	1220	2.4
	400	0.11	235	441	22.0	0.04	543	906	12.5
	800	0.15	238	388	35.4	0.06	-	-	-
	1200	0.15	238	381	38.8	0.07	565	798	23.8
CP2	0	0.04	386	512	13.8	0.02	1483	3104	1.3
	400	0.16	387	509	43.3	0.03	1466	2553	4.8
	800	0.20	389	500	59.0	0.04	1403	2412	6.4
	1200	0.20	382	418	182	0.03	1402	1990	12.9
CP3	0	0.05	587	780	14.4	-	-	-	-
	400	0.16	429	459	1500	-	-	-	-
	800	0.18	375	402	2126	-	-	-	-
	1200	0.23	321	325	1609	-	-	-	-

Capacitances and conductivities at +0.8 V and -0.8 V for CP1, CP2 and CP3 films are listed in **Table 5.6**. Like poly-(5-1), copolymer films exhibited a constant high frequency resistance at +0.8 V which indicated that the ionic resistance was negligible. Low frequency resistances decreased with increasing electrode rotation rate during polymerization. Capacitances increased with increasing rotation rate and capacitances which are proportional to the quantity of polymer, increased with increasing rotation rate. When we compare the capacitance values of CP1, CP2 and CP3 films, the maximum (p-type) capacitance of 4 mF was observed for CP3-(1200). On the other hand, CP1-(1200) exhibited the maximum n-type capacitance of ca. 0.1 mF. Further, the capacitance vs. potential plot (Fig. 5.13) showed an excellent coincidence with their respective cyclic voltammograms (Fig. 5.9). These results clearly substantiate the assignment of the capacitance seen in impedance as a Faradaic capacitance. It was also clear that conductivities of copolymer films (Table 5.6) increased with increasing electrode rotation rate during copolymerization and the maximum p-type conductivity for poly-(1200) was ca.  $1.6 \text{ mScm}^{-1}$ . This behavior can be attributed to the enhancement of grafting processes which was also observed for the poly-(5-1).

Thus estimated conductivity by impedance increases with the increase in EDOT units in the copolymer chain which was also observed in dual electrode sandwich voltammetric investigation of copolymers (chapter 4).

## 5.6 Conclusions

Electrode rotation enhances the grafting process during polymerization, resulting in faster polymer deposition. Also, the conductivity of the resulting polymer films increases with electrode rotation during polymerization, i.e. when the grafting process is enhanced. The influence of electrode rotation on conductivities of **5-1** was also reflected in its copolymers. The observation of faster polymerization with increasing rotation rate here is contrary to results previously reported for polythiophene and its derivatives [7-8]. The difference appears to be due to the lower monomer concentration used in this work.

**Reference:**

1. Skotheim, T.A.; Elsenbaumer, R.L.; Reynolds, J.R. *Handbook of Conducting Polymers*, Marcel Dekker, New York, **1998**.
2. Lang, P.; Chao, F.; Costa, M.; Lheritier, E.; Garnier, F. *Phys. Chem.* **1988**, *92*, 1528.
3. Raymond, D. E.; Harrison, J. D. *J. Electroanal. Chem.* **1993**, *361*, 65.
4. Lin, Y.; Wallace, G. G. *Electrochim. Acta* **1994**, *39*, 1409.
5. Fermin, D. J.; Scharifker, B. R. *J. Electroanal. Chem.* **1993**, *357*, 273.
6. Hoeben, F. J. M.; Jonkheijm, P.; Meijer, E. W.; Schenning, A. P. H. J. *Chem. Rev.* **2005**, *105*, 1491.
7. Otero, F.; Rodriguez, J. *J. Electroanal. Chem.* **1991**, *310*, 219.
8. Zhao, S. Z.; Pickup, P. G. *J. Chem. Soc., Faraday Trans.* **1994**, *90*, 3097.
9. Pickup, P. G. *J. Chem. Soc., Faraday Trans.* **1994**, *86*, 3631.
10. Ren, X.; Pickup, P. G. *Electrochim. Acta.* **2001**, *46*, 4177.

11. Raymond, D. E.; Harrison, J. D. *J. Electroanal. Chem.* **1990**, *296*, 269.
12. Wei, Y.; Chan, C-C.; Tian, J.; Jang, G-W.; Hsueh, K. F. *Chem. Mater.* **1991**, *3*, 888.
13. John, R.; Wallace, G. G. *J. Electroanal. Chem.* **1991**, *306*, 157.
14. Andrieux, C. P.; Audebert, P.; Hapicot, P.; Saveant, J-M. *J. Am. Chem. Soc.* **1990**, *112*, 2439.
15. Beck, F.; Oberst, M. Jansen, R. *Electrochim. Acta* **1990**, *35*, 1841.
16. Tanaka, K.; Schichiri, T.; Wang, S.; Yamabe, T. *Synth. Met.* **1988**, *24*, 203.
17. Marcos, M. L.; Rodriguez, I.; Gonzalez-Velasco, J. *Electrochimica Acta* **1987**, *32*, 1453.
18. Rodriguez, I.; Marcos, M. L.; Gonzalez-Velasco, J. *Electrochimica Acta* **1987**, *32*, 1181.
19. John, R.; Wallace, G. G. *Polym. Int.* **1992**, *27*, 255.
20. Li, F. B.; Albery, W. J. *Langmuir* **1992**, *8*, 1645.
21. Li, F. B.; Albery, W. J. *Electrochimica Acta* **1992**, *37*, 393.
22. Chao, F.; Costa, M.; Tian, C. *Synth. Met.* **1993**, *53*, 127.
23. Lukkari, J.; Alanko, M.; Heikkila, L.; Laiho, R.; Kankare, J. *Chem. Mater.* **1993**, *5*, 289.
24. Lukkari, J.; Tuomala, S.; Ristimaki, S.; Kankare, J. *Synth. Met.* **1992**, *47*, 217.
25. Kankare, J.; Vuorinen, M.; Alanko, M.; Lukkari, J. *J. Chem. Soc., Chem. Commun.* **1993**, 241.
26. Hillman, A. R.; Mallen, E. F.; Hamnett, A. *J. Electroanal. Chem.* **1988**, *244*, 353.

27. Morse, N. J.; Rosseinsky, D. R.; Mortimer, R. J.; Walton, D. J. *J. Electroanal. Chem.* **1988**, *255*, 119.
28. Genies, E. M.; Bidan, G.; Diaz, A. F. *J. Electroanal. Chem.* **1983**, *149*, 101.
29. Qui, Y. J.; Reynolds, J. R. *J. Poly. Sci. Part A, Poly. Chem.* **1992**, *30*, 1315.

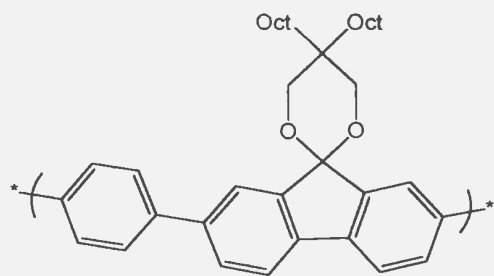
## *Chapter 6*

### **Studies on Fluorenone Based Copolymers**

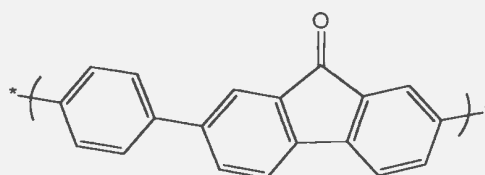
Polyfluorene derivatives are a particularly suitable class of materials for OLEDs because they contain a rigid biphenyl unit which leads to a large band gap with efficient blue emission [1, 2]. Most emitting polymers of fluorene are hole transporting (p-type) and the problem with such materials in OLEDs was that the positive charges (holes) created near the anode reach the cathode without recombination with opposite charges (electrons) [3]. There are only a few reports of electron-deficient (n-type) fluorene polymers which can enhance the probability of charge carrier recombination processes.

Substitution of a carbonyl group at the C-9 position of the fluorene ring produces a molecule that can be regarded as the phenyl analogue of cyclopenta[2,1-b:3,4-b']-bithiophen-4-one, which produces a polymer with a very low band gap [4]. Like bridged bithiophene systems, fluorenone produces a low band gap homopolymer with a low LUMO energy level [3]. Since polyfluorenone is an insoluble material, a polyketal precursor route was employed for its preparation. The LUMO energy of polyfluorenone is close to the work function of magnesium and therefore forms a contact with facile injection of electrons [3].

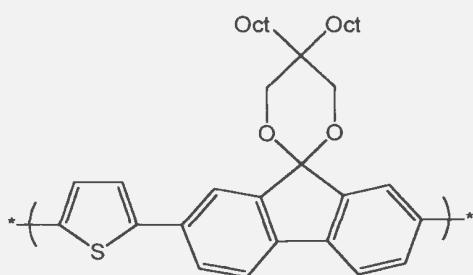




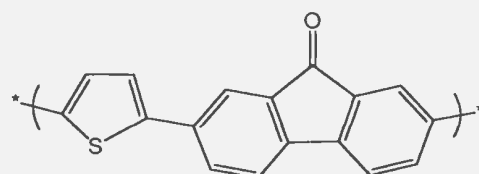
(a) PFKB



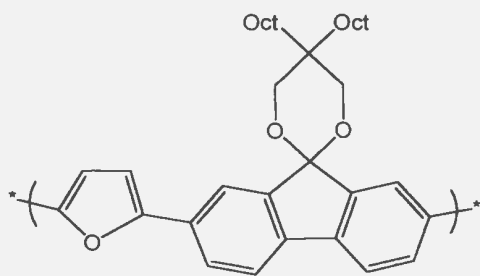
(d) PFB



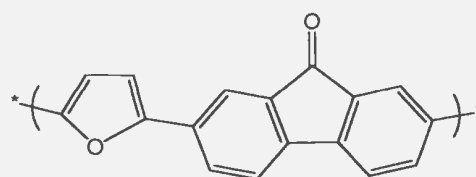
(b) PFKT



(e) PFT



(c) PFKF



(f) PFF

**Scheme 6.1.** Polyketal precursors and their respective polyfluorenone structures

Copolymerization of electron deficient and electron rich components (a donor-acceptor strategy) was found to be a successful approach to decrease band gaps in bridged bithiophenes [5], and the same approach can be extended to synthesize low band gap fluorenone derivatives [1]. In order to further study the use of the fluorenone building block in the construction of well defined polymeric systems, polyketal precursors of fluorene with thiophene (PFKT: poly2,7-spiro[4,4'-dioctyl-2',6'-dioxyocyclohexane]-1',9-fluorene-co-1,4-thiophene), furan (PFKF: poly2,7-spiro[4,4'-dioctyl-2',6'-dioxyocyclohexane]-1',9-fluorene-co-1,4-furan), and benzene (PFKB: poly2,7-spiro[4,4'-dioctyl-2',6'-dioxyocyclohexane]-1',9-fluorene-co-1,4-benzene) (**Scheme 6.1**) were chemically prepared [6]. Electrochemical studies on these materials and fluorenone copolymers produced from them are reported in this chapter. The goal of this work was to explore the applicability of the donor-acceptor strategy to fluorene based copolymers.

## **6.1 Experimental**

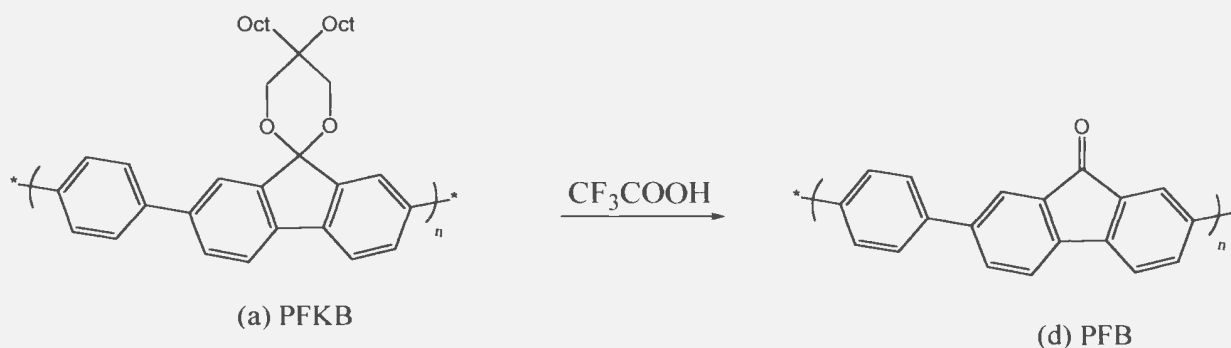
### **6.1.1 PFKB, PFKT, and PFKF Coated Electrodes**

The precursor copolymers were synthesized using a Stille coupling method by Fang Huang [6]. The reported molar masses of PFKB, PFKT and PFKF were 5000, 40400 and 4400 g mol<sup>-1</sup>, respectively. The precursor copolymers were dissolved in THF (5 mg/mL) and drop-coated onto the electrodes (or substrates) by a microsyringe.

### **6.1.2 Conversion of Ketals to Fluorenone Copolymers**

The ketal group was converted to the ketone (**Scheme 6.2**) by exposing the copolymer to trifluoroacetic acid vapour for ca. 30 minutes at ambient temperature [3].

The conversion proceeded spontaneously and was accompanied by a color change from yellow to red. After washing with acetone, insoluble, homogeneous copolymer films (PFB, PFT and PFF) were obtained.



**Scheme 6.2**

## 6.2 Characterization of PFB, PFT and PFF Films

### 6.2.1 IR Spectroscopy

IR spectra of PFB, PFT and PFF films are compared with the spectra of their respective ketal copolymers in **Fig 6.1**. Strong C-H bands at 2855, 2922, and 2955  $\text{cm}^{-1}$  are observed for the alkyl chains of the ketals (A1, B1 and C1). Bands due to the ketones are observed at 1720 and 1600  $\text{cm}^{-1}$  (A2, B2 and C2). Bands at ca. 1030 and 1070  $\text{cm}^{-1}$  in the ketal copolymer were shifted to 1130 and 1170  $\text{cm}^{-1}$  for the fluorenone copolymers. Most other bands are unchanged in the spectra of fluorenone copolymers when compared to the respective ketal copolymers.

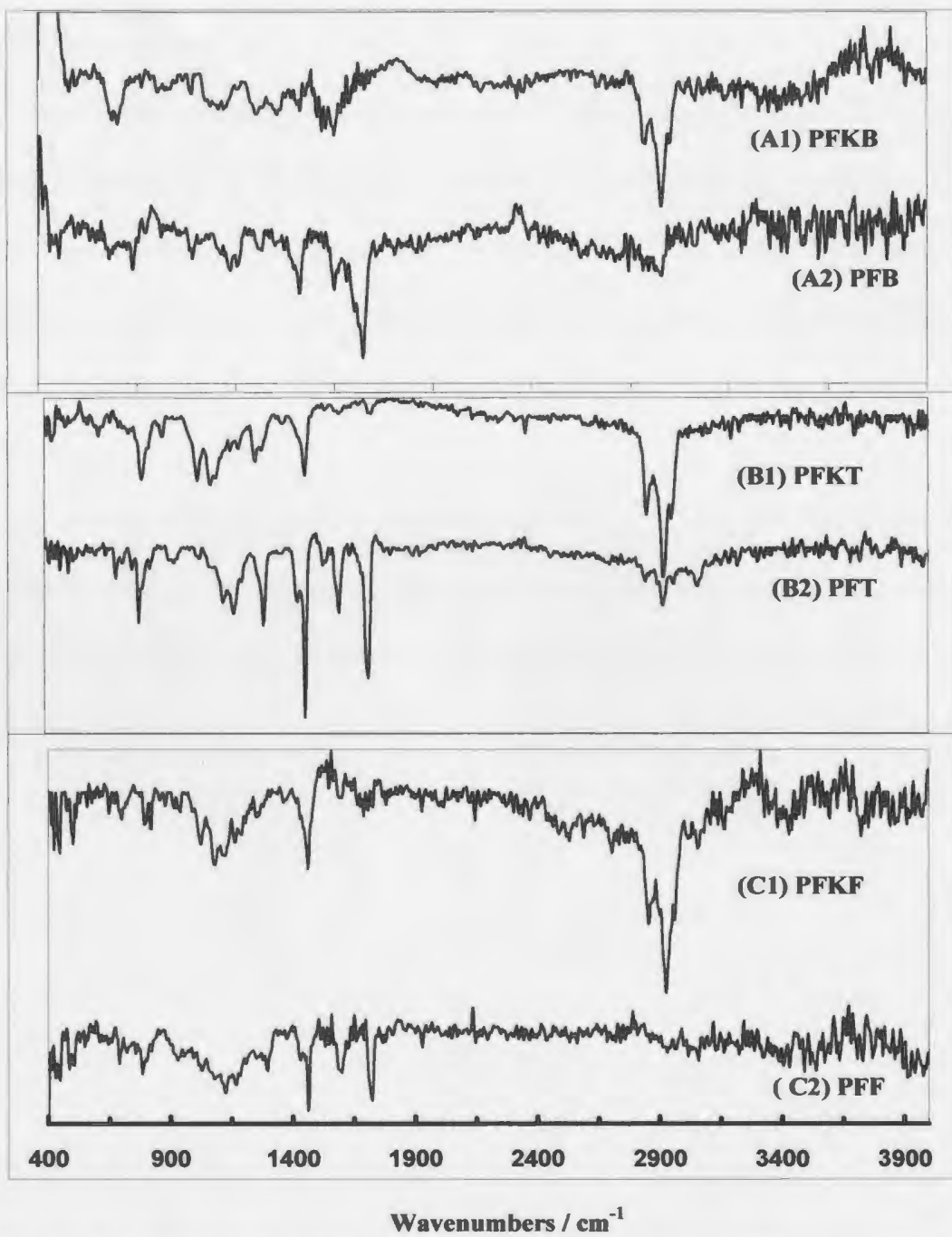


**Fig. 6.1.** IR spectra of PFB, PFT and PFF films on Si discs compared with their respective ketyl copolymers.

## 6.2.2 UV-Vis Spectroscopy

In **Fig 6.2**, curves A1 and A2 illustrate the UV-Visible spectra of PFKB and PFB, respectively on quartz discs. The optical absorption maximum of PFKB occurs at 430 nm, which is the result of a  $\pi$ - $\pi^*$  absorption transition. Absorption bands at 400 and 500 nm are observed for PFB. As shown in Fig 6.2, onset wavelengths for PFKB and PFB can be estimated to be ca. 510 and 650 nm, corresponding to optical band gaps of 2.4 and 1.9 eV, respectively.

Similarly, the absorption spectra of PFKT and PFT (**Fig 6.3**), and PFKF and PFF (**Fig 6.4**) differ significantly. Onset wavelengths for PFKT and PFT were estimated to be 536 and 647 nm, corresponding to optical band gaps of 2.3 and 1.9, respectively. Onset wavelengths of PFKF and PFF were 547 and 648 nm corresponding to optical bands gaps of 2.3 and 1.9 eV, respectively.

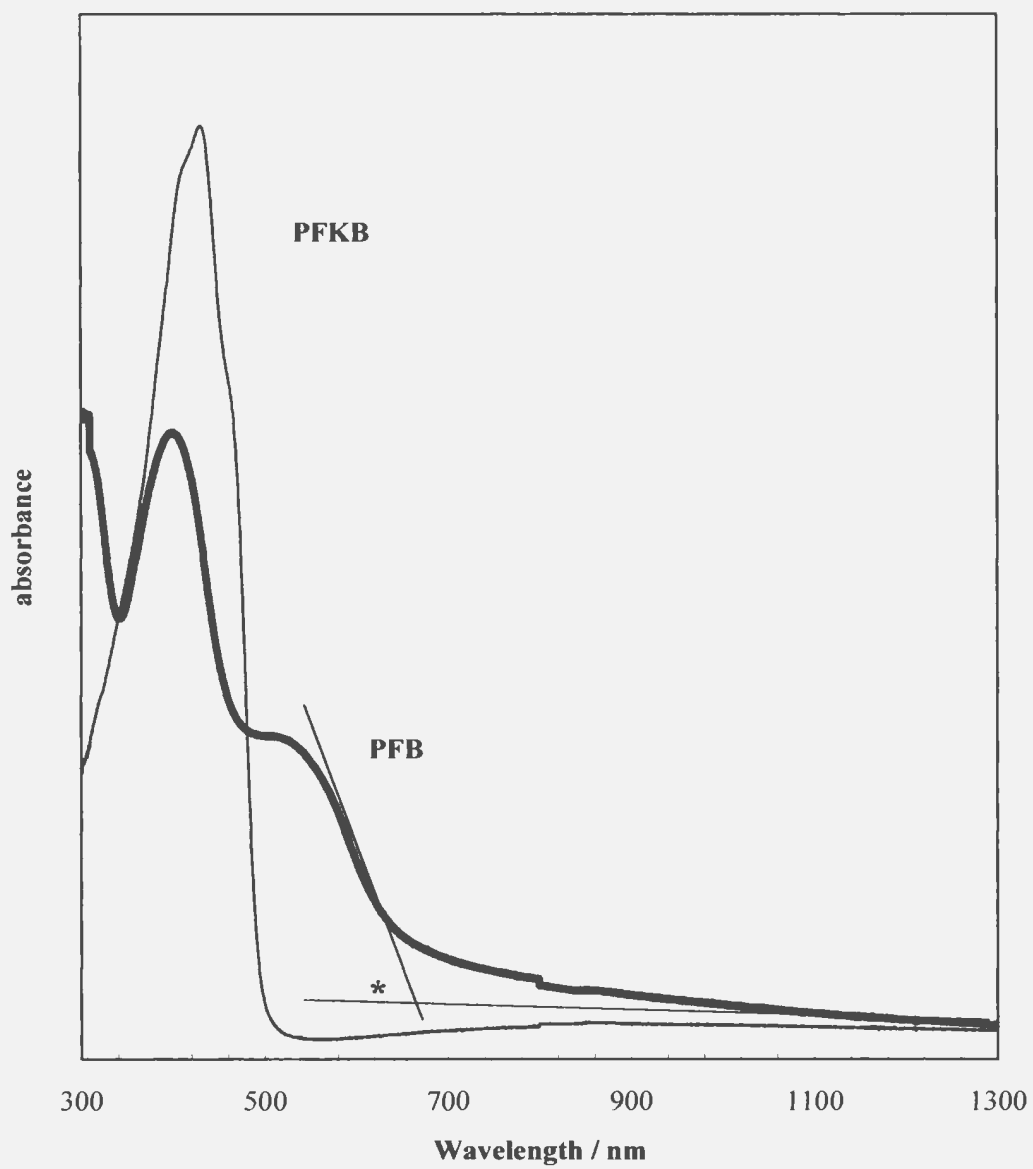


**Fig 6.2.** Electronic absorption spectra of a PFKB film on a quartz disc before and following exposure to trifluoroacetic acid vapour (PFB)  
The graphical method for estimating the absorption onset (\*) is illustrated.

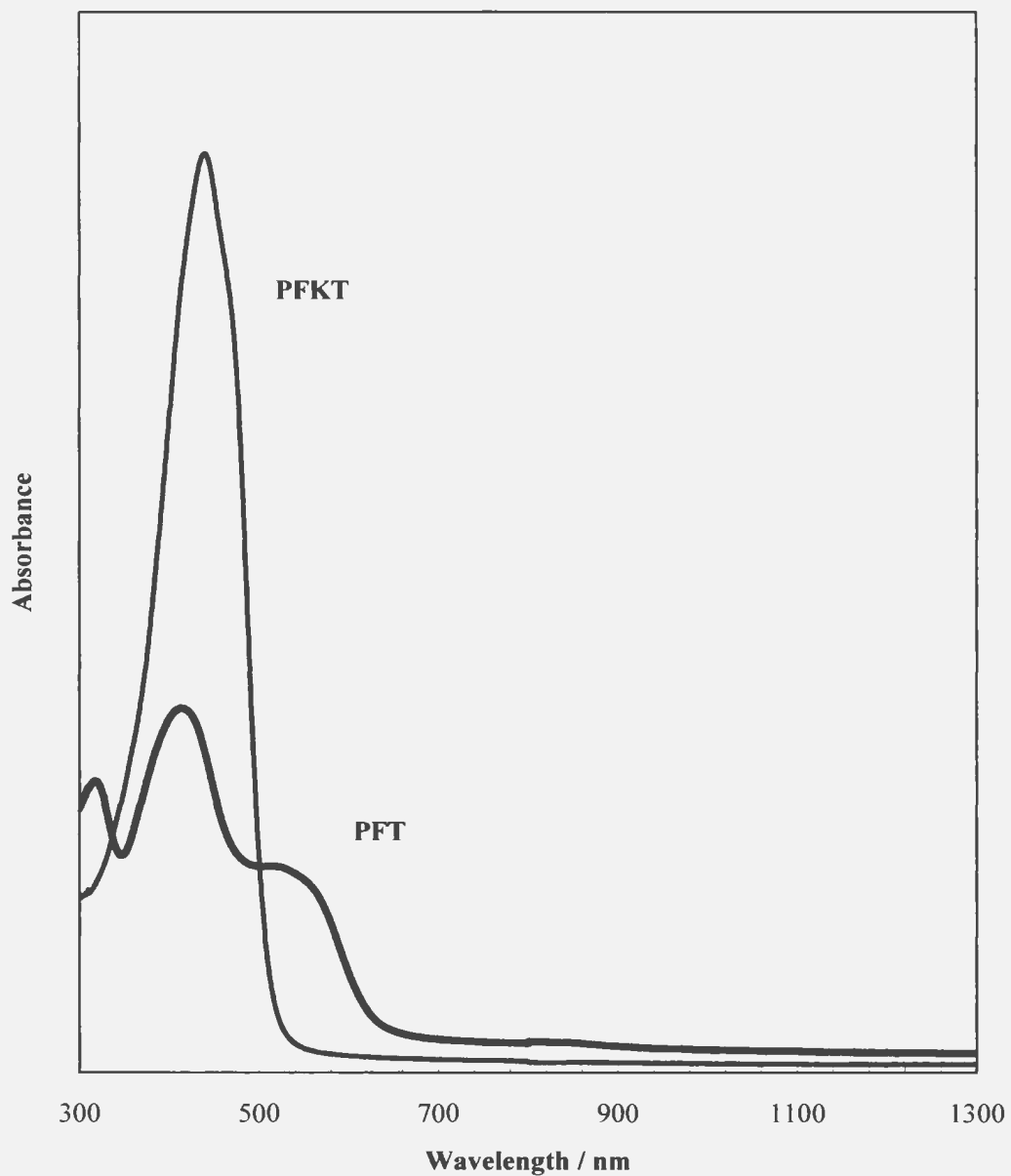


**Fig 6.3.** Electronic absorption spectra of a PFKT film on a quartz disc before and following exposure to trifluoroacetic acid vapour (PFT)

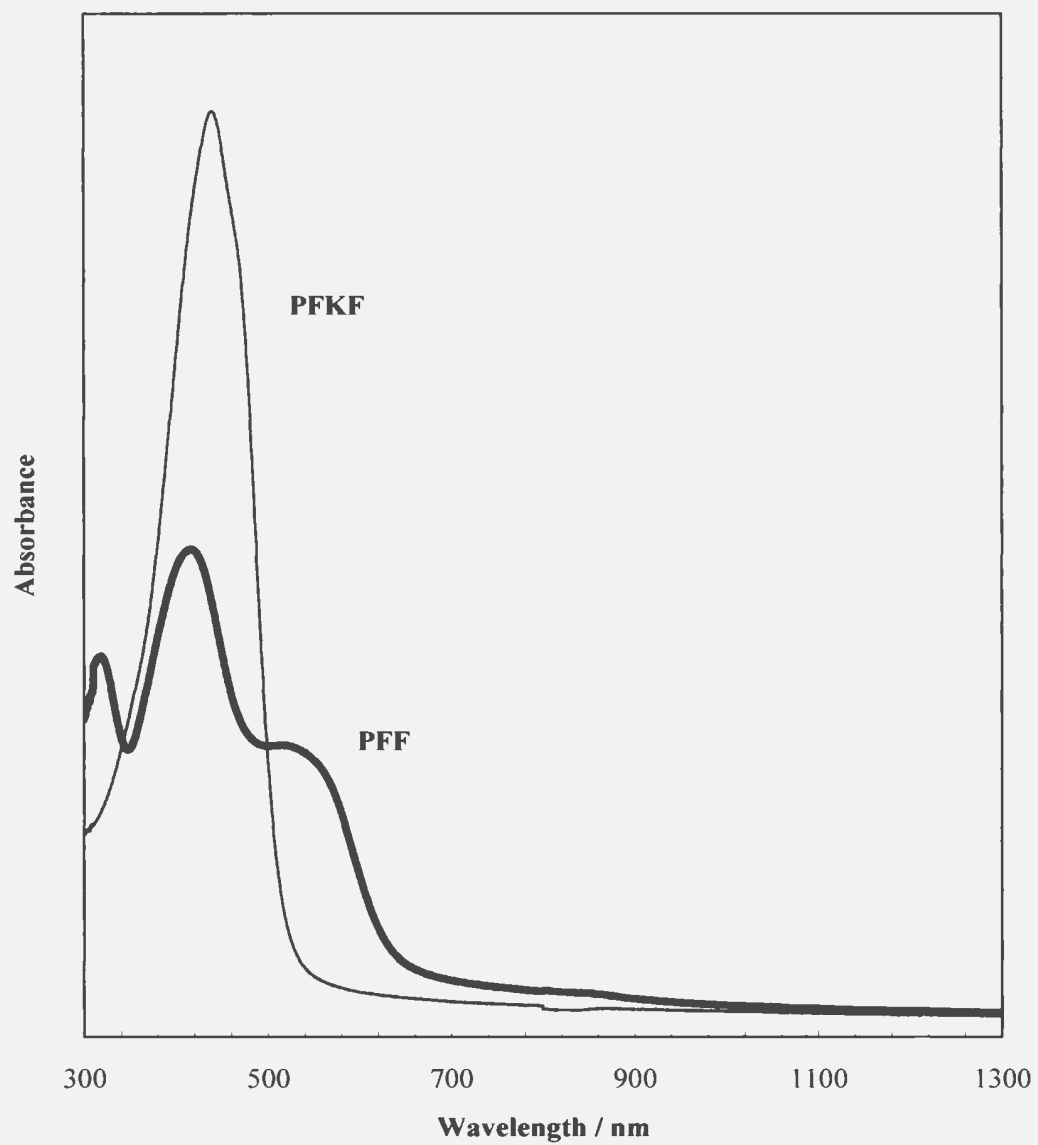


**Fig 6.4.** Electronic absorption spectra of a PFKF film on a quartz disc before and following exposure to trifluoroacetic acid vapour (PFF)



### 6.2.3 Cyclic Voltammetry

The precursor copolymers were dissolved in THF and drop coated onto glassy carbon electrodes for electrochemical characterization. The p-doping/undoping of PFKB (**Fig 6.5a**) exhibits an asymmetric voltammogram with an onset of ca. +1.2 V and a formal potential ( $E^0$ ) of ca. +1.4 V. n-Doping of the polymer film was not observed in the potential range ( $> -2.0$  V) of the experiment. Similar voltammograms were observed for PFKT and PFKF films with p-doping formal potentials at ca. +1.2 and +1.0 V, respectively.

**Fig 6.5b** shows a cyclic voltammogram of a PFKB coated electrode following exposure to trifluoroacetic acid vapour to convert it to the ketone derivative. The p-doping behavior of the PFB film is similar to that of the PFKB film, having a narrow p-doping peak (at +1.6 V) and a broad de-doping range (+1.6 V to +1.1 V). The n-doping of PFB exhibits reversible reduction doping and undoping peaks at ca. -1.4 V and -1.2 V, respectively. The formal potentials for p- and n-doping/undoping are ca. +1.4 V and -1.3 V, respectively, with a (band) gap of ca. 1.9 V between the onsets of p- and n-doping.

**Fig 6.3c** shows p- and n-doping/undoping peaks for PFT. The formal potentials are ca. +1.0 V and -1.1 V, respectively, with a (band) gap of ca. 1.6 V between the onsets of p and n-doping. PFF has p and n-doping/dedoping formal potentials at ca. +1.1 V and -1.3 V, respectively (**Fig 6.5d**), with a (band) gap of ca. 1.7 V between the onsets of p- and n-doping.

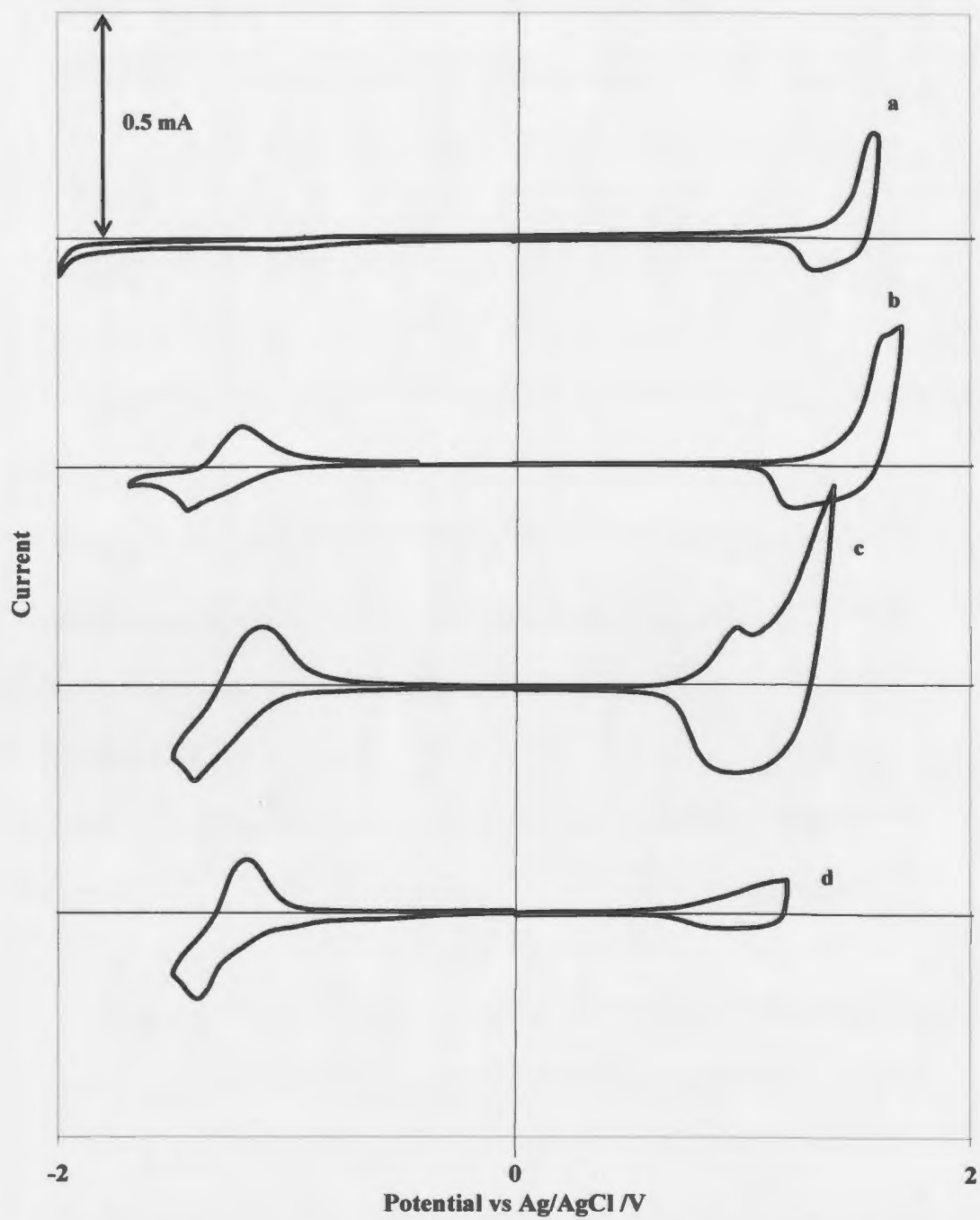


**Fig 6.5.** Cyclic voltammograms (100 mV/s) of films of (a) PFKB, (b) PFB, (c) PFT, and (d) PFF films on glassy carbon electrodes in acetonitrile containing 0.01 M  $\text{Bu}_4\text{NPF}_6$

**Table 6.1** Electrochemical data for the copolymers

Polymer	$E^{\circ}$ (p-doping) <sup>a</sup> / V	$E^{\circ}$ (n-doping) <sup>a</sup> / V	gap <sup>b</sup> / V
PFKB	1.4	-	
PFB	1.4	-1.3	1.9
PFKT	1.2	-	
PFT	1.0	-1.2	1.6
PFKF	1.0	-	
PFF	1.1	-1.3	1.7

a. average peak potential (vs Ag/AgCl) for doping and undoping

b. gap between onsets of n- and p- doping

- not observed

**Table 6.2** Optical properties of copolymers as films on quartz

Polymer	$\lambda_{\max}$ / nm	Band- gap <sup>a</sup> / eV
PFKB	430	2.4
PFB	400, 500	1.9
PFKT	440	2.3
PFT	414, 516	1.9
PFKF	440	2.3
PFF	416, 512	1.9

a. from onset of absorption

### 6.3 Discussion

The ketal groups of the PFKB, PFKT and PFKF copolymers protect a very reactive site at the C-9 position of fluorene rings and the alkyl chains add to the solubility of the polymers in organic solvents. Cleavage of the ketal group and formation of a carbonyl group at the C-9 position in the precursor copolymers was easily carried out by exposing films to an acidic atmosphere. This conversion was accompanied by a color change from yellow to red, reflecting the lower band gaps of the fluorenone copolymers. IR spectra (Fig 6.1) clearly show that acid treatment results in a high degree of conversion of the ketal groups to the ketone. The strong C-H bands at 2855, 2922, and 2955  $\text{cm}^{-1}$  observed for the alkyl chains of the ketals (A1, B1 and C1) are greatly diminished in the acid treated copolymers (A2, B2 and C2), and strong new bands due to the ketones are observed at 1720 and 1600  $\text{cm}^{-1}$ . The shift of the bands at ca. 1030 and 1070  $\text{cm}^{-1}$  to 1130 and 1170  $\text{cm}^{-1}$  has also been reported for the homopolymer [3] and it is clearly associated with the formation of a ketone conjugated to the fluorene unit.

Formal potentials for all the copolymer films in acetonitrile are summarized in **Table 6.1** and optical properties of the copolymer films are listed in **Table 6.2**. The ketal copolymer with benzene has a slightly higher optical band gap (2.4 eV) than the thiophene and furan polymers which have the same band gap (2.3 eV).

The p-doping/undoping of PFKB films (Fig 6.5a) exhibits an asymmetric voltammogram, which is characteristic behavior for most conducting polymers (due to conformational changes)[7], with an onset of ca. +1.2 V. An n-doping process was not observed for this or any of the other ketal precursor copolymers. From the optical

spectrum (onset), the band gap of PFKB can be estimated to be ca. 2.4 eV. n-Doping of PFKB would therefore be expected to begin at ca. -1.2 eV. It is therefore not clear why n-doping is not observed for the ketal copolymers.

The p-doping formal potential for PFKT is ca. +1.2 V and the optical band gap is ca. 2.3 eV. Thus the electron rich thiophene unit increases the HOMO energy of the polymer significantly relative to benzene. Based on the differences between the band gaps and HOMO energies, thiophene also increases the LUMO energy relative to benzene, but only by ca. 0.1 eV. The net effect is therefore in a slight lowering of the band gap, by ca. 0.1 eV.

PFKF has a significantly lower formal potential for p-doping (+1.0 V) than PFKT, but the same optical band gap (ca. 2.3 eV). PFKB, PFKT and PFKF copolymers possess lower optical band gaps, by ca. 0.5 eV, when compared to that of the ketal homopolymer, which has an absorption maximum of ca. 385 nm and the onset wavelength of ca. 430 nm corresponding to a band gap of ca. 2.9 eV [3].

Conversion to the ketone decreases the band gap of all three copolymers. All three ketone copolymers have an optical band gap of ca. 1.9 eV. PFB shows an electrochemical (band) gap of ca. 1.9 V between the onsets of p- and n-doping which agrees well with the optical band gap (Table 6.2). The p-doping formal potential of PFB is unchanged relative to that of PFKB, while the band gap is 0.5 eV lower. This indicates that the carbonyl group at the C9 position has little effect on the HOMO of the copolymer, but a large stabilizing effect on the LUMO energy level. This is consistent with experimental results for polyfluorenone itself [3].

The electrochemical (band) gap of PFT is ca. 1.6 V between the onsets of p and n-doping. The effects of replacing the benzene ring of PFB with thiophene are similar to those observed for the precursor polymers. The HOMO energy is increased by ca. 0.4 eV, while the LUMO energy is almost unchanged, and a decrease in band gap of ca. 0.4 eV is observed. But this decrease in band gap shown by the electrochemical results is not reflected in the optical band gap (Table 6.2). The reason can be attributed to the uncertainty in the measurement of the onset of absorption, since  $\lambda_{\max}$  values in Table 6.2 also show a slight red shift between PFB and PFT. A similar disagreement between electrochemical band gap and the optical band gap is also observed for PFF (Table 6.1 and Table 6.2). Fluorenone copolymers PFB, PFT and PFF possess low optical band gaps (1.9 eV) when compared that of the polyfluorenone homopolymer (ca. 2.5 eV, from the absorption onset) [3] which indicates the soundness of the donor-acceptor strategy. All three fluorenone containing copolymers possess the same n-doping potential (LUMO energy) which indicates that the LUMO is localized on the ketone group, and is not significantly influenced by changes in the conjugated  $\pi$ -system.

#### **6.4 Conclusions**

Copolymers of fluorenone with benzene, thiophene, and furan have band gaps of ca. 1.6-1.9 eV and can be easily p-doped and n-doped. Copolymerization of the electron deficient fluorenone moiety with the electron rich thiophene and furan units produces the lowest band gaps and the lowest p-doping potentials. The n-doping potential is insensitive to the nature of the spacer (donors) units between fluorenone units, indicating

localization of the LUMO on the ketone substituent. The band gaps of the copolymers are significantly lower than that of the fluorenone homopolymer. Thus PFB, PFT and PFF are promising candidates for use as an electron transport layer in multilayer LEDs.

#### References:

- (1) Scherf, U.; List, E. J. W. *Advan. Mater.* **2002**, *14*, 477.
- (2) Leclerc, M.; *J. Polym. Sci. Part A.* **2001**, *39*, 2868.
- (3) Uckert, F.; Setayesh, S.; Mullen, K. *Macromolecules* **1999**, *32*, 4519.
- (4) A. Cihaner, S. Tirkes, A. M. Onal, *J. Electroanal. Chem.* **2004**, *568*, 151.
- (5) Huang, H.; Pickup, P. G. *Chem. Mater.* **1998**, *10*, 2212
- (6) Fang, H.; Masters Thesis, Memorial University of Newfoundland, Canada **2004**.
- (7) Pickup, P. G. In *Modern aspects of Electrochemistry*; Convey, B. E.; Bockris, J. O'M.; White, R.E., Eds.; Plenum: New York, **1999**, *33*, 549.

## Chapter 7

### Synthesis of Fluorene Based Donor Acceptor Conjugated Molecules

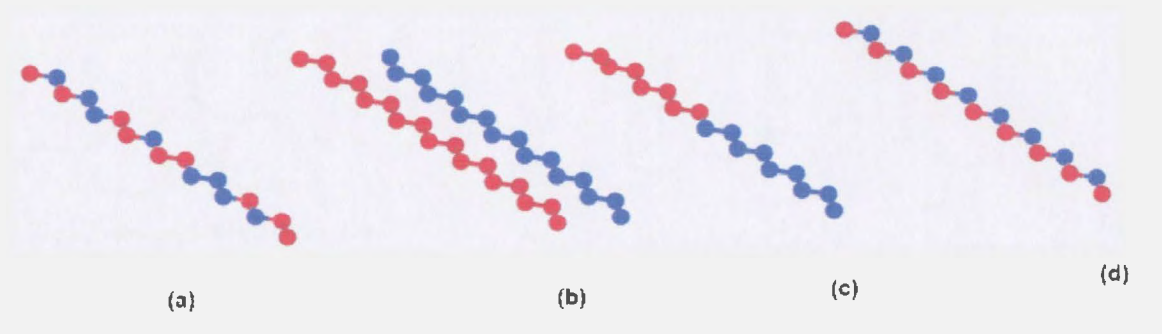
#### 7.1 Introduction

A color or spectral signature change with applied voltage, termed *electrochromism* (EC), is one of the most prominent and fundamental properties of conducting polymers. Normally, EC properties are tailored via modification of the polymer's structure. Through band gap control, one can vary the accessible color states in both the doped and neutral forms of the polymer [1]. Numerous synthetic strategies exist for tuning the band gaps of conjugated polymers [1]. Copolymerization of donor-acceptor monomers is one of the strategies that gives rise to a modification of main chain polymer structure and allows for an interesting combination of the properties supplied by each monomer unit.

For many copolymers synthesized by electrochemical methods from a solution of two or more monomers, exact structures have not been elucidated. Some of the possible structures for copolymers [2] synthesized by electrochemical oxidation of two monomers are shown in **Scheme 7.1**. Scheme 1(a) shows an irregular random copolymer, (b) and (c) show a mixture of homopolymer chains and block copolymer, respectively and (d) depicts a perfect alternating copolymer. In many cases of electrochemical polymerization,

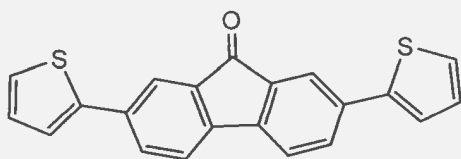


random copolymer formation has been observed [3-5]. Band gap tuning for these systems has been carried out by changing the feed ratio of the monomer solutions.



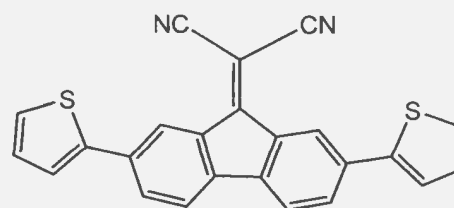
**Scheme 7.1.** Possible structures of copolymers synthesized by electrochemical oxidation of two monomers

Homopolymerization of a molecule containing both monomer units (comonomer) is a straightforward method to synthesize regular alternating copolymers and by changing the composition and structure of the comonomer one can tune the band gap [1]. Some of the examples of regular alternating thiophene based copolymers, prepared by electrochemical polymerization of donor-acceptor comonomers, are poly(EDOT-co-dicyanomethylene-fluorene), poly(EDOT-co-4-dicyanomethylene-cyclopenta[2,1-*b*:3,4,*b'*]bithiophene) [2, 6]. Copolymers consisting of alternating EDOT and DiCNFl units showed a decrease in electrochemical and optical band gaps when compared to their respective homopolymers. In order to explore this type of structure-property relationship, we have followed a similar comonomer strategy to design some new precursor materials for thiophene-fluorene based low band gap polymers.



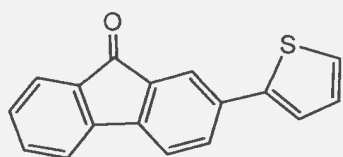
2,7-di-2-thienyl-9H-fluoren-9-one

7-3



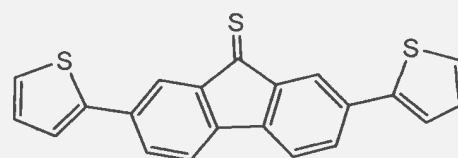
(2,7-di-2-thienyl-9H-fluoren-9-ylidene)malononitrile

7-5



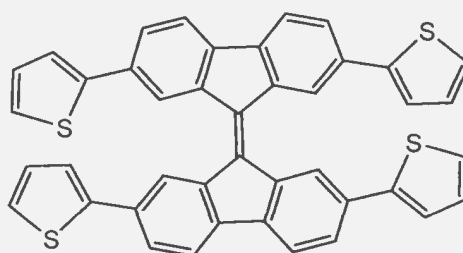
2-(2-thienyl)-9H-fluoren-9-one

7-4



2,7-di-2-thienyl-9H-fluorene-9-thione

7-6



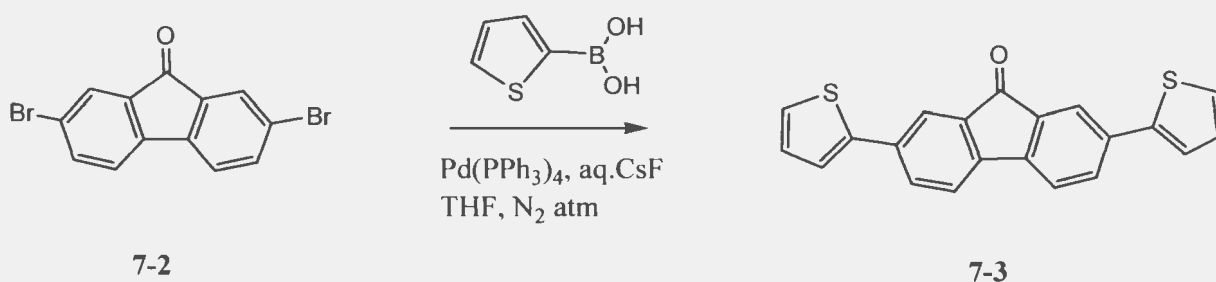
2,7,2',7'-tetra-2-thienyl-[9,9']bifluorenylidene

7-7

Our original interest was to study the effect of donor-acceptor units on cyclopenta[2,1-*b*:3,4-*b'*]bithiophen-4-one. We found difficulty in synthesizing that material in large amounts. Therefore we intended to study a similar structural analog, fluoren-9-one. Structure 7-4 shows a comonomer of fluoren-9-one with thiophene. The thiophene unit acts as a donor to the fluoren-9-one acceptor and was expected to lead to facile electrochemical polymerization. Moreover, it is the parent of thiophene system. Thiophene is attached to the 2 and 2,7 positions of fluoren-9-one in structures 7-4 and 7-3, respectively to study the effect of fluore-9-one to thiophene ratio. 7-5 and 7-6 were targeted to study the effect of changing the acceptor unit at the C-9 position of the fluoren-9-one. 7-7 was targeted as an analogue of the dimer in chapter 3. Synthetic routes to co-monomers 7-3, 7-4, 7-5 and results of the attempted synthesis of 7-6 and 7-7 are presented in this chapter.

## 7.2 Syntheses

### 7.2.1 Synthesis of 2,7-Di-2-thienyl-9H-fluoren-9-one, 7-3



**Scheme 7.2**

There are two common methods to synthesize **7-2**, one involving dihalogenation of fluoren-9-one [9] and the other by oxidation of 2,7-dibromofluorene[10]. In this work, 2,7-dibromo-fluoren-9-one (**7-2**) was synthesized by the dibromination of fluoren-9-one under Wohl-Ziegler conditions [9]. The reaction time was ca. 0.5 h and the product was obtained in 65% yield. The Wohl-Ziegler reaction is much faster than the oxidation of 2,7-dibromofluorene which requires at least five days [10].

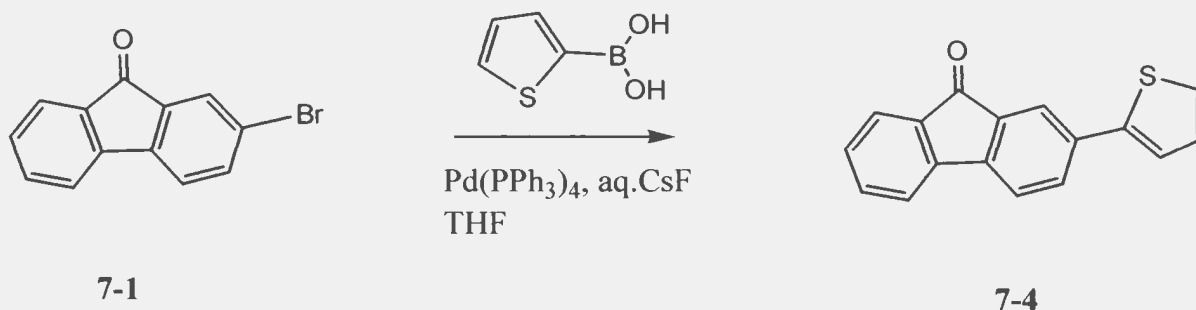
As shown in **Scheme 7.2**, 2,7-di-2-thienyl-9H-fluoren-9-one (**7-3**) was synthesized via a Suzuki-Miyaura coupling reaction using 2-thiopheneboronic acid (commercial sample, 3 equiv) and the dibromo compound **7-2** (1 equiv). The Suzuki-Miyaura coupling of boronic acid derivatives with aryl halides has become one of the most widely used methods for aryl-aryl bond formation due to its tolerance to a wide range of functional groups and the straight-forward separation of products [11]. The other advantages associated with this reaction include the low toxicity of the reagents and byproducts especially compared to tin containing compounds, mild reaction conditions, fewer side reactions, and higher conversions.

The catalyst tetrakis(triphenylphosphine)palladium is most common, but use of other homogeneous as well as immobilized heterogeneous palladium compounds has been reported [12]. Addition of base plays an important role in catalyst regeneration and speeds up the coupling reaction. Miyaura and co-workers found that bases such as NaOH, K<sub>2</sub>CO<sub>3</sub>, and K<sub>3</sub>PO<sub>4</sub> performed well in THF/H<sub>2</sub>O solvent systems [11]. In the present work, 2-thiopheneboronic acid was activated by aqueous K<sub>2</sub>CO<sub>3</sub> and the reaction time was 38 h. After re-crystallization from ethanol, the product **7-3** was obtained in 42%

yield. Later, the Suzuki-Miyaura coupling between **7-2** and 2-thiopheneboronic acid was carried out using cesium fluoride as the base under Wright-modified conditions [11] to accelerate the reaction rate. According to a previously proposed mechanism [11], fluoride ion displacement of the hydroxyl groups of the boronic acid to form an organotrifluoroborate ion *in situ* could occur, which would then undergo transmetallation. After 2 h of reaction, a red product was procured in 60-62% yield. A higher yield of compound **7-3** was obtained with CsF than in the reactions activated with K<sub>2</sub>CO<sub>3</sub> base. With this optimization, the starting material (**7-3**) for molecules **7-5**, **7-6** and **poly-7-3** was readily synthesized.

A C=O stretch at 1713 cm<sup>-1</sup> was observed in the FTIR spectrum of **7-3** and the <sup>1</sup>H NMR spectrum showed two doublets at 7.75 ppm and 7.41 ppm, characterizing the aromatic fluorene protons, H-3, H-6 and H-4, H-5, respectively. A singlet at 7.96 ppm identifies the H-1 and H-8 protons. Two doublets at 7.54 ppm and 7.34 ppm, and a triplet at 7.12 ppm characterize the thiophene protons, H-3, H-5, H-4, respectively. Also the elemental analysis data agreed well with the calculated values for **7-3**.

### 7.2.2 Synthesis of 2-(2-Thienyl)-9H-fluoren-9-one, **7-4**

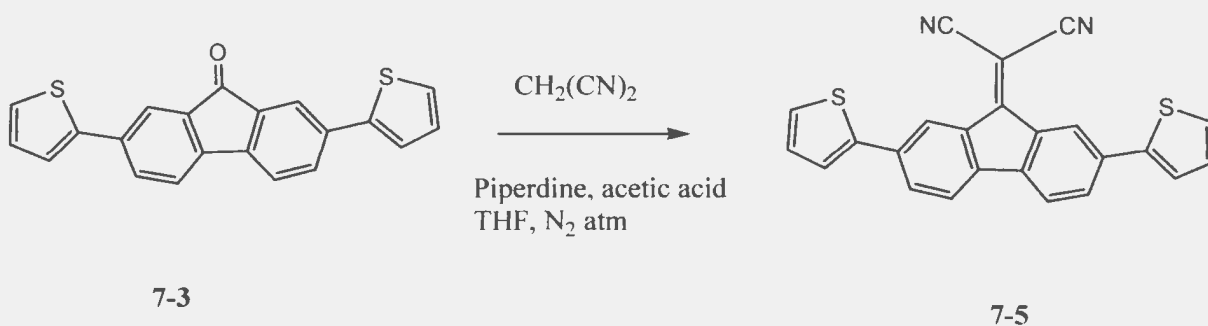


**Scheme 7.3**

A Wohl-Ziegler reaction between *n*-bromosuccinimide (1 equiv) and fluoren-9-one (1 equiv), under controlled conditions, resulted in 2-bromo-fluoren-9-one, **7-1** together with trace amounts of **7-2**. The separation of **7-1** from **7-2** was difficult, since both materials re-crystallized from ethanol. However, repeated re-crystallizations afforded yellow needles of pure 2-bromo-fluoren-9-one in 55% yield.

The synthesis of **7-4** was carried out as shown in **Scheme 7.3**. A Suzuki-Miyaura coupling reaction between 2-bromo-fluoren-9-one (1 equiv) and 2-thiopheneboronic acid (1.5 equiv) resulted in 2-(2-thienyl)-9H-fluoren-9-one (**7-4**) in 58% yield. The <sup>1</sup>H NMR spectrum of **7-4** showed one singlet at 7.87 ppm and two doublets at 7.69 ppm, 7.65 ppm characterizing H-1, H-3 and H-4, respectively. Two multiplets were observed at 7.28 ppm and 7.46 ppm characterizing the aromatic fluorene protons, H-5, H-6, H-7, H-8. Two doublets at 7.37 ppm, 7.32 ppm, and a triplet 7.10 ppm characterize the thiophene protons H-3, H-5, H-4, respectively. Also the MS and elemental analysis data agreed well with the calculated values for **7-4**.

### 7.2.3 Synthesis of (2,7-Di-2-thienyl-9H-fluoren-9-ylidene)malononitrile, **7-5**



**Scheme 7.4**

The carbonyl group in **7-3** is expected to be susceptible to nucleophilic attack. When heated with malononitrile in the presence of piperidine, a Knoevenagel condensation of **7-3** takes place and results in **7-5** (**scheme 7.4**). During a three hour reaction, a color change of the mixture from red to dark blue suggested the presence of a strong electron withdrawing ( $C=C(CN)_2$ ) group at the C-9 position of the fluorene unit and its existence was later confirmed by IR, NMR and mass spectra. The FTIR spectrum of compound **7-5** is shown in **Fig 7.1**. For comparison, the spectrum of the starting material (**7-3**) is also shown in Fig 7.1.

In the FTIR spectrum of 2,7-di-thiophen-2-yl-fluoren-9-one, the C=O group absorbs at  $1713\text{ cm}^{-1}$ . After condensation, the FTIR spectrum of **7-5** shows the absence of the C=O stretching vibration at  $1713\text{ cm}^{-1}$ , while there is a band at  $2225\text{ cm}^{-1}$  typical of a CN stretching vibration of a dicyanomethylene group. The  $^1\text{H}$  NMR spectrum showed two main groups of peaks associated with chemical shifts of 7.44-8.71 ppm and 7.13-7.57 that can be attributed to the fluorene and the thiophene protons, respectively.

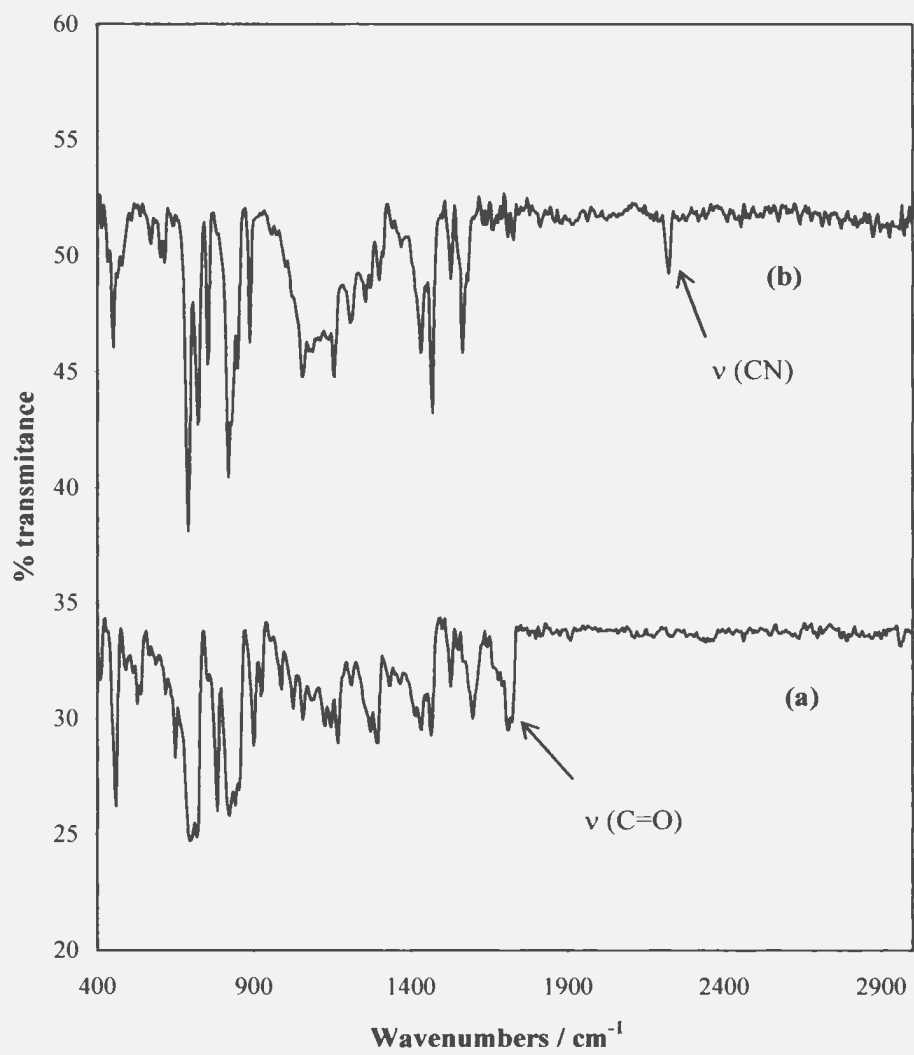


**Fig 7.1** IR spectra (KBr) of (a) 7-3 and (b) 7-5



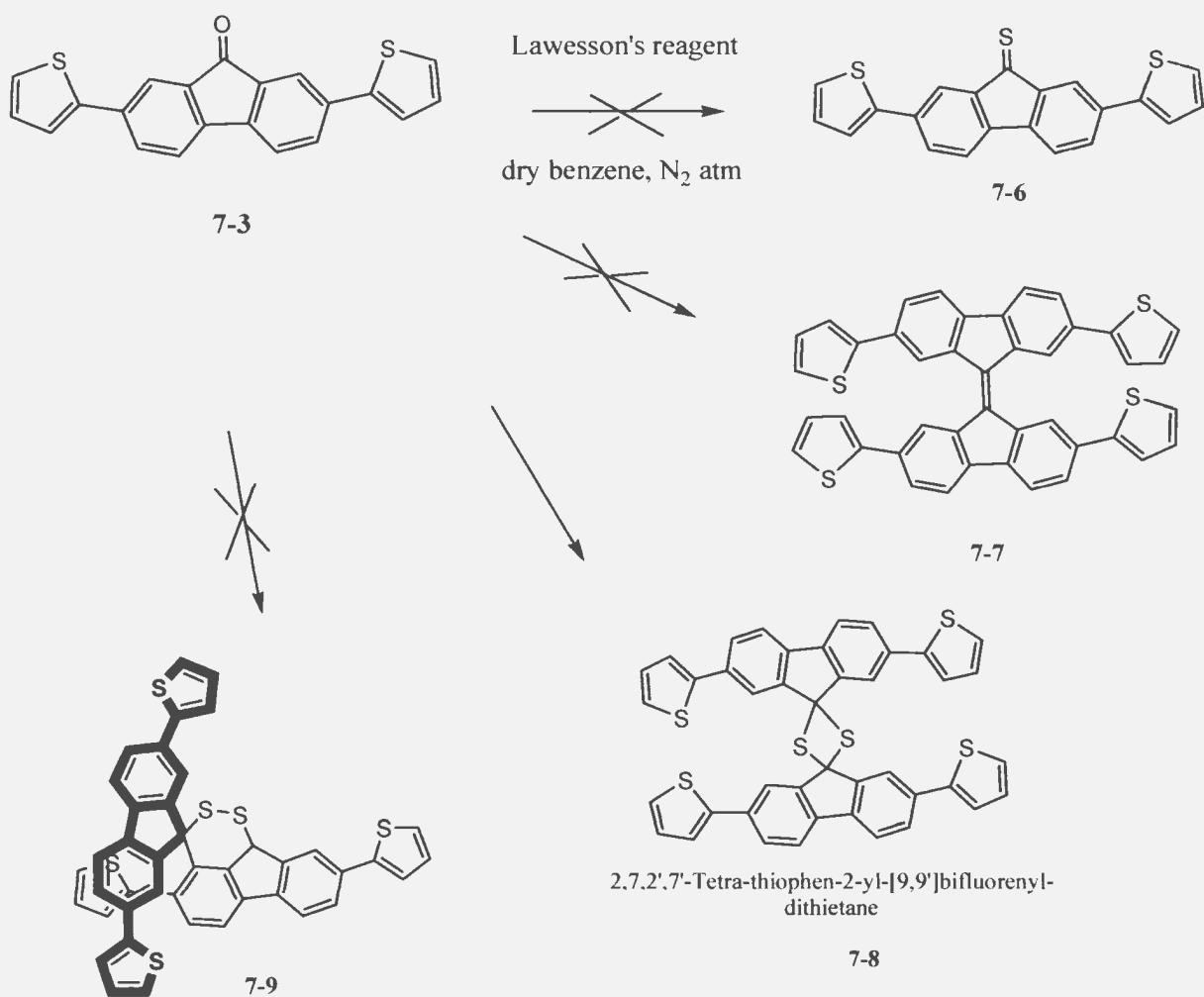
The resonance of the H-1 proton of the fluorene unit in **7-5** appears at a lower field of 8.71 ppm than the resonance, at 7.94 ppm, of the H-1 proton of **7-3**. This shift in resonance can be attributed to the presence of the strong electron withdrawing dicyanomethylene group of **7-5**. Furthermore, MS data provides further confirmation of the successful formation of **7-5**.

#### **7.2.4 Attempted Synthesis of 2,7-Di-2-thienyl-9H-fluorene-9-thione, 7-6 and/or 2,7,2',7'-Tetra-2-thienyl-[9,9']bifluorenylidene, 7-7**

Thionation, the conversion of a carbonyl group to a thiocarbonyl, is a widely used synthetic transformation for the preparation of organosulfur compounds. Typically this transformation is accomplished using either phosphorus pentasulfide (P<sub>4</sub>S<sub>10</sub>) or *Lawesson's* reagent [13]. 2,4-Bis(4-methoxyphenyl)-1,3,2,4-dithiadiphosphetane 2,4-disulfide, commonly known as *Lawesson's* reagent (**LR**), is one of the best known thionation reagents, and its advantage has been demonstrated for the thionation of a great variety of carbonyl compounds [14]. It tends to give good yields with fewer side reactions. However, because of the presence of highly electrophilic phosphorus species, reactions with **LR** require very dry conditions. To avoid unnecessary byproducts, benzene was dried with sodium prior to the reaction shown in **Scheme 7.5**.

Generally, thioketones are very reactive groups that have a tendency to undergo cycloadditions across a C=C bond or dimerization to form dithietanes. The formation of dithietanes has been mostly observed for aliphatic ketones[13]. In the case of aromatic

ketones other reactions occur. 9H-fluorene-9-thione, for example, dimerizes to form 9,9'-bifluorenylidene [14]. Thus, thioketones, dithietanes and C=C bonded dimers are the possible products of reactions involving aromatic ketones.



**Scheme 7.5**

With this knowledge of possible products during thionation, we carried out the reaction between **7-3** and **LR** in an attempt to synthesize 2,7-di-2-thienyl-9H-fluorene-9-thione (**7-6**) and/ or 2,7,2',7'-tetra-2-thienyl-[9,9']bifluorenylidene (**7-7**) **Scheme 7.5**. During a 5 h reaction, a color change from red to purple appeared but upon cooling, the product was unstable. Moreover, with longer reaction times, the color of the reaction mixture changed from red to purple and then to dark blue. Notably, the dark blue color remained stable upon cooling the reaction mixture, which tentatively indicated the stability of the product. Finally, blue needles were obtained after a straightforward separation by column chromatography and on subsequent re-crystallization from ethanol.

FT-IR,  $^1\text{H}$  NMR,  $^{13}\text{C}$  NMR, elemental analysis, and MS characterizations were performed. Elemental analysis data together with MS indicated that a dimer with six sulphur atoms had been obtained, suggesting the formation of the dithietane **7-8**. **Figure 7.2** shows a comparison of the FTIR spectra of **7-3** and the product of its thionation reaction (**7-8**). The C=O stretch at  $1713\text{ cm}^{-1}$  of **7-3** was noticeably absent in the spectrum of **7-8**. It is known that single bonds involving sulfur, such as the dithietane group give very weak infrared absorptions [15]. Nevertheless, the FTIR spectrum highlights the similarity of the carbon skeletons of **7-8** and **7-3**.

The  $^1\text{H}$  NMR spectrum of **7-8** (shown in **Fig 7.3**) is very similar to that of **7-3**, supporting the assignment of structure **7-8**, and ruling out the possibility of structure **7-9**. Two doublets at 7.73 ppm and 7.40 ppm, characterize the aromatic fluorene protons H-3, H-3', H-6, H-6' and H-4, H-4', H-5, H-5', respectively. A singlet at 7.98 ppm identifies the H-1/H-1' and H-8/H-8' protons.

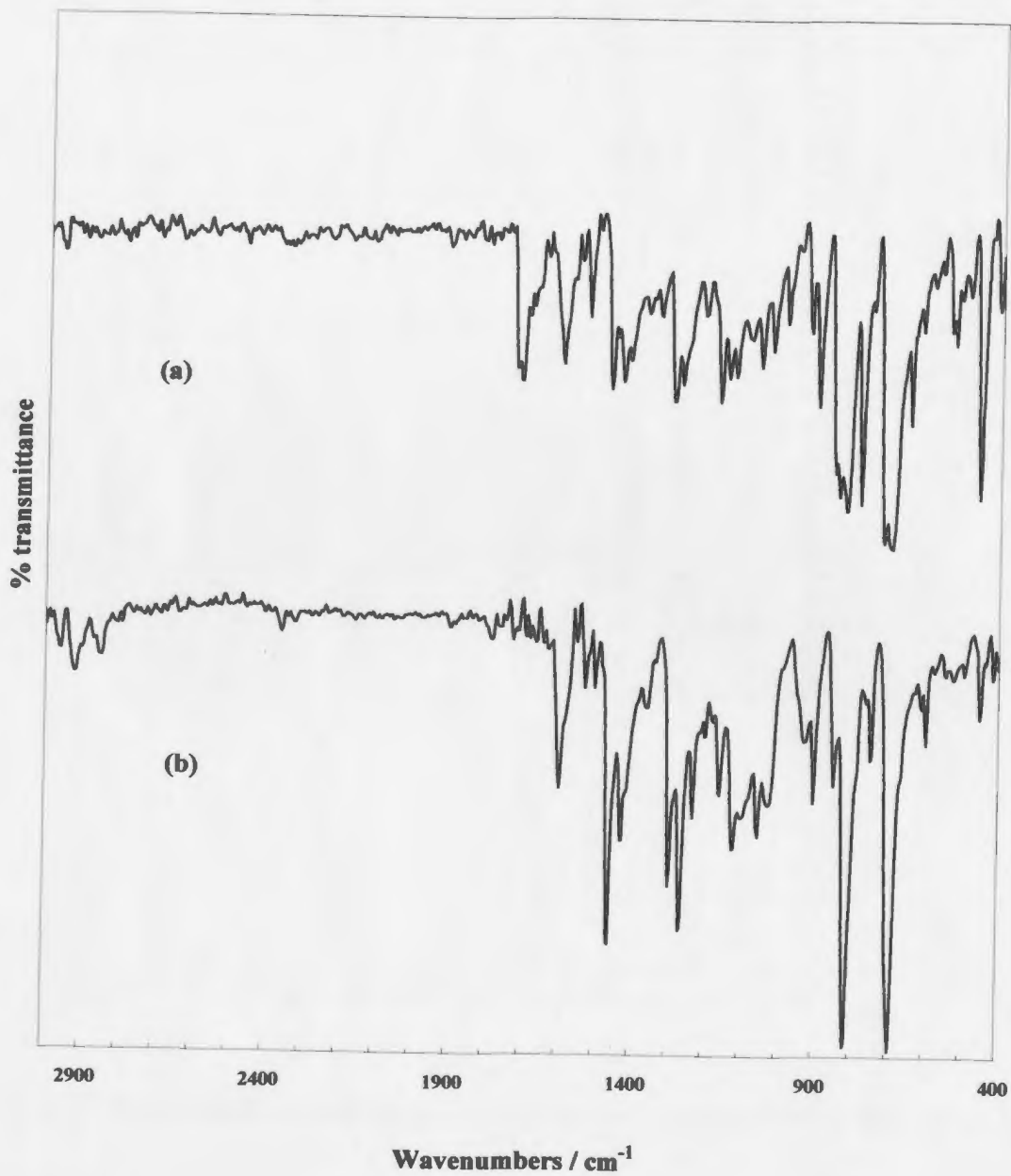


Fig 7.2 IR spectra (KBr discs) of a) 7-3, b) 7-8

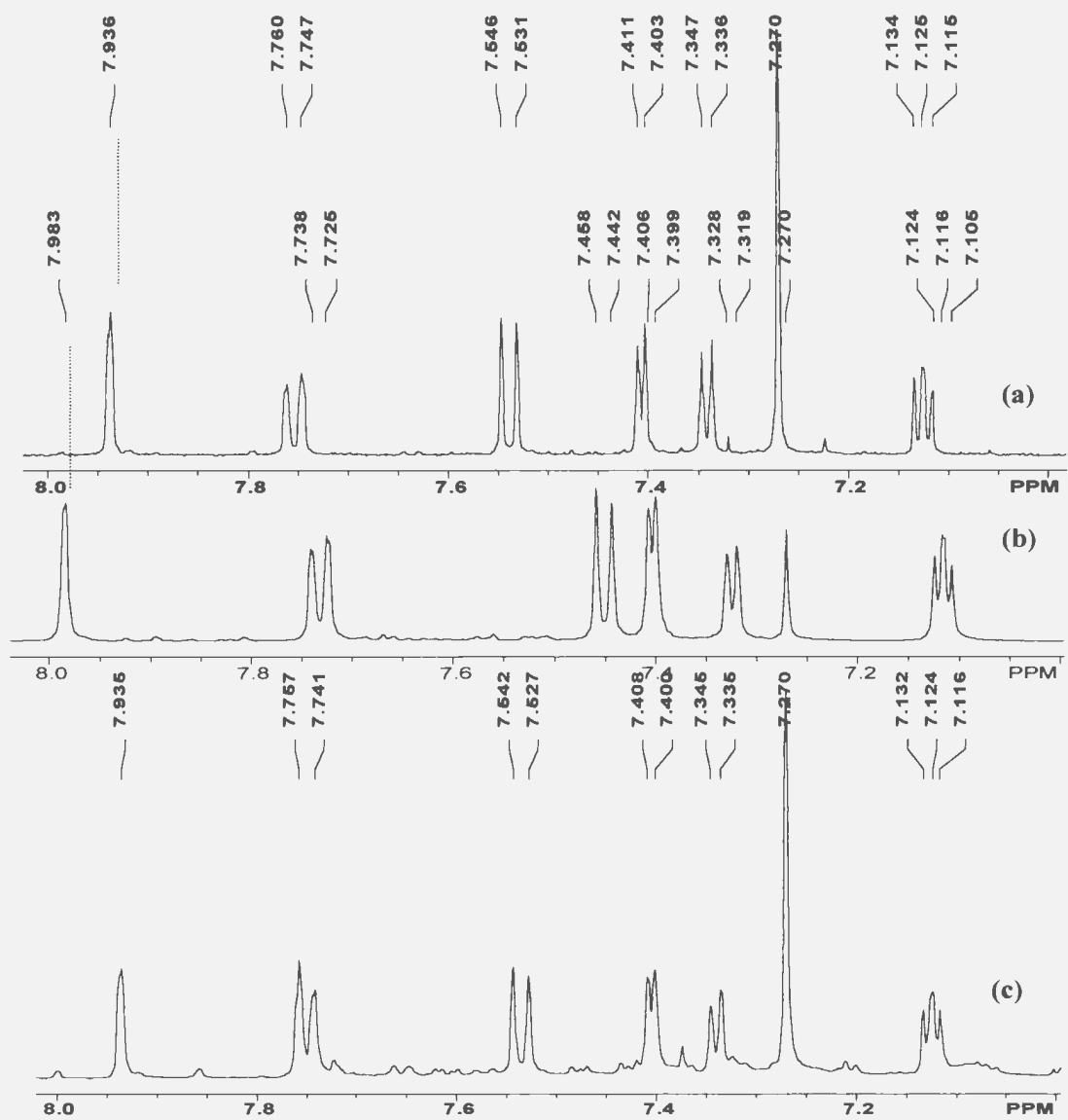


Fig 7.3 NMR spectra ( $\text{CDCl}_3$ ) of a) 7-3 b) 7-8 c) decomposition of 7-8 to 7-7

Two doublets at 7.54 ppm and 7.34 ppm, and one triplet at 7.12 ppm characterize the thiophene protons H-3'/H-3'', H-5'/H-5'', H-4''/H-5'', respectively.

MS analysis (Chemical ionization-CIMS) gave the molecular formula C<sub>42</sub>H<sub>24</sub>S<sub>6</sub> with a molecular ion peak at *m/z* 723. Also, daughter ion peaks at 689 (M-32), 657 (M-64), 361 were seen in the mass spectrum. The peak at *m/z* 689 represents the loss of one sulphur atom from the molecular ion peak. The peak at *m/z* 657 correspond to the dimer 7-7. The daughter ion peak at *m/z* 361 can be assigned to thioketone 7-6.

Compound 7-8 was stable as a solid but slowly decomposed in solution (> 12 h) at room temperature. This was indicated by a color change from dark blue to brown and the changes in the proton NMR spectrum shown in **fig 7.3**. The spectrum of the product was almost indistinguishable from that of 7-3. However, MS showed a molecular ion peak at 657 corresponding to the dimer 7-7. Purification and further characterization of this compound were unsuccessful due to the difficulties in scaling-up the decomposition reaction.

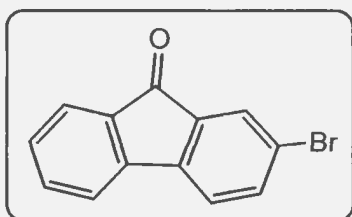
### 7.3 Conclusions

Donor-acceptor conjugated co-monomers with different D-A ratios, consisting of thiophene as the electron rich subunit (D) and fluoren-9-one as the electron deficient subunit (A), were synthesized in moderate yields by means of Suzuki cross-coupling reactions. (2,7-di-thiophen-2-yl-fluoren-9-ylidene)-isocyano-acetonitrile was synthesized by a Knoevenagel condensation of 2,7-di-thiophen-2-yl-fluoren-9-one. The reaction between 2,7-di-2-thienyl-9H-fluoren-9-one and *Lawesson's* reagent has yielded a new

precursor material 2,7,2',7'-tetra-thiophen-2-yl-[9,9']bifluorenyl-dithietane. The electrical and optical properties of these materials are discussed in the following chapter.

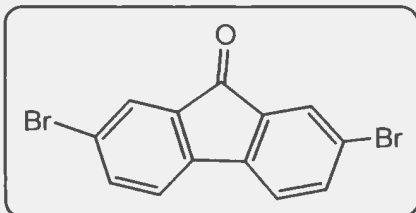
## 7.4 Experimental

### 2-Bromo-fluoren-9-one, 7-1



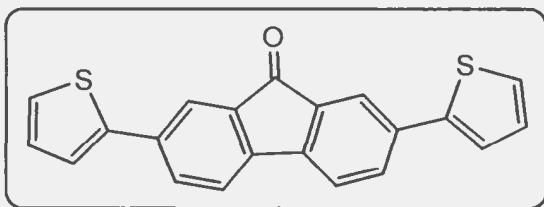
*N*-bromosuccinimide (1.78 g, 10 mmol) was slowly added in 100 mg portions to a solution of fluoren-9-one (1.80 g, 10 mmol) in 70% v/v sulphuric acid (150 mL); the mixture was kept at 40 °C for 1 h. Repeated re-crystallization of the product from ethanol gave yellow needles of 2-bromo-fluoren-9-one (1.42 g, 5.49 mmol, 55%): mp 145-147 °C (Lit [13]:148 °C): <sup>1</sup>H NMR (500 MHz, CDCl<sub>3</sub>) δ(ppm) 7.77 (s, 1H), 7.67 (d, *J* = 6.5 Hz, 1H), 7.62 (m, *J* = 9.5 Hz, 2H), 7.51 (d, *J* = 13.5 Hz, 1H), 7.39 (d, *J* = 13.0 Hz, 1H), 7.33 (d, *J* = 10.5 Hz, 1H) ; MS *m/z*: 260 (M<sup>+</sup>).

### 2,7-Dibromo-fluoren-9-one, 7-2



*N*-bromosuccinimide (1.78 g, 10 mmol) was added to a solution of fluoren-9-one (0.91 g, 5 mmol) in 85% v/v sulphuric acid (100 mL) and the mixture was vigorously stirred for 25 minutes at room temperature. Re-crystallization of the product from ethanol and then ethyl acetate gave a bright yellow compound (1.101 g, 3.25 mmol, 65%). Mp 197-198 °C (Lit [13]:199-200 °C); <sup>1</sup>H NMR (500 MHz, CDCl<sub>3</sub>) δ(ppm) 7.78 (s, 2H), 7.64 (d, *J* = 10.0 Hz, 2H), 7.40 (d, *J* = 8.5 Hz, 2H); MS *m/z*: 339 (M<sup>+</sup>).

### 2,7-Di-2-thienyl-9H-fluoren-9-one, 7-3

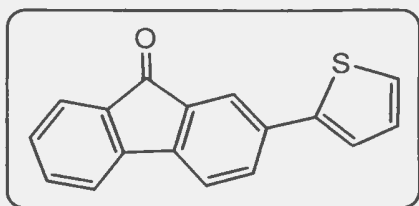


A mixture of 2,7-dibromo-fluoren-9-one (0.676 g, 2 mmol), tetrakis(triphenylphosphine)palladium(0) (0.043 g, 0.03 mmol), and 2-thiopheneboronic acid (0.768 g, 6 mmol) in THF (10 mL) with potassium carbonate (1.0 mL of 2 M solution in deoxygenated water) was heated to reflux (65-75 °C) for 38 h. The reaction mixture was poured into ice and the red precipitate was collected by filtration. The precipitate was then washed with hexane/CHCl<sub>3</sub> (1:1) and re-crystallized from ethanol to



afford. after drying in air, the title compound (0.28 g, 0.84 mmol, 42%). The above procedure was revised with cesium fluoride as the base (1.0 mL of 2 M solution in deoxygenated water) and the reaction mixture was heated to reflux for 2 h. After purification 0.42 g (1.22 mmol, 61%) of the title compound was obtained: mp 265 °C; FTIR (KBr)  $\nu_{\text{C=O}}$  1713  $\text{cm}^{-1}$ ;  $^1\text{H NMR}$  (500 MHz,  $\text{CDCl}_3$ )  $\delta$ (ppm) 7.94 (s, 2H), 7.75 (d,  $J = 6.5$  Hz, 2H), 7.54 (d,  $J = 7.5$  Hz, 2H), 7.41 (d,  $J = 4.0$  Hz, 2H), 7.34 (d,  $J = 5.5$  Hz, 2H), 7.12 (t,  $J = 9.5$  Hz, 2H). Anal. Calc'd for  $\text{C}_{21}\text{H}_{12}\text{OS}_2$ : C, 73.23%; H, 3.51%; S, 18.62%. Found: C, 72.76%; H, 3.91%; S, 18.02%. MS  $m/z$ : 345 ( $\text{M}^+$ ).

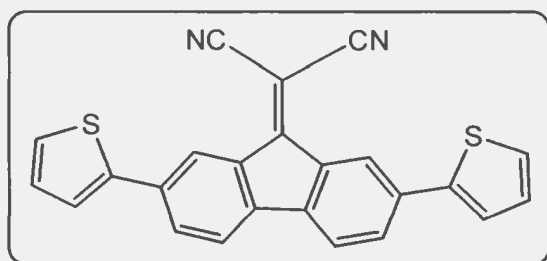
#### 2-(2-Thienyl)-9H-fluoren-9-one, 7-4



A mixture of 2-bromo-fluoren-9-one (0.518 g, 2 mmol), tetrakis(triphenylphosphine)-palladium(0) (0.027 g, 0.023 mmol), and 2-thiopheneboronic acid (0.384 g, 3 mmol) in THF (10 mL) with cesium fluoride (1.0 mL of 2 M solution in deoxygenated water) was heated at 65-75 °C for 2 h. The reaction mixture was poured into ice and the precipitate was collected by filtration, dissolved in THF, dried over magnesium sulphate and the solvent was removed by rotatory evaporation. The dried product was then washed with hexane/ $\text{CHCl}_3$  (1:1), air-dried and re-crystallized with ethanol to afford 0.304 g (1.16 mmol, 58%) of the titled compound as fine yellow needles: mp 150 °C; FTIR (KBr)  $\nu_{\text{C=O}}$  1713  $\text{cm}^{-1}$ ;  $^1\text{H NMR}$  (500 MHz,  $\text{CDCl}_3$ )  $\delta$ (ppm) 7.87 (s, 1H), 7.69 (d,  $J = 8.0$  Hz, 1H),

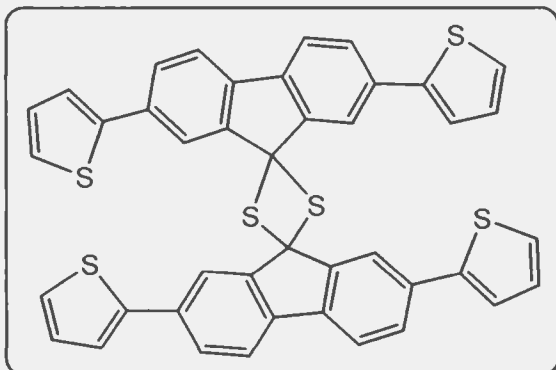
7.65 (d,  $J = 7.0$  Hz, 1H), 7.48 (m,  $J = 13.0$  Hz, 3H), 7.37 (d,  $J = 4.0$  Hz, 1H), 7.32 (d,  $J = 5.0$  Hz, 1H), 7.29 (m,  $J = 13.5$  Hz, 1H), 7.10 (t,  $J = 8.5$  Hz, 1H). Anal. Calc'd for  $C_{17}H_{10}OS$ : C, 77.84%; H, 3.84%; S, 12.22%. Found: C, 77.22%; H, 3.93%; S, 11.12%. MS  $m/z$ : 263 ( $M^+$ ).

**(2,7-Di-2-thienyl-9H-fluoren-9-ylidene)malononitrile, 7-5**



A solution of 2,7-di-thiophen-2-yl-fluoren-9-one (1.032 g, 3 mmol) in THF (30 mL), malononitrile (0.396 g, 6 mmol), glacial acetic acid (0.01 mL, 0.19 mmol) and a catalytic amount of piperidine (0.1 mL, 0.6 mmol) was stirred for 0.5 h at room temperature and then refluxed at 65-75 °C for 3 h. The reaction mixture was poured into ice water and the dark blue precipitate was collected by filtration. Then the precipitate was washed with copious amounts of water, dissolved in THF, dried over magnesium sulphate and the solvent was removed by rotatory evaporation. The obtained solid was re-crystallized from ethanol to yield 0.78 g (2 mmol, 67%) of the title compound as fine blue needles: mp 282 °C; FTIR (KBr)  $\nu_{CN}$  2223  $cm^{-1}$ ;  $^1H$  NMR (500 MHz,  $CDCl_3$ )  $\delta$ (ppm) 8.71 (s, 2H), 7.74 (d,  $J = 6.5$  Hz, 2H), 7.56 (d,  $J = 7.5$  Hz, 2H), 7.43 (d,  $J = 4.0$  Hz, 2H), 7.36 (d,  $J = 5.5$  Hz, 2H), 7.14 (t,  $J = 9.5$  Hz, 2H); CIMS  $m/z$ : 393 ( $M^+$ ).

### 2,7,2',7'-Tetra-2-thienyl-[9,9']bifluorenyl-dithietane, 7-8



To a solution of 2,7-di-thiophen-2-yl-fluoren-9-one (1.032 g, 3 mmol) in dried benzene (50 mL) was added Lawesson's reagent (2.42 g, 6 mmol). The mixture was heated to reflux (80-90 °C) under a nitrogen atmosphere. The reaction was followed every hour by TLC and the color changes during the course of the reaction were monitored. After 5 hours the color of the reaction mixture had changed from red to purple and on overnight reflux a further change from purple to dark blue had occurred. After cooling the reaction to room temperature, the solvent was removed by rotatory evaporation and the product was then purified by column chromatography (silica gel, hexane/dichloromethane 9:1) and re-crystallized from ethanol to give a dark blue compound (0.108 g, 0.15 mmol, 5%): mp 135 °C;  $^1\text{H}$  NMR (500 MHz,  $\text{CDCl}_3$ )  $\delta$ (ppm) 7.98 (s, 4H), 7.73 (d,  $J = 6.5$  Hz, 4H), 7.45 (d,  $J = 8.0$  Hz, 4H), 7.40 (d,  $J = 3.5$  Hz, 4H), 7.32 (d,  $J = 4.5$  Hz, 4H), 7.11 (t,  $J = 9.5$  Hz, 4H);  $^{13}\text{C}$  NMR (500 MHz,  $\text{CDCl}_3$ )  $\delta$ (ppm) 143.5, 142.5, 141.8, 135.4, 131.4, 128.3, 125.4, 123.9, 121.4, 120.4, 96.3. Anal. Calc'd for  $\text{C}_{42}\text{H}_{24}\text{S}_6$ : C, 69.96%; H, 3.36%; S, 26.68%. Found: C, 70.58%; H, 3.56%; S, 25.25%. MS  $m/z$ : 722 (M+1), 657, 361, 331.

## References:

- 1 Argun, A. A.; Aubert, P. H.; Thompson, B. C.; Schwendeman, I.; Gaupp, C. L.; Hwang, J.; Pinto, N. J.; Tanner, D. B.; MacDiarmid, A. G.; Reynolds, J. R. *Chem. Mater.* **2004**, *16*, 4401.
- 2 Rault-Berthelot, J.; Raoult, E.; Le Floch, F. *J. Electroanal. Chem.* **2003**, *546*, 29
- 3 Manisankar, P.; Vedhi, C.; Selvanathan, G.; Somasundaram, R. M. *Chem. Mater.* **2005**, *17*, 1722.
- 4 Gaupp, C. L.; Reynolds, J. R. *Macromolecules* **2003**, *36*, 6305.
- 5 Demadrille, R.; Rannou, P.; Bleuse, J.; Oddou, J.-L.; Pron, A.; Zagorska, M. *Macromolecules* **2003**, *36*, 7045.
- 6 Berlin, A.; Zotti, G.; Zecchin, S.; Schiavon, G.; Vercelli, B.; Zanelli, A. *Chem. Mater.* **2003**, *16*, 3667.
- 7 Uckert, F.; Setayesh, S.; Mullen, K. *Macromolecules* **1999**, *32*, 4519.
- 8 Cihaner, A.; Tirkes, S.; Onal, A. M. *J. Electroanal. Chem.* **2004**, *568*, 151.
- 9 Dewhurst, F.; Shah, P. K. *J. Chem. Soc. (C)* **1970**, 1738
- 10 Huang, F. *M.Sc. Dissertation*. Memorial University of Newfoundland, St. John's, Canada, **2004**
- 11 Miyaura, N.; Suzuki, A. *Chem. Rev.* **1995**, *95*, 2457.
- 12 Heidenreich, Köhler, K. ; Krauter, J. G. E.; Pietsch, J. *Synlett* **2002**, *7*, 1118.
- 13 Nakamura, M.; Isobe, H.; Nakamura E. *Chem. Rev.* **2003**, *103*, 1295.
- 14 Scheibye, S.; Shabana, R.; Lawesson, S.O.; Romming, C. *Tetrahedron* **1982**, *38*, 993.

15 Lambert, J. B. et al. *Organic Structural Spectroscopy* Prentice-Hall, Inc. New Jersey **1998**.

## *Chapter 8*

# **The Influence of Donor Acceptor Units on the Band gaps of Fluorene Based Copolymers**

### **8.1 Introduction**

Since  $\pi$ -conjugated polymers allow virtually endless manipulation of their chemical structure, control of the band-gaps of these semiconductors is a research issue of ongoing interest. This band-gap engineering can give the polymer its desired electrical and optical properties; reduction of the band-gap to approximately zero is expected to give an intrinsically conducting polymer [1]. One of the most successful approaches to low band-gap polymers is the application of an alternating sequence of donor-acceptor (D-A) units in the  $\pi$ -conjugated polymer chain [2-5]. Many fluorene based conducting polymers have been investigated to explore the applicability of the donor-acceptor strategy [3, 6-7].

Fluorenone is an attractive precursor material to produce low band gap polymers with a low LUMO energy level [8]. The presence of an electron withdrawing group at the C-9 position of a fluorenone unit reduces the reduction potential to -1.3 V but at the expense of an increased oxidation potential when compared to that of fluorene [9]. The co-polymerization of  $\pi$ -rich units such as EDT, with electron deficient fluorene

derivatives was found to facilitate the p-doping process, lower the band-gap and improve the stability of the resulting copolymers [10-11]. Furthermore, the band-gap of the

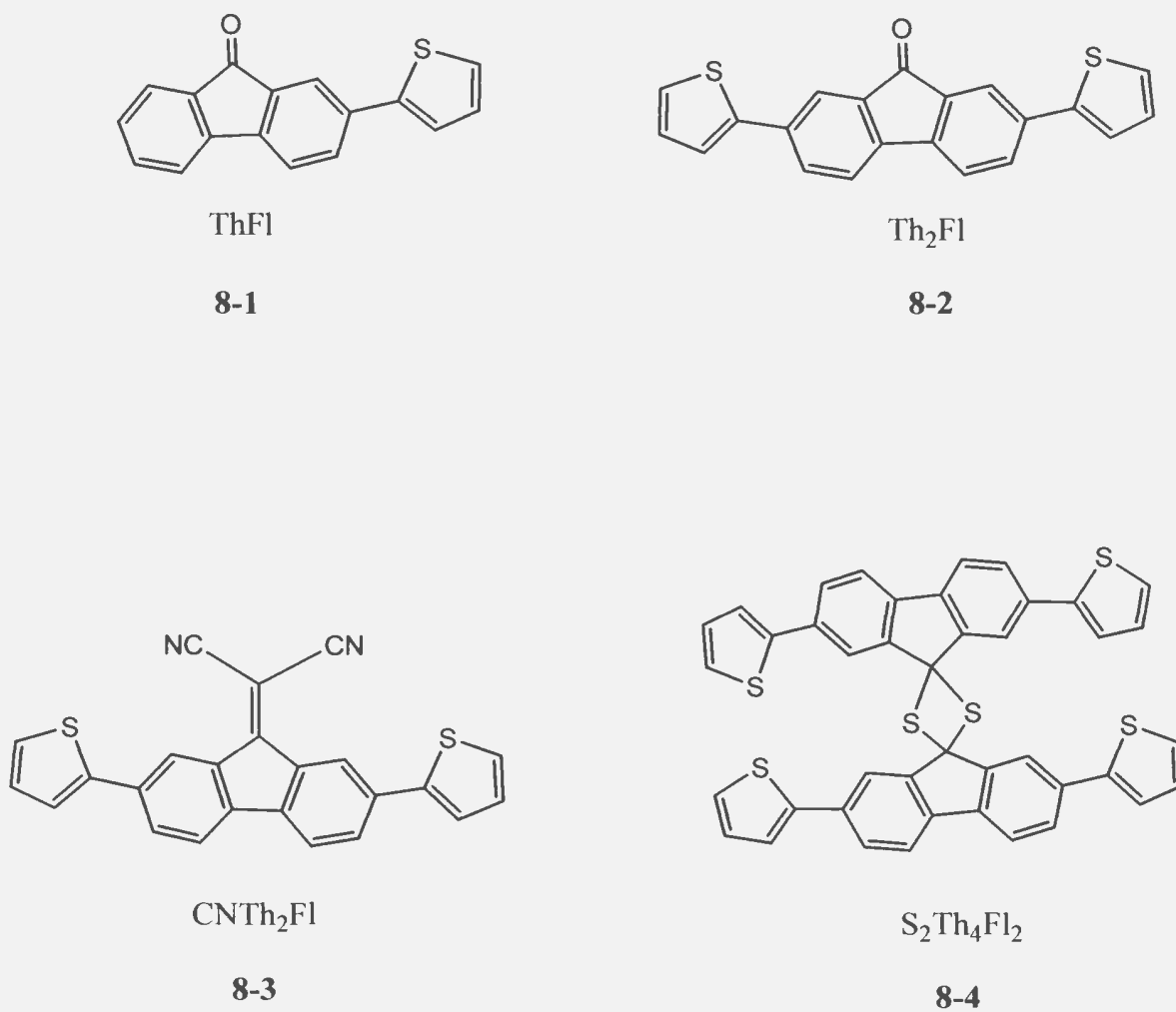
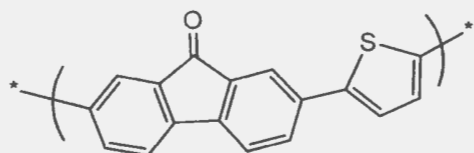
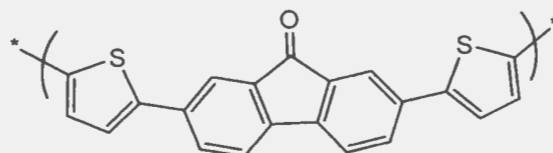


**Fig 8.1.** Structures of fluorene based comonomers



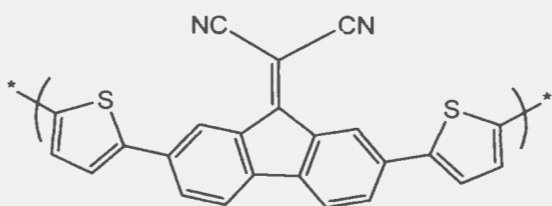
poly-(ThFl)

8-5



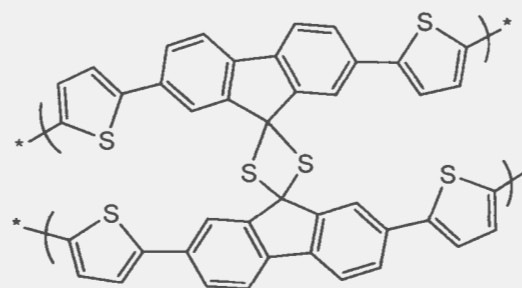
poly-(Th<sub>2</sub>Fl)

8-6



poly-(CNTh<sub>2</sub>Fl)

8-7



poly-(S<sub>2</sub>Th<sub>4</sub>Fl<sub>2</sub>)

8-8

**Fig 8.2.** Structures of fluorene based copolymers



copolymers can be easily controlled by changing/altering the number of donor units and by increasing the electronegativity difference between donor and acceptor units [10-12]. We have studied both of these issues with the monomeric and polymeric fluorene-thiophene systems shown in structures 8-1 to 8-8 (**Fig 8.1** and **Fig 8.2**), and report here on the effect of D-A units on band-gaps and conductivities of polyfluorene derivatives.

## **8.2 Redox Potentials and Band Gaps of ThFl, Th<sub>2</sub>Fl and CNTh<sub>2</sub>Fl**

### **8.2.1 Redox Potentials of ThFl, Th<sub>2</sub>Fl and CNTh<sub>2</sub>Fl**

**Fig 8.3** represents cyclic voltammograms, from two different experiments, for the reduction and oxidation of ThFl at a Pt electrode. During the cathodic cycle, reduction of ThFl occurs with a peak potential of ca. -1.35 V and in the reverse scan, a peak indicating a reversible solution process was seen at -1.2 V. During the anodic cycle, an oxidation wave was observed with a peak potential of +1.55 V. In the reverse scan, a broad reduction wave between +1.35 and +0.80 V was seen, which can be attributed to the undoping of a polymer formed on the electrode during the forward scan.

The oxidation and reduction behavior of Th<sub>2</sub>Fl (**Fig 8.4**) at a Pt electrode was similar to that of ThFl. In this case, the cathodic cycle was performed first to avoid contamination of the electrode surface by the polymer formed during anodic cycling. The formal potential for reduction was ca. -1.30 V. During the positive scan, the anodic peak potential at +1.33 V and, a broad de-doping range (+1.22 to +0.55 V) were observed. Reduction of CNTh<sub>2</sub>Fl (**Fig 8.5**) occurs with a formal potential of -0.75 V. During the

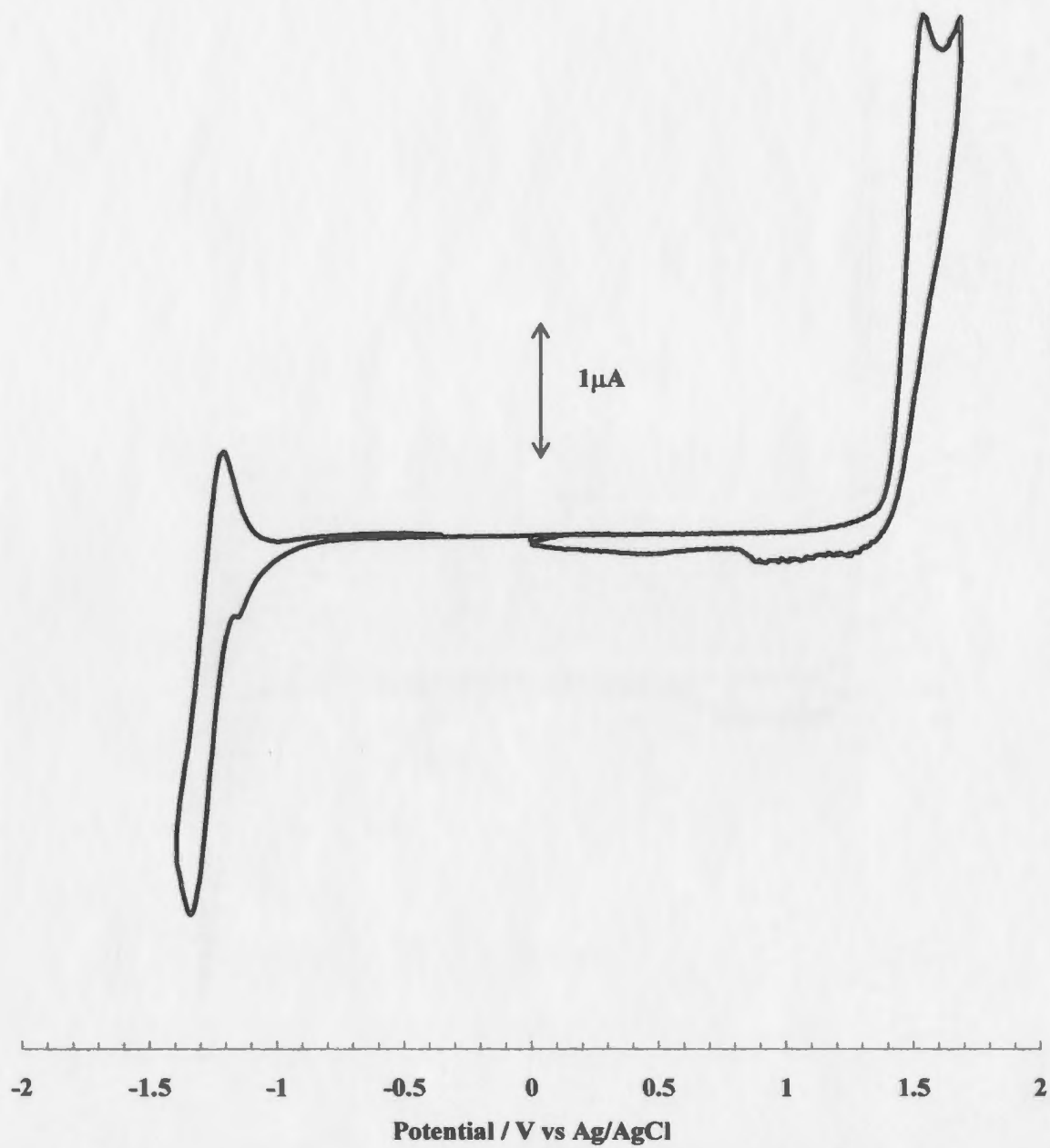


**Fig 8.3.** Cyclic voltammograms ( $100\ \text{mV s}^{-1}$ ) of ThFl (2 mM) in dichloromethane containing 0.1 M  $\text{Bu}_4\text{NPF}_6$

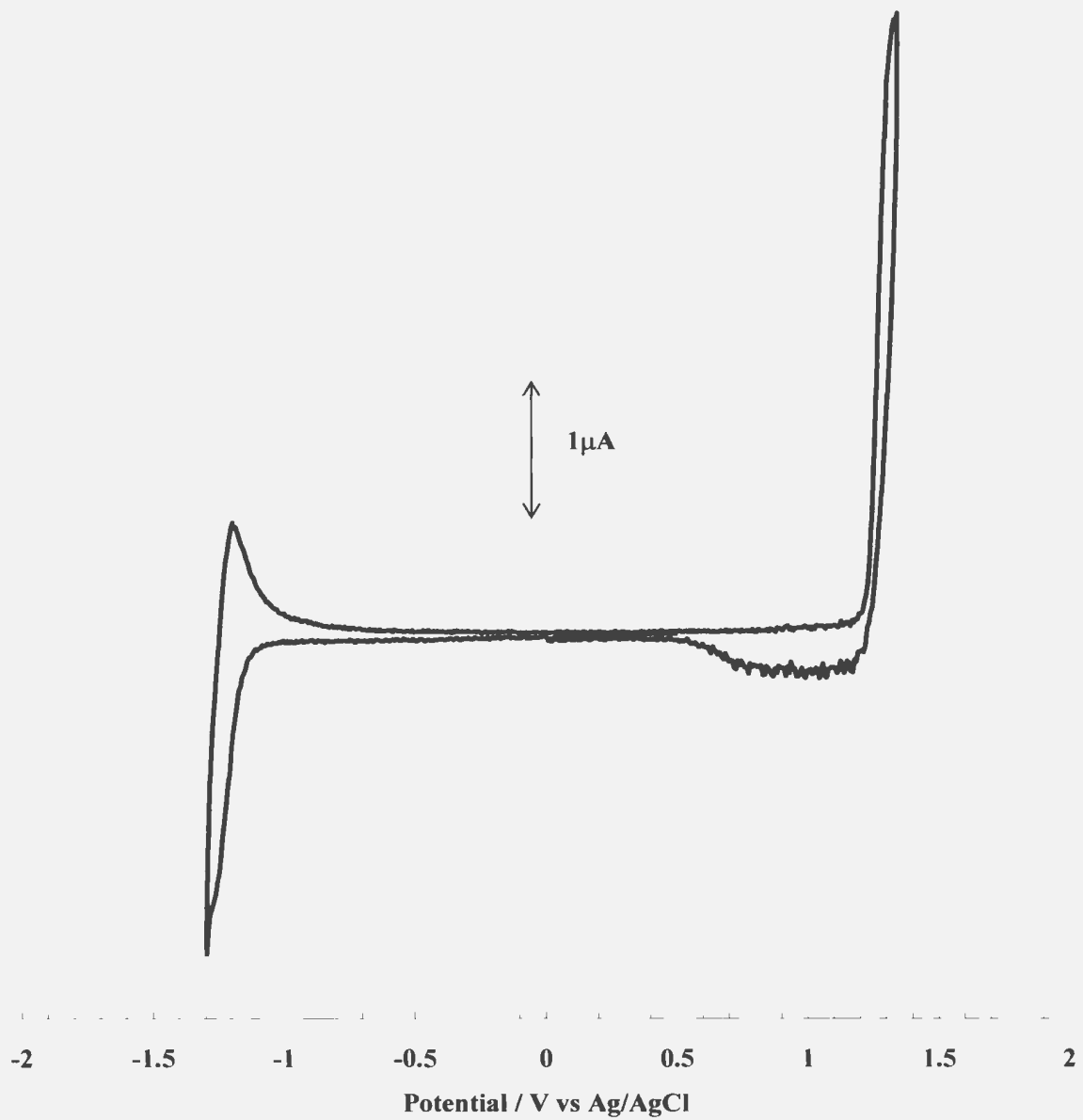


**Fig 8.4.** Cyclic voltammograms ( $100\ \text{mV s}^{-1}$ ) of  $\text{Th}_2\text{FI}$  (2 mM) in dichloromethane containing 0.1 M  $\text{Bu}_4\text{NPF}_6$

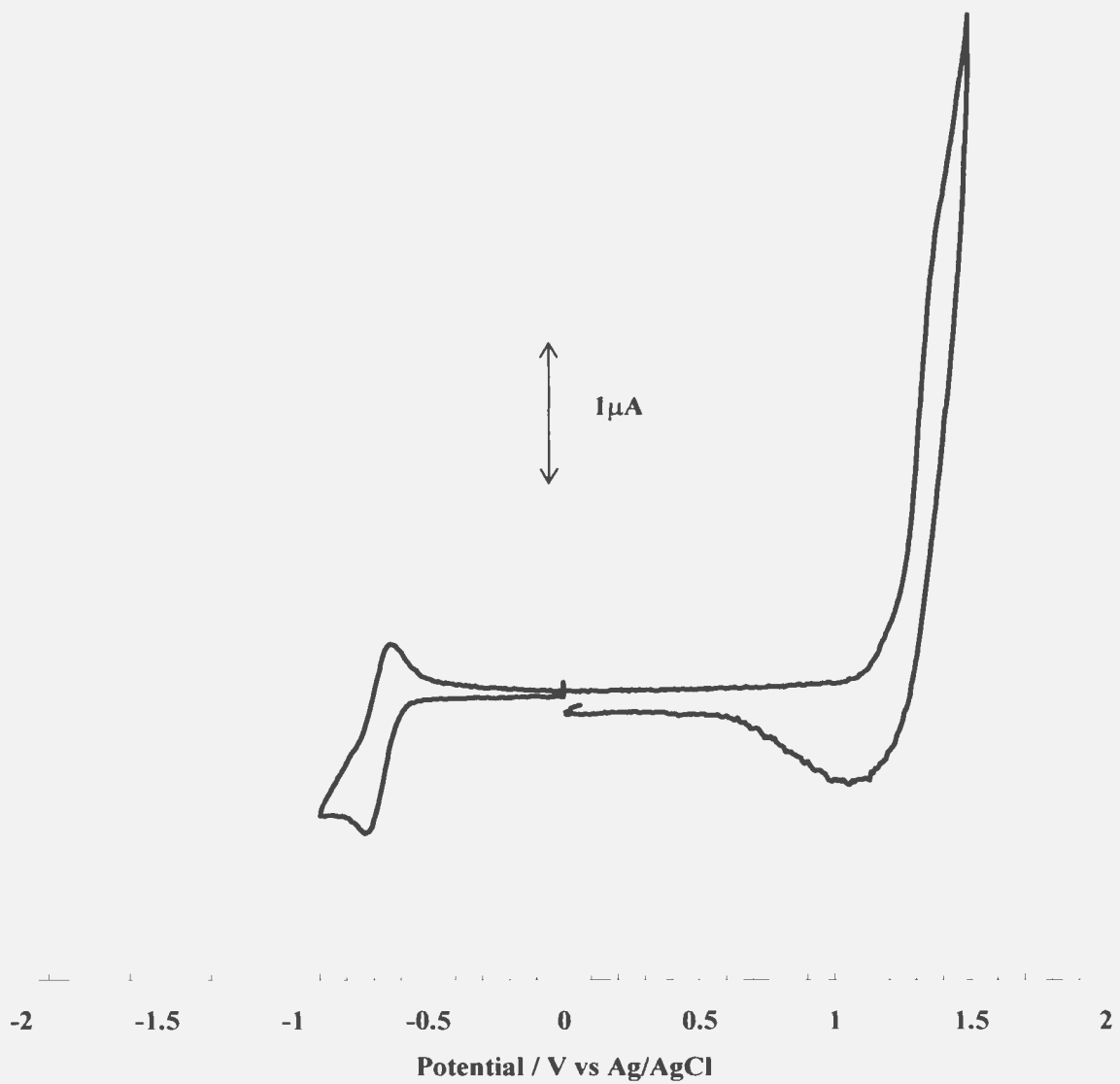


**Fig 8.5.** Cyclic voltammograms ( $100 \text{ mV s}^{-1}$ ) of  $\text{CNTh}_2\text{F1}$  (2 mM) in dichloromethane containing 0.1 M  $\text{Bu}_4\text{NPF}_6$

positive scan, an oxidation wave was observed with a peak potential of ca. +1.40 V. In the reverse scan, there was a reduction (undoping) wave at ca. +1.00 V.

### 8.2.2 UV-Visible Spectroscopic Results of ThFl, Th<sub>2</sub>Fl and CNTh<sub>2</sub>Fl

UV-vis absorption spectroscopy of ThFl, Th<sub>2</sub>Fl and CNTh<sub>2</sub>Fl was carried out in chloroform. ThFl (Fig 8.6, curve a) exhibits a  $\pi$ - $\pi^*$  absorption with a maximum at ca. 433 nm (2.9 eV) and an onset of ca. 525 nm (2.4 eV). Onset wavelengths and the optical absorption maximum of Th<sub>2</sub>Fl (Fig 8.6, curve b) were estimated to be 580 nm (2.1 eV) and 563 nm (2.2 eV), respectively. Also shown in Fig 8.6 (curve c) is an absorption spectrum of CNTh<sub>2</sub>Fl, with an onset wavelength at ca. 770 nm (1.6 eV) and a maximum at ca. 580 nm (2.1 eV).

### 8.3 Electropolymerizations of ThFl, Th<sub>2</sub>Fl and CNTh<sub>2</sub>Fl

A film of poly-ThFl was formed (Fig 8.7, CV a) on a Pt electrode by the anodic polymerization of ThFl (ca. 2mM) in dichloromethane containing 0.1 M Bu<sub>4</sub>NPF<sub>6</sub>. On continuous potential scanning between 0.4 and +1.8 V, a current increase in a region between ca. 0.9 and ca. 1.4 V was observed. Following this experiment, a yellow film was seen coating the electrode.

Similarly, polymerization and film deposition were characterized by increasing peak currents for oxidation of Th<sub>2</sub>Fl on successive cycles while potential scanning between 0.4 and +1.4 V. A red poly-Th<sub>2</sub>Fl film was visible on the electrode after multiple cycles as illustrated in Fig 8.7, CV b. Electrochemical generation of a poly-CNTh<sub>2</sub>Fl film

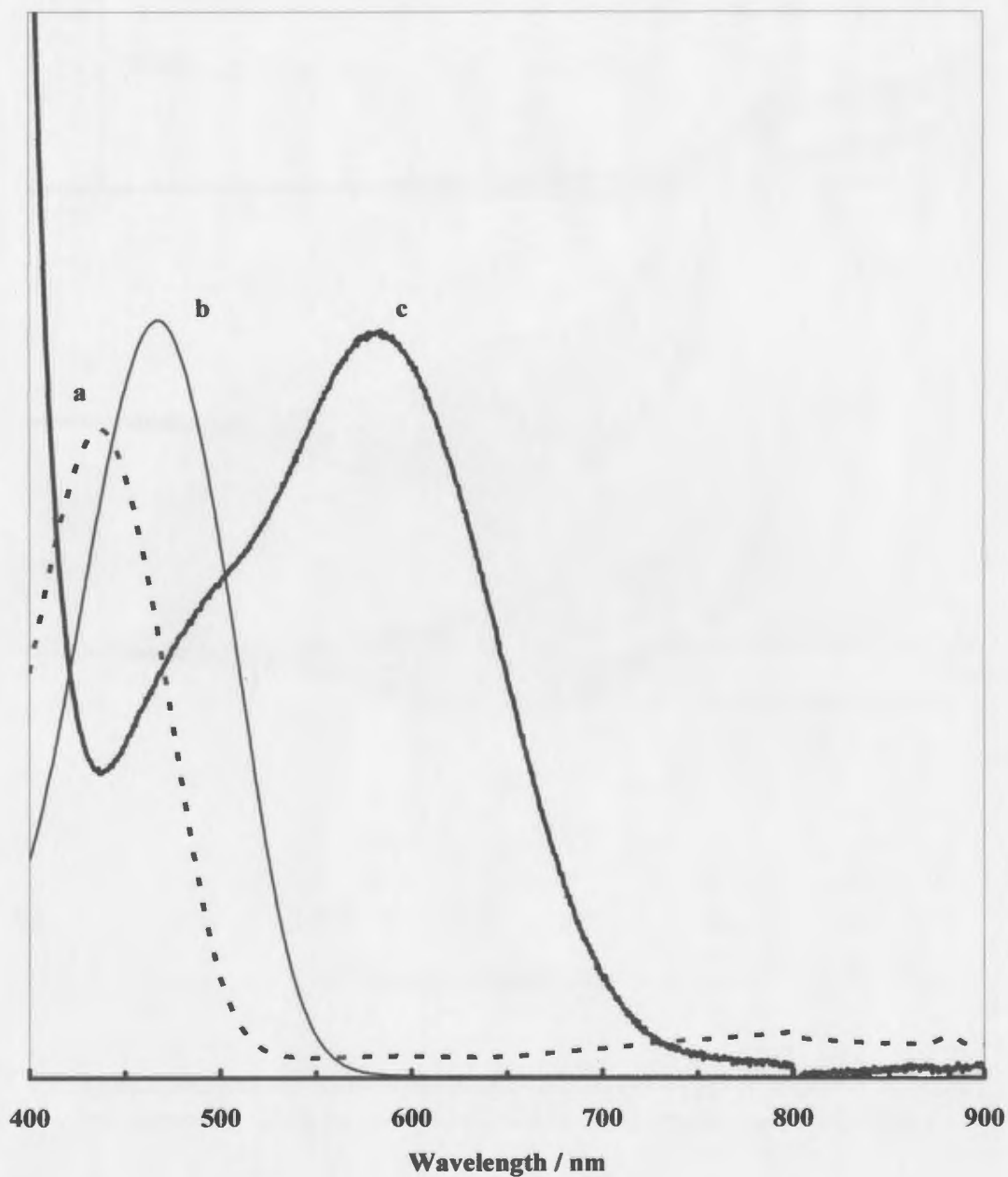


**Fig 8.6.** Comparison of UV-Visible spectra of (a) ThFI, (b) Th<sub>2</sub>FI and (c) CNTh<sub>2</sub>FI recorded in CHCl<sub>3</sub> solution.

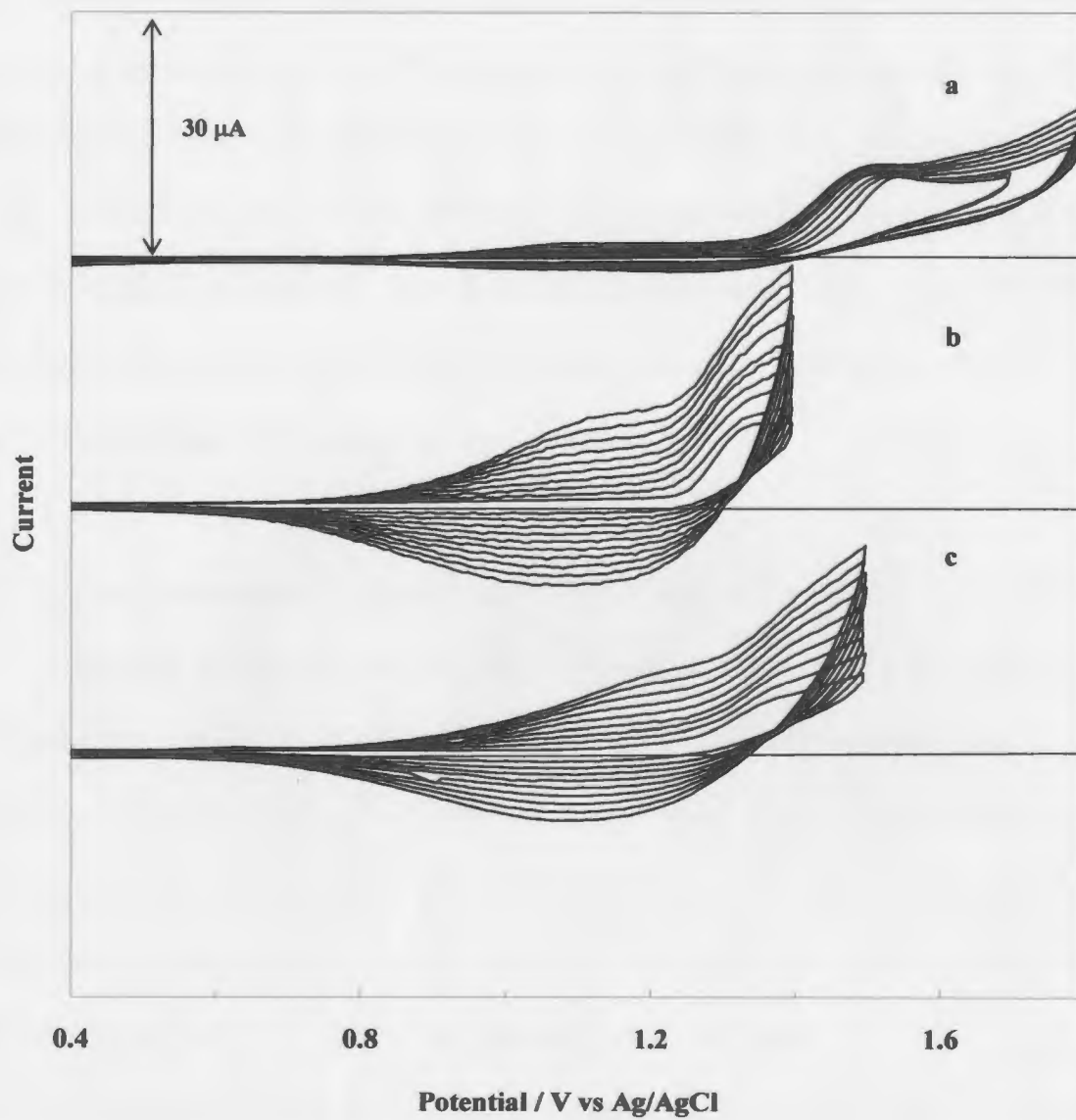


**Fig 8.7.** Multisweep cyclic voltammograms (100 mV/s) at a Pt electrode of 2 mM precursors (A- ThFl; B- Th<sub>2</sub>Fl; C- CNTh<sub>2</sub>Fl) in dichloromethane containing 0.1 M Bu<sub>4</sub>NPF<sub>6</sub>

on a Pt electrode by potential scanning between 0.4 and 1.5 V is shown in Fig 8.7 (CV c). On continuous potential scanning, a broad wave extending from +0.8 V to +1.3 V became progressively higher indicating the growth of the polymer. A dark blue film was observed on the electrode after the final electrochemical oxidation. Copolymer films were rinsed with acetone and dried in air before further experiments. Film thicknesses of polymer films were estimated from the charge (integrated to the formal potential) under the final voltametric scan during film synthesis by using the relationship of 31 mC cm<sup>-2</sup> per μm established by scanning electron microscopy.

#### **8.4 Electrochemical Studies of Poly-ThFl, Poly-Th<sub>2</sub>Fl and Poly-CNTh<sub>2</sub>Fl**

A cyclic voltammogram of a poly-ThFl coated Pt electrode in monomer-free acetonitrile containing 0.1 M Bu<sub>4</sub>NPF<sub>6</sub> is shown in **Fig 8.8 (a)**. p-Doping of the copolymer film was observed as a reversible wave in the +0.6 to +1.5 V region, while n-doping appeared as a less reversible wave in the -0.6 to -1.4 V region. The formal potentials of p- and n-doping/undoping are ca. +1.25 and -1.25 V, respectively, with a (band) gap of ca. 2.0 V between the onsets of p- and n-doping.

Fig 8.8 (b) shows a cyclic voltammogram for a poly-Th<sub>2</sub>Fl film in acetonitrile containing 0.1 M Bu<sub>4</sub>NPF<sub>6</sub>. p-Doping was carried out between 0 and +1.1 V while n-doping between 0 and -1.5 V. The formal potentials for p- and n-doping/undoping from the voltammograms are ca. +0.9 and -1.3 V, respectively. From the onsets of p- and n-doping, the (band) gap was estimated to be ca. 1.8 V.



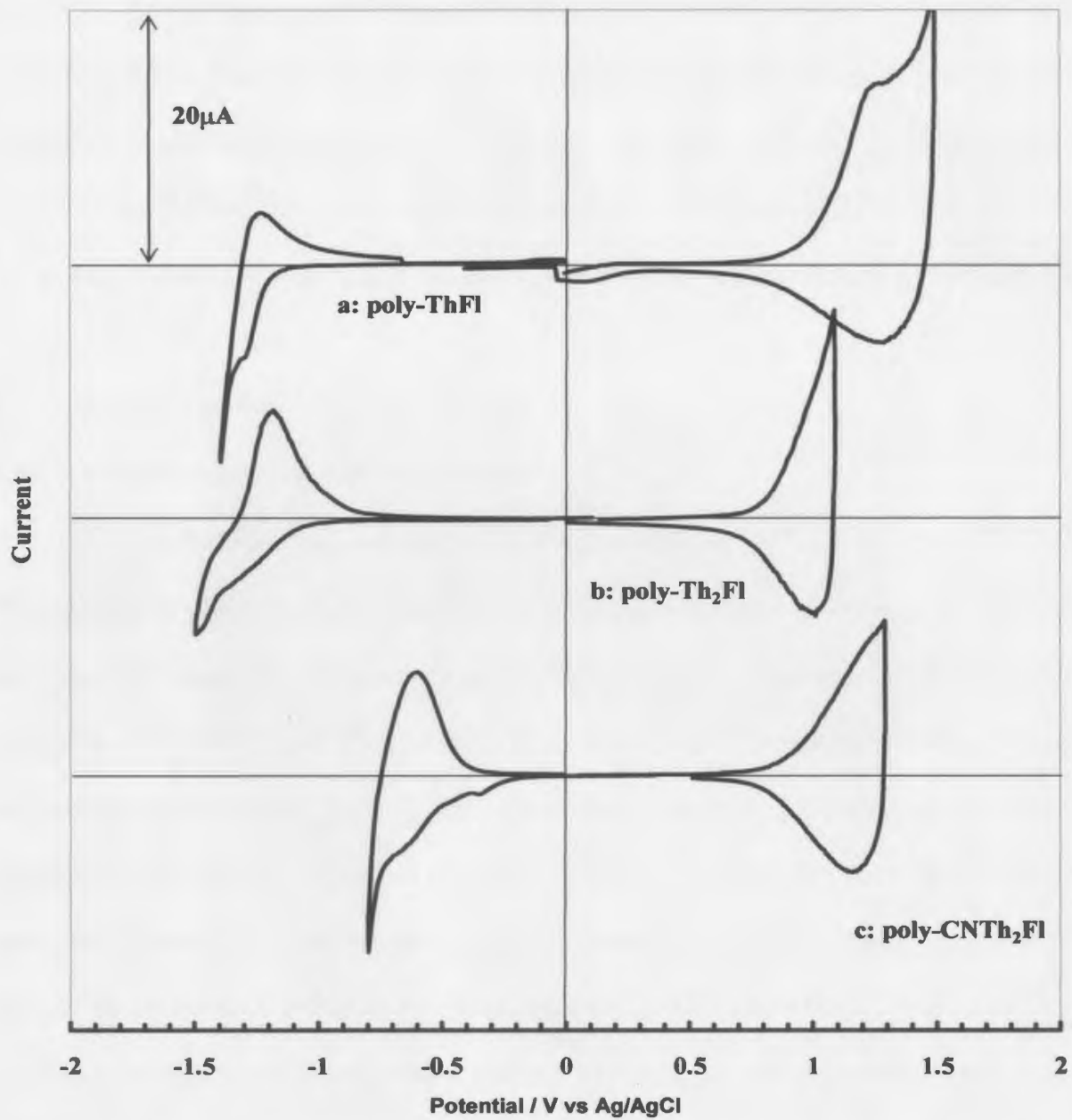


**Fig. 8.8.** Comparison of cyclic voltammograms of (A) poly-ThFl, (B) poly-Th<sub>2</sub>Fl and (C) poly-CNTh<sub>2</sub>Fl in acetonitrile containing 0.1 M Bu<sub>4</sub>NPF<sub>6</sub>  
Scan rate: 100 mV/s

Also shown in Fig 8.8 (c) is a cyclic voltammogram illustrating p- doping (from 0 to +1.3 V) and n-doping processes (from 0 to -0.8 V) of poly-CNTh<sub>2</sub>Fl in acetonitrile containing 0.1 M Bu<sub>4</sub>NPF<sub>6</sub>. Both the p- and n-doping of the copolymer film appeared as reversible waves in the region between +0.5 and +1.3 V and -0.1 and -0.8 V, respectively.

Poly-CNTh<sub>2</sub>Fl has p- and n-doping/dedoping formal potentials at ca. +1.1 and -0.6 V, respectively; with a (band) gap of ca. 1.2 V between the onsets of p- and n-doping.

## 8.5 *In Situ* Conductivity Measurements

### 8.5.1 Dual Electrode Sandwich Method

The in situ electronic conductivities of poly-ThFl, poly-Th<sub>2</sub>Fl and poly-CNTh<sub>2</sub>Fl films against potential were measured in acetonitrile containing 0.1 M Bu<sub>4</sub>NPF<sub>6</sub> by using dual electrode sandwich voltammetry. Fig 8.9 displays a conductivity vs. potential plot for a poly-ThFl film. In the positive scan, the p-type conductivity was investigated in the region between 0.0 V and +1.30 V. The p-type conductivity of the copolymer rises to a maximum of ca.  $3.1 \times 10^{-5} \text{ S cm}^{-1}$  at ca. +1.25 V. During the negative scan, in the region between 0.0 and -1.3 V, the n-type conductivity reached at  $5.6 \times 10^{-7} \text{ S cm}^{-1}$  at -1.3 V and was ca. 50 times smaller than the p-type conductivity. This conductivity was reproducible over multiple scans. The conductivity was slightly higher at lower potentials, but was unstable.

Fig 8.10 shows a plot of conductivity vs. potential obtained for a poly-Th<sub>2</sub>Fl film. The p-type conductivity of the copolymer rose to a maximum of ca.  $4 \times 10^{-4} \text{ S cm}^{-1}$  at ca.

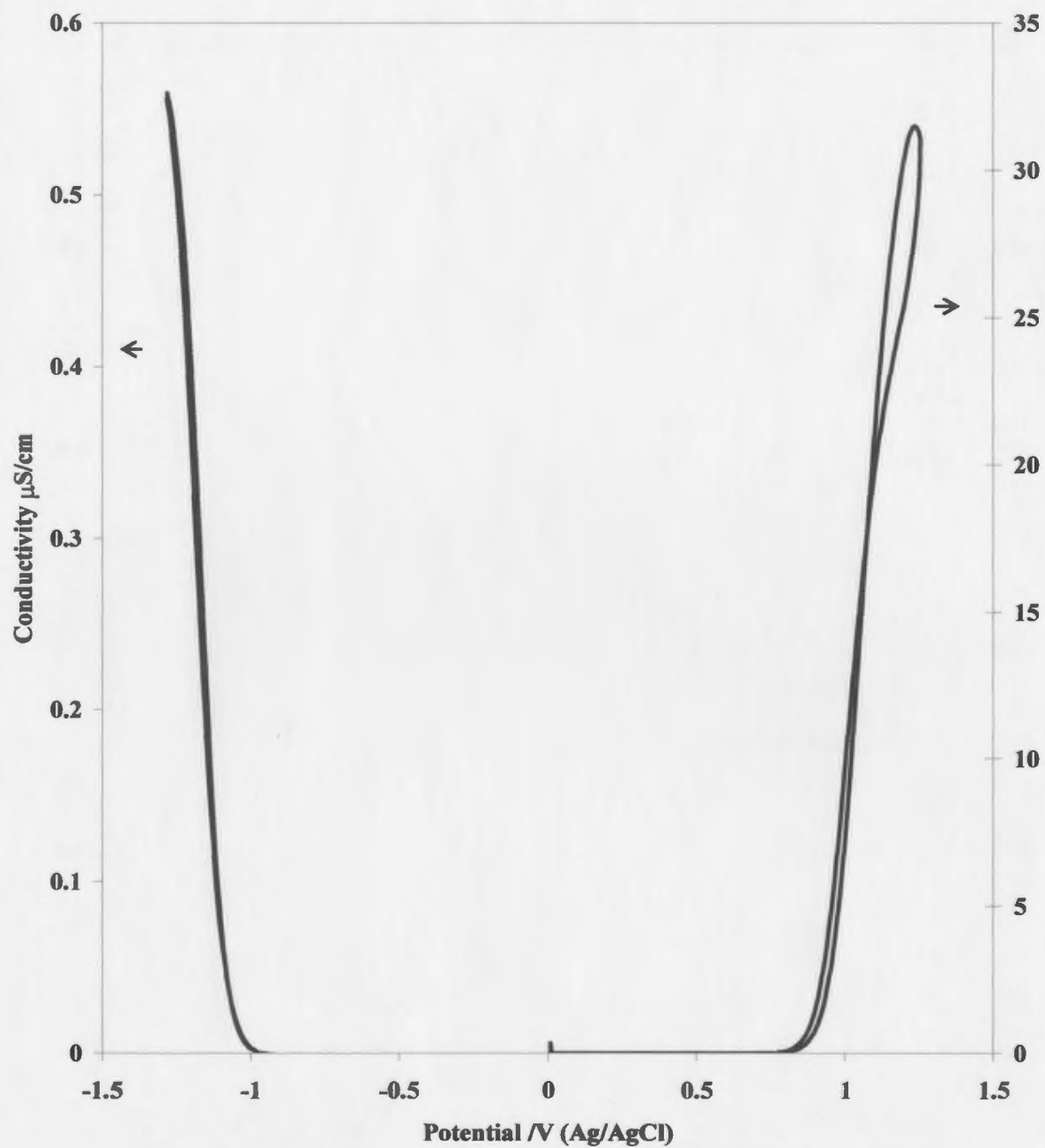


**Fig 8.9.** In situ conductivity as a function of potential (in acetonitrile containing 0.01 MBu<sub>4</sub>NPF<sub>6</sub>) for a 0.1 μm poly-ThFI film sandwiched between a Pt disk electrode and a porous gold film

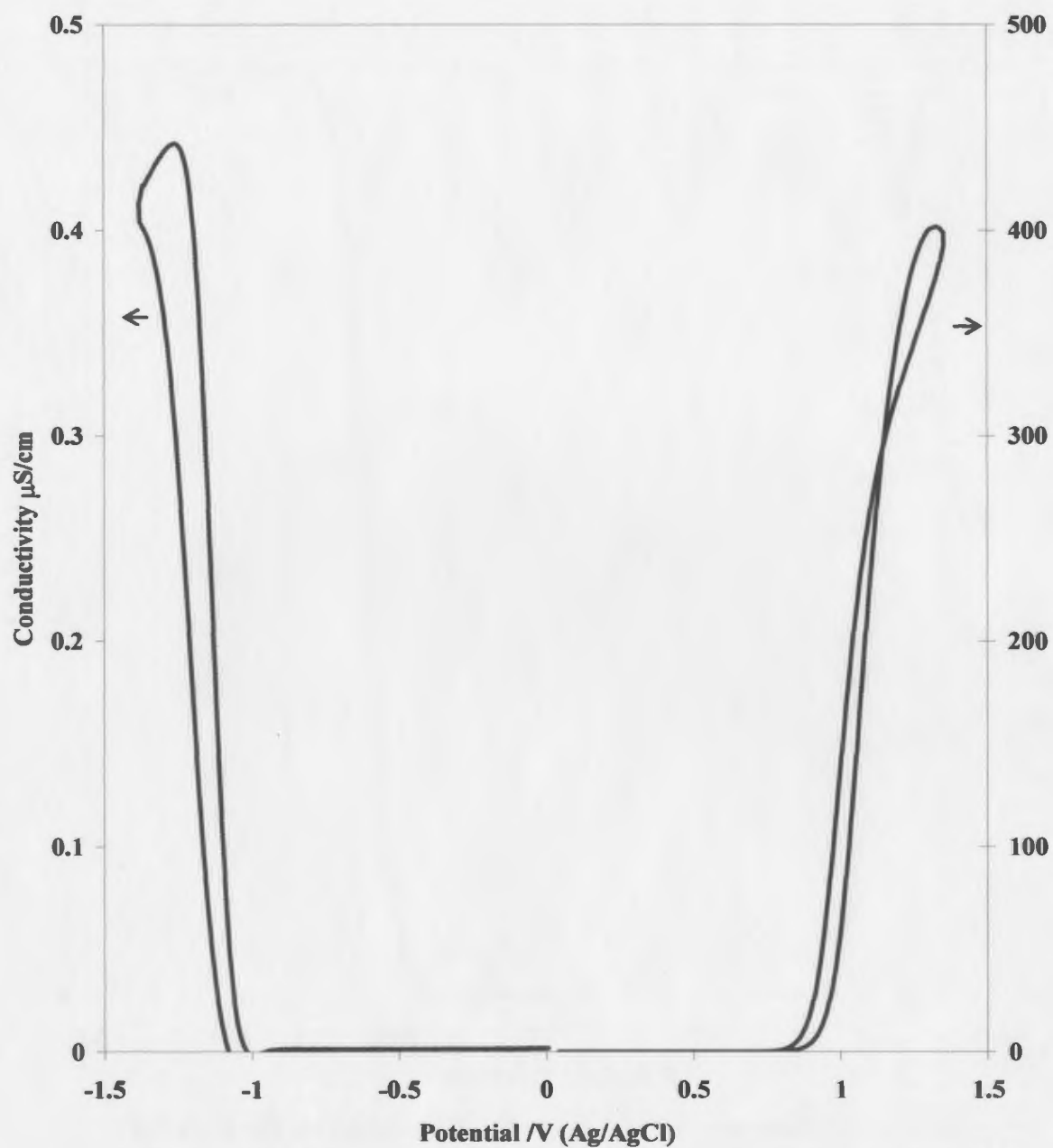


**Fig 8.10.** In situ conductivity as a function of potential (in acetonitrile containing 0.01 MBu<sub>4</sub>NPF<sub>6</sub>) for a 0.1 μm poly-Th<sub>2</sub>Fl film sandwiched between a Pt disk electrode and a porous gold film

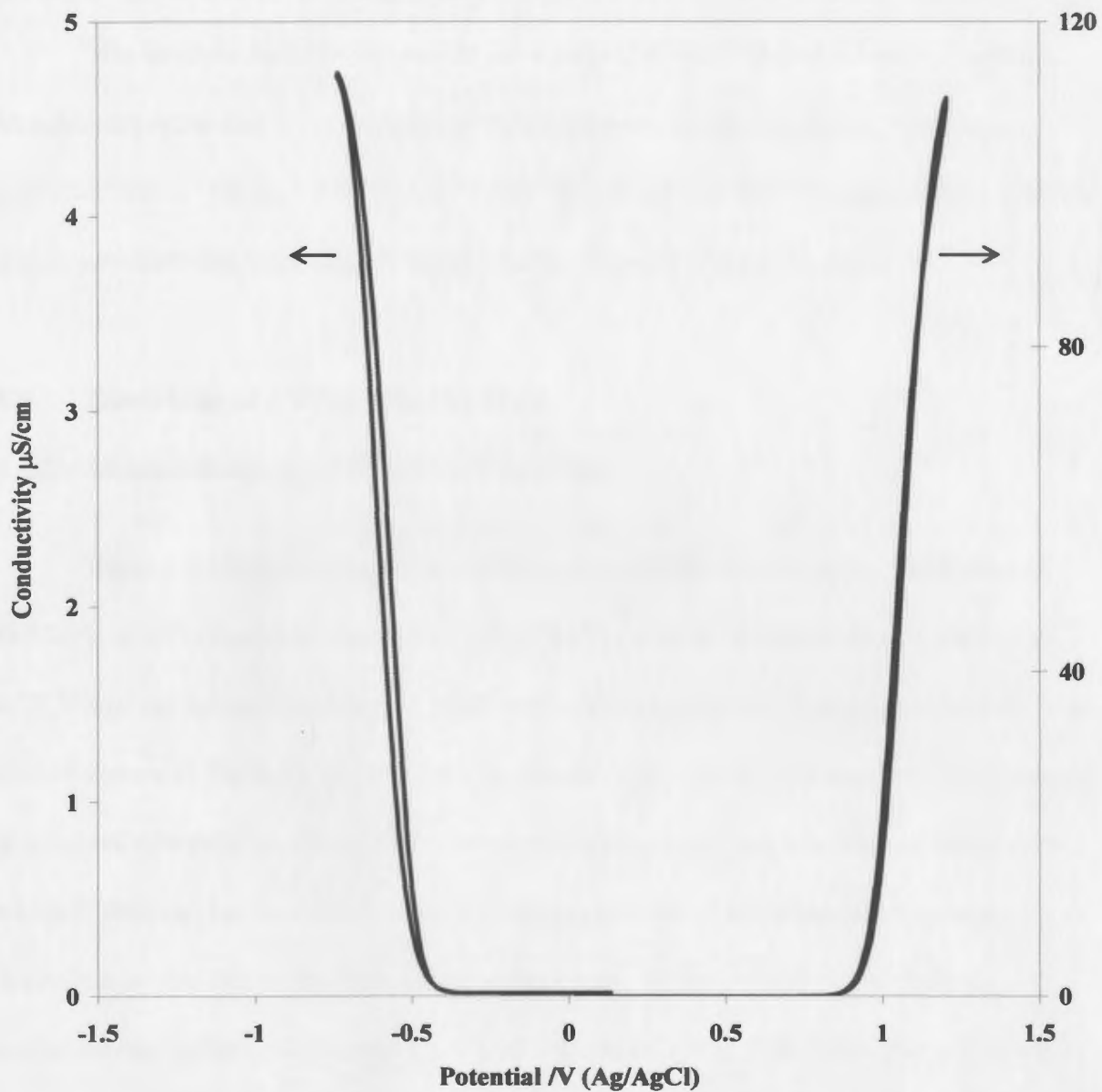


**Fig 8.11.** In situ conductivity as a function of potential (in acetonitrile containing 0.01 MBu<sub>4</sub>NPF<sub>6</sub>) for a 0.1 μm poly-CNTh<sub>2</sub>FI film sandwiched between a Pt disk electrode and a porous gold film

+1.3 V. The n-type conductivity, observed in the negative scan, was much smaller than the p-type conductivity, peaking at  $4.22 \times 10^{-7} \text{ S cm}^{-1}$  at ca. -1.25 V.

The in situ conductivity profile for a poly-CNTh<sub>2</sub>Fl film is shown in **Fig 8.11**. Maximum p-type and n-type conductivities observed for the copolymer film were  $1.10 \times 10^{-4} \text{ S cm}^{-1}$  (at ca. 1.2 V) and  $4.71 \times 10^{-6} \text{ S cm}^{-1}$  (at ca. -0.7 V), respectively, with the n-type conductivity being ca. 20 times smaller than the p-type conductivity.

## **8.6 Band Gap of Poly-(S<sub>2</sub>Th<sub>4</sub>Fl<sub>2</sub>) (8-4)**

### **8.6.1 Electrochemical and Optical Band Gap**

**Figure 8.12** shows cyclic voltammograms for the reduction and oxidation of S<sub>2</sub>Th<sub>4</sub>Fl<sub>2</sub> at a Pt electrode. Reduction of S<sub>2</sub>Th<sub>4</sub>Fl<sub>2</sub> occurred at a formal potential of ca. -0.75 V and on further scanning, it exhibited a second reduction formal potential at -1.46 V (not shown in Fig 8.7). During the first anodic cycle, an oxidation wave was observed at a formal potential of +1.38 V. In the reverse scan, there was a reduction wave at ca. +1.08 V that can be attributed to the undoping (reduction) of polymeric material deposited on the electrode during the forward scan. In the second cycle, both the oxidation and reduction currents increased compared to the first cycle, and a new anodic wave appeared at a lower potential of ca. +1.17 V. From the onsets of oxidation and reduction, the electrochemical (band) gap of S<sub>2</sub>Th<sub>4</sub>Fl<sub>2</sub> was estimated to be 1.7 V. The inset of Fig 8.12 shows the UV-Vis spectrum of S<sub>2</sub>Th<sub>4</sub>Fl<sub>2</sub> in chloroform. S<sub>2</sub>Th<sub>4</sub>Fl<sub>2</sub> has an optical absorption maximum of 570 nm (2.2 eV), associated with the  $\pi$ - $\pi^*$  electronic

transition. The onset wavelength at 710 nm corresponds to an optical band gap of ca. 1.7 eV.

### 8.6.2 Theoretical Estimation of Bandgap

Semi-empirical calculations for  $S_2Th_4Fl_2$  were performed using the AM1 method using Hyperchem pro7.1 (Hypercube Inc.). **Fig 8.13** shows the structure of  $S_2Th_4Fl_2$  with the LUMO population. After geometry optimization, HOMO and LUMO energies were calculated to be -8.306 and -1.623 eV, respectively. Similarly, HOMO and LUMO energies of terthiophene (Th3) were calculated to be -8.29 and -0.82 eV respectively. By using the HOMO and LUMO energy values, and the oxidation formal potential of ca. 1.05 V and the reduction formal potential of ca. -2.2 V of terthiophene [13], the formal potentials of  $S_2Th_4Fl_2$  were estimated as shown below.

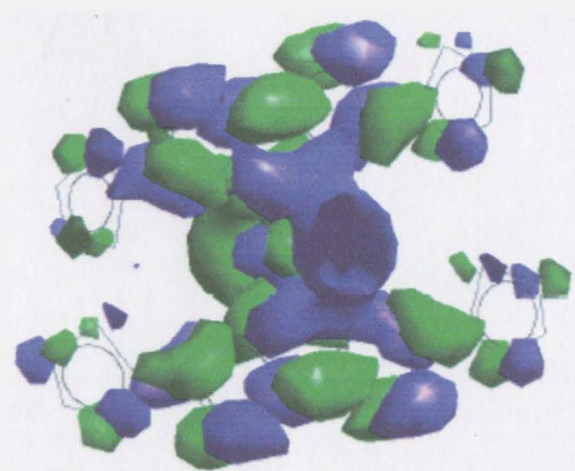


**Fig 8.13.** Structure of  $S_2Th_4Fl_2$  representing LUMO population

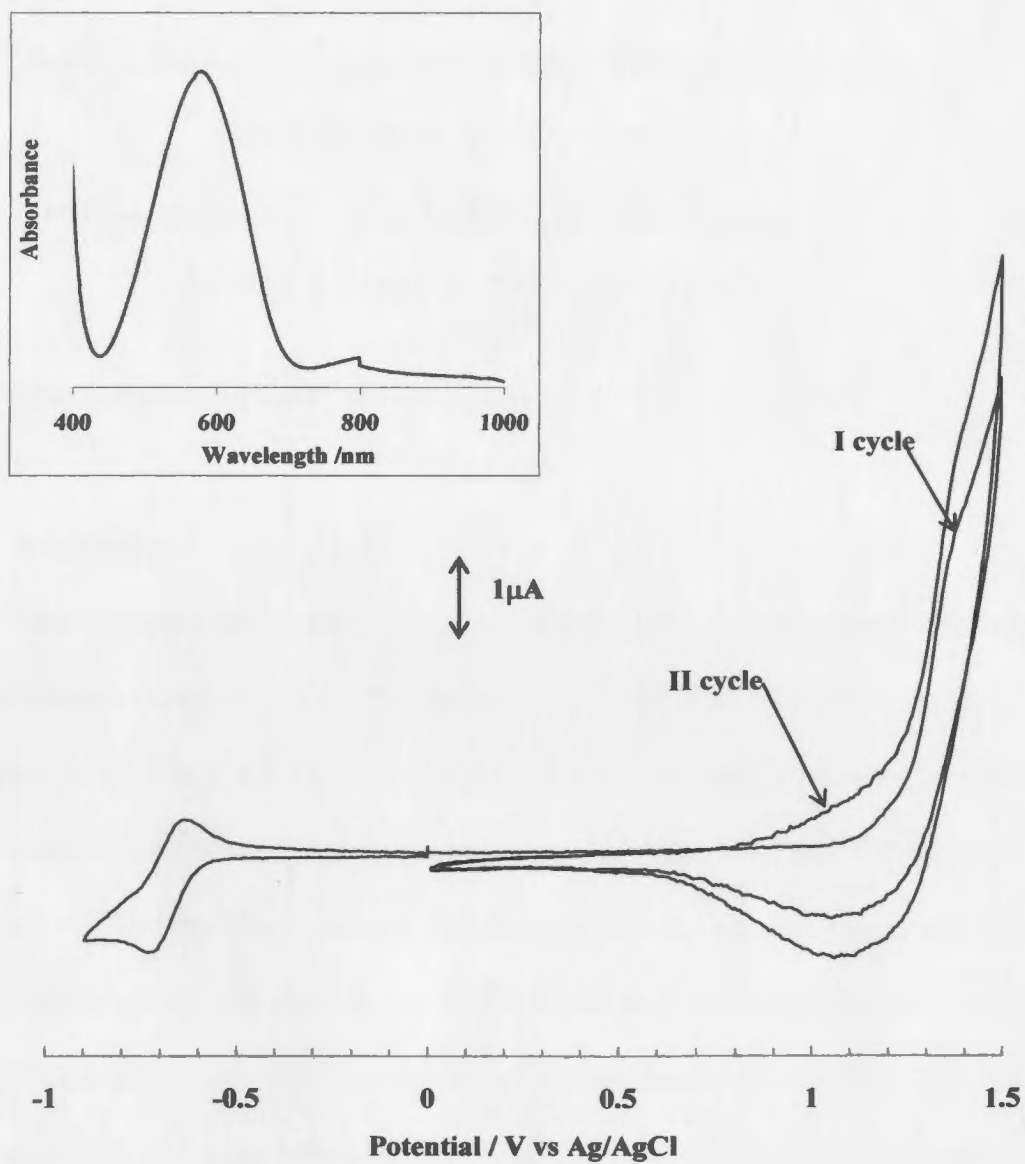


**Fig 8.12** Electrochemistry of S<sub>2</sub>Th<sub>4</sub>Fl<sub>2</sub> in acetonitrile containing 0.01 M Bu<sub>4</sub>NPF<sub>6</sub>. Inset: UV-Visible absorption spectrum of S<sub>2</sub>Th<sub>4</sub>Fl<sub>2</sub> in chloroform



$$\begin{aligned} \text{For } E_{\text{ox, S}_2\text{Th}_4\text{Fl}_2}^{0'} &= E_{\text{ox, Th}_3}^{0'} + \text{HOMO}_{\text{Th}_3} - \text{HOMO}_{\text{S}_2\text{Th}_4\text{Fl}_2} \\ &= + 1.05 - 8.29 + 8.31 = +1.07 \text{ V} \end{aligned}$$

$$\begin{aligned} \text{For } E_{\text{red, S}_2\text{Th}_4\text{Fl}_2}^{0'} &= E_{\text{red, Th}_3}^{0'} + \text{LUMO}_{\text{Th}_3} - \text{LUMO}_{\text{S}_2\text{Th}_4\text{Fl}_2} \\ &= - 2.2 - 0.82 + 1.62 = - 1.40 \text{ V} \end{aligned}$$

This estimation gave a HOMO-LUMO gap of 2.5 eV for S<sub>2</sub>Th<sub>4</sub>Fl<sub>2</sub>.

## 8.7 Discussion

The electrochemical and optical properties of the fluorene based molecules studied here are summarized in **Tables 8.1** and **8.2**. ThFl and Th<sub>2</sub>Fl have electrochemical band gaps of ca. 2.9 and 2.6 eV. Optical HOMO-LUMO gaps (Table 8.2) of ThFl and Th<sub>2</sub>Fl agree well with the respective electrochemical gaps. The reduction formal potentials of ThFl and Th<sub>2</sub>Fl are almost the same, whereas the oxidation peak potential of ThFl is higher (ca. 0.3 V) than that of Th<sub>2</sub>Fl. Moreover the HOMO-LUMO gaps of ThFl and Th<sub>2</sub>Fl are ca.0.7 and 1.0 eV, respectively, lower than the HOMO-LUMO gap of fluorenone. The n-doping formal potentials of ThFl and Th<sub>2</sub>Fl were unchanged relative to that of fluorenone, while the HOMO-LUMO gap is lower. This indicates that the thiophene units at the 2, 7 positions have little effect on the LUMO of the comonomer, but have a significant effect on the HOMO energy level. This result indicates that the HOMO energy level can be increased by varying the chain length of donor units in the fluorenone backbone of the comonomers. The HOMO-LUMO gap of fluorenone (2.8 eV) was estimated from ref. [9] for this comparison.

**Table 8.1** Summary of electrochemical properties of fluorene based molecules

	$E_{p, ox}$ /V	$E^{0}_{red}$ /V	$E_{g(electrochem)} = E_{p, ox} - E^{0}_{red}$ /V
ThFl	1.55	-1.35	2.9
Th <sub>2</sub> Fl	1.33	-1.30	2.6
CNTh <sub>2</sub> Fl	1.40	-0.75	2.1
Fluorenone	2.40 <sup>a</sup>	-1.30 <sup>a</sup>	3.6 <sup>a</sup>

a estimated from reference [9]

$E_p$  taken as approximation of  $E^{0}$

**Table 8.2** Summary of spectroscopic properties of fluorene based molecules

	$\lambda_{max}$ /nm	$\lambda_{onset}$ /nm	HOMO-LUMO gap <sup>b</sup> <sub>(optical)</sub> /eV
ThFl	433	525	2.9
Th <sub>2</sub> Fl	563	580	2.3
CNTh <sub>2</sub> Fl	580	770	2.1
Fluorenone	400 <sup>a</sup>	460 <sup>a</sup>	3.4 <sup>a</sup>

a estimated from reference [9]

b based on  $\lambda_{max}$

**Table 8.3** Summary of electrochemical properties of fluorene based polymers

	$E^{\circ}$ (p-doping)/ V	$E_{p(\text{ox onset})}$ /V	$E^{\circ}$ (n-doping)/ V	$E_{n(\text{re onset})}$ /V	$E_g^b$ (electrochem) /V
Poly-ThFl	1.25	0.90	-1.25	-1.10	2.00
Poly-Th <sub>2</sub> Fl	0.95	0.70	-1.30	-1.10	1.80
Poly-CNTh <sub>2</sub> Fl	1.10	0.80	-0.60	-0.40	1.20
PFT <sup>c</sup>	1.00	0.70	-1.20	-0.90	1.60
Poly-Fluorenone	1.55 <sup>a</sup>	1.40 <sup>a</sup>	-1.20 <sup>a</sup>	-1.10 <sup>a</sup>	2.50 <sup>a</sup>

a estimated from reference [9]

b gap between onsets of n- and p-doping

c 6.1e from chapter 6

**Table 8.4** Conductivities of fluorene based copolymers

	$\sigma_{\text{max, p}}$ /S cm <sup>-1</sup>	$\sigma_{\text{max, n}}$ /S cm <sup>-1</sup>	$\sigma_{\text{intrinsic}}$ /S cm <sup>-1</sup>
Poly-ThFl	$3.15 \times 10^{-5}$	$5.60 \times 10^{-7}$	$1 \times 10^{-12}$
Poly-Th <sub>2</sub> Fl	$4.00 \times 10^{-4}$	$4.22 \times 10^{-7}$	$1 \times 10^{-11}$
Poly-CNTh <sub>2</sub> Fl	$1.10 \times 10^{-4}$	$4.71 \times 10^{-6}$	$1 \times 10^{-10}$

Substitution of a dicyanomethylene group at the C-9 position of Th<sub>2</sub>Fl decreases the HOMO-LUMO gap further. CNTh<sub>2</sub>Fl has an absorption maximum of ca. 580 nm and the onset wavelength of ca. 770 nm corresponds to a HOMO-LUMO gap of ca. 1.6 eV. The absorption maximum and onset wavelength of CNTh<sub>2</sub>Fl are red shifted when compared to those of fluorenone, ThFl, and Th<sub>2</sub>Fl (Table 8.2). Moreover, CNTh<sub>2</sub>Fl has an electrochemical band gap of ca. 1.7 eV with a reduction formal potential of -0.7 V. The oxidation formal potential of CNTh<sub>2</sub>Fl is slightly higher (by ca. 0.1 V) than Th<sub>2</sub>Fl but lower (by ca. 0.1 V) than observed for ThFl. The reduction onset and formal potentials of CNTh<sub>2</sub>Fl are ca. 0.5 V lower than those of Th<sub>2</sub>Fl. This indicates that the dicyanomethylene group at the C9 position of CNTh<sub>2</sub>Fl has little effect on the HOMO of the comonomer, but a large effect on the LUMO energy level.

Copolymer films poly-ThFl, poly-Th<sub>2</sub>Fl and poly-CNTh<sub>2</sub>Fl were prepared by the potential cycling method. This mode of polymerization is advantageous because the film growth can be monitored and some useful mechanistic information can be obtained, which can be applied to interpretation of the electrochemical behavior of the new conducting polymers [13]. Since the potential cycling method worked well for homopolymerizations of comonomers, constant potential or constant current polymerizations were not performed.

The electrochemical properties of poly-ThFl, poly-Th<sub>2</sub>Fl and poly-CNTh<sub>2</sub>Fl together with the properties of polyfluorenone [9] are summarized in **Table 8.3**. Poly-ThFl has a (band) gap of ca. 2.0 V between the p- and n-doping onset potentials of ca.

+0.9 V and ca. -1.1 V, respectively. The electrochemical (band) gap of poly-Th<sub>2</sub>Fl is ca. 1.8 V between the onsets of p and n-doping at ca. +0.7 and -1.1 V, respectively. By increasing the thiophene units in the copolymer chain, the p-doping onset potential is decreased by 0.2 V whereas the n-doping potential remains almost unchanged, and the band gap, therefore, is 0.2 eV lower for poly-Th<sub>2</sub>Fl. Moreover, the band gaps of poly-ThFl and poly-Th<sub>2</sub>Fl are ca.0.5 and 0.7 eV lower when compared to that of polyfluorenone (Table 8.3). The n-doping onset potentials of poly-ThFl, poly-Th<sub>2</sub>Fl and polyfluorenone are the same. This indicates that the copolymerization of thiophene with fluorenone increases the HOMO energy level of the resulting copolymer.

It is of interest to compare the electrochemical band gap of poly-ThFl, the copolymer obtained by homopolymerization of comonomer **8-1**, and PFT **6.1e** (a copolymer drop coated on to the electrode which was synthesized by a Stille coupling method; chapter 6). The p and n-doping onsets of PFT at ca. +0.7 V and ca. -0.9 V corresponds to a (band) gap of ca.1.6 eV, which is ca. 0.4 eV less than that obtained for poly-ThFl. But the electrochemical band gap of poly-ThFl agrees well with the optical band gap of PFT (ca. 1.9 eV; Table 6.2, chapter 6). Inhomogeneities and deposition conditions of PFT film should be the reason for a slight disagreement between the electrochemical band gaps of PFT and poly-ThFl.

Poly-CNTh<sub>2</sub>Fl has a (band) gap of 1.2 V between the onsets of p- and n-doping (Table 8.3). The n-doping onset potential of poly-CNTh<sub>2</sub>Fl is ca. 0.7 V more positive than those obtained for poly-ThFl and poly-Th<sub>2</sub>Fl. This shift can be attributed to the large electron withdrawing effect of acceptor units [12] in the copolymer chain of poly-

CNTh<sub>2</sub>Fl. The p-doping onset potential of poly-CNTh<sub>2</sub>Fl is slightly more positive, (by ca. 0.1 V) than that of poly-Th<sub>2</sub>Fl. This slight lowering of the HOMO energy level of poly-CNTh<sub>2</sub>Fl is also due to the strong electron withdrawing effect of dicyanomethylene groups in the copolymer chain [12]. These results indicate that the presence of a strong electron acceptor in the copolymer chain lowers the LUMO energy. Thus poly-CNTh<sub>2</sub>Fl is a lowest band gap donor-acceptor (alternating) copolymer of those studied here.

Maximum p-type, n-type and intrinsic conductivities of poly-ThFl, poly-Th<sub>2</sub>Fl and poly-CNTh<sub>2</sub>Fl, calculated from the dual electrode voltammetric experiments, are listed in **Table 8.4**. The maximum p-type conductivity of poly-Th<sub>2</sub>Fl is ca. 10 times higher than observed for a poly-ThFl film. The maximum n-type conductivity observed for poly-Th<sub>2</sub>Fl is very small when compared to the maximum p-type conductivity of the same film and the n-type conductivity of poly-ThFl. The reason for a low n-type conductivity of poly-Th<sub>2</sub>Fl can be attributed to the resistance caused by additional (regularly spaced) thiophene units to the mobility of the n-type charge carriers.

Maximum p- and n-type conductivities of poly-CNTh<sub>2</sub>Fl are ca. 5 times higher than those observed for poly-ThFl. The p-type conductivity of poly-CNTh<sub>2</sub>Fl was slightly lower when compared to that of poly-Th<sub>2</sub>Fl.

The intrinsic conductivities of the copolymers were obtained from (dual electrode sandwich voltammetry) log conductivity vs potential plots using the intercept method (Table 8.4). Poly-CNTh<sub>2</sub>Fl exhibited a higher intrinsic conductivity of 0.01  $\mu\text{S cm}^{-1}$  than those of poly-ThFl and poly-Th<sub>2</sub>Fl. Therefore, substitution of a strong electron withdrawing groups (such as dicyanomethylene) at the C-9 position of the comonomer

has a significant effect on the n-type and the intrinsic conductivities of the copolymers. On the other hand, the donor chain length of the copolymer strongly influences its p-type conductivity and enhances the intrinsic conductivity.

The oligomer  $S_2Th_4Fl_2$  has an oxidation formal potential of ca. +1.4 V and a reduction formal potential of ca. -1.4 V. A (HOMO-LUMO) gap of ca. 2.5 V was observed between the formal potentials for oxidation and reduction. There is good agreement between the experimental (electrochemical and optical) and theoretically estimated HOMO-LUMO gaps. Theoretical formal potentials for  $S_2Th_4Fl_2$  were estimated based on HOMO and LUMO energies from AM1 calculations and experimental formal potentials of terthiophene (a molecule with 3 thiophenes). The theoretically estimated reduction formal potential of  $S_2Th_4Fl_2$  agrees well with the experimental value. The oxidation formal potential of  $S_2Th_4Fl_2$  was slightly (ca. 0.3 V) higher than the theoretically estimated value. Moreover, the LUMO of  $S_2Th_4Fl_2$  is conjugated between the fluorene moieties via the bridging sulphur units as shown in **Fig 8.13**. Thus,  $S_2Th_4Fl_2$  is a new conjugated precursor for low band gap polymers.

## **8.8 Conclusion**

Homopolymerization of comonomers leads to the formation of alternating copolymers. By increasing the D-A ratio of the comonomers, the band gaps of fluorenone and polyfluorenone can be decreased. Substitution of a strong electron acceptor in the comonomer chain lowers the LUMO energy, decreases the band gap and enhances the intrinsic conductivity of the copolymer.  $S_2Th_4Fl_2$  is a new conjugated

precursor for low band gap polymers. These results for monomeric and polymeric materials support the applicability of the donor acceptor strategy in the design of low band gap conducting materials.

#### References:

1. van Mullekom, H. A. M.; Vekemans, J. A. J. M.; Havinga, E. E. *Mater. Sci. Eng. R.* **2001**, *32*, 1.
2. Bakhshi, A. K; Bhalla, G. *J. Sci. Ind. Res.* **2004**, *63*, 715.
3. Chen, M. X.; Perzon, E.; Robisson, N. *Synth. Met.* **2004**, *146*, 233.
4. Ajayaghosh, A. *Chem. Soc. Rev.* **2003**, *32*, 181.
5. Huang, H.; Pickup, P. G. *Chem. Mater.* **1998**, *10*, 2212.
6. Liu, S. P.; Chan, H. S. O.; Ng, S. C. *J. Polym. Sci., Part A: Polym. Chem.* **2004**, *42*, 4792.
7. Kong, X. X.; Kulkarni, A. P.; Jenekhe, S. A. *Macromolecules*; **2003**, *36*, 8992.
8. Uckert, F.; Setayesh, S.; Mullen, K. *Macromolecules* **1999**, *32*, 4519.
9. Cihaner, A; Tirkes, S; Onal, A. M, *J. Electroanal. Chem.* **2004**, 568, 151.
10. Rault-Berthelot, J.; Raoult, E.; Le Floch, F. *J. Electroanal. Chem.* **2003**, *546*, 29.
11. Rault-Berthelot, J.; Raoult, E. *Adv. Mat. Opt. Elect.* **2000**, *10*, 267.
12. Salzner, U.; Lagowski, J. B.; Pickup, P. G.; Poirier, R. A. *J. Org. Chem.* **1999**, *64*, 7419.



13. Naudin, E.; El Mehdi, N.; Soucy, C.; Breau, L.; Belanger, D. *Chem. Mater.* **2001**, *13*, 634.

## Chapter 9

### Summary

Polymerization of bridged bithiophene (structure, **3-3**) has produced a very low band gap ( $E_g = \text{ca. } 0.5 \text{ eV}$ ) polymer. The very low HOMO-LUMO gap of **3-3** together with its four linkable thiophene terminals may make it a useful component for cross-linking low band gap systems and of value as a building block for molecular electronic systems. Copolymerization of bridged bithiophene with EDOT produces materials with reduced electrochemical band gaps, enhanced conductivities and faster electrochemical kinetics. However, poor conjugation of the resulting materials leads to low charge carrier mobilities and conductivities relative to the poly-EDOT homopolymer. The donor-acceptor method for band gap reduction is again shown to be effective, but at the expense of charge carrier mobility. Thus, the expected gains in intrinsic conductivity with band gap reduction have not been realized. Electrode rotation enhances the grafting process during polymerization, resulting in faster polymer deposition. Also, the conductivity of the resulting polymer films increases with electrode rotation during polymerization, i.e. when the grafting process is enhanced. The influence of electrode rotation on conductivities of bridged bithiophene was also reflected in its copolymers. The observation of faster polymerization with increasing rotation rate here is contrary to results previously reported for polythiophene and its derivatives. The difference appears to be due to the lower monomer concentration used in this work.

Copolymers of fluorenone with benzene, thiophene, and furan have band gaps of ca. 1.6-1.9 eV and can be easily p-doped and n-doped. Copolymerization of the electron deficient fluorenone moiety with the electron rich thiophene and furan units produces the lowest band gaps and the lowest p-doping potentials. The n-doping potential is insensitive to the nature of the spacer (donors) units between fluorenone units, indicating localization of the LUMO on the ketone substituent. The band gaps of the copolymers are significantly lower than that of the fluorenone homopolymer. PFB, PFT and PFF are promising candidates for use as an electron transport layer in multilayer LEDs.

Donor-acceptor conjugated co-monomers with different D-A ratios, consisting of thiophene as the electron rich subunit (D) and fluorenone as the electron deficient subunit (A), were synthesized in moderate yields by means of Suzuki cross-coupling reactions. (2,7-di-thiophen-2-yl-fluorenone-ylidene)-isocyano-acetonitrile was synthesized by a Knoevenagel condensation of 2,7-di-thiophen-2-yl-fluorenone. The reaction between 2,7-di-thienyl-9H-fluorenone and *Lawesson's* reagent has yielded a new precursor material 2,7,2',7'-tetra-thiophen-2-yl-[9,9']bifluorenyl-dithietane.

Homopolymerization of comonomers leads to the formation of alternating copolymers. By increasing the D-A ratio of the comonomers, the band gaps of fluorenone and polyfluorenone can be decreased. Substitution of a strong electron acceptor in the comonomer chain lowers the LUMO energy, decreases the band gap and enhances the intrinsic conductivity of the copolymer.  $S_2Th_4Fl_2$  is a new conjugated precursor for low band gap polymers.

## 9.2 Future Work

The linkage of two bridged bithiophene moieties by a double bond can be performed by McMurry reaction. The concentration of monomer solution used for electropolymerizations under hydrodynamic conditions can be further optimized to enhance grafting processes. It's understood that the bridged fluorene moieties by sulphur atoms can produce low band gap materials with low LUMO energy levels. Therefore, a very low band gap and highly conducting materials can be designed by copolymerization of electron deficient bridged fluorenes with electron rich EDOT.

## Appendix A

### $^1\text{H}$ NMR Spectra

